ECOLE POLYTECHNIQUE FEDERALE DE LAUSANNE

ISRF / EPFL

Translation of the Doctoral Thesis N^{O} 1169

Strength and Deformability of Jointed Rock Masses Reinforced by Rock Bolts

By

Frédéric Pellet

Department of Civil Engineering - Rock Mechanics Laboratory
Swiss Federal Institute of Technology - 1015 - Lausanne - Switzerland

Foreword

This study was carried out at the Rock Mechanics Laboratory of the Swiss Federal Institute of Technology in Lausanne.

I wish to express my best thanks to Professor F. Descoeudres who accepted to supervise this work and who provided facilities and support to complete it.

I express my sincere gratitude to Professor P. Egger for his precious scientific advice as well as for his kind encouragements.

The participation of Professors E. Recordon, G.P. Giani, J.P. Piguet and R. Favre in the evaluation of this work was really appreciated. The author thanks each of them for their valuable contribution.

The sientific assistance of Dr M. Kharchafi and Mr J.F. Mathier was of the most importance in the completion of this work. Moreover, their friendly support was very helpful.

The technical assistance of Mr J.F. Mottier was really appreciated as well as the help of Mrs G. Neidhart who prepared drawings.

The author thanks Dr L. Zabuski for translating this thesis and Dr A.M. Ferrero and Dr L. Thorel for the fruitful scientific discussions they had together.

Finally, thanks are extended to all colleagues of the Rock Mechanics Laboratory.

Lausanne, March 1994

Abstract

Nowadays, the technique of employing passive anchors for rock mass reinforcement is frequently used to ensure the stability of rock slopes and underground cavities. Even though the technology is in common practice, the description of the reinforced rock's mechanical behaviour is not always clearly understood. The present study aims to determine, in terms of strength and deformability, the effect of a rock bolt on the behaviour of a rock joint in order to rationalize the dimensioning of rock structures.

The physical mechanisms of reinforcements are described in **chapter 2.** The principal works published to this date in the experimental, analytical and numerical fields are summarized in **chapter 3**.

Chapter 4 describes the experimental program which was conceived to illustrate the principal factors affecting the behaviour of a volume of reinforced rock. The tests were carried out using a triaxial cell which permitted the testing of large samples having one or several discontinuities reinforced with steel bolts. The results show that in addition to the bolts' inherent properties, the rock's strength, the bolts' orientation and its fixing conditions are parameters which also influence the strength and the deformability of the reinforced joint.

The analytical development presented in **chapter 5** allows the calculation of the complete curve of a bolt's contribution to the shear strength of a rock joint as a function of the movement along the joint. This model is based on the description of the process of the bolts' deformations illustrated by tests and characterized at the end point by a mechanism involving two plastic hinges.

In the elastic range, the evolution of the mobilized forces in the bolt as a function of the displacements is obtained with the help of a variational

formula. The deformed shape of the bolt is described by a hyperbolic cosine function. The forces at the elastic limit are calculated by a plastic hinge formation criterion, established by taking into consideration the interaction of the bending moment and the normal force. **In the plastic range,** it is assumed that the normal force mobilized in the bolt continues to increase. The displacements are calculated using an axial rigidity secant which progressively decreases as a function of the plastic lengthening of the bolt. **At failure**, the mobilized forces in the bolt flush with the joint are determined by a formula of the interaction between the normal force and the shear force based on the Tresca criterion. The displacements are calculated by a large displacement formula assuming that the length delimited by the plastic hinges attains the material's failure strain. Knowing the orientation and the intensity of the mobilized resultant force in the bolt, one can determine the reinforced joint's shear strength by dissociating the bolt cohesion and the confinement effects.

Chapter 6 evaluates the performance of the analytical development and shows its capacity to describe the observed phenomena. The effect of inclining the bolt on the strength and the deformability of the reinforced joint is clearly established, as is the influence of the rock strength and the friction angle on the joint. The comparison of the performances of this model with experimental results demonstrates that it may be employed for a wide range of parameters.

Calculation for rock structures is covered in **chapter 7** in which examples of a slope and a shallow tunnel are treated. We show that the analytical development can be used to dimension the bolting system for a project and predict the displacements of the rock mass. On the basis of the experimental and theoretical conclusions, some practical suggestions were made in order to aid those conceiving projects and works in this field.

Contents

formula. The deformed shape of the bolt is described by a hyperbolic cosine function. The forces at the elastic limit are calculated by a plastic hinge formation criterion, established by taking into consideration the interaction of the bending moment and the normal force. **In the plastic range,** it is assumed that the normal force mobilized in the bolt continues to increase. The displacements are calculated using an axial rigidity secant which progressively decreases as a function of the plastic lengthening of the bolt. **At failure**, the mobilized forces in the bolt flush with the joint are determined by a formula of the interaction between the normal force and the shear force based on the Tresca criterion. The displacements are calculated by a large displacement formula assuming that the length delimited by the plastic hinges attains the material's failure strain. Knowing the orientation and the intensity of the mobilized resultant force in the bolt, one can determine the reinforced joint's shear strength by dissociating the bolt cohesion and the confinement effects.

Chapter 6 evaluates the performance of the analytical development and shows its capacity to describe the observed phenomena. The effect of inclining the bolt on the strength and the deformability of the reinforced joint is clearly established, as is the influence of the rock strength and the friction angle on the joint. The comparison of the performances of this model with experimental results demonstrates that it may be employed for a wide range of parameters.

Calculation for rock structures is covered in **chapter 7** in which examples of a slope and a shallow tunnel are treated. We show that the analytical development can be used to dimension the bolting system for a project and predict the displacements of the rock mass. On the basis of the experimental and theoretical conclusions, some practical suggestions were made in order to aid those conceiving projects and works in this field.

Contents

Chapter 6. Parametric Study and Theory Evaluation

Chapter 7.Applications to the Dimensioning of Rock Engineering Structures

Chapter 1

Introduction

Historical development in human activity involved the realization of numerous infrastructures, among which the construction of communication ways and buildings seems to be essential. The constructor, in his activity, is often confronted with problems of stability of structures, which are connected with material strength or with stability of masses forming foundations.

The common property of all geomaterials which constitute the Earth's crust is their mechanical behaviour, characterized by a very low ratio of tension to compressive strength. To overcome the influence of this unfavorable intrinsic property, the first important structures made of building stones were constructed in the form of arches or cupolas, to avoid any tension. Innovations introduced in the nineteenth century, i.e., reinforced and later prestressed concrete, illustrate the constant care of engineers to find appropriate protection against the development of tension stresses in structural elements.

Reinforcement of in situ soils and rocks were always the subject of the constructor's considerations. One can still find traces of ancient slope stabilization by bamboo stems. The theoretical explanation of the instability phenomenon was furnished in the eighteenth century by Coulomb, who found that the material shear strength increases as a function of the mean stress level. Thereby, he established the fundamental rule of the failure analysis. Thus, due to application of overloading or to unloading of the mass by excavation, the danger of failure always appears when the deviator of stresses is too high. As the geostatic stresses prevailing at the horizon of the Earth's surface are low, it is obvious that the shear strength of the material

is not significant. This peculiarity is accented in the case of rock masses because of the presence of tectonic or orogenic discontinuities, which constitute potential failure planes.

Although man had built superficial and underground structures for a long time, it was only in the nineteenth century that the first great constructions were realized. Development of hydro-electricity, as well as the initial projects of the great alpine crossing, allowed for significant acceleration in technology. During the realization of the Mont-Cenis tunnel (1857-1871), Germain Sommeiller introduced the pneumatic hammer, allowing for the mechanical boring of rocks. Later, this technique would allow the installation of steel bars for rock reinforcement.

However, initial applications of metallic elements for stabilization of structures were not introduced until the first decades of the twentieth century. André Coyne, in 1934, stabilized the Cheurfas Dam (Algeria) using prestressed cables. Yet, the main growth of this technique began in the second half of our century. At the very beginning, reinforcing elements were used in mining, and next in civil engineering. Introduction of this method was the answer to lowering costs and reducing delays in the structure's construction. One of the important consequences of this technological progress was a considerable reduction in the heavy "contribution" paid in human lives. From that time, stabilization of rock masses by systematic bolting spread widely in the field of superficial workings (slopes and embankments) as well as in underground excavations. The acceleration in the continuous development of these new technologies is due to the improvement of rock perforation methods and to the applications of some new materials, such as mortar and reinforcing elements of better quality.

From the very beginning, reinforcement by bolting has been the result of intuition and observation of experimenting miners. Until today, however, the available tools for the dimensioning of rock structures have been rudimentary. Despite the experience gained during realization of numerous constructions being very valuable, it is necessary to quantify the action of the rockbolts, to satisfy economic limitations and security requirements. In the same time, the development of supercomputers offers the possibility of establishing increasingly sophisticated models for the description of the

mechanical behaviour. Nevertheless, until now, "shaded zones" existed in the description of the action of the anchored bar and thus, none of the calculation models could be unanimously accepted.

The presented work is devoted to the continuation of earlier studies dealing with the comprehension of the action mode of passive bolts installed in rock masses. After the description of the general concept of rock mass reinforcement in **chapter 2**, the principal published results are reviewed in **chapter 3**. In **chapter 4**, the conditions and the results of the experiments realized on the reinforced models are described. The theory is developed in **chapter 5**, which consists of analytic formulation allowing for the quantitative description of rockbolt action in terms of strength and deformability of the reinforced rock joint. This formulation is discussed in **chapter 6** and then it is compared with other analytical predictions as well as with principal results of the experiments. Application of this analytical model to two important classes of practical problems, i.e., to superficial and underground excavations, is presented in **chapter 7**. In this chapter practical conclusions are formulated, which are in fact some guides for the designer. At the end, in **chapter 8**, a few remarks regarding possible future lines of investigations are presented.

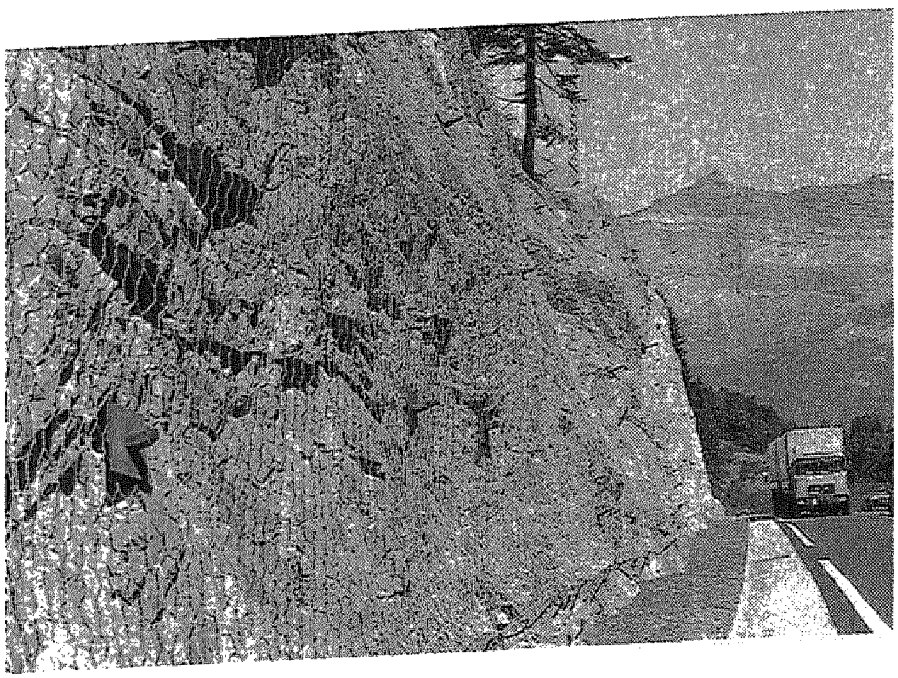

Figure 1 : *View of the rock slope reinforced by passive bolts located on the access road of the Mont- Blanc tunnel*

Chapter 2

Concept of Rock Masses Reinforcement

The principal aim of rock mass reinforcement by passive rockbolts is stabilization of the mass, by increasing its shear strength. When the construction is realized in the site, deformations of the rock mass must be limited, to avoid any damage to the nearby environment and constructions.

When the temporary or long-term stability of constructions is considered, the effectiveness of the reinforcement system depends on many factors, such as the mechanical and geometric characteristics of the reinforcement system, the quality and actual conditions of the rock mass, and the geometry of the construction under study. A typical situation is presented in Figure 2.1. In this case, both the stability of the slope and that of the underground cavity should be ensured.

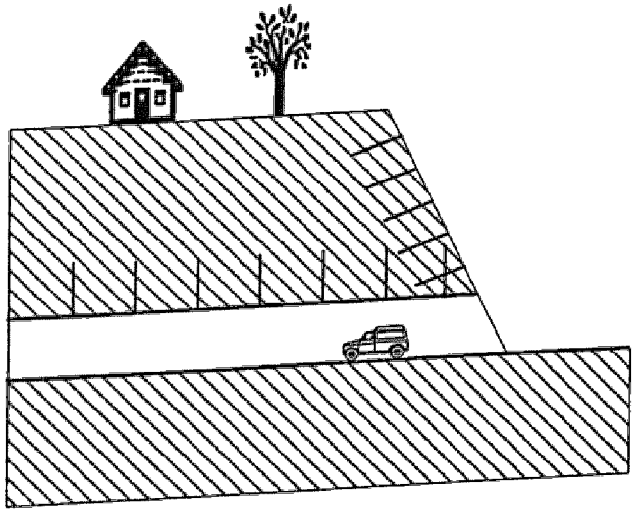

Figure 2.1 : *Typical situation in stability problem of the rock mass*

2.1. Technical elements

Rock mass reinforcement is realized by using many different techniques that introduce various kinds of mechanisms, principally differing in the nature and the fixing conditions of the reinforcement elements.

From the point of view of their mechanical action, many reinforcing elements could be generally divided into two categories: stiff elements, which are able to sustain bending moment and flexible elements, which can only carry axial forces. Stiff elements are represented by bars with circular cross-sections, made of high resistant steel, or glass fiber. Flexible elements, composed of single wire cables, are frequently used in mining works. Other elements, such as tubular friction anchored bolts (e.g. Swellex or Split Set type) have increasing importance in underground workings. One should also mention multiple-wire cables, which are used first of all as pretensioned elements. The mode of their action will be described later.

The action of the reinforcement system depends on the fixing conditions of the anchoring elements to the rock mass. Fixing can be achieved punctually, by fixing extreme points of the bar, or continuously, by grouting the whole length of the bar. From a mechanical point of view, it becomes obvious that the axial force is constant along the free length of the bar. It can be somewhat pre-tensioned (at time of installation). Continuous connection is realized most frequently by using grout or synthetic mixtures, such as epoxy resins. In the case of Swellex bolts, the contact is assured by expanding the tube in the borehole. From the mechanical point of view, continuously fixed bolts sustain the forces, which can differ along their length as a function of displacements occurring in the surrounding rock mass.

To ensure long-term action, rockbolts are often encapsulated before installation with polyvinyl chloride (PVC), to avoid any corrosion. The scheme of an anchor, mechanically fixed at its ends is shown in Figure 2.2a, whilst a fully grouted rockbolt is presented in Figure 2.2b. The reader can find more details concerning construction and installation in the book of **Stillborg (1986).**

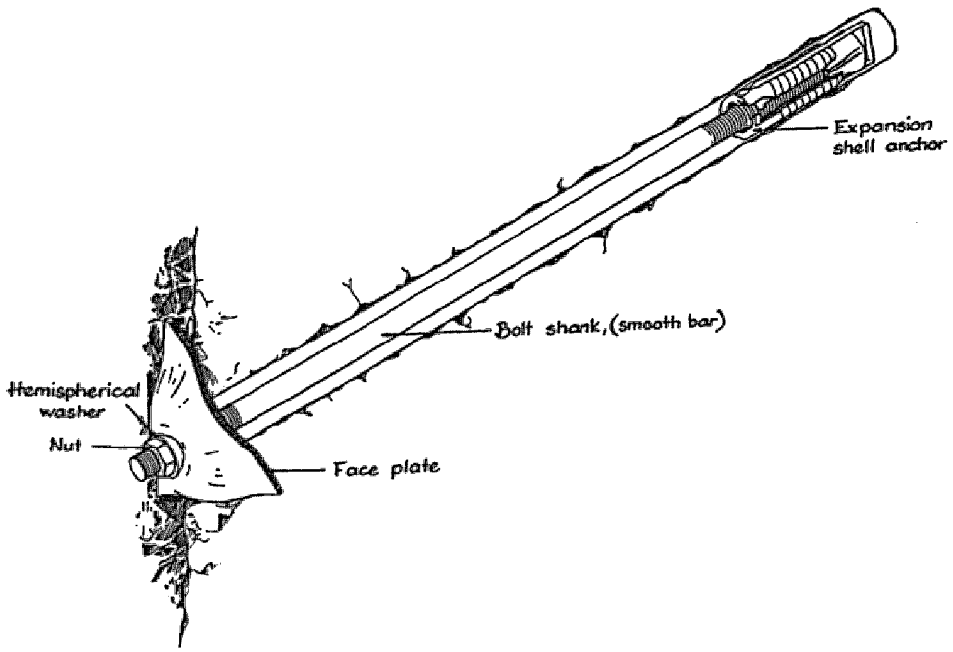

a- Mechanically anchored rockbolt

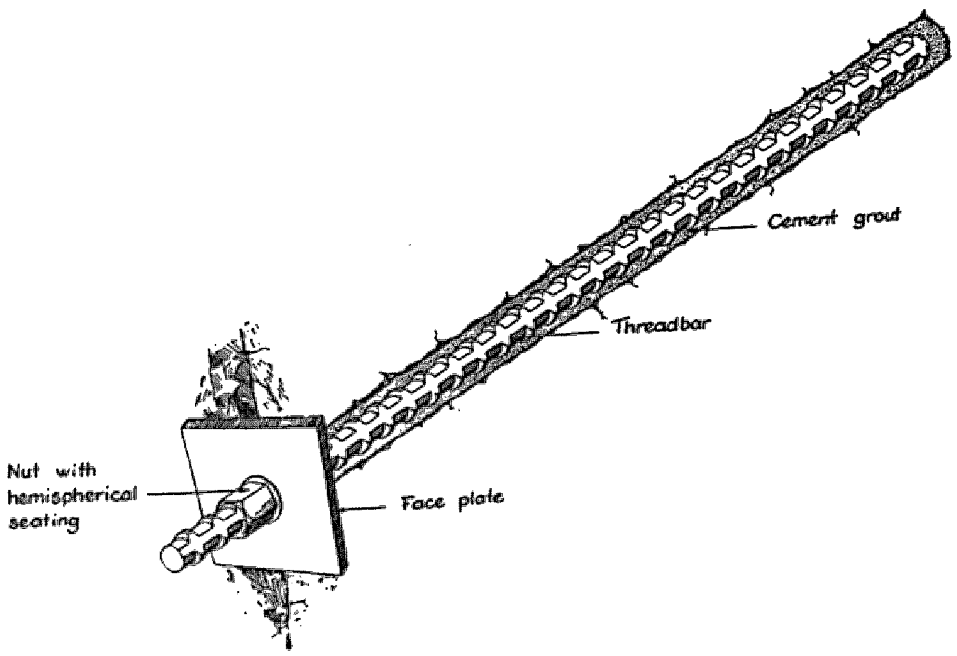

b- Fully grouted rockbolt

Figure 2.2 : *Rockbolts after Stillborg (1986)*

2.2. Nature and conditions of the in situ rock mass

Geomaterials constituting the Earth's crust exhibit various geologic forms. From the mass built of sound rock to extremely pulverized soil, the product of rock alteration, all situations are represented in nature. In most cases, potentially unstable rock masses are intersected by numerous discontinuities of different kinds, such as diaclases, joints, interbedding and foliation fissures. Thus, the analysis of rock mass stability requires one to identify, at the appropriate scale of the mass, all the discontinuity sets. It requires to define the fracturing degree, the orientation and the extension of discontinuities, as well as the properties of individual joints (i.e., aperture, roughness, filling material).

The fracturing degree, which can be appreciated through R.Q.D. (Rock Quality Designation), determines the average dimensions of individual rock blocks and the spacing of the discontinuities. The knowledge of orientation and persistence of principal discontinuities allows one to estimate the kinematics of potential movements. Some of the rock masses are "hierarchical". This signifies that rock mass stability depends on the stability of so called "key blocks".

Properties such as aperture of individual discontinuities, as well as rock mass tightness, influence rock mass mechanical behaviour to a very high degree. The mode of shear strength mobilization depends on the intensity of dislocation and loosening of the rock mass. If the mass is highly loosened, mobilization of the shear strength can be increased by increasing the extent of contacts between rock blocks. To the contrary, when the rock mass is tight and discontinuity apertures are very small, the positive role of the dilatancy phenomenon should be exploited. It must also be mentioned that the presence of filling material in discontinuities can strongly influence mechanical behaviour of the medium.

The elements described above allow one to approximately evaluate rock mass mechanical behaviour, and to define the mechanisms of the potential failure. A few examples of possible situations are presented in Figure 2.3, illustrating the above considerations. If the rock mass is comprised of parallel arranged layers (Figure 2.3.a) it can be expected that potential

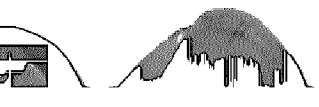

instability will appear by translative movement along a single discontinuity (or discontinuity set). If two sets of discontinuities are present, then such a movement will cause the opening of discontinuities in the second set (Figure 2.3b). Rotation phenomenon is also possible, causing slides between individual rock blocks (Figure 2.3c). If the rock mass is randomly and densely fractured (Figure 2.3.d), the slide surface and the failure mechanism can not be preliminary determined with a sufficient degree of accuracy.

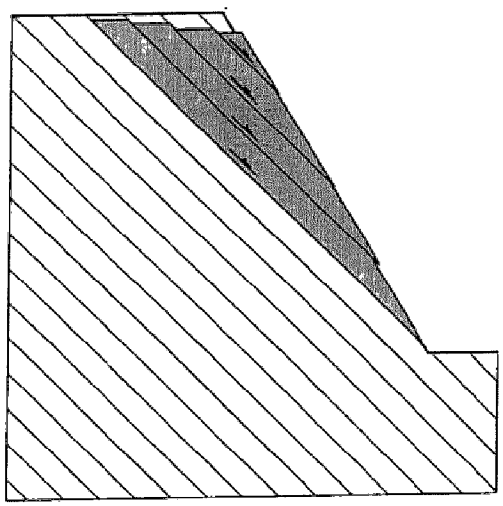

a - Plane sliding along one set of joints

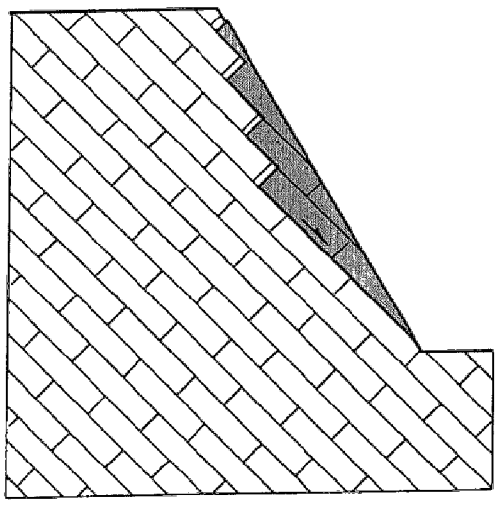

b - Sliding with opening of one set of joints

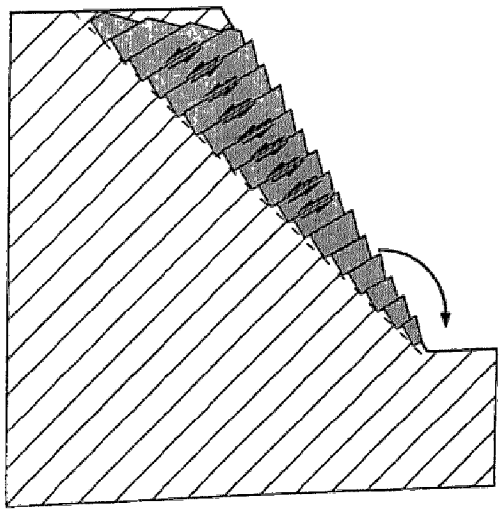

c - Rotation of layers with sliding along one set of joints

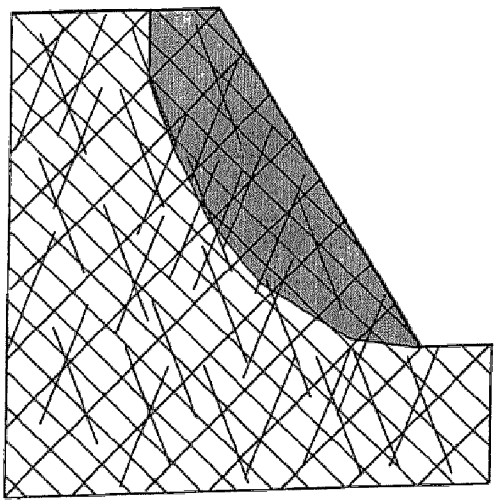

d - Sliding without any preferred direction

Figure 2.3 : *In situ rock conditions*

It should be finally emphasized, that the description of rock masses as well as the preliminary determination of kinematics of potential movements must precede any stability analysis. Heterogeneity and discontinuity of the rock mass in the construction scale should not be neglected, as these properties are intrinsic to the rock medium.

2.3. Active and passive anchors

A short reminder of the difference between active and passive anchors should be useful. These concepts seem to be not univocal, as some passive bolts (rebars) can also be preliminary tensioned. This problem was discussed by **Descoeudres (1985)**.

Pretensioned (i.e., active) rockbolts introduce into the rock mass some force of known intensity and orientation. As a consequence, shear strength is increased owing to normal stress augmentation across discontinuity planes. Exact information concerning orientation and extension of discontinuities, in which shear deformations can be expected, must be provided to fully utilize the anchoring action. The effectiveness of a bolting system depends on the conditions of the rock mass and on its characteristics. If the rock is not sufficiently competent and is susceptible to creep, some stress dissipation can be expected as well as a loss of tension in the anchor. If the rock mass is highly fractured and discontinuities are open, the action of the anchor cannot close the openings and consequently, shear strength cannot be satisfactorily mobilized. These considerations allow one to formulate, as a general conclusion, that the active anchors are not efficient in case of systematic reinforcement of the rock mass. Additionally, the cost of such an installation is unacceptable from the economic point of view. To the contrary, this kind of reinforcement could be used in stabilization of rock volumes with clear and well-identified discontinuities. Active rockbolts are frequently installed to stabilize retaining walls, foundations of columns or dams.

Reinforcement of rock masses by passive rockbolts is based on a different idea. As it was originally explained by **Londe & Bonazzi (1974)**, the idea consists of creating composed material, called "roche armée", with better mechanical characteristics. The forces are mobilized in bolts because of

displacements along the joints. Thus, there is the interdependence between these displacements and the forces mobilized in the bolts.

2.4. Mechanics of the rock mass reinforced by passive rockbolts

Stability analysis of rock mass requires preliminary determination of its probable failure. Reinforcement can be recognized as optimal when the specific resistance of the bolt is fully utilized. Thus, it is necessary, first of all, to find the proper dependence between the position of the bolt and the direction of potential displacements.

On the other hand, bolt's ability to accommodate deformations depends on the fracturation degree of the rock mass, as well as on the deformability of the rock matrix. If the rock mass is highly fractured, then the bolt can be easily adapted to the deformations; in such a case the mode of its functioning is similar to that exhibited by a bolt used in soil nailing. If rock mass fracturation is feeble, then the bolt acts rather as a support, transferring the forces from unstable to stable parts of the rock mass. Bolt deformations in this case are localized along the rock joint. Different tasks and effects of bolts in functions of rock mass structure were analyzed by **Piguet & Revalor (1988)**.

In most cases, deformations of rock mass essentially result from displacements along the discontinuities. Thus, the reinforcement effectiveness depends first, on the size and the arrangement of rock blocks, as well as on the structure of rock joints. **Panet (1986)** shows the very favorable dilatant behaviour of the rough joint.

The knowledge of physical laws, describing the relations between stress and displacement along the joint, is therefore of the greatest importance in the analysis of the behaviour of the jointed rock mass. As illustrated in Figure 2.4, the slide of the rock blocks along one set of discontinuities causes the opening of the second set. The action of the bolt crossing the first set is different in comparison to that which crosses the second set.

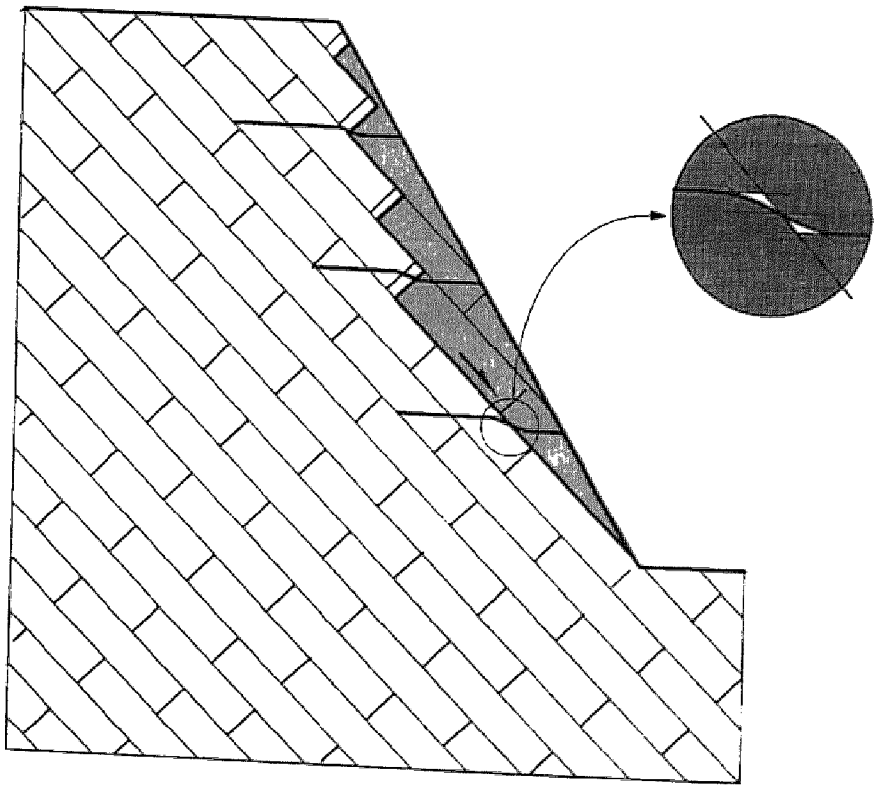

Figure 2.4 : *Mechanism of deformation of reinforced rock mass*

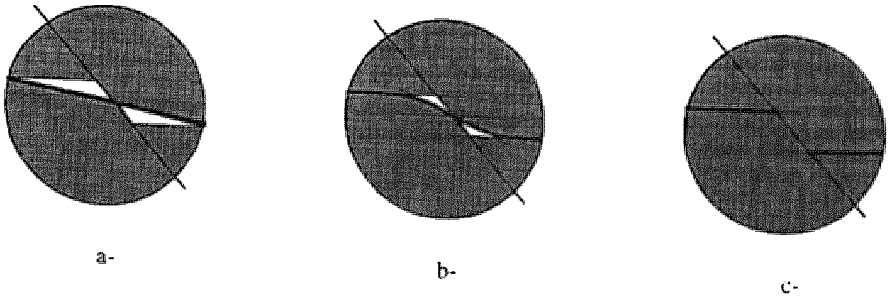

Figure 2.5 : *Failure modes of reinforced joint*

2.5. Mechanical behaviour of individual reinforced joints

Analysis of the behaviour of a single bolted joint must take into account multiple interaction phenomena between the bolt and the rock, followed by analysis of the mechanisms, which are responsible for the transfer of loading between the stable and unstable parts of the mass.

Strength and deformability of the rock matrix directly influence the failure mode of the reinforced joint. The forces associated with the displacement occurrence in the unstable parts of the mass are principally transmitted by anchored bolts into the stable parts of the rock matrix. Different kinds of ruptures are shown in Figure 2.5.

In the case of very weak and strongly deformable mediums, such as soil, the failure process can develop without any permanent deformation of the bolt (see Figure 2.5a). To the contrary, if the medium is very strong and exhibits small deformability, the failure can take place without any deformation of the rock (see Figure 2.5c). The intermediate situation is most frequently met in practice. Failure is accompanied by the appearance of plastic hinges, which are localized on both sides of the joint, at a distance dependent on the rock strength (see Figure 2.5b). The problems that need to be solved are determination of the direction and the intensity of the resultant force, R_o, mobilized in the bolt and the calculation of the associated displacement, U_j, along the joint.

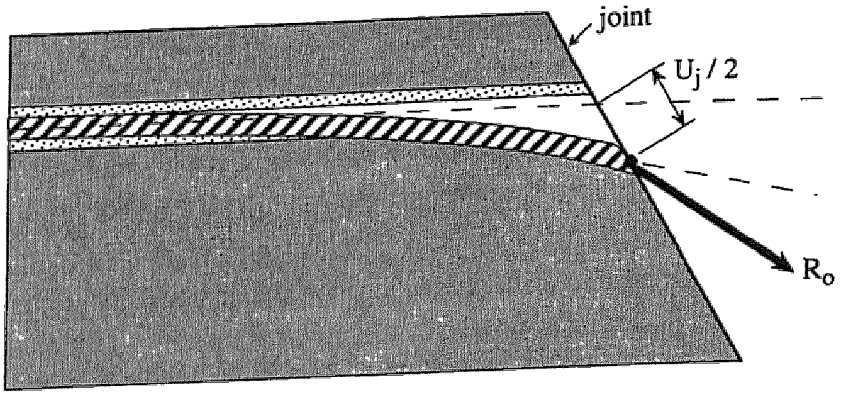

Figure 2.6 : *Deformation and loading conditions of a grouted bolt*

2.6. Analysis of mechanical behaviour of reinforced structures

The analysis can be performed with the help of different techniques, ranging from simple methods based on the limit equilibrium principle to more sophisticated methods, such as modern numerical methods. The possible approaches to the analysis of mechanical behaviour of reinforced structures were summarized in the paper of **Gerrard (1983)** and **Stille (1992)**.

Each analysis starts from the exact description of the geometry of the structure being studied. In the problem of slope stability, any symmetry cannot be taken into consideration. The boundary conditions of the problem are relatively known and assumption of the plane strain condition is taken into account. To the contrary, the geometry in three dimensions must be analyzed in case of underground excavations (such as tunnels); axial symmetry can be assumed in some situations. In this case the determination of the boundary conditions is generally more difficult.

In other words, establishment of an analytical solution for the stress-strain problem depends on the geometry of the structure and requires recognition of the boundary conditions. The problems of slopes are traditionally solved by the methods of failure calculation, whereas the stability of any section of tunnel can be studied by analytical solutions based on different hypotheses.

These two approaches, which are frequently presented as being in opposition, seem to be complementary. It is a fact that the methods of calculation which consider deformational processes are relatively well adapted to the situations where pre-failure processes are analyzed. They become ineffective after the development of failure surfaces where large plastic deformations occur. The methods of failure calculations do not provide any information concerning displacements, yet they allow one to obtain the value of loading, which can be sustained by the structure.

In the analysis of reinforced structures by the methods of failure calculation, equilibrium of potentially unstable volumes should be checked. The forces mobilized in the reinforcing bolts are introduced in the equilibrium equations. It can be said, based on actual state of knowledge that these methods are not satisfactory, as the intensity and direction of forces mobilized in the bolts are not a priori known. Thus, no calculation can be

performed before some simplifying hypotheses are assumed. These methods are applied only if the failure mechanism is identified. The schemes of different potential failure mechanisms above the tunnel roof are shown in Figure 2.7.

Conventional analytic solutions for calculations of underground works were developed for some initial stress conditions and for a continuous medium. Consequently, the above theories cannot be directly applied to the rock masses intersected by discontinuities. Many scientists have investigated more general models, based on the concept of homogenizing the rock material, allowing for application of the continuous medium theory.

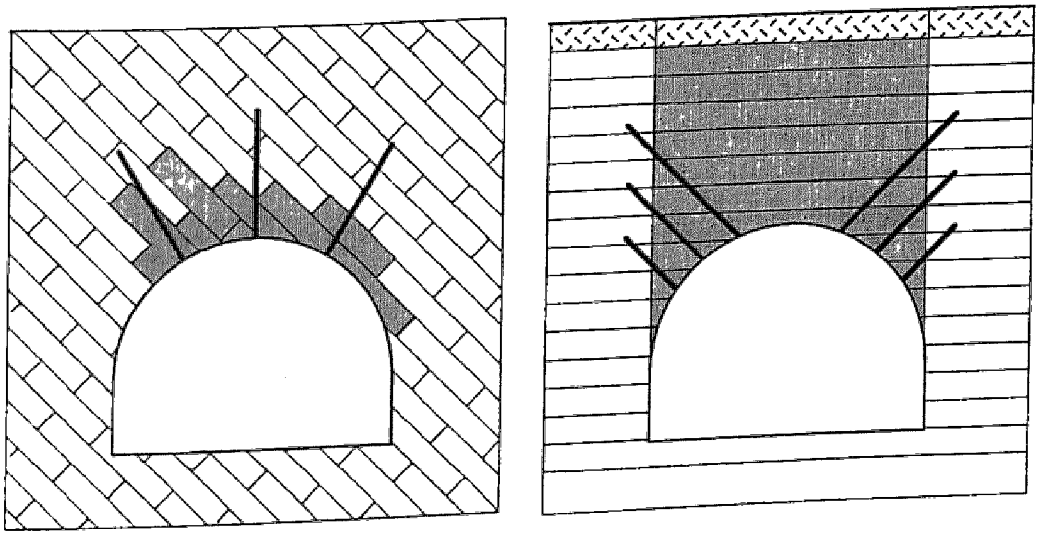

a- tunnel in fractured medium *b- shallow tunnel in stratified medium*

Figure 2.7 : *Different failure mechanisms for a tunnel cross-section*

Numerical methods can be divided into two categories. The first consists of a discrete approach, in which discontinuities are taken explicitly. The second is based on the global approach, in which the material such as "roche armée" is homogenized.

It should be emphasized, that in each of the considered approaches i.e., in analytical or numerical solutions (in discrete or global approach), the description of the behaviour of the discontinuities cannot be neglected. This

requires determination of the influence of the anchored bar on the strength and deformability of the reinforced joint.

2.7. Objectives and limitations of the study

The actual study is intended to improve the dimensioning methods of reinforced structures, such as excavated slopes and underground cavities. It makes possible the better comprehension of behaviour of the rock masses reinforced by passive rockbolts. The aim is to express in a quantitative way the influence of bolts on the strength and the deformability of rock joints.

The scope of the study is limited to the case of the rock mass having one discontinuity set of known orientation, in which shear displacements can develop. The analytic solution allowing the determination of the influence of the rockbolt is valid in the case of the rock mass intersected by smooth joints, reinforced by fully bonded steel bolts. However, it can also be adapted in any case of dilatant joints.

Chapter 3

State of the Art

Traditionally, geomechanical problems are simultaneously approached by experimental, analytical and numerical methods. It is also well known that each physical phenomenon reveals its own properties and it is thus, necessary to provide an appropriate combination of the methods of analysis. Numerous investigations have been carried out in past decades studying rock masses reinforced by passive rockbolts. One can distinguish many levels of study, corresponding to different degrees of material homogenization (Figure 3.1).

The first level of study considers the analysis of the working mode of axially and transversely loaded rockbolts. In this approach special attention is paid to accurate description of the behaviour of each element (i.e. bolt, rock, bonding mortar). It is also necessary to take into account the constitutive laws which govern the interface behaviour (i.e. bolt-mortar, mortar-rock). Pull-out tests and bending tests of fully grouted bolts were performed for the validation of different analytical formulations.

The second level consists of the description of the mechanical behaviour on the scale of the individual joints. The first degree of homogenization is involved here, where the average mechanical characteristics of the joint plane are considered. The problem was analyzed with the help of experimental studies, based essentially on the results of direct shear tests, realized on site or in the laboratory, on the specimens having the joint reinforced by steel bolts. A considerable number of such studies allowed the establishment of analytical formulae having more or less empirical natures. These formulae make possible the calculation of the contribution of the bolt to the total joint shear strength.

requires determination of the influence of the anchored bar on the strength and deformability of the reinforced joint.

2.7. Objectives and limitations of the study

The actual study is intended to improve the dimensioning methods of reinforced structures, such as excavated slopes and underground cavities. It makes possible the better comprehension of behaviour of the rock masses reinforced by passive rockbolts. The aim is to express in a quantitative way the influence of bolts on the strength and the deformability of rock joints.

The scope of the study is limited to the case of the rock mass having one discontinuity set of known orientation, in which shear displacements can develop. The analytic solution allowing the determination of the influence of the rockbolt is valid in the case of the rock mass intersected by smooth joints, reinforced by fully bonded steel bolts. However, it can also be adapted in any case of dilatant joints.

Chapter 3

State of the Art

Traditionally, geomechanical problems are simultaneously approached by experimental, analytical and numerical methods. It is also well known that each physical phenomenon reveals its own properties and it is thus, necessary to provide an appropriate combination of the methods of analysis. Numerous investigations have been carried out in past decades studying rock masses reinforced by passive rockbolts. One can distinguish many levels of study, corresponding to different degrees of material homogenization (Figure 3.1).

The first level of study considers the analysis of the working mode of axially and transversely loaded rockbolts. In this approach special attention is paid to accurate description of the behaviour of each element (i.e. bolt, rock, bonding mortar). It is also necessary to take into account the constitutive laws which govern the interface behaviour (i.e. bolt-mortar, mortar-rock). Pull-out tests and bending tests of fully grouted bolts were performed for the validation of different analytical formulations.

The second level consists of the description of the mechanical behaviour on the scale of the individual joints. The first degree of homogenization is involved here, where the average mechanical characteristics of the joint plane are considered. The problem was analyzed with the help of experimental studies, based essentially on the results of direct shear tests, realized on site or in the laboratory, on the specimens having the joint reinforced by steel bolts. A considerable number of such studies allowed the establishment of analytical formulae having more or less empirical natures. These formulae make possible the calculation of the contribution of the bolt to the total joint shear strength.

The objective of the third level is to describe the global mechanical behaviour of the rock mass. The mechanical characteristics of the material equivalent to the "roche armée", considered homogeneous and continuous, are defined here by the homogenization in the total volume scale. From the experimental point of view, this approach was the object of numerous tests carried out on reduced models.

The mechanical behaviour in each of the above levels can be determined by numerical methods. These can be divided into two categories, i.e., discrete and global. In the former, the elements and their interfaces are modeled separately, whereas in the latter the mechanical characteristics of homogenized material are taken.

After the behaviour of the model is established, it is possible to perform calculations for the structure. Its geometry imposes the utilization of one of the described approaches. Finally, the comparison of the results obtained in the analysis with those collected in measurements performed in the structure allows one to determine the rules of dimensioning. The experimental part of the presented study concerns the second and third level (see Figure 3.1), whilst the analytical considerations are situated within the first and second levels.

3.1. Working mode of fully bonded rockbolt

3.1.1. Axially loaded rockbolt

The case of fully bonded and axially loaded rockbolt occurs in particular situations, e.g. in the reinforcement of the roof of underground excavation. Analysis of this situation allows one to appreciate the bonding quality between the bolt and the surrounding rock mass and allows one to estimate the required length of bonding. **Littlejohn & Bruce (1975)** inspected different modes of the failure and they ascertained following types :

- failure of rock mass (Figure 3.2a),
- failure at interfaces bolt-grout or grout-rock (Figure 3.2.b),
- failure of bolt (Figure 3.2.c).

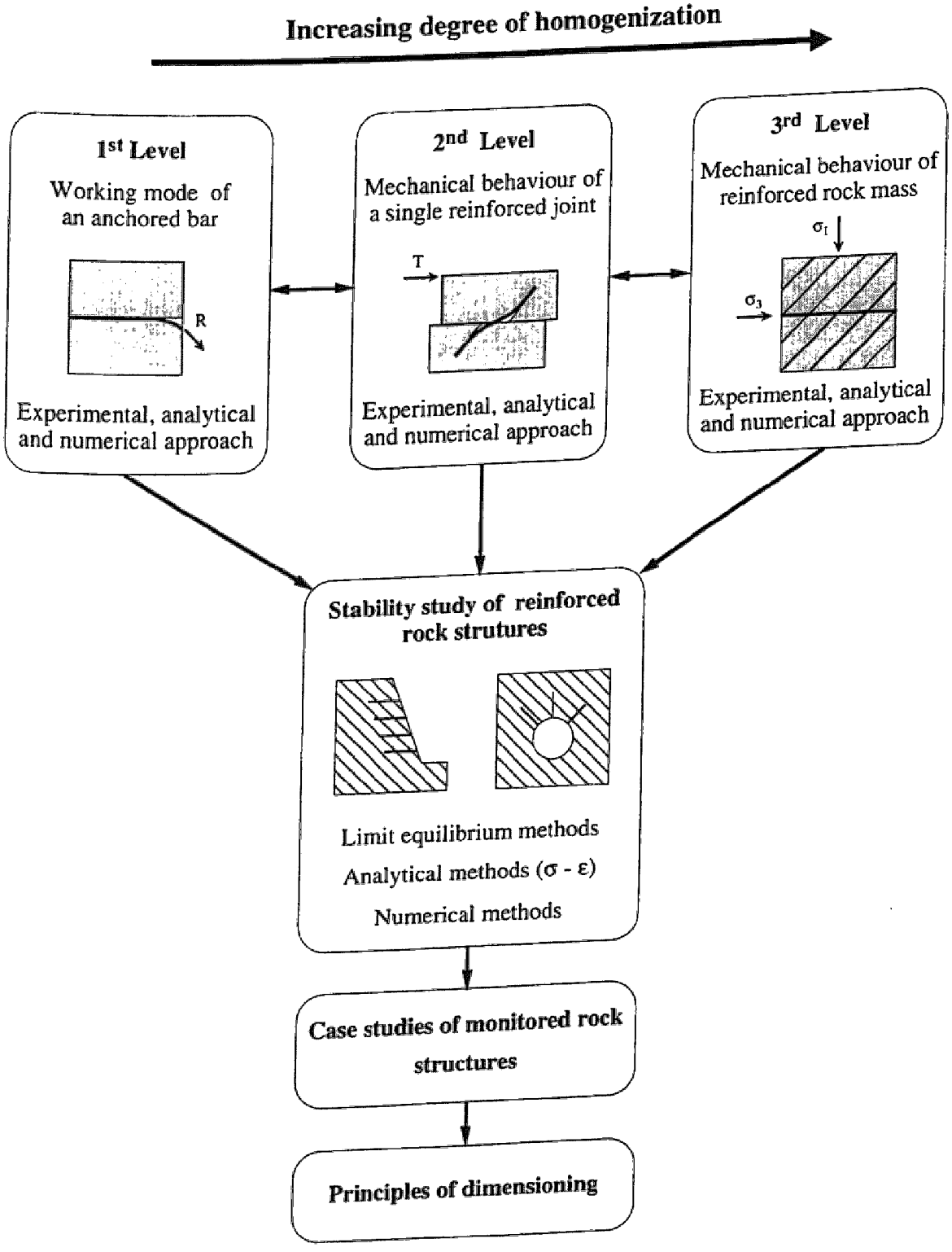

Figure 3.1 : *Interconnection scheme for different approaches in the studies of reinforced rock masses*

They recommended a semi-empirical formula for calculation of bolt capacity :

$$N_{ult} = 0.1\ \sigma_c\ \pi\ r_h\ L_g$$

where : N_{ult} : maximum normal force in bolt,
σ_c : uniaxial compressive strength of surrounding rock,
r_h : borehole radius,
L_g : bonded length of bolt.

Farmer (1975) studied the section of bolts bonded to the rock masses by resin (Figure 3.3). He found that failure occurred by breaking the bolt or the bolt-grout interface and he proposed the following expression to calculate shear stress distribution along the bolt-grout interface :

$$\tau_{(x)} = \frac{1}{2}\ a\ r_b\ \sigma_o\ e^{-ax}$$

where: r_b : radius of bolt,
σ_o : normal stress at bolt head.

He also found, that when the thickness of the grout annulus is small [$(r_h - r_b) < r_b$], the shear stresses have the same value in the bolt as well as at the interface. The constant "a" is expressed in this case as:

$$a = \sqrt{\frac{E_g}{E_b\ r_b\ (r_h - r_b)}}$$

If this thickness is larger, i.e., $(r_h - r_b) > r_b$, then :

$$a = \sqrt{\frac{E_g}{E_b\ r_b^2\ \ln (r_h / r_b)}}$$

where, E_b : elasticity modulus of bolt material,
E_g : elasticity modulus of grout.

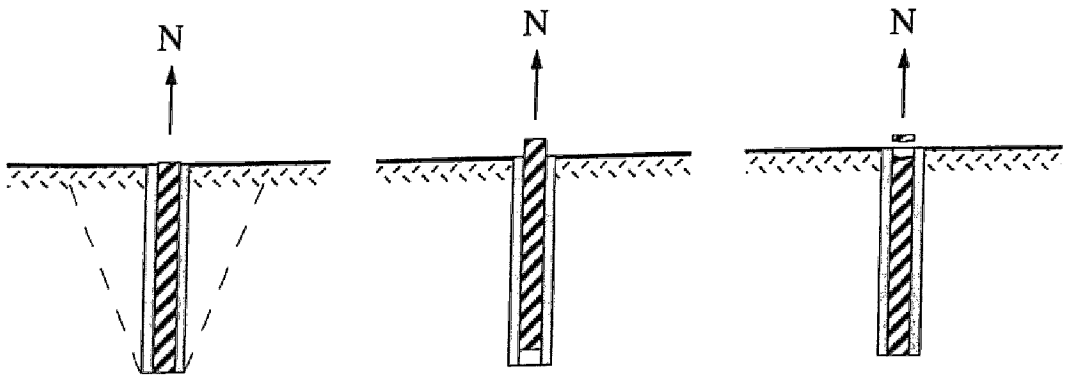

a- failure in rock *b- failure of the grout-bolt interface* *c- failure of the bolt*

Figure 3.2 : *Failure modes of an axially loaded bolt, after Littejohn & Bruce (1975)*

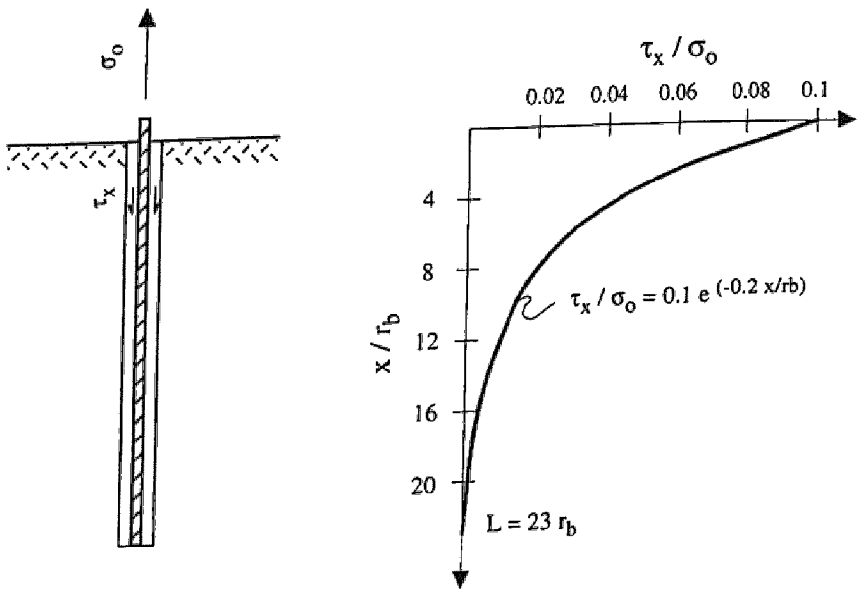

Figure 3.3 : *Distribution of shear stress along the bolt, after Farmer (1975)*

When the ratio of the grout to the bolt moduli is equal to 0.01 and the thickness of the grout is equal to $0.25r_b$, the distribution of shear stress along the bolt is expressed by :

$$\tau_{(x)} = 0.1\ \sigma_o\ e^{-(0.2\ x/r_b)}$$

Numerous authors have presented results of pull tests carried out on grouted bolts. **Pells (1974)** realized laboratory pull tests on bolts grouted by resin as well as by cement mortar. He found, that the length along which the bolt is loaded is relatively small.

Duhnam (1976) carried out pull-out tests on bolts instrumented by strain gauges. His results confirmed the previously dicussed Farmer's formula in the case of small loading. However, as the load increased, the contact between the bolt and the grout was lost and the shear stress dropped along an increasing length.

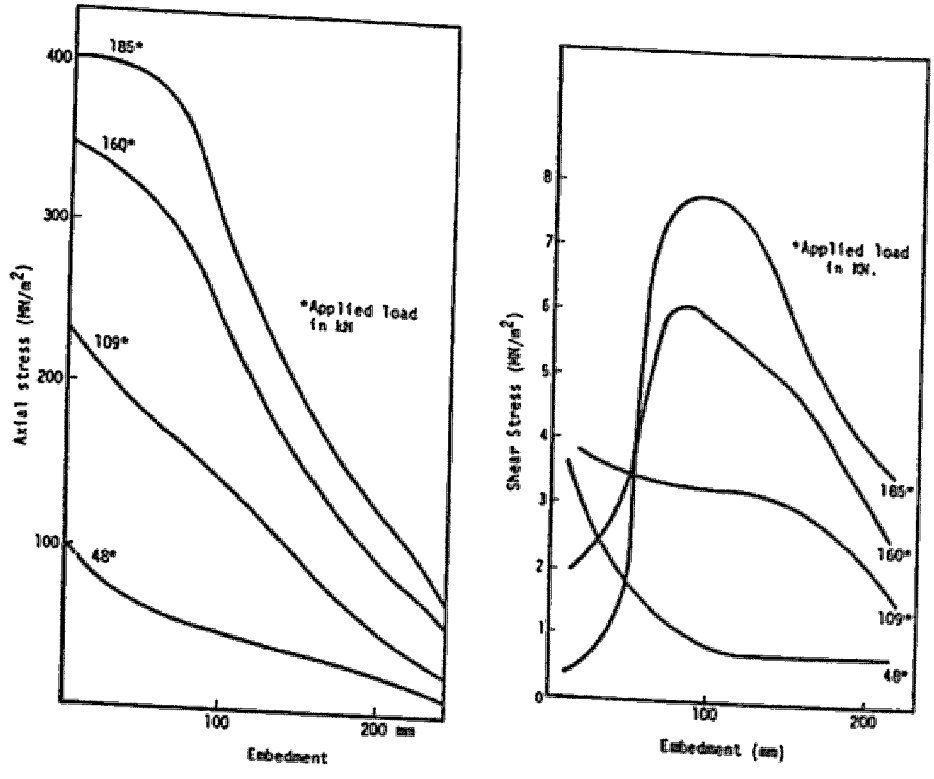

a- normal stress in the bolt *b- shear stress at the bolt/grout interface*

Figure 3.4 : *Results of instrumentation of the bolt with the diameter of 25mm , 300mm long, resin-grouted, after Duhnam (1976)*

Ballivy et al. (1986) noticed the influence of the quality of fixing grout. They recommended utilization of cement grout having low shrinkage, high compressive strength and dilatant behaviour.

3.1.2. Transversely loaded rockbolt

The case of the transversely loaded bolt was initially investigated by different scientists studying reinforced concrete (**Hofbeck et al. 1969, Dulascka 1972**). Their objective was the determination of the transversal force mobilized in the bolt after concrete cracking.

Di Prisco (1989) analyzed this phenomenon, realizing tests on steel bolts installed inside concrete blocks. The bolts were loaded transversely at one extremity. One series of inductive tranducers was installed in regular intervals along the bolt axis, allowing one to record its deformations as a function of loading. Figure 3.5 illustrates the scheme of the test and one example of the results. The curves represent the force versus displacement at the bolt head as well as its deformation in different stages of loading.

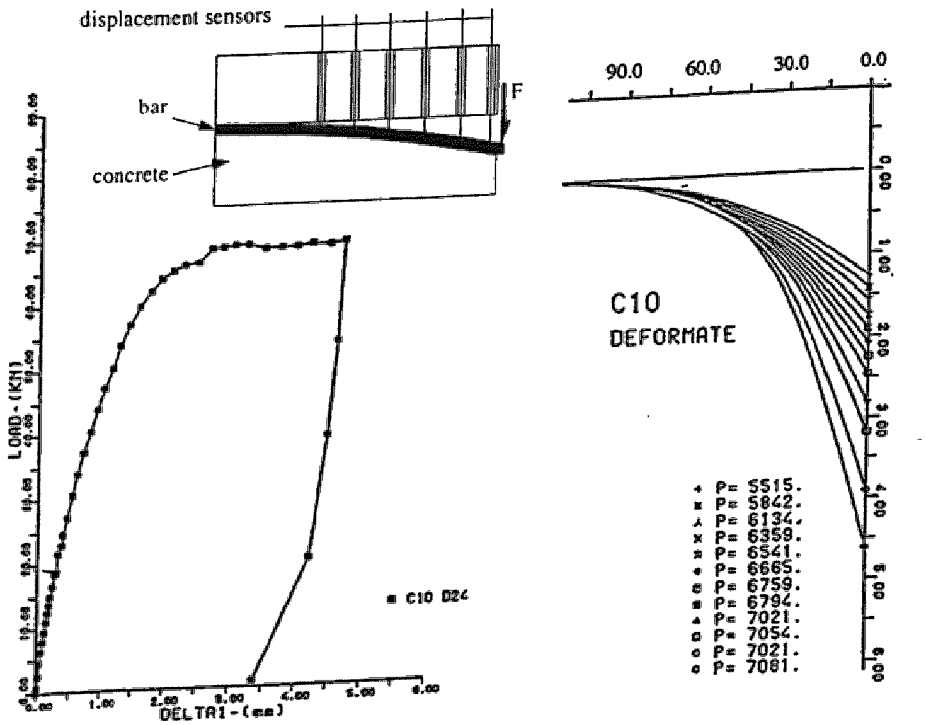

a- force versus head displacement b- deformation line of the bolt

Figure 3.5 : *Schematic principle and test results for the bolt of 24mm in diameter, after Di Prisco (1989)*

3.2. Mechanical behaviour of individual bolted rock joints

3.2.1. Model of behaviour

As the reinforced rock joint is subjected to shear, the displacement progressively increases, until the reinforcing bolt is broken. The bolt is axially loaded by a normal force, N, and transversely by a shear force, T. At the point of intersection between the joint and the bolt, the force resulting from N and T, R_o, can be decomposed into the force, R_n, acting perpendicularly to the joint plane and the force, R_t, which acts parallelly to this plane (Figure 3.6).

During this process, the length on which the pressure of the rock reaction is exerted increases continuously and thus, the bolt, which is initially in elastic state, eventually yields. In almost all practical cases, the bolt breaks after two plastic hinges appear at some distance from the joint.

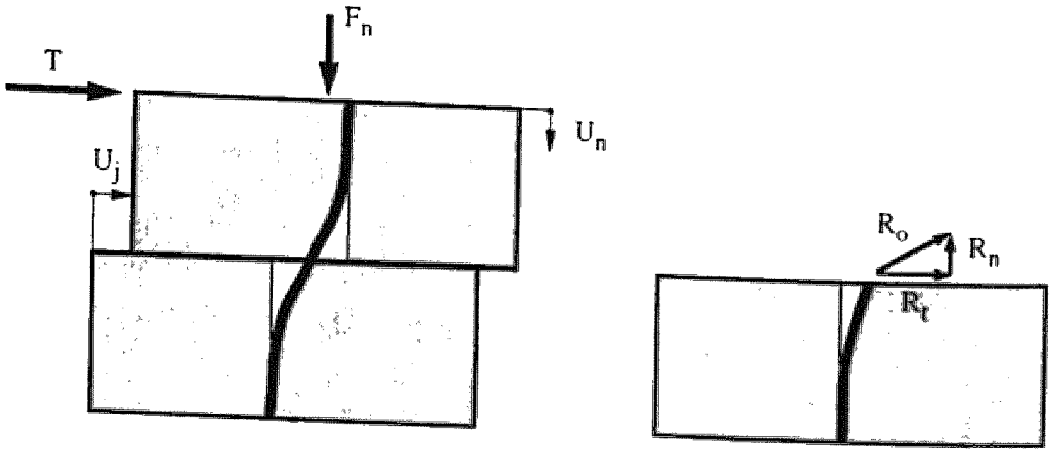

Figure 3.6 : *Forces developed in the bolt on the joint level during shear test*

Total shear force T is the sum of force T_j, mobilized in the joint without reinforcement and force T_b, which expresses contribution of the bolt :

$$T = T_j + T_b$$

Mechanical behaviour of the reinforced joint can be described with the help of the elasto-plastic model, after the stresses and mechanical characteristics of joint plane are homogenized :

$$\tau = \frac{T}{A_j} \qquad \text{and} \qquad \sigma_n = \frac{F_n}{A_j}$$

Where, τ : shear stress on joint plane,
σ_n : normal stress on joint plane,
A_j : surface area of joint.

Such as in the case of failure, total shear stress is the sum of the shear strength of the joint and the additional strength provided by the bolt, i.e. :

$$\tau = \tau_j + \Delta\tau_b$$

where, τ : total shear strength of reinforced joint,
τ_j : shear strength of unreinforced joint,
$\Delta\tau_b$: strength increment provided by bolt.

Based on the Mohr-Coulomb criterion the shear strength of the joint is described as :

$$\tau_j = c_j + \sigma_{no} \tan \phi_j$$

where, c_j : joint cohesion,
ϕ_j : angle of friction along joint,
σ_{no} : initial normal stress on joint plane.

The bolt contribution to the shear strength of the joint is taken into account by consideration of the cohesion augmentation due to the tangential component of the force mobilized in the bolt at failure, R_t, as well as the augmentation of normal stress on the joint plane due to the R_n component of the same force. The increase of strength caused by the bolt can be expressed as :

$$\Delta\tau_b = \Delta c_b + \Delta\sigma_{nb} \tan \phi_j$$

where Δc_b is the cohesion increment due to the tangential component of the force mobilized in the bolt and $\Delta\sigma_{nb}$ represents an increase of normal stress due to the normal component of force mobilized in the bolt. These two terms, known as the reinforcement cohesion and the effect of confinement are calculated by the following formulae :

$$\Delta c_b = \frac{R_t}{A_j}$$

$$\Delta\sigma_{nb} = \frac{R_n}{A_j}$$

where, A_j : surface area of joint,
R_n : component of force in bolt, normal to joint plane,
R_t : component of force in bolt, tangential to joint plane.

When the intrinsic strength of the joint and the additional strength provided by the bolt are added, the total strength of reinforced joint can be obtained from :

$$\tau = \left(c_j + \Delta c_b\right) + \left(\sigma_{no} + \Delta\sigma_{nb}\right) \tan \phi_j$$

The state of stresses at the point of failure for unreinforced and reinforced joints are represented in the Mohr diagram (Figure 3.7).

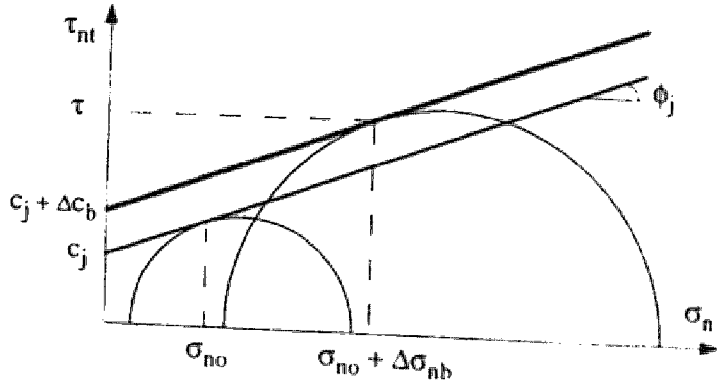

Figure 3.7 : *State of stresses at failure for unreinforced and reinforced joints*

For the rough joints, the behaviour is dilatant and failure occurs by sliding along the joint asperities or by shearing through them. **Patton (1966)** and later, **Heuze (1979)**, elaborated the relationships allowing one to define the transition between these two modes of failure. If the failure develops by sliding along asperities, the shear strength can be expressed by the following formula :

$$\tau_j = c_j + \sigma_n \tan(\phi_j + i)$$

where, i : angle of dilatation.

Supposing a linear behaviour of reinforced joints in elastic phase, the relations between applied stresses and resulting displacements can be formulated in matrix form as :

$$\begin{bmatrix} \sigma_n \\ \tau_{nt} \end{bmatrix} = \begin{bmatrix} k_n & k_{nt} \\ k_{tn} & k_t \end{bmatrix} \begin{bmatrix} u_n \\ u_t \end{bmatrix}$$

with :
$$\Delta\sigma_n = k_n\ u_n + k_{nt}\ u_t$$

$$\Delta\tau_{nt} = k_{tn}\ u_n + k_t\ u_t$$

where, k_n : normal stiffness of reinforced joint,
k_t : shear stiffness of reinforced joint,
k_{nt} : coupled stiffness or indirect normal of reinforced joint.

It should be noted, that in the general case, the terms k_n and k_t vary as a function of the applied stress level. If the asperities of the rough joint are symmetrical with respect to the average joint plane, the terms k_{nt} and k_{tn} are identical. In the opposite case, behaviour of the joint depends on the loading path. For unreinforced, smooth or non-dilatant joints, the terms situated out of the matrix diagonal, i.e., k_{nt} and k_{tn} are equal to zero. On the other hand, if the joint is reinforced, the normal stress increment due to the lengthening of the bolt is not associated with the normal displacement :

$$\Delta\sigma_{nb} = k_{nt}\ u_t \qquad \Delta\tau_{nt} = k_t\ u_t$$

3.2.2. Shear tests on joints reinforced by bolts

Many authors have conducted shear tests for determination of bolt contribution to the strength of the reinforced joint and for evaluation of the associated displacement.

Bjurstrom (1974) tested the influence of different factors affecting the shear strength of the reinforced rock joint. He carried out many direct shear tests, in laboratory and on site, on granite specimens reinforced by fully bonded steel bolts. He found that both the rock strength and the bolt orientation with respect to the joint influence the strength of the joint (Figure 3.8). He also observed that when the angle between the bolt and the joint is smaller than 35 degrees, the bolt failure occurs by tension. In the opposite case failure results from the combined action of tension and shear stresses. **Haas (1976, 1981)** compared the performance of bolts simply fixed at their ends with that of fully bonded bolts. The bolts were pretensioned in each of the cases. The tests were carried out on limestone specimens with an artificially cut joint. He stated that fully bonded bolts cause the diminution of displacements and provide a greater contribution to the joint shear strength than the bolts fixed only at their ends.

Azuar (1977) and later **Azuar et al. (1979)** conducted research on reinforced mediums, realizing direct shear tests on concrete specimens of large dimensions (60 x 40cm). Smooth or undulating joints were artificially created in the specimens. The steel bolts were either directly casted in concrete or grouted by polyester resin. The angles between the bolt and the joint were equal to 90, 60 and 30 degrees. He found the bolt contribution to the shear strength to be greater, and the displacements smaller, in the case of inclined bolts (Figure 3.9).

Hibino & Motojima (1981) realized direct shear tests, using specimens built of concrete reinforced either by fully bonded bolts or by pretensioned cables. The diameter of the borehole, the inclination of the bolt and the level of pretensioning were varied. He established, on one hand, that the greater the pretensioning of the bolt, the smaller the maximum displacement will be. On the other hand, he stated that the greater the angle between the bolt and the normal to the joint, the smaller the joint displacement will be (Figure 3.10).

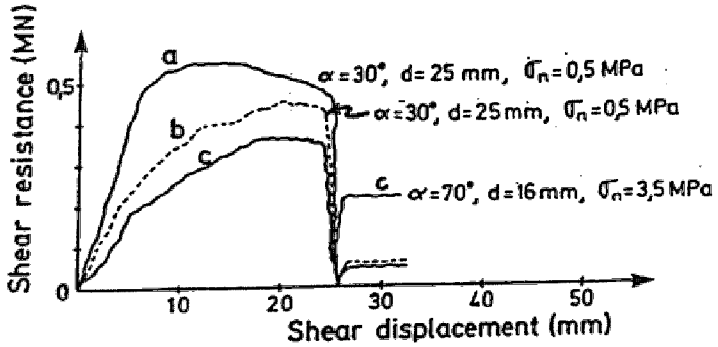

Figure 3.8 : *Shear force versus joint displacement , after Bjurstrom (1974)*

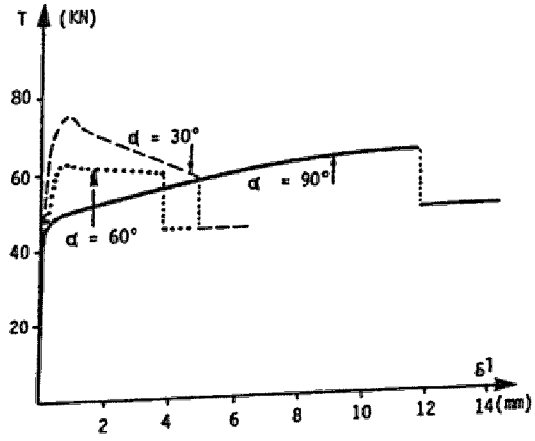

Figure 3.9 : *Shear force versus joint displacement for specimens reinforced by one bolt of 6mm in diameter, after Azuar (1977)*

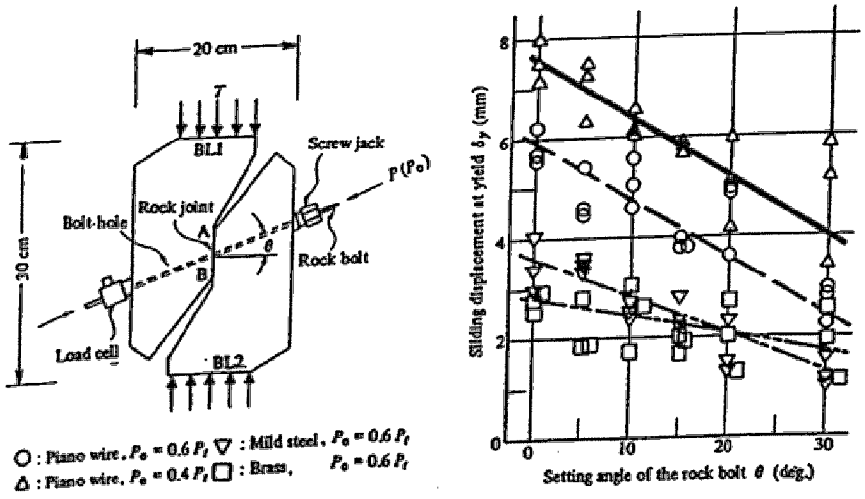

Figure 3.10 : *Influence of bolt orientation on joint displacement for reinforced specimens, after Hibino & Motojima (1981)*

Dight (1983a) carried out one series of tests with varying rock strength. He used a mixture of gypsum with sand and basalt. Steel bolts were fully bonded by epoxy resin. He also observed the dependence between the bolt inclination and the strength of the joint. **Ludvig (1983)** compared the efficiency of tubes and conventional bolts. He found that in the case of equal cross-sections, the efficiency of the tube is lower compared with that of bolt. The displacement necessary to mobilize the resistance of the element is clearly more important in the case of tubes. **Egger & Fernandes (1983)** realized the tests using concrete specimens, reinforced with steel bolts. The uniqueness of this study lay in the direction of loading which represents realistic loading paths (Figure 3.11). The authors observed that the optimum angle between the joint and the bolt is approximately equal to the joint friction angle. The tests also show that the angle between the bolt and the joint, at the point of failure, considerably decreases.

Yoshinaka et al. (1987) presented the results of a testing program and concluded, that the angle of bolt inclination directly influences the strength and deformablity of the reinforced joint (Figure 3.12).

Spang (1988) performed a series of direct shear tests using sandstone, concrete and granite specimens with uniaxial compressive strength changing from 10 to 105 MPa. The bolts were grouted by cement mortar in holes having a diameter two times greater than the bolt diameter. The inclination angle between the bolt and the joint varied from 45 to 90 degrees. The test results confirm the influence of the bolt inclination. **Egger & Zabuski (1991)** realized direct shear tests using concrete specimens with a single joint having regular asperities. The steel bolts with small diameters were placed perpendicularly to the joint plane. The results show that the joint dilatancy causes an increment of bolt contribution and reduces the displacement along the joint.

Ferrero (1993) carried out direct shear tests on specimens built of concrete or granite. The reinforcement was achieved by fully bonded bolts or tubes, which were placed perpendicularly to the joint and then pretensioned. The author concluded that the pretensioning effect causes a reduced displacement (Figure 3.13).

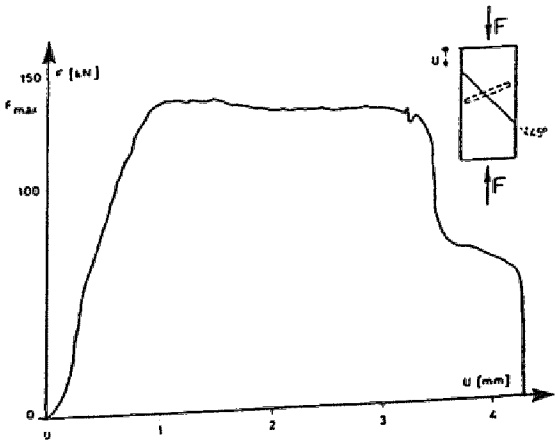

Figure 3.11 : *Vertical force versus vertical displacement for reinforced specimens, after Egger & Fernandes (1983)*

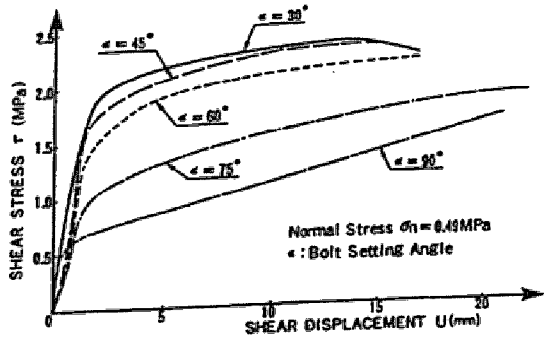

Figure 3.12 : *Shear stress versus joint displacement, after Yoshinaka (1987)*

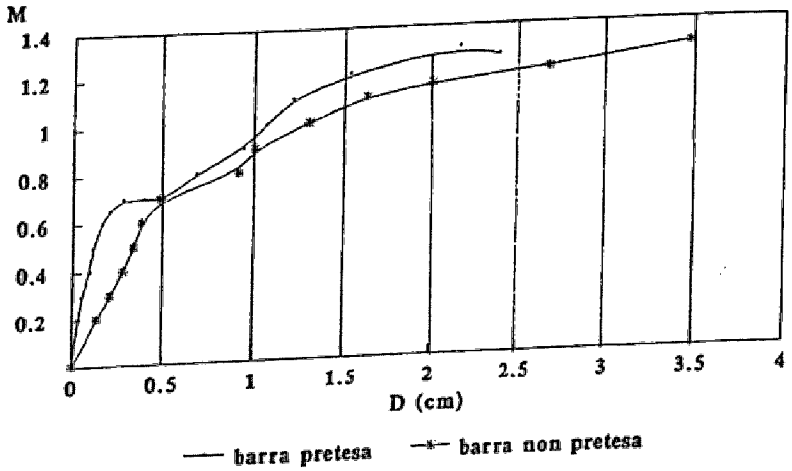

Figure 3.13 : *Normalized contribution of the bolt of 8mm in diameter as a function of joint displacement, after Ferrero (1983)*

3.2.3. Analytical formulation for calculation of bolt contribution

Based on experimental results, many authors attempted to describe the behaviour of reinforced joints for the determination of bolt contribution to the joint shear strength and for calculation of the joint displacement.

Dulascka (1972) established the following expression, based on idealized stress distribution at the bolt contact (Figure 3.14) :

$$T = 0.2\ D_b^2\ \sigma_y\ \sin\alpha \left[\sqrt{1 + \left(\frac{\sigma_c}{0.03\ \sigma_y\ \sin^2\alpha} \right)} - 1 \right]$$

where, T : shear force carried by bolt,
σ_c : uniaxial compressive strength of rock,
D_b : diameter of bolt,
σ_y : stress corresponding to yield limit of bolt,
α : angle between bolt and normal to joint.

Bjurström (1974) proposed calculation of the total contribution T_b of the bolt to the joint shear strength, by decomposing the force into a normal T_N and a shear T_Q component , also known as the "dowel action". Each of the terms is calculated using the following formula :

$$T_N = N_y \left(\cos\beta + \sin\beta\ \tan\phi_j \right)$$

$$T_Q = 0.67\ D_b^2\ \sqrt{\sigma_y\ \sigma_c}$$

where, N_y : normal force corresponding to yield limit of bolt,
β : angle between bolt and joint,
ϕ_j : angle of friction of joint.

Figure 3.15 (after **Bergman & Bjurström, 1983**), illustrates the variation of bolt contribution as a function of the bolt inclination for different diameters of the bolt.

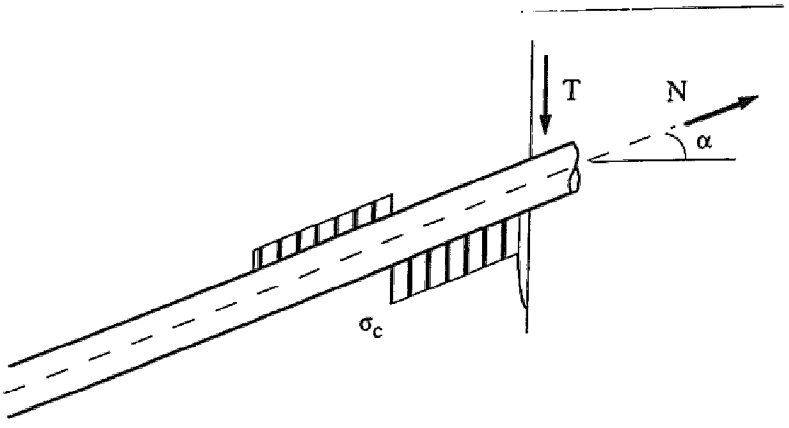

Figure 3.14 : *Scheme of transversely loaded bolt, after Dulascka (1972)*

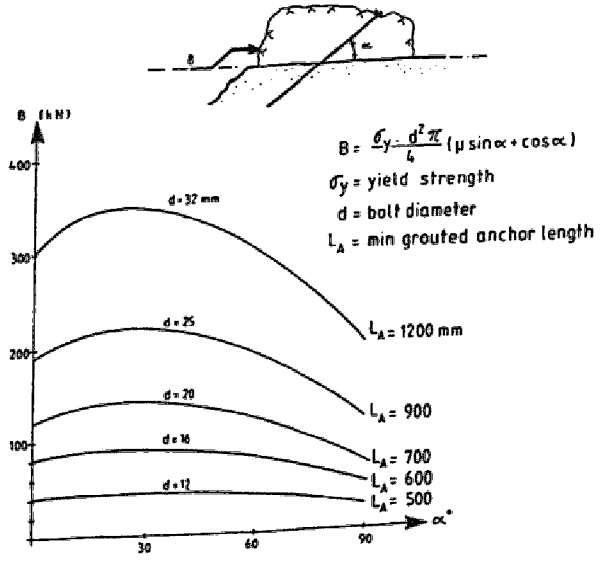

Figure 3.15 : *Variation of bolt contribution as a function of angle between the bolt and joint, for different diameters of the bolts, after Bergman & Bjurstrom (1983)*

It should be noted that the above formulae are simplified because rotation related to the deformation of the bolt is not taken into account. In addition, the effect of the shear force is independent of the orientation of the bolt.

Fuller & Cox (1978) developed an analytical expression allowing one to calculate the bolt contribution. It is based on the mechanism of deformation, which is presented in Figure 3.16. The segment of the bolt between the two plastic hinges has the form of a straight line. The angle between the initial and final positions of the bolt (i.e., rotation with respect to the joint) is taken into account and the shear strength increment caused by the bolt is calculated using the following formula :

$$\Delta\tau = \frac{N_y}{A_j} \left[\cos(\beta - \omega) + \sin(\beta - \omega) \tan\phi_j \right]$$

where, N_y : maximum normal force in bolt,
A_j : surface area influenced by bolt,
β : angle between bolt and joint,
ω : angle between initial and final position of bolt,
ϕ_j : angle of friction of joint.

with : $$\omega = \beta - \arctan\left(\frac{L_s + \delta_n}{(L_s / \tan\beta) + \delta_s} \right)$$

In this approach it is necessary to know a priori the position of the plastic hinges (L_s). The authors propose to determine this position by pull-out tests. Moreover, the calculation of displacement increments is required. The displacements components, parallel and perpendicularly to joint plane, are δ_s and δ_n, respectively.

Azuar & Panet (1980) proposed decomposition of the shear force into two components. One corresponds to the work necessary for bending the bolt, T_a^b, and the second corresponds to the work required for rock crushing, T_a^r, (Figure 3.17). The authors suggested calculating the joint displacements with the help of the first order theory, in the case of elastically supported beams. The disadvantage of this formulation is its limited validity. In fact, it can only be used for the elastic state of the bolt, and it represents a small part of the phenomenon, which is being observed.

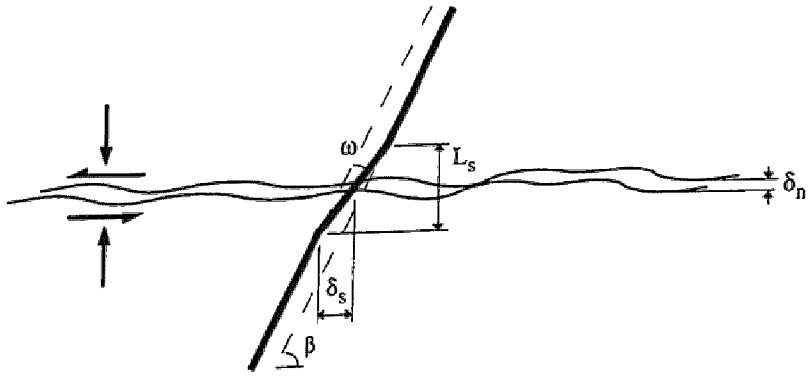

Figure 3.16 : *Mechanism of bolt deformation, after Fuller & Cox (1978)*

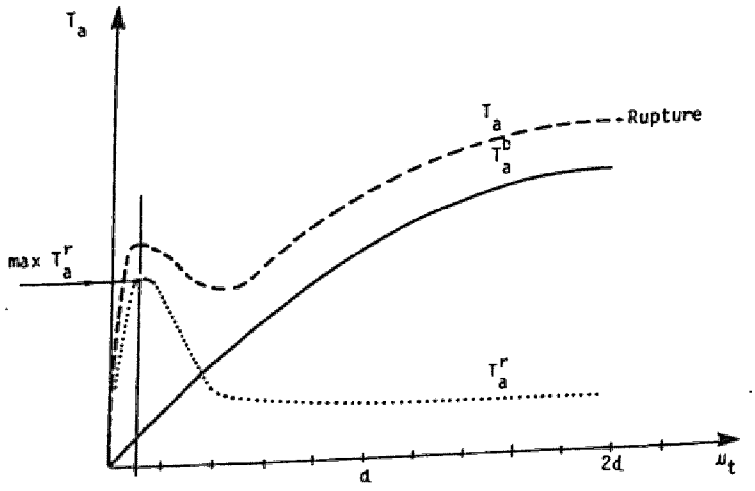

Figure 3.17 : *Decomposition of the steel bolt contribution as a function of tangential displacement, after Azuar & Panet (1980)*

Dight (1983a, 1985) proposed an analysis of bolt equilibrium, supposing the force distributions shown in figure 3.18. He elaborated the following formulae, taking into account the equation of moments and Tresca's criterion for steel failure :

$$T_Q = \frac{1}{\cos(\beta-\omega)} \frac{D_b^2}{4} \sqrt{1.7\ \pi\ p_u\ \sigma_y \left[1 - \left(\frac{N}{N_y}\right)^2\right]}$$

$$T_N = N_y \left[\sin(\beta-\omega) + \cos(\beta-\omega)\ \tan(\phi + i)\right]$$

where, p_u: maximum pressure exerted by rock or by grout,
i : angle of dilatation.

Maximum pressure p_u can be determined using the theory of the expansion of a cylindrical cavity in elasto-plastic medium, revealing brittle fracture. Dight established the relation between p_u and joint displacement U_j, for the calculation of the rotation angle (ω) corresponding to the displacement.

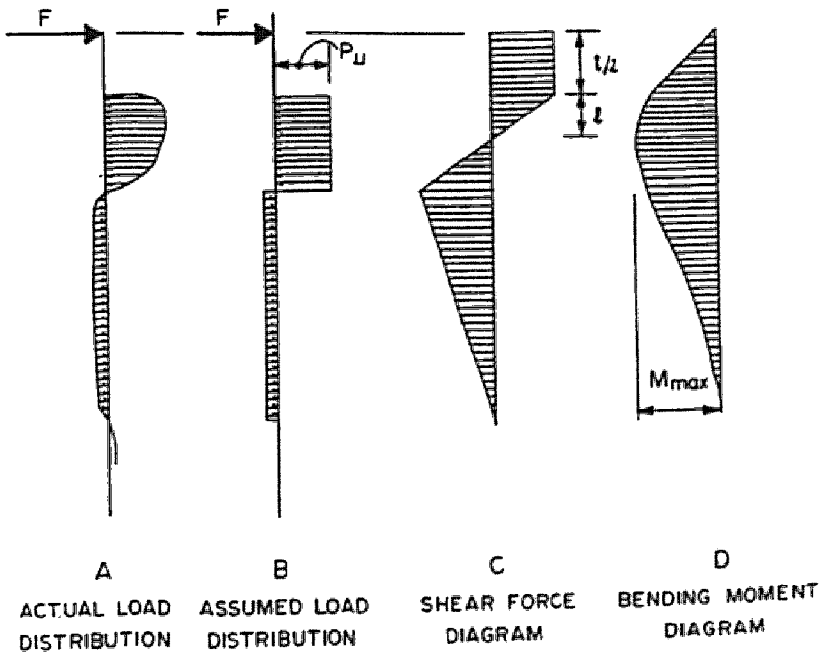

Figure 3.18 : *Reaction pressure and forces acting on the bolt, after Dight (1983)*

Egger & Fernandes (1983) suggested the simplified formula for the calculation of the bolt contribution :

$$F = N_y \frac{\cos\left(\beta - \phi_j\right)}{\cos\left(\theta' + \phi_j\right)}$$

where, N_y : normal force in bolt at yield limit of steel,
θ' : angle between joint and vertical direction,
β : angle between bolt and joint.

Figure 3.19 illustrates the example of the forces measured as a function of the orientation β of the bolts. It can be observed, that the angles measured at the bolt failure (empty squares) are generally lower than the initial angles (filled triangles).

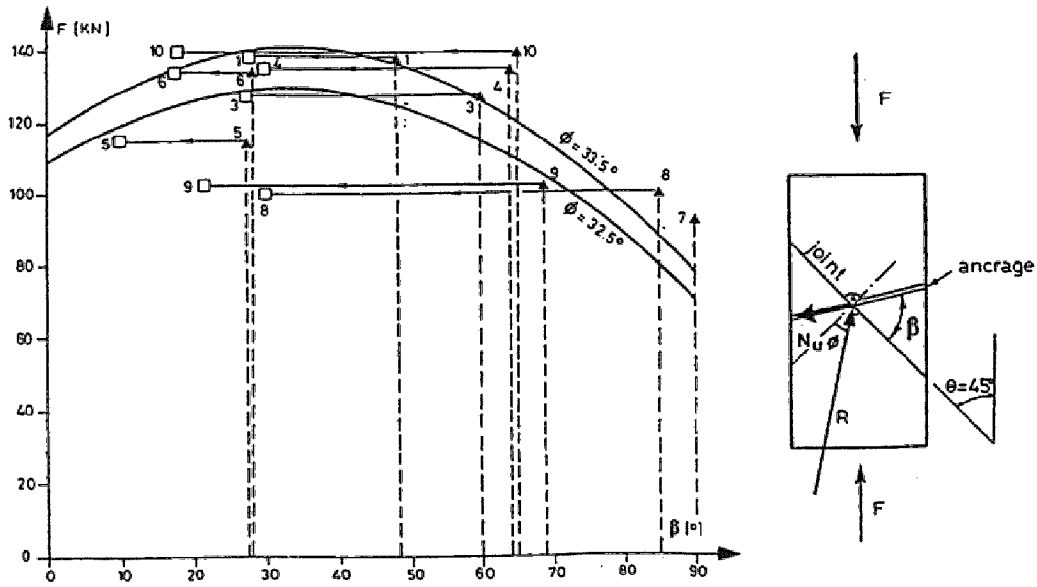

Figure 3.19 : *Variation of vertical forces as a function of the angle between the bolt and the joint, after Egger & Fernandes (1983)*

Gaziev & Lapin (1983) proposed calculating the increase of shear strength of the reinforced rock joint, by the following empirical formula :

$$\Delta\tau = m\ \sigma_b \left[\cos\beta + \sin\beta \tan\left(i_o \left(1 - \frac{\sigma_{no}}{\sigma_c}\right)^{10} + \phi_j\right)\right]$$

where, m : density of reinforcement (A_b/A_j),
σ_b : normal stress in bolt,
i_o : initial angle of dilatation.

They also determined the optimum angle between the bolt and the joint :

$$\beta_{opt} = i_o \left(1 - \frac{\sigma_{no}}{\sigma_c}\right)^{10} + \phi_j$$

Blondeau et al. (1984) developed a method for the case of soil nailing, based on the principle of maximum work. The force mobilized in the bolt at the failure is decomposed into normal the N_{oy} and the shear force Q_{oy} . As the steel obeys Tresca's criterion, possible combinations of forces in the N_o-Q_o plane are represented in the form of an ellipse. The couple of forces at failure is obtained when the normal to the displacement direction is tangential to the ellipse. Other criteria are also taken into account. Thus, the normal force is limited by the pull-out strength of the bolt while, the shear force is limited by soil strength.

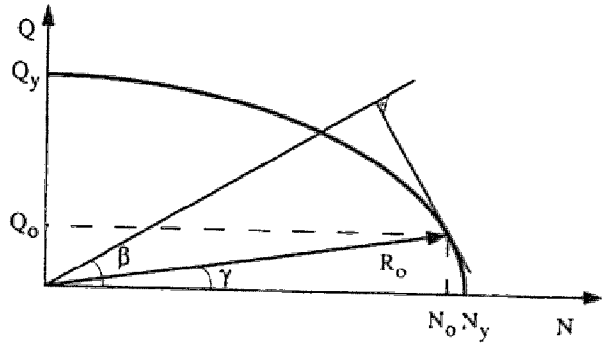

Figure 3.20 : *Principle of maximum work, after Blondeau et al.(1984)*

Schubert (1984) analyzed the behaviour of axially and transversely loaded bolts. He characterized the reaction of the surrounding rock by the so called penetration modulus, defined as the ratio of the force necessary to push in a steel ball of 20 mm in diameter to the depth of rock penetration. He used a numerical iterative procedure, in which the bolt was loaded step by step, until its failure occurred. The interaction between the bending moment and the normal force, as well as shear force, is taken into account in the failure criterion.

Stimpson (1987) established an expression for the determination of the stiffness of the reinforced joint. His approach, which is based on the theory

of beams, is only valid if the bolt is in the elastic range. **Rosengren et al. (1987)** proposed the simplified equation for calculation of fully bonded cables. The authors formulated the hypothesis that cables deform in the form of a circular arc.

Based on experimental results, **Spang (1988)** derived the empirical rules for calculation of the bolt contribution, T_b, as well as for the determination of the associated joint displacement, U_j :

$$T_b = N_y \left[1.55 + 0.011\ \sigma_c^{1.07}\ \sin^2(\alpha + i)\right]\ \sigma_c^{-0.14}\ (0.85 + 0.45\ \tan\phi)$$

$$U_j = D_b \left(15.2 - 55.2\ \sigma_c^{-0.14} + 56.2\ \sigma_c^{-0.28}\right) \left[\ 1 - \frac{\tan\alpha}{\cos\alpha^{0.5}} \left(\frac{70}{\sigma_c}\right)^{0.125}\right]$$

where, σ_c : uniaxial compressive strength of rock, in MPa,
α : angle between bolt and normal to joint,
N_y : normal force at the yield limit of bolt, in MPa,
D_b : diameter of bolt.

The above equations are valid for rocks with uniaxial compression strengths within the range of 10-70 MPa and for angles between the bolt and the joint within the range of 60-90 degrees.

Aydan (1989) elaborated the following formula, which describes the bolt contribution :

$$T_b = A_b\ \sigma_b \left(\ 1 + \frac{1}{2}\ \tan\phi_j\ \sin 2\theta\right)$$

where, A_b : cross-sectional area of bolt,
σ_b : stress in bolt in direction of shearing,
θ : angle between bolt and joint.

and : $$\sigma_b = \frac{\sigma_y}{\sqrt{3\ \cos^2\theta + \sin^2\theta}}$$

where σ_y : stress corresponding to yield limit of steel.

Figure 3.21 presents the variation of the bolt contribution as a function of the angle between the bolt and the joint. It should be mentioned that in the case of a bolt placed perpendicularly to the joint, the bolt contribution is independent of the joint friction angle. This does not agree with reality.

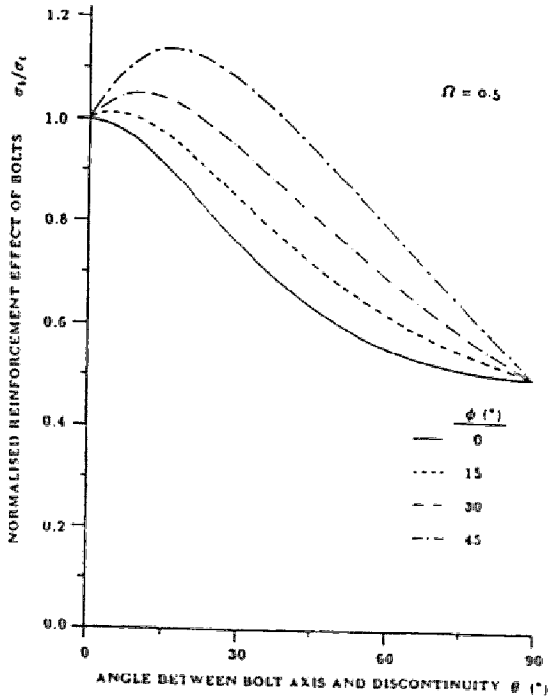

Figure 3.21 : *Bolt contribution versus angle between the bolt and joint for different values of friction angle, after Aydan (1989)*

Egger & Zabuski (1991) proposed the calculation of bolt contribution in the case of the dilatant joint, according to the following formula :

$$T_b = R_o \cos(\gamma + \omega) \tan(\phi_j + i) + R_o \sin(\gamma + \omega)$$

The force decomposition is shown in Figure 3.22. The angle γ and the resultant force R_o are determined, based on the principle of maximum work (**Blondeau et al. 1984**, see Figure 3.20). Accordance between theory and experimental results was observed.

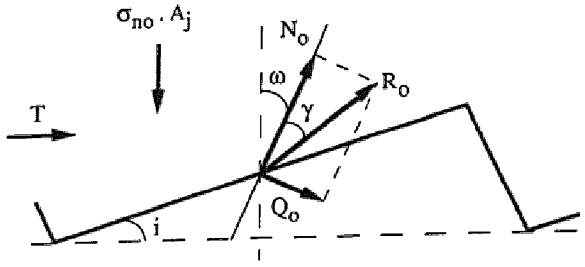

Figure 3.22 : *Loading in reinforced rough joint, after Egger & Zabuski (1991)*

Holmberg (1991) developed the analytic formulation allowing for calculation of bolt contribution :

$$T_b = T_s \left(\sin \beta - \cos \beta \tan \phi_j\right) + T_t \left(\cos \beta + \sin \beta \tan \phi_j\right)$$

where the parameters after transposition to our notation are as follows :

$T_t = N_o$: normal force in bolt at intersection with joint,
$T_s = Q_o$: shear force in bolt at intersection with joint,
$\beta = \beta_o - \omega$: angle between deformed bolt and joint.

The author distinguished three stages and finally the ultimate state; these are shown in figure 3.23:

- bolt and surrounding medium are in elastic state (Figure 3.23a),
- bolt is in elastic state and surrounding medium is yielded (Figure 3.23b),
- bolt and surrounding medium are yielded (Figure 3.23c).

In the first stage, behaviour in the axial direction is described based on **Farmer's** theory **(1975)**, whereas the lateral behaviour is described by the first order theory for elastically supported beams. No coupling between normal and shear force exists, thus the formulae are :

$$N_o = \pi E_b r_b^2 a u_t$$

$$Q_o = \frac{2\ E_b\ I}{l_o^3}\ u_s$$

where, a : integration constant defined by Farmer (see p.3.2.1),
l_o : length of transfer characterizing the stiffness of bolt-rock system, calculated as follows :

$$l_o = \sqrt[4]{\frac{E\ I}{k\ D_b}}$$

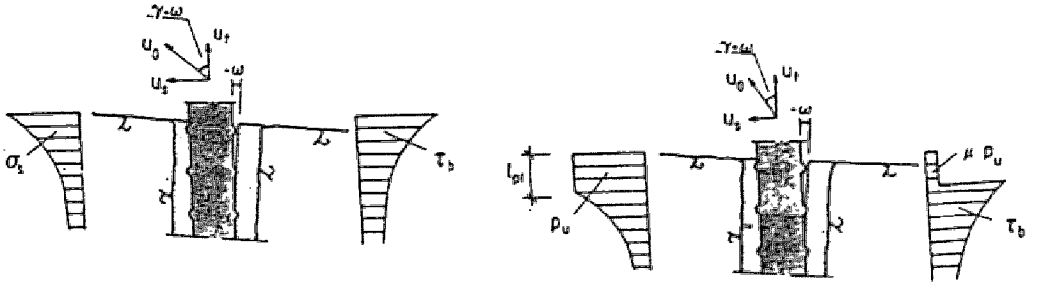

a- bolt and grout in elastic state

b- elastic bolt, yielded grout

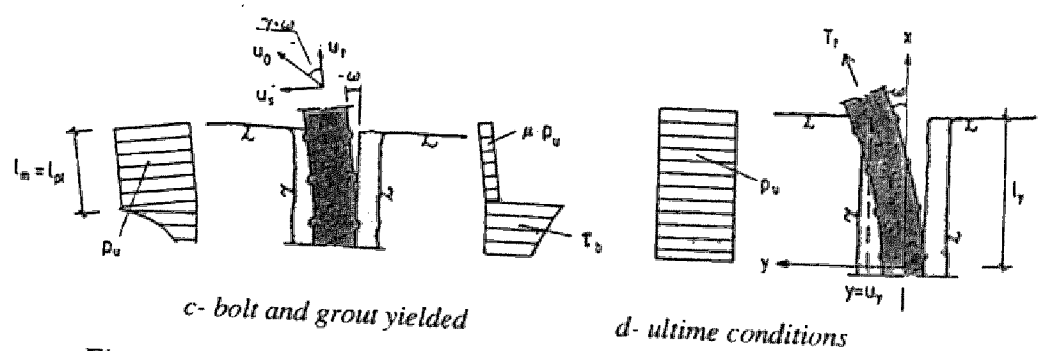

c- bolt and grout yielded

d- ultime conditions

Figure 3.23 : *Forces and displacements in bolt, after Holmberg (1991)*

The following equations are obtained for the second stage:

$$N_o = \mu\ p_u\ D_b\ l_{pl} + \pi\ E_b\ r_b^2\ a\ u_t$$

$$Q_o = \frac{\dfrac{p_u\ D_b\ l_{pl}}{2}\left(l_{pl} + 2l_o\right) + \dfrac{2\ p_u\ E_b\ I}{k_s\ l_o^2}}{\left(l_o + l_{pl}\right)}$$

where, μ : coefficient of friction at bolt-grout interface,
l_{pl} : plastic length of bolt.

It is supposed that in the third stage, the bolt behaves like a cable i.e., it does not sustain any shear force. Thus:

$$N_o = N_y \, e^{\left(\mu \, p_u \, D_b \, l_y \, / \, N_y\right)}$$

The above theory furnishes an appropriate estimate for the maximum bolt contribution, as well as for the joint displacement. It roughly follows the complete force-displacement curve in the case of a bolt placed perpendicularly to the joint.

The study performed by **Jewell & Pedley (1992)** concerning soil reinforcement should finally be mentioned. The authors proposed a simplified analysis, taking into account the bending stiffness of the bolt. The approach allowing one to calculate the bolt contribution in the case of soil is somewhat different, as the failure surface is not a priori determined and as the orientation angle of the bolt is unknown.

3.3. Mechanical behaviour of reinforced rock mass

As mentioned above, rock mass heterogeneity and discontinuity complicates the description of rock's mechanical behaviour in terms of deformability and shear strength. In the following section, homogenization of the mechanical characteristics is considered, i.e., the substitution of rock mass by equivalent material, macroscopically homogeneous and continuous, which exhibits the same mechanical characteristics as the original rock mass. The considered case deals with stratified rock mass with a single joint set of infinite extension, corresponding to a periodic structure.

3.3.1. Deformability of the equivalent reinforced rock material

The principle supposes a uniform distribution of the mechanical characteristics over the considered volume. It is also supposed that the spacing between the discontinuities should be regular and small enough, with respect to the critical dimension of the structure under study (e.g. slope height or diameter of tunnel). The concept of equivalent material is illustrated in figure 3.24.

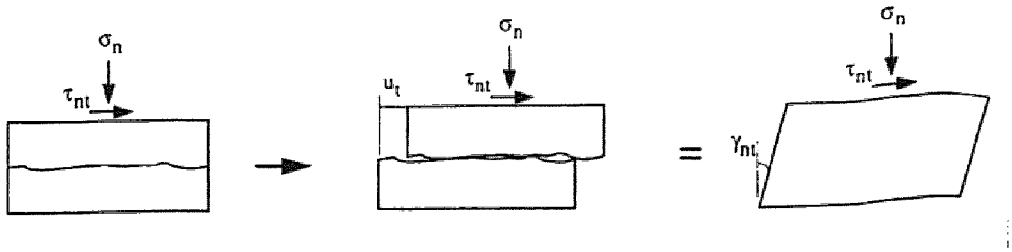

Figure 3.24 : *Concept of equivalent material*

The plane strain problem is studied for application of this principle. When the intact rock exhibits elastic linear and isotropic behaviour, the generalized Hooke's law can be applied :

$$\sigma_{ij} = D_{ijkl}\ \varepsilon_{ij}$$

where, σ_{ij} : tensor of stresses,
D_{ijkl} : matrix of elastic constants,
ε_{ij} : tensor of strains.

and, $\varepsilon_{ij} = C_{ijkl}\ \sigma_{ij}$

where C is the inverse matrix of **D**, known as the "compliance matrix". The above expression can be formulated in terms of Young's modulus E and Poisson's coefficient ν as below :

$$\begin{bmatrix} \varepsilon_n \\ \varepsilon_t \\ \gamma_{nt} \end{bmatrix} = \begin{bmatrix} 1/E & -\nu/E & 0 \\ -\nu/E & 1/E & 0 \\ 0 & 0 & 1/G \end{bmatrix} \begin{bmatrix} \sigma_n \\ \sigma_t \\ \tau_{nt} \end{bmatrix}$$

where G is the shear modulus calculated from the formula :

$$G = \frac{E}{2\,(1+\nu)}$$

Amadei & Goodman (1981) calculated the total deformation by adding the rock matrix deformation to the sum of the joint deformations :

$$\varepsilon^{rj} = \varepsilon^{r} + \sum_{1}^{n_j} \varepsilon^{j}$$

where, ε_{rj} : sum of strains of intact rock and joints,
ε_r : strain of intact rock,
ε_j : strain of joints,
n_j : number of joints in volume which is being studied.

Matrix C is thus expressed in following form :

$$\begin{bmatrix} \varepsilon_n \\ \varepsilon_t \\ \gamma_{nt} \end{bmatrix} = \begin{bmatrix} 1/E_n & -\nu/E_t & 0 \\ -\nu/E_t & 1/E_t & 0 \\ 0 & 0 & 1/G_{nt} \end{bmatrix} \begin{bmatrix} \sigma_n \\ \sigma_t \\ \tau_{nt} \end{bmatrix}$$

where:
$$\frac{1}{E_n} = \frac{1}{E} + \frac{1}{k_n\ s}$$

$$\frac{1}{G_{nt}} = \frac{1}{G} + \frac{1}{k_t\ s}$$

and, E : elasticity modulus of intact rock,
G : shear modulus of intact rock,
k_n : stiffness normal to joint plane,
k_s : tangential (shear) stiffness of joint,
s : spacing between joints,
E_n : elastic modulus of equivalent material normal to joint,
E_t : elastic modulus of equivalent material parallel to joint,
G_{nt} : shear modulus of equivalent material.

It should be noted that the behaviour of the equivalent material is anisotropic. A medium a having a single set of joints is axially orthotropic or transversely isotropic.

Gerrard (1982) extended this approach to the case of reinforced rock mass. He assumed the equivalence of rock mass and reinforcement strains :

$$\varepsilon^{b} = \varepsilon^{rj}$$

where, ε^{b} : strain of reinforcing bolt.

The total stress acting in the reinforced rock mass can be calculated by adding the stresses carried by the rock mass and by the reinforcement :

$$\sigma^{*} = \sigma^{rj} + \sum\sigma^{b}$$

where, σ^{*} : resultant stress in rock, bolt and joint system,
σ_{rj} : stress in rock-joint system,
σ_{b} : stress in reinforcement bolt.

Gerrard & Pande (1983-1985) presented the rheologic scheme for equivalent material in the simple case of uniaxial loading (Figure 3.25). In this particular case, each element (i.e., rock, bolt and joint) exhibits elasto-visco-plastic behaviour.

Larsson & Olofsson (1983,1985) proposed a similar approach, in which the elastic and the shear moduli of reinforced medium are calculated as follows :

$$E_{b}^{*} = \frac{2\ E_{b}\ \tau_{b}\ s}{r_{b}\ \sigma_{y}}$$

$$G_{b}^{*} = \frac{2\ \sqrt{3}\ G_{b}\ \sigma_{cg}\ s}{\pi\ r_{b}\ \sigma_{y}}$$

where σ_{cg} means uniaxial compressive strength of cement grout.

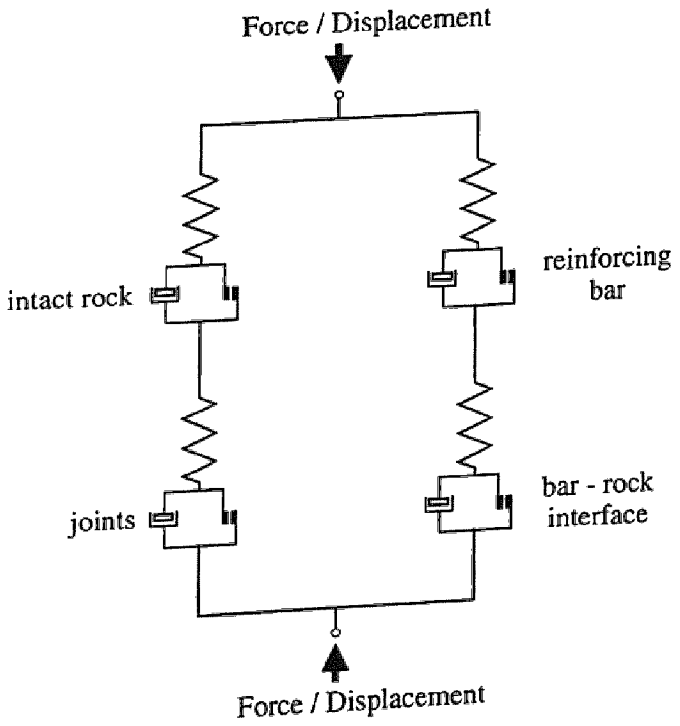

Figure 3.25 : *Rheological unit, after Gerrard et al . (1984)*

Chappell (1989) studied the behaviour of filled joints with non-zero thicknesses. He defined an upper and a lower limit of the elastic characteristics for the case of uniaxial loading.

The lower limit corresponds to the case of loading in the direction perpendicular to the joint (Figure 3.26a). Thus, the total deformation of equivalent material is the sum of the deformations of the joint and the intact rock. To the contrary, stresses are identical in each of the compounding elements. This model, which is called the "equilibrium model" can be illustrated as a series of springs.

$$\frac{1}{E_L} = \frac{V_{ni}}{E_i} + \frac{V_{nj}}{E_j}$$

$$\frac{1}{G_L} = \frac{V_{ni}}{G_i} + \frac{V_{nj}}{G_j}$$

where, E_L : lower limit of elasticity modulus,
G_L : lower limit of shear modulus,
E_i : elasticity modulus of intact rock,
G_i : shear modulus of intact rock,
E_j : elasticity modulus of filling material,
G_j : shear modulus of filling material,
V_{ni} : relative volume of intact rock,
V_{nj} : relative volume of joint.

The upper limit corresponds to the case in which loading is parallel to the joint (Figure 3.26b). The total stress in the equivalent material is the sum of the stresses in the joint and in the intact rock. Their deformations, however, are equal to one another. This model is called the "compatibility model" and can be illustrated as a set of parallel arranged springs.

$$E_u = V_{pi}\ E_i + V_{pj}\ E_j$$

$$G_u = V_{pi}\ G_i + V_{pj}\ G_j$$

where, E_u : upper limit of elasticity modulus,
G_u : upper limit of shear modulus,
V_{pi} : relative volume of intact rock,
V_{pj} : relative volume of joint.

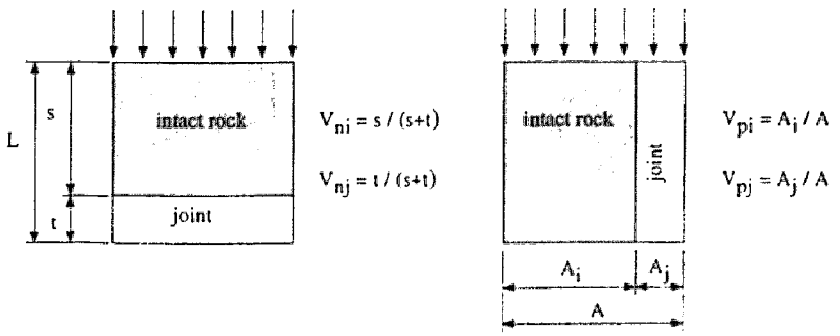

Figure 3.26 : *Definition of relative volumes, after Chappell (1989)*

If loading is arbitrarily oriented with respect to the joint direction, the value of the elastic modulus lies between the two limits and can be calculated by the following formula :

$$\frac{1}{E_y} = \frac{\cos^4\theta}{E_L} + \frac{\sin^4\theta}{E_u} + \cos^2\theta\,\sin^2\theta\left[\left(\frac{1}{G_L} + \frac{1}{G_u}\right) - \left(\frac{\nu_{12}}{E_u} + \frac{\nu_{21}}{E_L}\right)\right]$$

where, E_y : modulus of elasticity in considered direction,
θ : angle of joint orientation,
ν : Poisson's coefficient in considered direction.

In the case of reinforced material, these moduli are calculated taking into account a volumetric proportion of reinforcing bolts. Figure 3.27 presents an example of the variation of E_y modulus as a function of the joint's inclination. Reinforced and unreinforced cases are shown. It can be noted, that the reinforcement considerably reduces the deformability anisotropy of the equivalent model.

3.3.2. Strength of the equivalent reinforced rock material

In the case of stratified rock mass, Coulomb-Mohr's equation of failure for intact rock can be written as follows :

$$\sigma_1 = 2\,c_r\,\mathrm{tg}\left(\frac{\pi}{4} + \frac{\phi_r}{2}\right) + \sigma_3\left[1 + 2\,\mathrm{tg}\phi_r\,\mathrm{tg}\left(\frac{\pi}{4} + \frac{\phi_r}{2}\right)\right]$$

where: σ_1 , σ_3 : major and minor principal stress, respectively,
ϕ_r : friction angle of rock,
c_r : rock cohesion.

Failure along joint can be described by :

$$\sigma_1 = \left[c_j\left(1 + \mathrm{tg}^2\theta\right) + \sigma_3\,\mathrm{tg}\theta\left(1 + \mathrm{tg}\phi_j\,\mathrm{tg}\theta\right)\right]\frac{1}{\mathrm{tg}\theta - \mathrm{tg}\phi_j}$$

where, θ : angle of joint inclination to σ_1 plane,
ϕ_j : friction angle along joint,
c_j : joint cohesion.

Figure 3.28 presents the variation of strength as a function of joint orientation. It should be noticed that for some specific cases of stresses and mechanical characteristics, the strength decreases with increasing joint inclination angle. On the other hand, when the confining component of stress (i.e., σ_3) is higher, the development of the failure mechanism in intact material is more intensive.

Based on the above principles, **Wullschlager & Natau (1983)** defined shear strength, using the Mohr-Coulomb criterion. They proved that the installation of anchored bolts produces reduction of cohesion anisotropy, whereas the joint friction angle remains constant.

3.3.3. Experimental models

Experimental verification is most frequently performed using reduced models, as the testing of large volumes of rock is rather difficult.

Einstein & Hirschfeld (1973) carried out tests on specimens built up from plaster. They proved the influence of joint orientation on the strength and the deformability of the medium. **Reik & Zacas (1978)** realized the tests in truly triaxial conditions, using unreinforced models. They demonstrated that the strength and the deformability of rock mass depends on the level of the applied confining stress.

Indraratna (1990) and **Yamachi et al. (1989)** realized simple compression tests on models built up from plaster and reinforced by steel bolts. They showed, qualitatively, that the greater the density of reinforcement, the higher the strength of the model will be (Figure 3.29). **Egger & Pellet (1990, 1991)** extended this conclusion. They performed triaxial tests and found that depending on the confining stress level, failure develops either along joints or in intact rock. Thus, realizing the tests with different confining stresses, one can determine the increase of both normal stress and cohesion provided by the bolts.

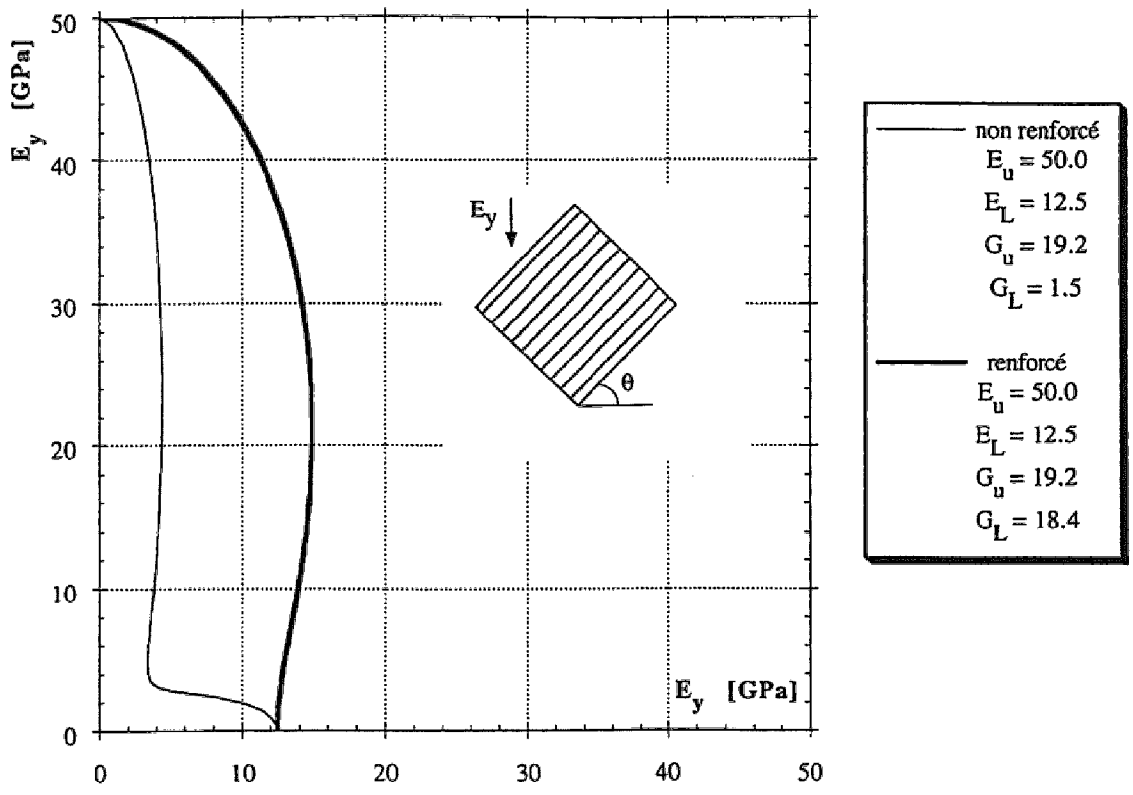

Figure 3.27 : *Variation of E_y modulus versus angle θ, after Chappell (1989)*

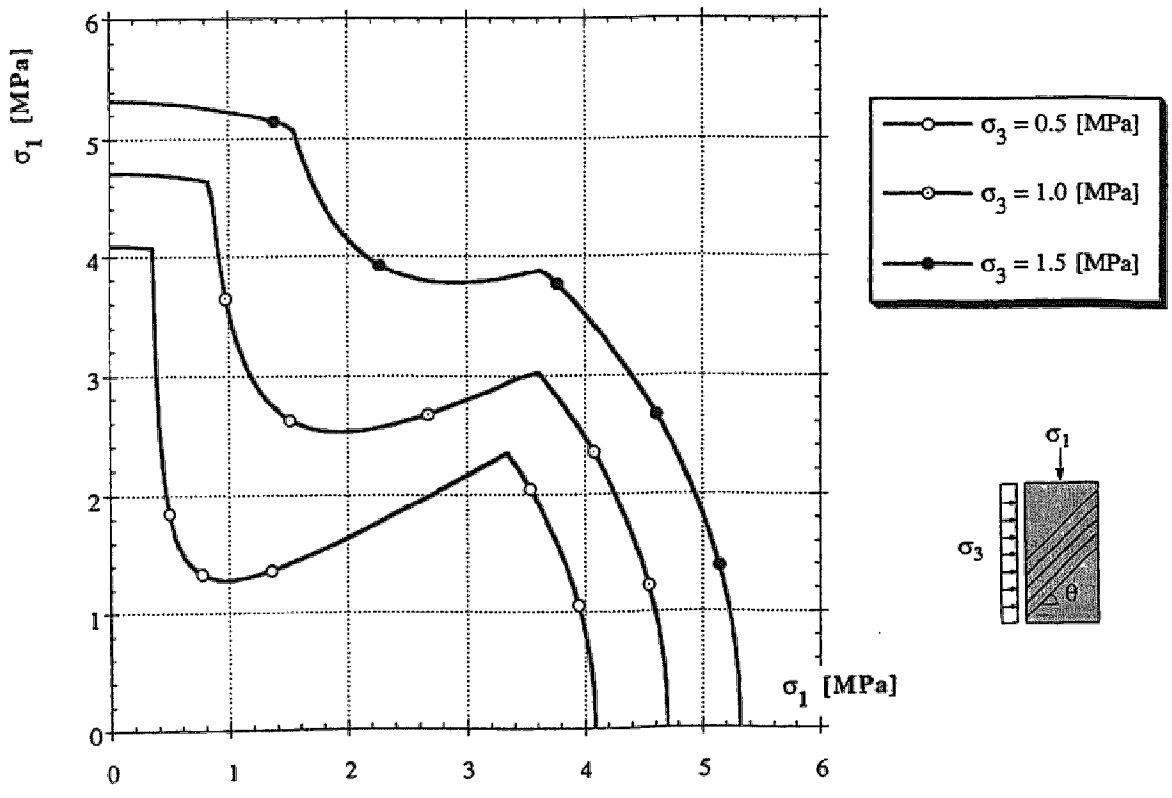

Figure 3.28 : *Strength variation versus angle θ*

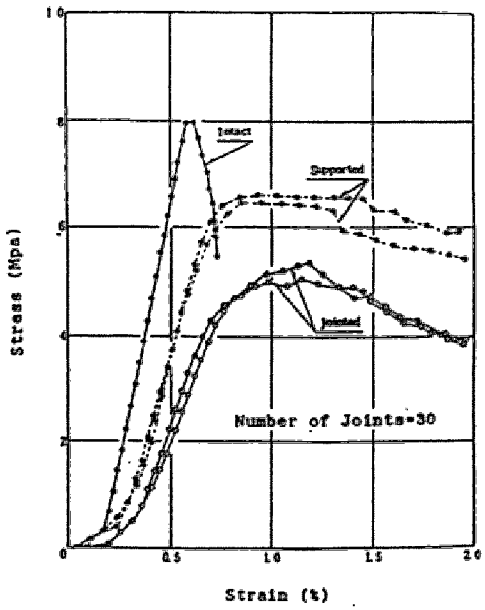

Figure 3.29 : *Stress-strain relationship for the reinforced models, after Yamachi et al. (1989)*

3.4. Numerical modeling of reinforced rock masses

As was mentioned in the introductory section, numerical modeling can be used to describe mechanical behaviour of reinforced rock mass at every level.

Different approaches can be distinguished, depending on their degree of discretization. In any discrete approach, each of the constitutive elements is taken separately. The reason for this attempt is the necessity for the most accurate description of the bolt behaviour, filling grout and surrounding rock. It is necessary to take into account not only the constitutive equations for each element but also the behaviour of the different interfaces. In some global approaches, mechanical characteristics of equivalent homogeneous materials are introduced and discontinuities are ignored, as their treatment frequently causes numerical problems.

The discrete approach is handled by the Distinct Element Method (DEM) or by the Finite Element Method (FEM), with the help of some special elements. The global approach is treated by the Finite Element Method, as well as by the Boundary Element Method (BEM). In fact, there is no purely discrete or completely global approach. In most cases, intermediate

situations are encountered, differing from each other by different homogenization degrees.

3.4.1. Modeling of axially and transversally loaded bolt

First attempts at numerical modeling concerned the simulation of pull-out tests of anchored bolts. **Coates & Yu (1970)** conducted analyses by the Finite Element approach, assuming elastic behaviour of the elements (i.e., rock, grout, bolt). Next, **Ballivy et al. (1987)** performed numerical tests, taking into account a failure criterion for the grout material.

Concerning the behaviour of a transversely loaded bolt, **Yoshinaka et al. (1986)** simulated the bolt element as an elastically supported beam (Figure 3.30). **Spang & Egger (1990)** modeled a shear test of the reinforced rock joint, adopting the mesh presented in Figure 3.31. **Keddi (1992)** proceeded with systematic numerical studies, applying the FE method, which took into account large displacements exhibited by the bolt during the loading process.

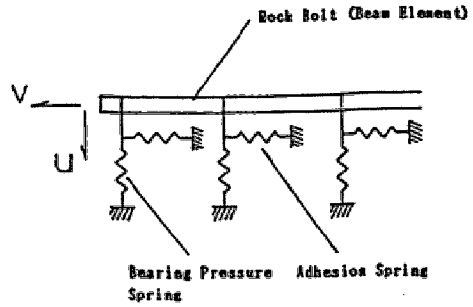

Figure 3.30 : *Representation of bolt, after Yoshinaka (1986)*

3.4.2. Modeling of a reinforced joint

In the study of the behaviour of any construction, it is necessary to assume certain simplifications for representation of bolt elements and their interfaces.

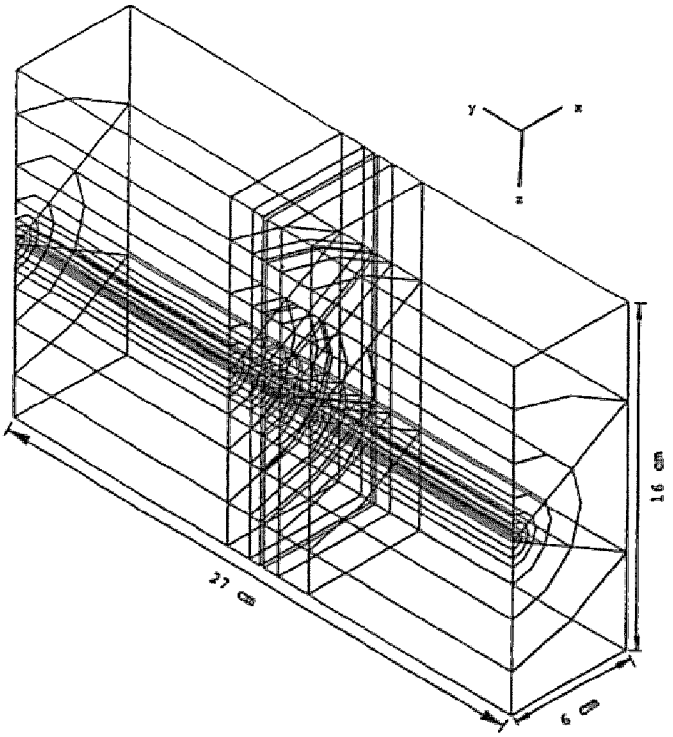

Figure 3.31 : *Three-dimensional mesh of bolt, after Spang & Egger (1990)*

In the first attempts of FE modeling of reinforced structures, the bolts were represented by a one-dimensional element with axial stiffness (**Heuze & Goodman, 1973**). This approach can be accepted in the case of punctually fixed or pretensioned anchors, when the displacements are parallel to the bolt axis. Such an approach is not acceptable in the case of fully bonded bolt, which intersects a rock joint. As proved above, the axial and the shear force mobilized in the bolt increase the strength and the deformation capability of the joint.

St John & van Dillen (1983) elaborated a three-dimensional element (Figure 3.32), also taking into account the tangential stiffness of the bolt and the grout. The elementary matrix **[D]** of the elastic constants in the local coordinate system is expressed in the following form :

$$[D] = \begin{bmatrix} E_b\ A_b & 0 & 0 & 0 \\ 0 & G_b 2\pi r & 0 & 0 \\ 0 & 0 & G_b A_b & 0 \\ 0 & 0 & 0 & G_b A_b \end{bmatrix}$$

where, E_b : elasticity modulus of bolt,
G_b : shear modulus of bolt,
A_b : cross-sectional area of bolt,
r : radius of bolt.

Aydan (1989) developed a three-dimensional element with 8 nodal points. Two of these are connected to the bolt, whereas the six others are jointed to the rock mass (Figure 3.33). Interpolation functions are linear. The number of nodes in the two-dimensional case is reduced to six. This element is associated with an interface element, representing the rock joint, which was developed by **Ghaboussi et al.(1973)**.

Both the axial and transversal behaviour of the element, representing the bolt and the grout are taken into the analysis. The local elementary stiffness matrix in cylindrical coordinates can be expressed as follows :

$$\mathbf{K}^{e}_{b,ga} = \begin{bmatrix} [K]_b & \\ & [K]_{ga} \end{bmatrix}$$

where $[K]_b$ represents the bolt contribution and has the form :

$$\mathbf{K}_b = \begin{bmatrix} K^r_b & 0 & -K^r_b & 0 \\ 0 & K^z_b & 0 & -K^z_b \\ -K^r_b & 0 & K^r_b & 0 \\ 0 & -K^z_b & 0 & K^z_b \end{bmatrix}$$

with $K^z_b = \dfrac{E_b\ A_b}{L}$ term of axial stiffness

$K^r_b = \dfrac{G_b\ A_b}{L}$ term of radial or transversal stiffness

where, L : length of element.

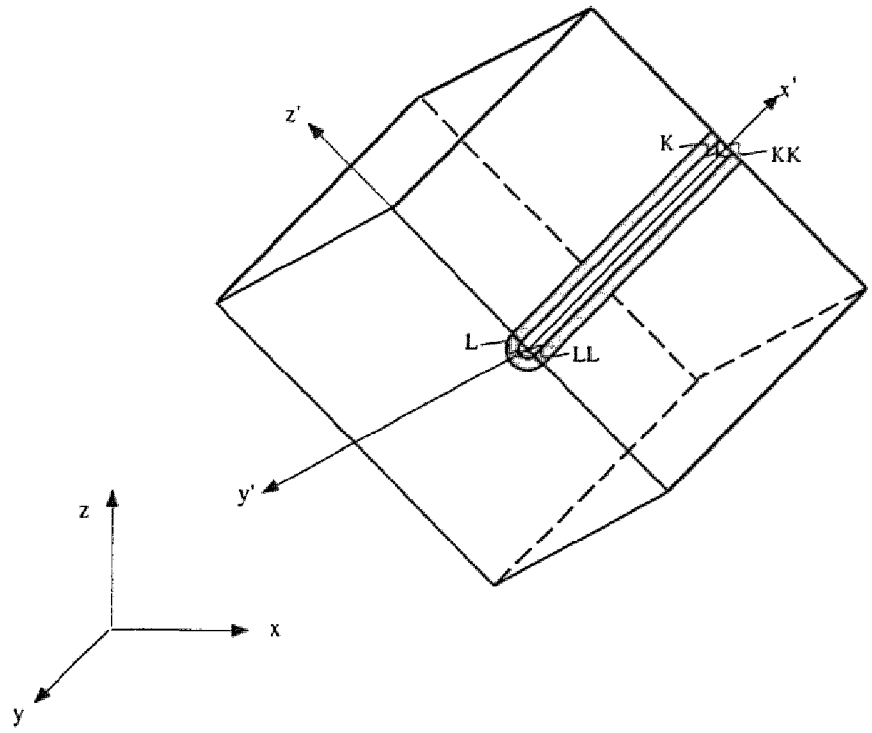

Figure 3.32 : *Three-dimensional representation of element with 4 nodal points*

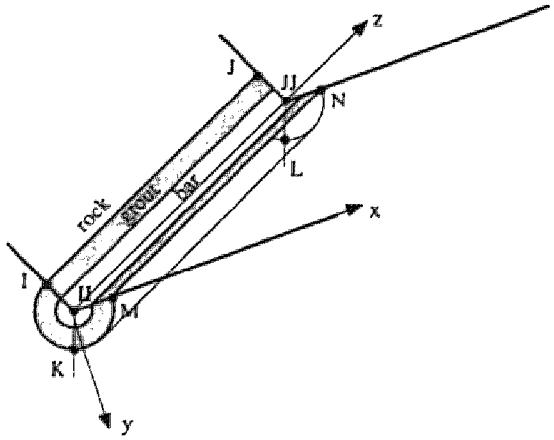

Figure 3.33 : *Three-dimensional representation of element, after Aydan (1989)*

Matrix $[K]_{ga}$ describes the contribution of the grout ring and is expressed in the following form :

$$\mathbf{K}_{ga} = \begin{bmatrix} 2K^{r}_{ga} & 0 & K^{r}_{ga} & 0 \\ 0 & 2K^{z}_{ga} & 0 & K^{z}_{ga} \\ K^{r}_{ga} & 0 & 2K^{r}_{ga} & 0 \\ 0 & K^{z}_{ga} & 0 & 2K^{z}_{ga} \end{bmatrix}$$

with : $K^{r}_{ga} = \dfrac{\pi\ E_{ga}\ L}{3\ \ln\left(r_h\ /\ r_b\right)}$ term of axial stiffness

$K^{z}_{ga} = \dfrac{\pi\ G_{ga}\ L}{3\ \ln\left(r_h\ /\ r_b\right)}$ term of radial or transversal stiffness

where:
- E_{ga} : elasticity modulus of grout,
- G_{ga} : shear modulus of grout,
- L : length of element,
- r_b : radius of bolt,
- r_h : radius of borehole.

The global stiffness matrix of the system is obtained by assembling all of the elementary matrices. These are subjected to a transformation from the local to the global system of coordinates. The disadvantage of this formulation lies in the fact that only the axial and shear stiffnesses are considered, neglecting the bending stiffness of the bolt.

Swoboda & Mareñce (1991-1992) modified the above formulation, assigning different coordinates for the bolt nodes and the nodes of rock-grout interfaces (Figure 3.34). Thus, the bolt and rock displacements are different at the bolt-joint intersection. In this case, the parameters in the stiffness matrix are not constant. They depend on joint displacement and are independently calculated by an iterative procedure. The bolt is represented as a beam element analysed by the large displacements theory. The beam element is settled on elastic supports, representing normal and tangential reaction with respect to the bolt. Moreover, the failure criterion of the beam

element takes into account the interaction between the bending moment, the normal force and the shear force.

Egger & Pellet (1992) defined an interface element whose the thickness corresponds to the distance between the two plastic hinges in the bolt. This distance is calculated according to the beam theory, based on the equilibrium of the bolt. This approach allows one to consider the augmentation of tangential stiffness due to the bolt action. Nevertheless, discretization of the bolt elements should be done for the simulation of confining effect.

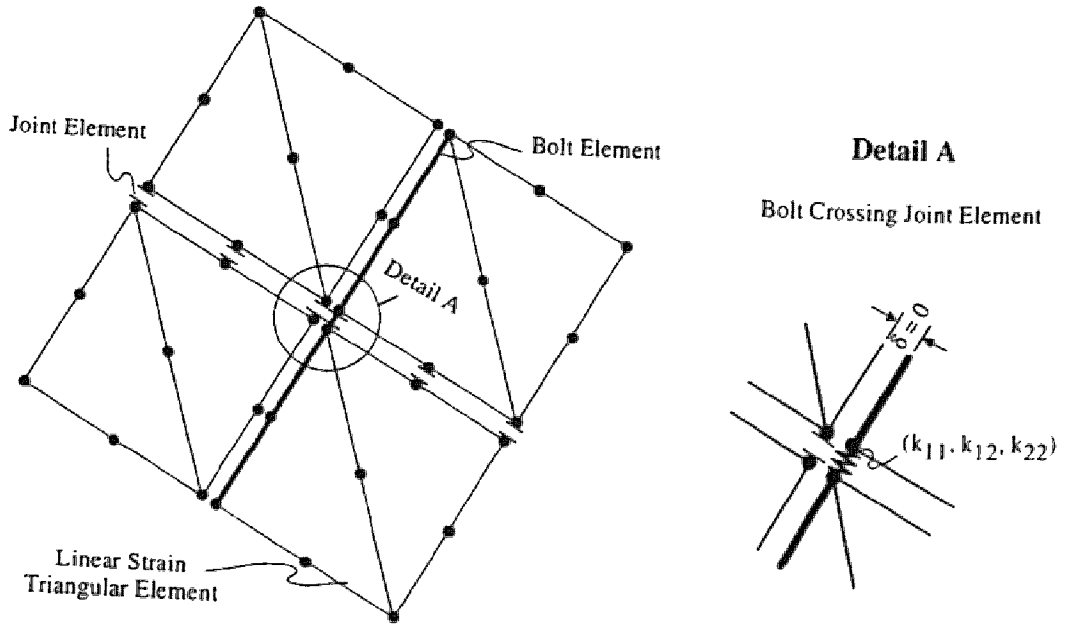

Figure 3.34 : *Joint element, after Swoboda & Marence (1991)*

The Distinct Element Method (DEM), described in details by **Hart (1991)**, is based on the numerical integration of movement law. The force-displacement relations introduced in the solution are expressed as follows :

$$\Delta F_n = K_n \Delta u_n$$

$$\Delta F_s = K_s \Delta u_s$$

where, ΔF_n, ΔF_t : force acting normally and tangentially to joint
u_n , u_s : normal and tangential displacement of joint,
K_n , K_s : normal and tangential stiffness of joint.

Lorig (1985) elaborated a DE solution, enabling one to include the effect of fully bonded bolt. The force-displacement relations for the bolt can be directly evaluated, based on the results of pull-out tests (axial behaviour) and shear tests (transversal behaviour). If the results are not determined in the appropriate tests, the following procedure is proposed for evaluation of the above relation.

The axial stiffness K_a is calculated from the formula :

$$K_a = \pi \; k \; r_b$$

with : $$k = \sqrt{\frac{G_g \; E_b}{2(r_h / r_b - 1)}}$$

where, E_b : elasticity modulus of bolt,
G_g : shear modulus of grout,
r_b : radius of bolt,
r_h : radius of borehole,

For the determination of the transversal stiffness, K_s, the bolt is considered as an elastically supported beam and the following formula can then be used:

$$K_s = E_b \; I \; \beta^3$$

$$\beta = \sqrt[4]{\frac{K}{4 \; E_b \; I}}$$

$$K = \frac{2 \; E_g}{(r_h / r_b - 1)}$$

where, I : moment of inertia of the bolt,
E_g : Young modulus of the grout.

The bolt capacity in the axial direction can be calculated using the formula proposed by **Littlejohn & Bruce (1975)**, (see section 3.2.1), whereas the tangential capacity can be determined with the help of the solution elaborated by **Bjurstrom (1974)**, (see section 3.3.2).

3.4.3.Modeling of a volumetric element of reinforced rock

In this approach representative volumetric elements of reinforced rock are treated as a continuous medium having homogeneous mechanical characteristics.

Pande & Gerrard (1983) and later **Pande et al. (1990)** presented the results of the numerical simulations performed by the Finite Element Method for a mining pillar (Figure 3.35). **Larsson et al. (1985)** simulated the direct shear tests and obtained significant agreement with the results of the experiments, although this model is not yet appropriate for simulation of three-dimensional loading.

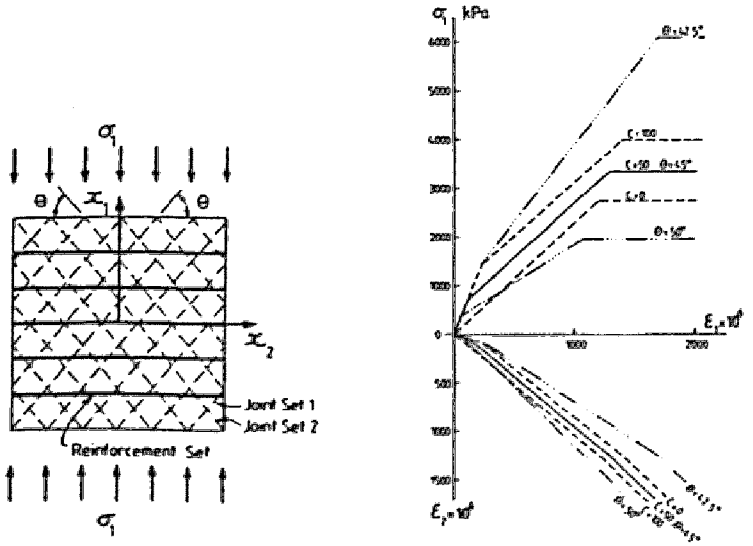

Figure 3.35 : *Simulation of the failure of the reinforced rock volume, after Pande & Gerrard (1983)*

3.5. Stability analysis of reinforced structures and case studies

Different approaches allowing quantification of action of anchored bolts in rock masses were presented in the preceding chapters. The results should allow one to analyze the behaviour of reinforced rock structures.

Structures in rock can be generally divided into two broad categories, i.e., constructions realized on the ground surface (slopes and embankments) and

underground excavations (such as tunnels and caverns). As shown in chapter 2, the choice of the appropriate method for analysis depends on the geometry and the type of the structure.

3.5.1. Superficial structures

Superficial structures concern mainly the natural or the artificially formed slopes in civil engineering works and in open-pit mining.

The slope geometry is unsymmetrical and therefore, no analytic solution of the stress-strain problem exists for this case. Thus, the problems of the stability of slopes are analyzed with the help of limit equilibrium methods or through the use of numerical models. **Aydan (1992)** presented the possible approaches for the studies of reinforced slopes stability. **Sharma & Pande (1988)** analyzed the case of a slope by the Finite Element approach (Figure 3.36).

Concerning in situ observations, **Dight (1983b)** demonstrates the favorable effect of cables, grouted along their whole length, for the case of a slope in an open pit mine. **Colombet & Glories (1983)** presented the positive effect of bolting on the stabilization of a channel slope, subjected to rapid emptying. **Moore & Imbrie (1982)** described the case of a slope stabilization in a dam site. **Egger & Spang (1987)** presented the example of utilizing grouted bolts in the reinforcement of the rock mass in the gravity dam foundation. Few examples of experimental slopes are reported in the literature (e.g. **Gudehus, 1982**).

3.5.2. Underground structures

In the case of underground works, excavations can be often modeled as axisymmetric cases and thus, the analytic solutions can be formulated for a stress-strain problems. The stability of a reinforced section is traditionally studied by the convergence-confinement method. Determination of the equilibrium point between the characteristic curve of the rock mass and the reaction provided by the support is the main principle of this method.

Egger (1973) is one of the first to propose a method of calculation, taking into account the influence of a systematic bolting on the stability of a circular excavation. He assumed that the bolts provide reactions uniformly distributed around the excavation. The bolts are considered as external elements producing the appropriate reaction to balance the overburden pressure.

Stille et al. (1989) and later **Indraratna & Kaiser (1990)** considered the reinforcement as part of the rock mass. They proposed a method of calculation for the rock mass characteristic curve, which directly includes the influence of reinforcement. This idea presents some form of homogenization, where only the axial behaviour of bolts is considered. In Figure 3.37 the characteristic curve of reinforced material is shown (see **Stille et al.**, 1989). Having in mind this same idea, **Wullschlager & Natau (1987)** proposed to model the ring of reinforced rock as a material with additional cohesion, calculated based on the bolts density.

An example of experimental measurements, realized in the Kielder tunnel, was reported by **Freeman (1978)** and **Ward et al. (1983)**. The authors have shown the distribution of forces along the bolt length and the influence of reinforcement stiffness on the displacements reduction.

3.6. Synthesis

3.6.1. Experimental studies

Results of the tests are conformable between themselves in various experimental studies and allow one to formulate the following conclusions :

- If the angle between the bolt and the joint decreases, the tangential stiffness and the bolt contribution to the shear strength considerably increases. In other words, the greater the bolt is engaged in tension, the higher its efficiency will be. Thus, in the case of rough joint, dilatancy phenomenon has a positive influence on the bolt contribution.

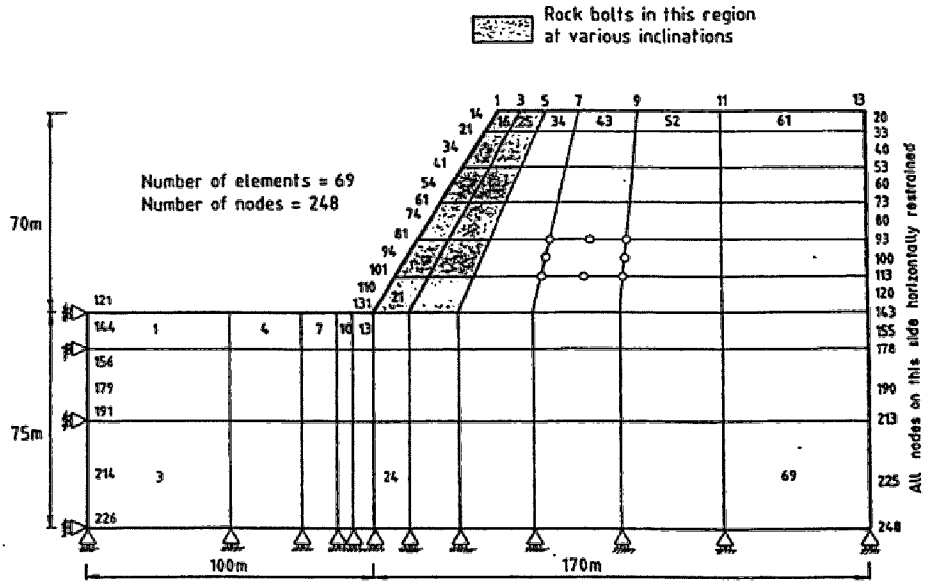

Figure 3.36 : *Finite Element Mesh for a problem of reinforced slope stability, after Sharma & Pande (1988)*

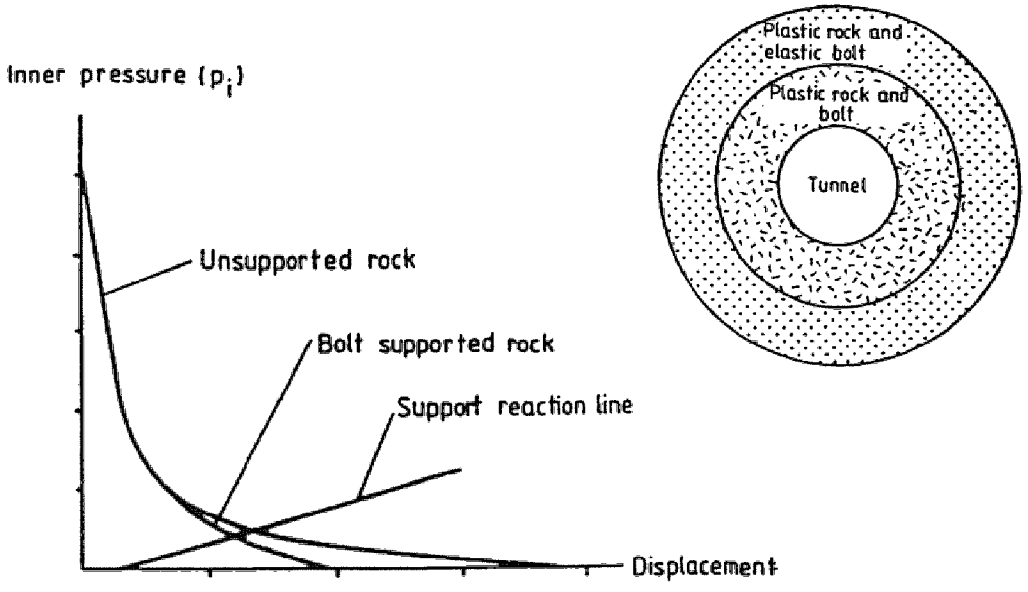

Figure 3.37 : *Characteristic curves for reinforced mass, after Stille et al. (1989)*

- Initial tensioning of bolts plays a favorable role, as it increases the initial joint stiffness and thus, its strength characteristic.

- Properties of grout are of principal importance. If the grout exhibits lower strength than the surrounding rock, the maximum force is mobilized only after the contact between the grout and the rock is reached. In such a

situation, a small space between the bolt and the borehole will allows one to limit the joint displacements.

- The total bolt contribution to the shear strength of the reinforced joint increases in proportion to the bolt cross-section area. As in the reviewed literature, all bolts were built of steel, it is impossible to determine the influence of the elastic modulus on the reinforcing effect of the bolt.

- Tubular bolts provide lower strength than traditional ones. In addition they require a larger displacement to reach the maximum bolt contribution.

3.6.2. Analytic formulations

All the authors generally agree that the bolt contribution to the shear strength of the reinforced joint partially results from the mobilization of the normal force in the bolt and partially from generating a force in the direction parallel to the joint. This behaviour is known as the "dowel action" of the bolt. It should be emphasized, however, that the shear force acting in the bolt does not act parallel to the joint. Thus, it is recommended to first determine the resultant force of the normal and shear forces and then, to decompose it into the force acting parallel and the force acting perpendicularly to the joint plane. It is evident that the augmentation of the joint shear strength is partially the effect of normal stress augmentation and partially the result of the force acting parallel to the joint plane. The latter can be considered as the additional cohesion of reinforcement.

The first formulations proposed for calculation of the bolt contribution to the shear strength of the joint furnished rather conservative solutions, as the shear force mobilized in the bolt was not taken into account. Moreover, the bolt rotation with respect to the joint was neglected and the direction of the normal force was assumed to be in the original position of the bolt.

In most cases, the formulations that consider deformations of the bolt as a function of loading are based on the theory of elastically supported beams. There are first order calculations in which the interdependence between normal and shear forces is not taken into account and the theory of small

displacements is applied. The application of these methods is possible in the calculation of displacements along the joint, associated with the force mobilized in the bolt. Their validity is still limited, as the elastic behaviour of surrounding rock can not be assumed, except for the very beginning of the loading process. The rock failure in the bolt proximity occurs very quickly. Additionally, the bolt itself is yielded and large displacements occur. It must be finally pointed out, that the benefits of formulations of empirical nature are rather limited as they cannot be extrapolated without complementary verification.

3.6.3. Numerical modeling

Although the actual models of the bolt action are simplified, the authors obtain satisfactory descriptions of the behaviour of reinforced rock in the elastic, pre-failure domain. Modeling of large plastic displacements, however, is always very difficult. On the other hand, this approach does not give any indications regarding the forces generated in the bolts and as a consequence it is a handicap in the construction dimensioning.

3.7. Conclusion

It seems to be necessary, from the analytic point of view, to develop a formula which can establish the relation between the force effectively mobilized in the bolt and the corresponding displacement along the joint. In doing this, it is necessary to consider not only the rock failure at the point of contact with the bolt, but also the bolt yield. Bolt yield occurs due to the combination of the normal force, the shear force, and the bending moment. It is also necessary to formulate the problem taking into consideration large displacements, which appear during the loading process.

Chapter 4

Experimental Study of Reinforced Models

Previous experimental studies described in chapter 3 highlighted the influence of the anchored bar on the mechanical behaviour of the rock joint. Most of the direct shear tests mentioned, whether realized in laboratory or on site, used specimens with single discontinuity.

The experimental study presented in this chapter extends these conclusions by approximation of the in situ conditions. The study concerns representative volume material, containing one or more joints, subjected to loading from potentially triaxial state of stress. Figure 4.1. illustrates a typical situation, in which reinforced rock volume, initially subjected to a triaxial state of stress, is unloaded due to excavation and then loaded by a surcharge.

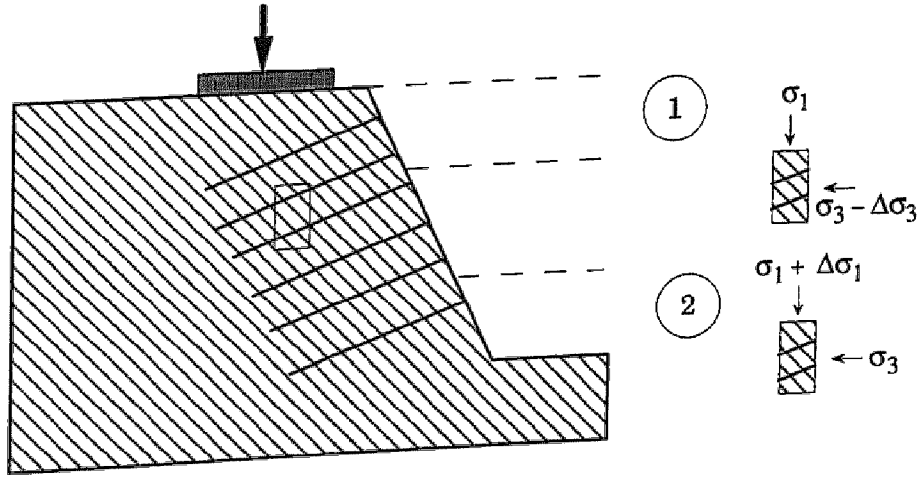

Figure 4.1 : *Modification of initial stress state in reinforced rock mass*

The experimental program which is described in this chapter was realized on specimens of large dimensions. The TRIROC press, utilized in the tests, was constructed at the end of the seventies in the Rock Mechanics Laboratory of the Federal Institute of Technology in Lausanne.

4.1. Presentation of the TRIROC press

The TRIROC is a triaxial press of great dimensions, enabling one to test specimens having a height of 60 cm, a square base of 30 x 30 cm or a circular base with a diameter of 30 cm. It allows for studying of continuous materials, such as fine molded soils and homogeneous rocks, as well as discontinuous media, such as stratified rocks. The first study of bolted discontinuous medium carried out by this apparatus was reported by **Egger & Fernandes (1983).**

4.1.1. Principle of the tests

Parallelepiped specimen can be subjected to a truly triaxial state of stress (Figure 4.2). The major stress component σ_1 is applied vertically, whereas the intermediate (σ_2) and the minor component (σ_3) act horizontally.

Each of the stress components is independently controlled during the test. The major stress component results from a vertical force, applied by the bottom plate of the press. The minor stress component is developed by the pressure of fluid in the cell and is kept constant during the test. The intermediate stress component is applied by means of three removable and independent loading frames. It can be kept constant or can vary to provide plane strain conditions (i.e. $\varepsilon_2 = 0$).

4.1.2. Construction of the press

The scheme of the press is presented in figure 4.3. It is comprised of three prestressed columns, producing high rigidity (up to 1.5 GN/m) of the press.

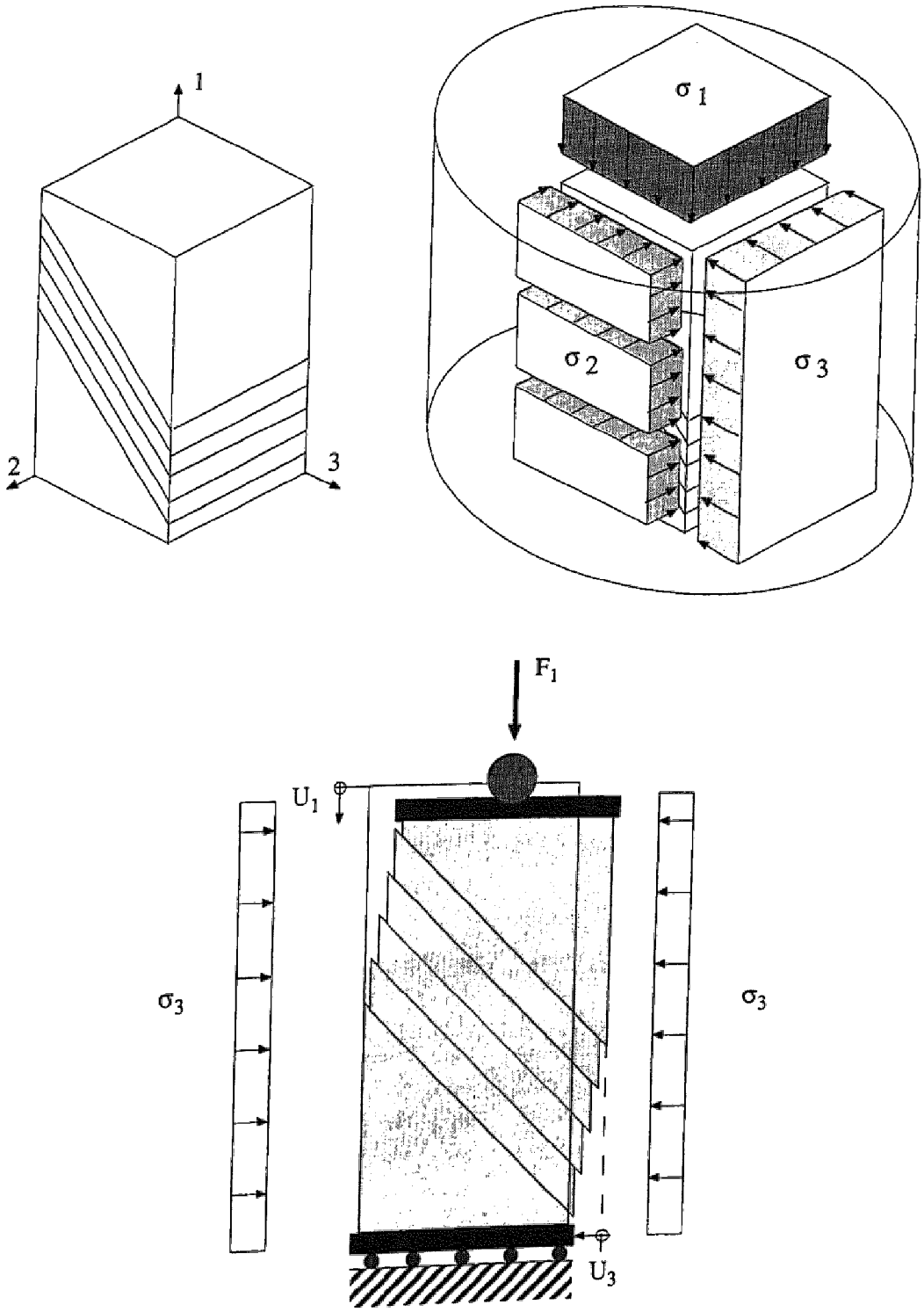

Figure 4.2 : *Triaxial loading of the specimen*

The top plate is mounted on a spherical seat. This arrangement assures uniform distribution of stresses, by eliminating the possible non-parallelism between the upper and lower surface of the specimen. The bottom plate is placed on rollers arranged in two layers, crossing one another. Owing to this, the plate can freely move in the horizontal plane. It is put in motion by the principal hydraulic jack, which can develop a vertical force of up to 3.5 MN.

Lateral loading plates generate the intermediate stress on the two side walls of the specimen. The specimen is installed in the apparatus after setting in it a rubber membrane. Each plate is composed of two steel plates, one connected to another by two double effect jacks. The contact between the specimen and the plates is therefore always maintained, whatever the sign of the lateral deformation may be (i.e., positive or negative dilatancy).

Confining stress, which can reach a value of up to 5 MPa, is applied by water pressure, generated by a set of independent pumps. The cell is comprised of a cylindrical metallic casing which can slide vertically. The water-tightness between the casing and the press is assured by special joints (O-rings). The casing is also equipped with illuminators and a fiber optical lighting system, thus direct observations are possible during the test.

Figures 4.4a shows the press when the cell is opened, after the installation of the specimen. Figures 4.4b shows the press when the cell is closed during a triaxial test. Installation of the specimen is facilitated, due to a special table mounted on the track equipped with rollers. It enables one to slide the specimen, until the proper position is reached.

4.1.3.Installation and data acquisition

Horizontal displacements are measured by means of inductive sensors at the level of the bottom plate (Figure 4.2). Vertical displacement of this plate, having a travel range equal to 10 cm, is simultaneously measured with the help of a sensor incorporated into the jack and by means of an external sensor.

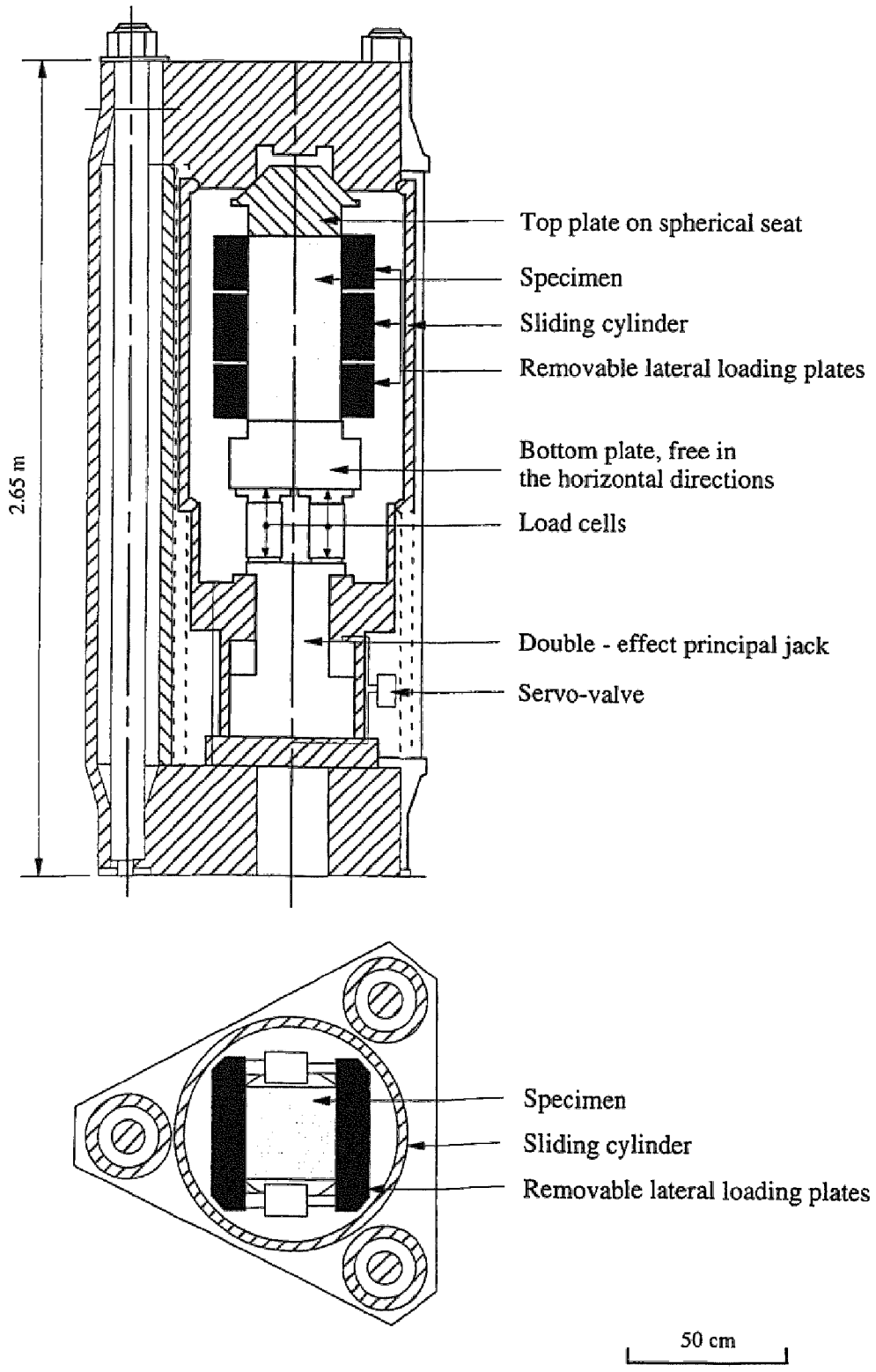

Figure 4.3 : *Vertical and horizontal cross-sections of the Triroc press*

Displacement between the lateral plates is measured using a water-tight sensor. If the tests in plane strain conditions are realized, the sensor allows one to keep the plates in a mode ensuring zero lateral deformation. The oil circuit supplying the jacks which load the plates is connected in series. Two cells allow one to measure the pressure in the high and low pressure chambers of the jack.

The vertical force is measured by means of three load cells displayed in a triangle, each of capacity equal to 1.8 MN. The confining pressure is measured by one incorporated pressure cell.

The rate of vertical displacement is controlled by an automatic system supplied with servo-valves. As the tests should be performed at a constant rate, this device allows one to properly control the pressure in the principal jack, especially in the post-failure range. It is thus, possible to continue the test in this range. The advancing rate of the plate is controlled by the functional generator and can follow monotonic or cyclic functions. The test parameters are determined and continuously recorded at intervals prescribed by the operator.

It should be added that if simple compression tests are realized, two sensors fixed on the specimen allow for the direct measurement of the displacement along the joint.

4.1.4. Advantages of the TRIROC press in comparison to conventional testing apparatus

In comparison with traditional presses, the TRIROC press, due to the movable bottom plate, considerably reduces the parasitic forces. Kinematic conditions do not disturb the formation of the failure plane in the specimen. Moreover, jointing the top plate to the circular seat ensures the uniform stress distribution on the upper and lower surface of the specimen, even in the case when these are not perfectly parallel to one another.

High rigidity of the press, associated with the controlling system of vertical force and with the movable bottom plate, allows for the study of the behaviour of brittle materials in the post-failure range.

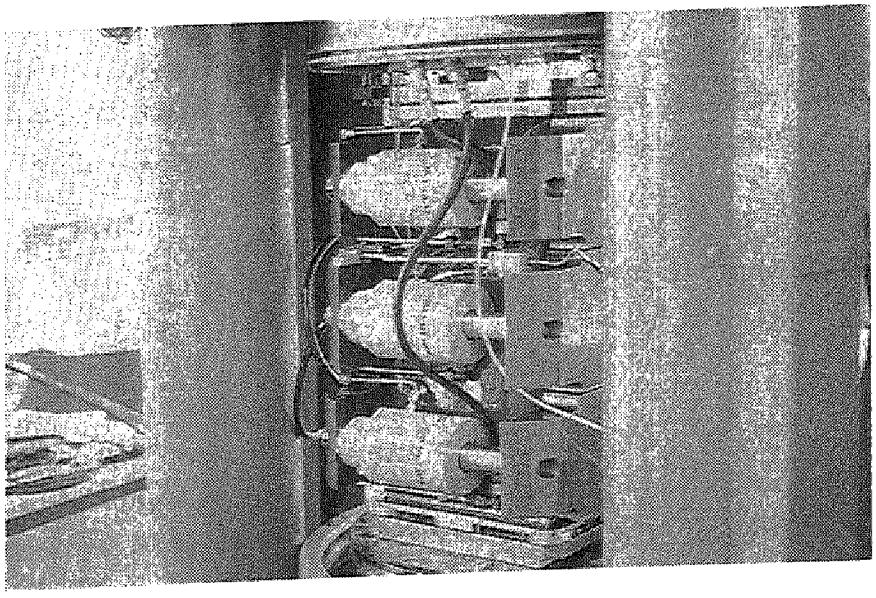

a- open cell after specimen installation

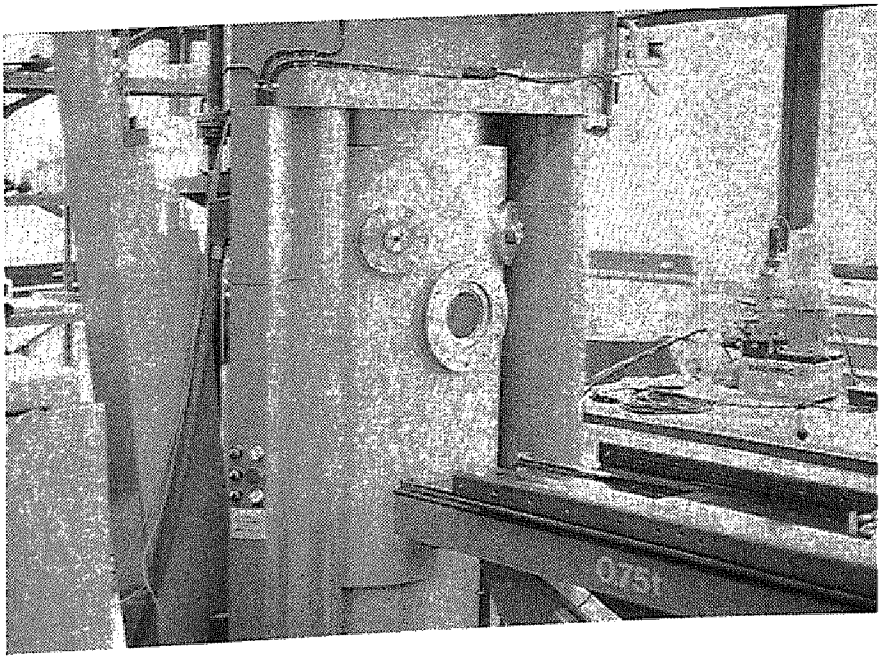

b- closed cell in time of triaxial test

Figure 4.4 : *View of the TRIROC press*

The TRIROC allows one to apply uniform loading in the case of tests performed on reinforced models with originally existing discontinuities. In comparison to the tests realized in the shear box here, the normal force can be applied without compression of the bar. Moreover, joint displacement measurements are more accurate and parasitic forces are avoided, which can be generated due to the rotation of the two halves of the shear box.

4.2. Concept of the physical models

4.2.1. Geometry of the models

Parallelepiped blocks were chosen as models, having heights equal to 60 cm and square bases with sides of 30 cm. Two configurations were established, i.e., the blocks with the joints inclined at an angle of 45 degrees and 60 degrees to the horizontal. For the first configuration the number of joints was varied from 1 to 5 (Figure 4.5).

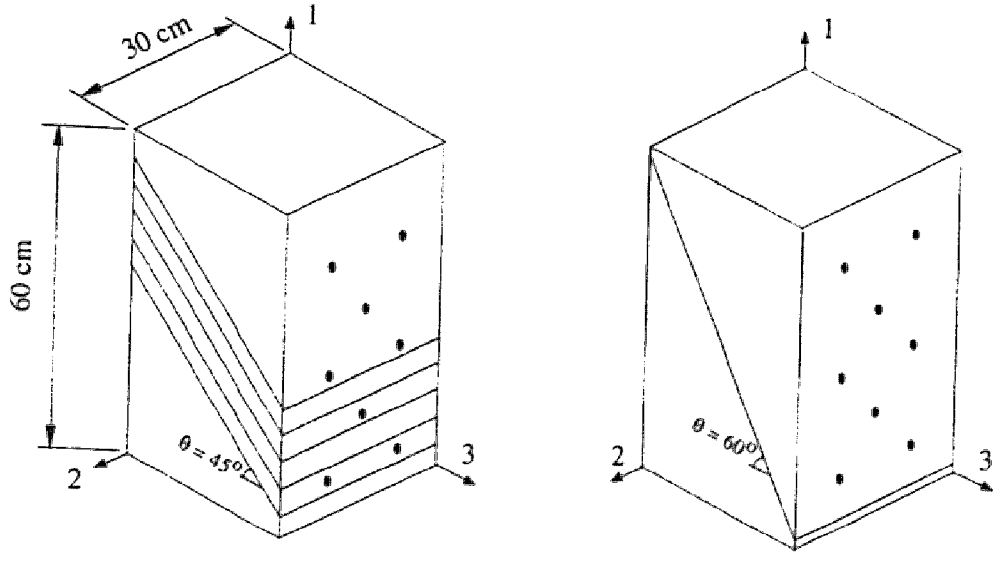

Figure 4.5 : *Geometry of tested models*

4.2.2. Models materials

Two materials were utilized, i.e., one with low strength, representing soft rock and the other with high strength.

Plaster was used to simulate soft rock. It was commercially available in the form of 4 cm thick plates with the following mechanical characteristics :

- simple (uniaxial) compressive strength	$\sigma_c = 7.0$ MPa
- elastic modulus	$E_r = 3.0$ GPa
- Poisson's coefficient	$\nu_r = 0.05$
- angle of internal friction	$\phi_r = 0$ degree
- cohesion	$c_r = 3.5$ MPa

The hard material was an Urgonian limestone, coming from the quarry in Sixt (Haute Savoie). It contains 90 % calcium carbonate ($CaCO_3$), and exhibits the following mechanical properties :

- simple compressive strength ,	$\sigma_c = 150$ MPa
- elastic modulus ,	$E_r = 80$ GPa

Each model was simply juxtaposed before final assembly. Thus, the cohesion of joints is equal to zero. Values of the friction angle for the two types of model materials are equal to :

- friction angle of plaster,	$\phi_j = 40$ degrees
- friction angle of limestone ,	$\phi_j = 25$ degrees

4.2.3. Reinforcing bars

The models were reinforced by bars of 3 mm diameter, constituted of cold drawn steel with the following mechanical characteristics :

- elasticity limit	$\sigma_{el} = 600$ MPa
- yield limit	$\sigma_{ec} = 650$ MPa
- strain at failure	$\varepsilon_f = 20\%$
- elastic modulus	$E = 210$ GPa

4.2.4. Installation and fixing of the bars

The bars were installed horizontally, and thus, the angle between the bar and the joint was equal to the angle of joint inclination ($\beta = \theta$).

In plaster models the bars were driven and bolted at both their extremities. The washer diameter in the first series of the specimens was equal to 15 mm, whereas it was equal to 50 mm in the second series. Figure 4.6 illustrates the installation of the bars and details of the fixing system.

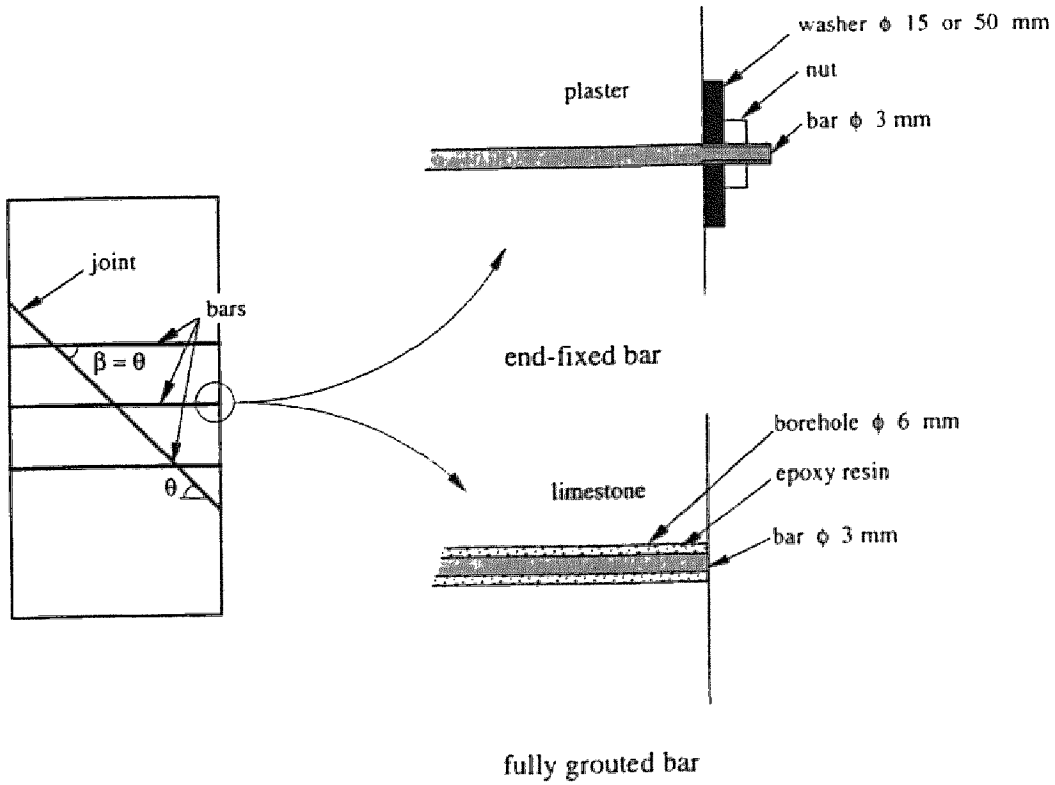

Figure 4.6 : *Scheme of the bar installation and detail of the fixing system*

The maximum normal force mobilized at the bar extremity was determined during the test. In the case of bars bolted by washers of 15 mm in diameter, the force corresponds to plaster punching due to the washer action. If the bar is fixed by washers of 50 mm in diameter, the force corresponds to its tension strength, taking into account diminution of the diameter due to the thread. The values of forces listed below can be compared to the maximum normal force sustainable by the bar with full cross-section :

- washer ϕ 15mm , $N_{max} = 3.0$ kN
- washer ϕ 50mm , $N_{max} = 3.5$ kN
- full cross-section, $N_{max} = 4.6$ kN

The bars in the limestone models are bonded along their whole length in prebored holes of 6 mm diameter (Figure 4.6). Epoxy resin Sikadur 52 was used as a bonding agent, having the following mechanical characteristics :

- simple compressive strength , $\sigma_{cg} = 60$ MPa
- tension strength, $\sigma_{tg} = 25$ MPa
- elastic modulus , $E = 1.1$ GPa

4.3. Testing program

Two types of tests were performed : simple compression tests (without confining pressure) and triaxial tests (confining pressure applied).

The first series of tests (PL series) was realized on plaster models reinforced by 8 bars bolted with 15 mm washers. These tests were performed for three configurations of joints. In the first case, 5 joints were inclined at 45 degrees. In the second and third, one joint was present, inclined at 45 degrees and 60 degrees, respectively. Three tests were carried out for each of the configurations: one simple compression test and two triaxial tests in plane strain state, with confining pressures equal to 200 and 400 kPa.

The second series of tests (PF series) was executed in simple compression conditions, using plaster models reinforced with bars, bolted by washers of 50 mm in diameter. Two configurations were tested, in which one joint was inclined at angles of 45 degrees and 60 degrees, respectively. Two tests were realized for each configuration: one with four and the other with eight reinforcing bars.

Limestone, reinforced by fully bonded bars, was tested in the third (CE series). Two configurations were investigated, differing by joint inclination. An angle of 45 degrees was chosen in the first configuration and 60 degrees

was chosen in the second. Four tests were realized for each of two configurations. The number of bars was varied in two simple compression tests, whereas two other tests were performed in triaxial conditions, with different confining pressures.

Characteristics of the tests are summarized in the table 4.1. The parameters are explained below (see also Figure 4.7) :

σ_c = simple compressive strength
ϕ_j = joint friction angle
β = angle between bar and joint
n_j = number of joints
n_b = number of reinforcing bars
σ_3 = initial confining pressure

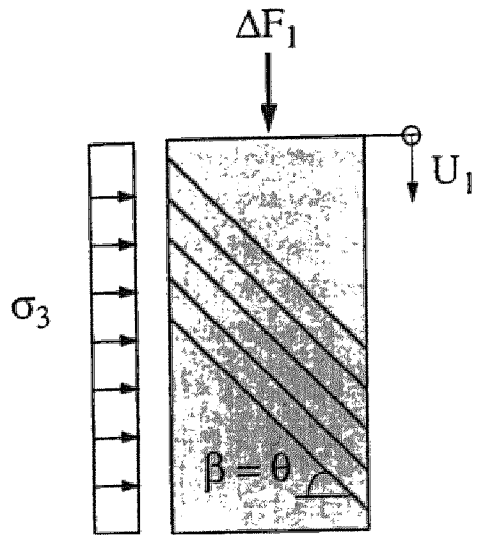

Figure 4.7 : *Illustration of principal quantities in the tests*

4.4. Results and comments on the development of the tests

4.4.1. Tests of plaster models - PL series

The failure of the models occurred by sliding along the joints. The washers penetrated into the specimen, punching plaster on the external surfaces of the model.

	Test -	σ_3 [MPa]	β degrees	n_b -	n_j -
PL SERIE Plaster $\sigma_c = 7.0$ MPa $\phi_j = 40$ degrees $N_{max} = 3.0$ kN	**PL45.01**	0.0	45	8	5
	PL45.02	0.2			
	PL45.03	0.4			
	PL45.04	0.0	45	8	1
	PL45.05	0.2			
	PL45.06	0.4			
	PL60.07	0.0	60	8	1
	PL60.08	0.2			
	PL60.09	0.4			
PF SERIE Plaster $\sigma_c = 7.0$ MPa $\phi_j = 40$ degrees $N_{max} = 3.5$ kN	**PF45.10**	0.0	45	4	1
	PF45.11	0.0	45	6	1
	PF60.12	0.0	60	6	1
	PF60.13	0.0	60	8	1
CE SERIE Limestone $\sigma_c = 150$ MPa $\phi_j = 25$ degrees $N_{max} = 4.6$ kN	**CE45.14**	0.0	45	6	1
	CE45.15	0.0	45	6	1
	CE45.16	0.2	45	6	1
	CE45.17	0.4	45	8	1
	CE60.18	0.0	60	6	1
	CE60.19	0.0	60	8	1
	CE60.20	0.4	60	8	1
	CE60.21	0.4	60	10	1

Table 4.1 : *Recapitulating of the testing program*

In all the tests, the curves representing the vertical force, ΔF_1, versus vertical displacement, U_1, are linear in the initial stages (Figures 4.8, 4.9, 4.10). Following the initial stages, the force increases less steeply and after reaching a maximum, it tends to some constant value. It was observed that the initial tangent modulus, corresponding to the original slope of the load-displacement curve, increases with the confining pressure.

Vertical displacement, corresponding to the maximum force was greater for the case of the specimen having 5 joints, oriented at an angle of 45 degrees (Figure 4.8) in comparison to the case with only one joint (Figure 4.9). Displacement in the first of the above cases is in fact the sum of the displacements of the individual joints. It should be noted, however, that the displacements of each joint were not equivalent.

In the models with a single joint, the transition zone between the linear and the plastic portions of the curve was approximately extended over a length equal to the diameter of the bar. The force reached peak value and then it diminished, tending towards the residual value. The displacement corresponding to the maximum force was approximately equal to twice the diameter of the bar. Comparing the Figures 4.8 and 4.9 one can conclude that the number of joints slightly influences the specimen strength.

In the models with a single joint oriented at 60 degrees, the length of the transition zone between the linear and the plastic portions of the curve was equal to about one half of the bar diameter. After reaching this value, the force continued to increase very slowly.

4.4.2. Tests of plaster models - PF series

The bars in this series of tests were broken at their end points. Due to the great diameter of the washers (i.e., 50 mm) the load which was necessary to punch the plaster was higher than the strength of the reduced section of the bar.

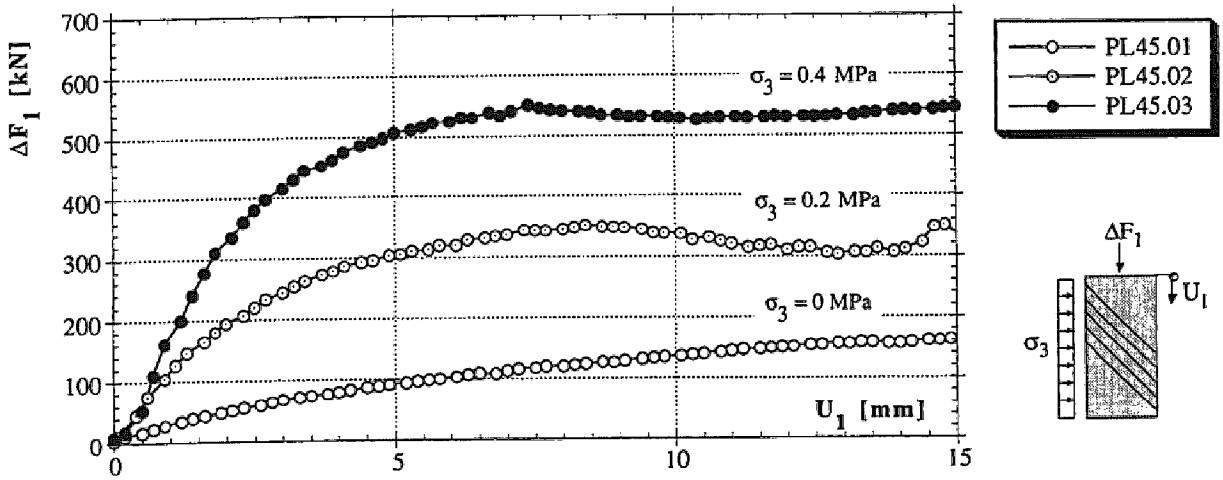

Figure 4.8 : *Plaster models with 5 joints, oriented at 45 degrees and reinforced by 8 bars*

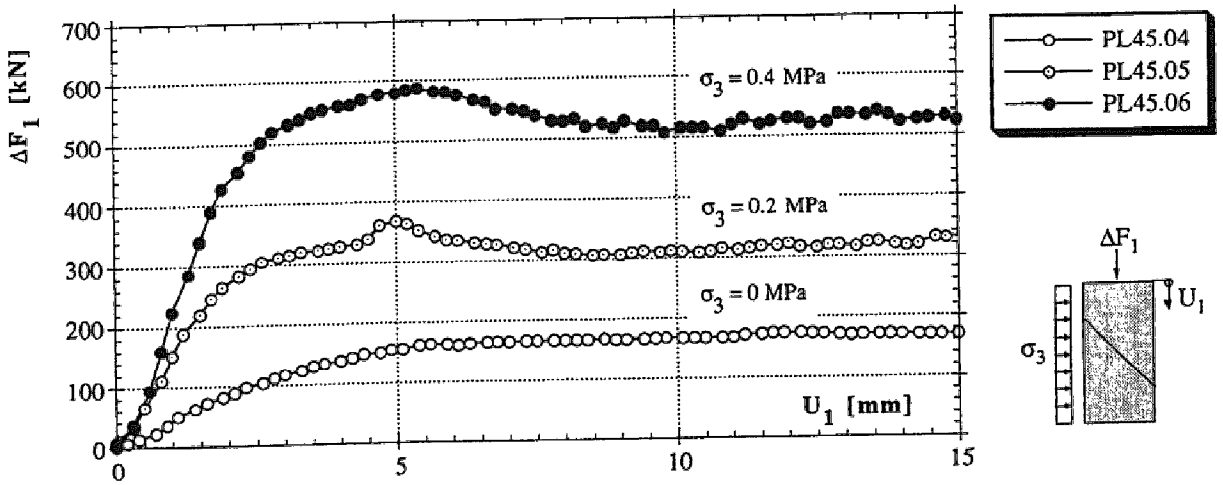

Figure 4.9 : *Plaster models with one joint, oriented at 45 degrees and reinforced by 8 bars*

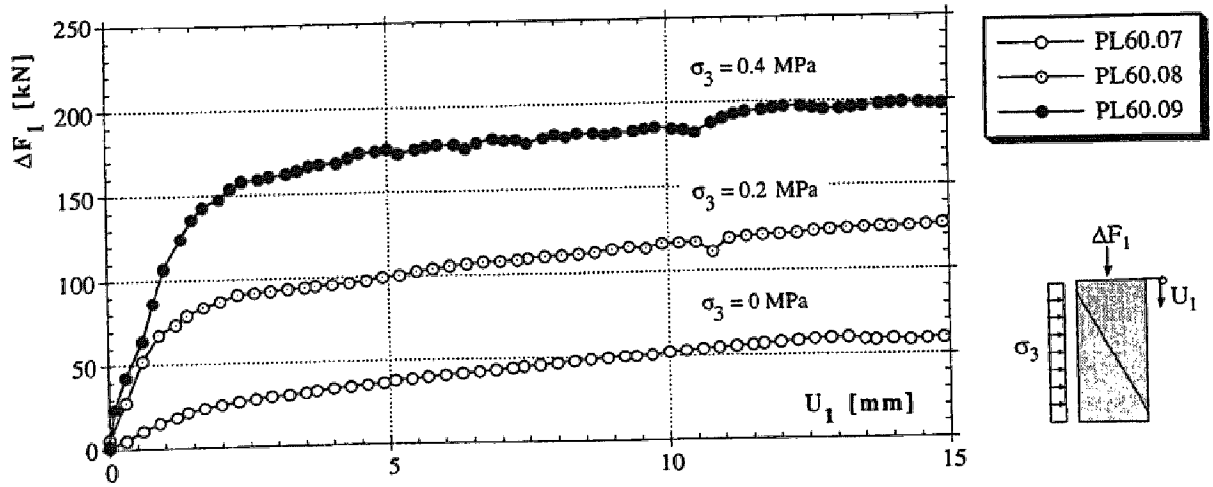

Figure 4.10: *Plaster models with one joint, oriented at 60 degrees and reinforced by 8 bars*

Curves representing vertical force versus vertical displacement (Figures 4.11 and 4.12) show a linear portion, corresponding to the first testing stage. Non-linear behaviour occurs in the next stage, until the maximum force is achieved. In the final stage, the rupture appears suddenly, without any significant plastic deformations (unlike the tests described in the previous section).

In the tests of models with a single joint inclined at an angle of 45 degrees (Figure 4.11) the bars broke at the same time. The rupture occurred when displacement was equal to about 50% of the bar diameter.

To the contrary, in the models with one joint oriented at an angle of 60 degrees (Figure 4.12), the bars broke at different times. It is clearly visible in Figure 4.12 that the irregular shape of the descending part of the force-displacement curve results from the failure of the individual bars during the test. The maximum value of the force is reached for a displacement approximately equal to the bar diameter. In the PF60.12 test, the first ruptures appeared before all the bars were fully loaded. Therefore, the maximum force in this test was lower in comparison to the real capacity of the model.

4.4.3. Tests of limestone models - CE series

The rupture of the models in this series occurred by failure of the bars across the joint.

The early portions of the curves representing vertical force versus vertical displacement show quasi-linear behaviour (Figures 4.13 and 4.14). The force progressively increases, until the maximum value is reached, which corresponds to the entire yielding of the bar. Subsequently, the force remains constant and a large plastic zone appears, resulting from bar lengthening, continuing until its failure is achieved.

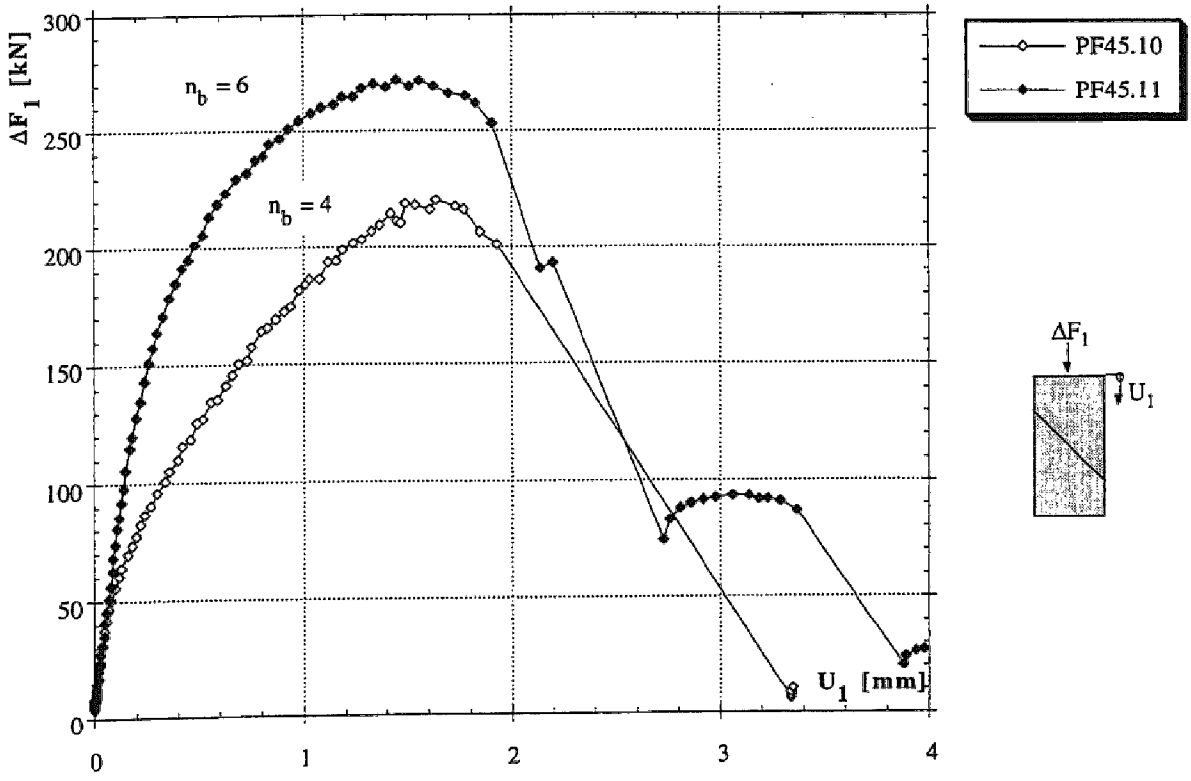

Figure 4.11 : *Plaster models with one joint, oriented at 45 degrees and reinforced by bars fixed at extremities*

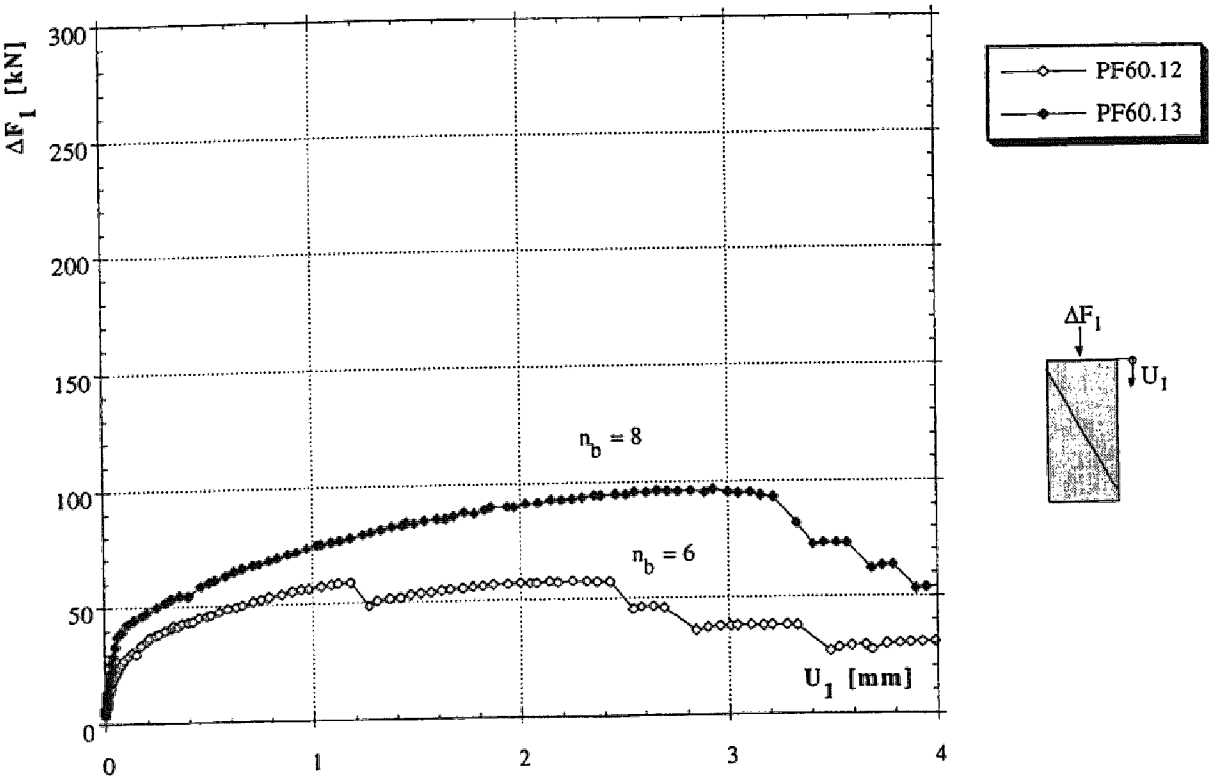

Figure 4.12 : *Plaster models with one joint, oriented at 60 degrees and reinforced by bars fixed at extremities*

In the tests of models with a single joint inclined at an angle of 45 degrees realized in simple compression conditions (Figure 4.13), the displacements at the maximum forces were rather small i.e., equal to 0.25 - 0.50 mm. Rupture occurred when the displacements were equal to about one half of the bar diameter. For the triaxial tests, the maximum forces were attained for larger displacements (Figure 4.13).

Displacements were also relatively small in simple compression tests of the models having a single joint, inclined at an angle of 60 degrees (Figure 4.14). Rupture was observed when displacements were slightly greater than one half of the bar diameter, whereas in triaxial conditions these were slightly smaller than the bar diameter (see Figure 4.14).

4.5. Interpretation and discussion of the experimental results

4.5.1. Failure modes

Before the comparison of the results is done, allowing one to describe the mechanical behaviour of the reinforced models in terms of strength and deformability, it is convenient to define the different modes of observed failures.

As shown in the photograph (Figure 4.15), the bars in the plaster models did not fail across the joints. The maximum force carried by the specimen was achieved when the capacity of the fastening system of the bar extremities was attained. In the case of the bars bolted at the ends by washers of 15 mm in diameter, plaster punching was observed on the external faces of the specimen. To the contrary, in the case of models with bars bolted by washers of 50 mm in diameter, the necessary force for plaster punching was higher than the strength of the bars. Thus, these failed at the extremities, in their reduced sections. Based on this observation, it can be stated that the friction at the interface between the bar and plaster is low and as a result, the normal force mobilized in the bar is quasi-constant along its whole length.

In the cases in which the bars were not broken across the joint plane, the

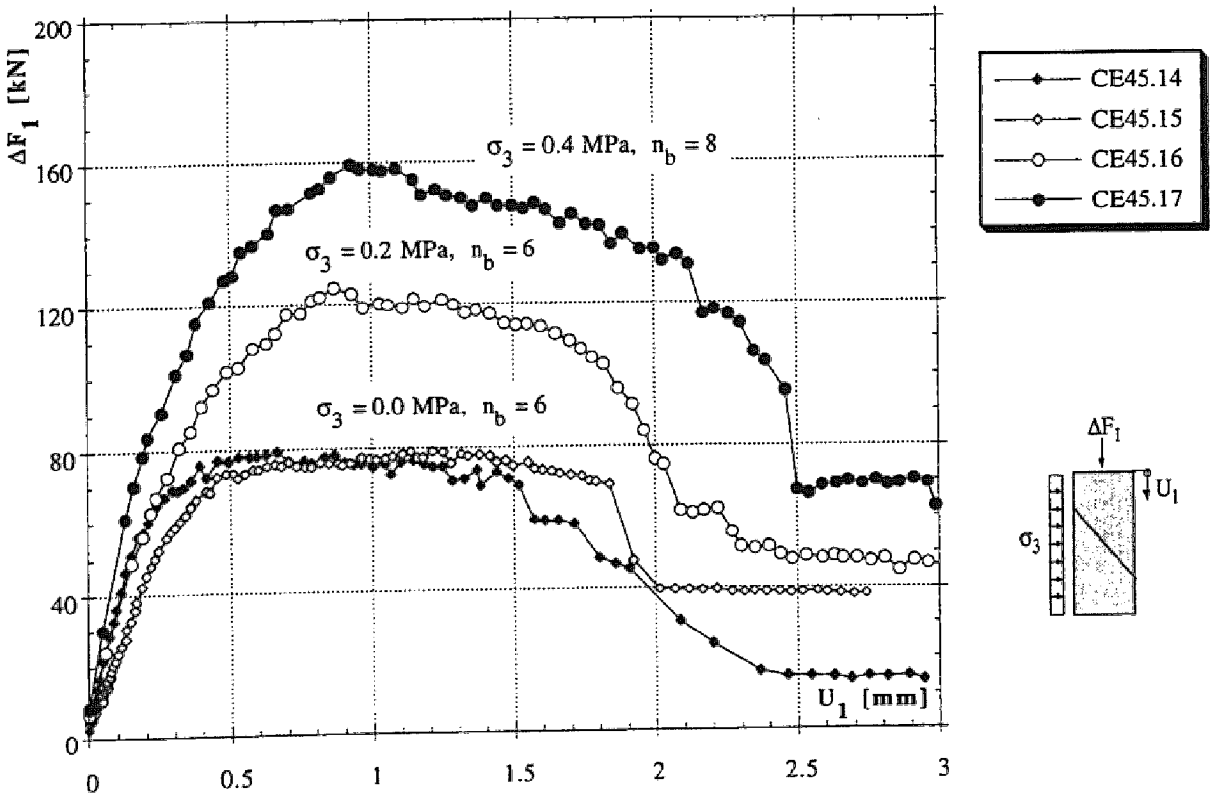

Figure 4.13 : *Limestone models with one joint, oriented at 45 degrees and reinforced by bars grouted with epoxy resin*

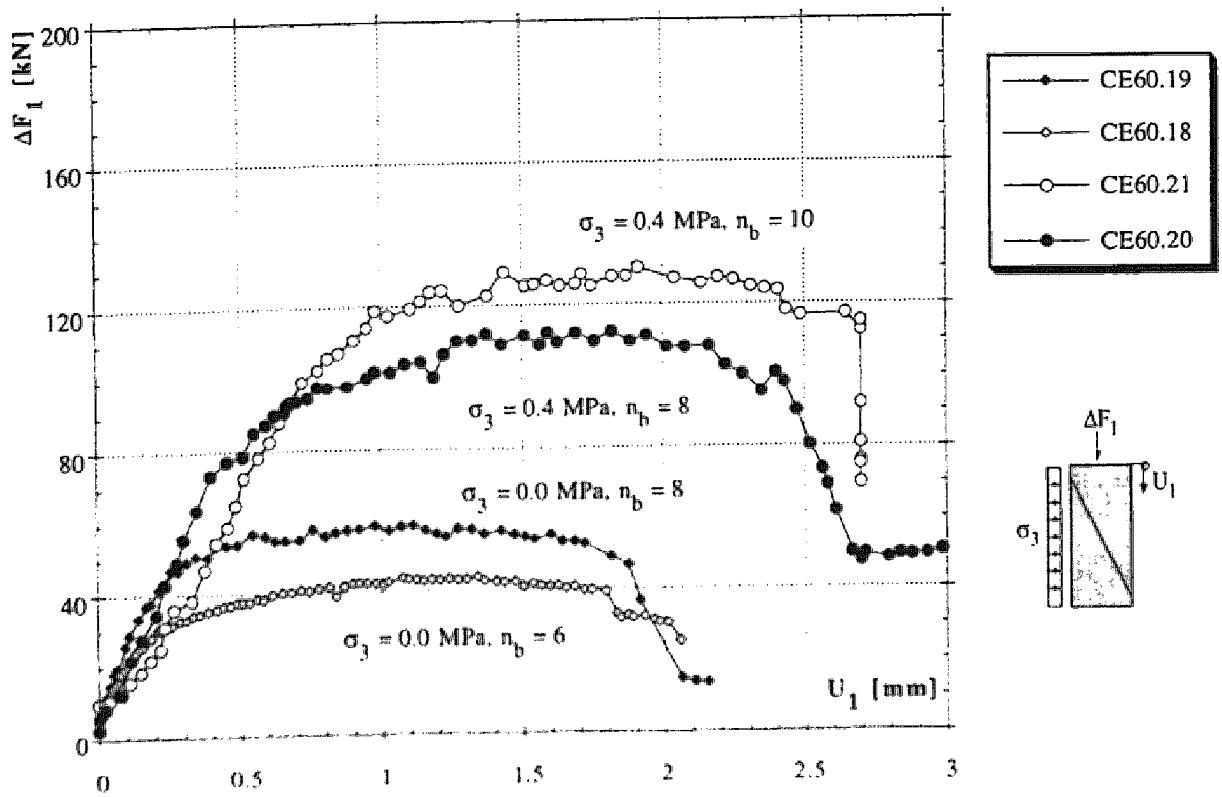

Figure 4.14 : *Limestone models with one joint, oriented at 60 degrees and reinforced by bars grouted with epoxy resin*

bars were considerably deformed and the failure mechanism was characterized by two plastic hinges, localized on both sides of the joint. Permanent deformations of the bars, equal to about four times the bar diameter were observed. The photograph (Figure 4.16a) presents the deformed bar in the model having 5 joints, inclined at 45 degrees. Only small permanent deformations appeared in the case of bars bolted by 50 mm washers.

In the tests on limestone models, specimen failure corresponds to the failure of the bars across the joint planes. The bars were deformed over a length equal to about one half of the diameter. Very nearly spaced plastic hinges were also visible. A view of the deformed bar in the model with a single joint inclined at 60 degrees is presented in the photograph (Figure 4.16b). It can be observed that the displacements at failure were not sufficient to provide contact between the bar and the rock.

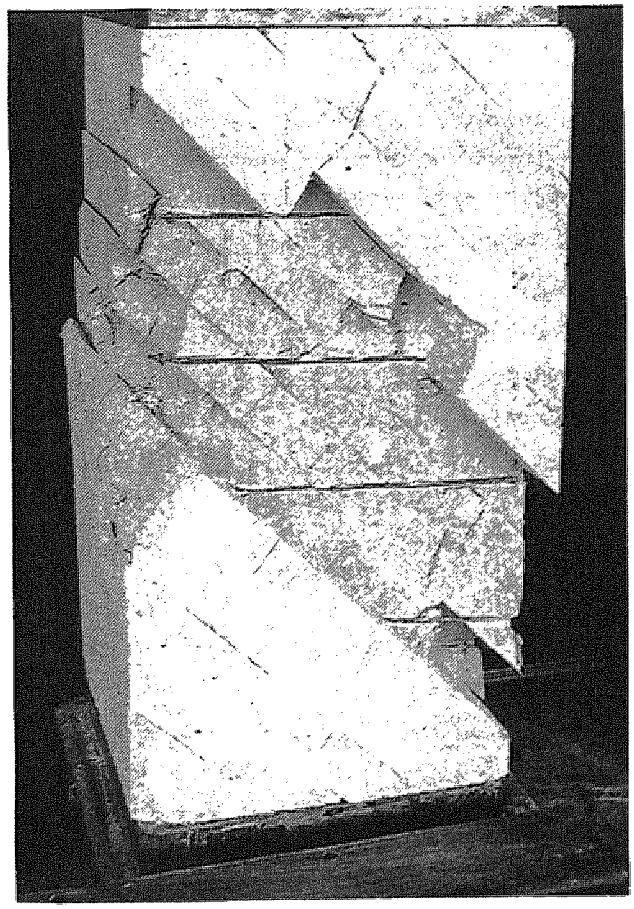

Figure 4.15 : *View of plaster models after failure in the test of PL series the bars are not broken*

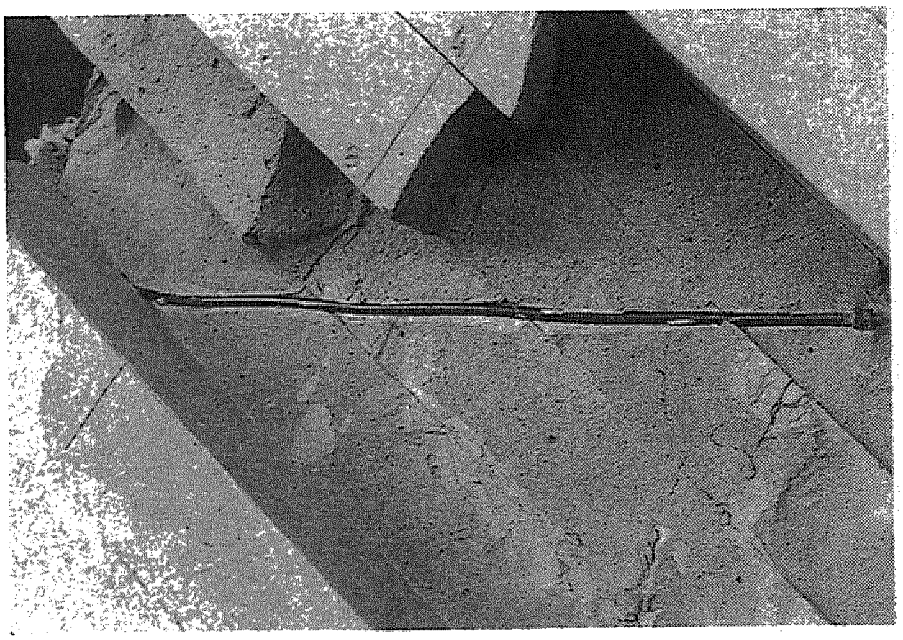

Figure 4.16a : *Enlargement of the separated zone - the bars are subjected to permanent deformations at the level of each joint*

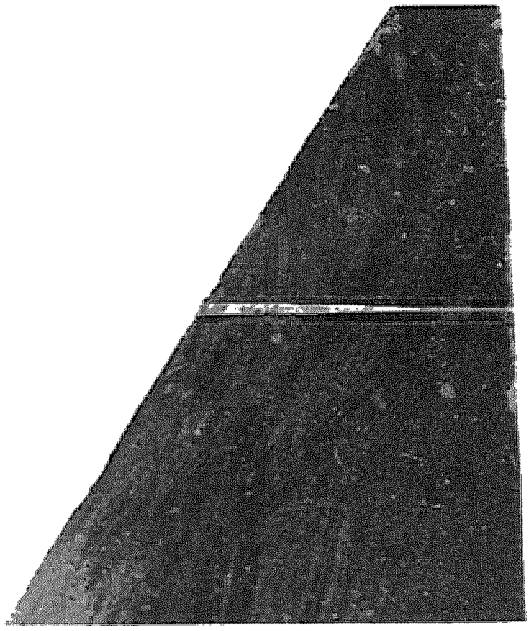

Figure 4.16b : *Cross-section in the plane of axis of grouted bar in limestone - the broken bar is deformed in a small zone without entering in contact with the surrounding rock*

4.5.2. Bar contribution to the joint shear strength

For a comparative study of experimental results, the forces acting on the specimen should be decomposed with respect to the joint direction, as shown in Figure 4.17. The force carried by the bars can be calculated, taking into account the equilibrium equation in the joint direction. The contribution of a single bar to the joint shear strength can be then obtained by dividing this force by the total number of bars crossing a joint. Thus :

$$T_b = \left[F_1 \left(\sin\beta - \cos\beta \tan\phi_j\right) - F_3 \left(\cos\beta + \sin\beta \tan\phi_j\right)\right] / n_b$$

where,
- T_b : contribution of a single bar,
- F_1 : total vertical force acting on the specimen,
- F_3 : initial horizontal force acting on the specimen,
- β : angle between bar and joint,
- ϕ_j : joint friction angle,
- n_b : number of bars installed across joint.

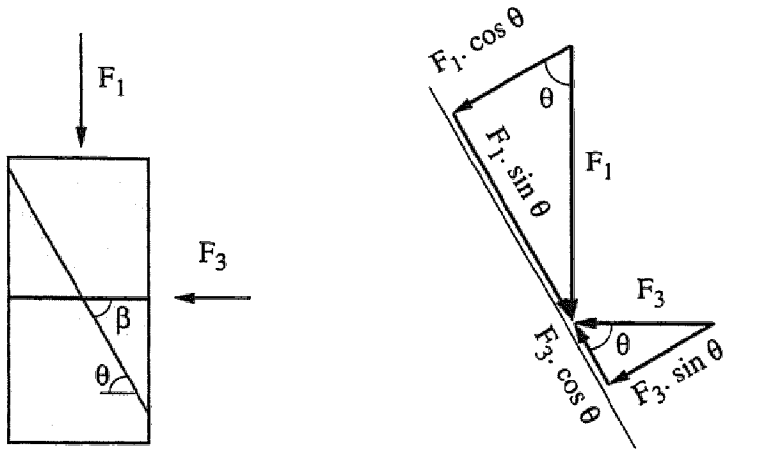

Figure 4.17 : *Decomposition of forces acting in joint plane*

When triaxial conditions are considered, the total vertical force, F_1, can be taken as the sum of the initial force, F_{1o}, and the increment, ΔF_1 :

$$F_1 = F_{1o} + \Delta F_1$$

where :

$$F_{1o} = \frac{F_{3o}}{tg\beta}$$

The displacement along the joint is obtained by projection of the vertical displacement on the joint direction :

$$u_j = \frac{u_1}{\sin \beta}$$

The results of the tests, namely the calculated maximal contributions of the bars, as well as the corresponding displacements, are assembled in table 4.2.

The bar contribution in the PL series of tests, realized on the plaster models with the bars bolted by the 15 mm washers, is not very high. The reason for this is that the force mobilized in the bar across the joints is limited by the plaster punching strength on the external faces of the specimen. The smaller the angle between the bar and joint is, the more the bar is tensioned. This explains that the bar contribution is smaller for an angle of 45 degrees than for an angle equal to 60 degrees. It also seems that the number of joints does not affect total strength of the reinforced models.

The maximum bar contribution for models with a single joint inclined at 45 degrees is achieved when the magnitude of the joint displacement is 2.5 times the bar diameter. This magnitude is higher for models with a joint inclined at 60 degrees.

The plaster punching does not appear in the PF tests realized on the models with the bars bolted by the 50 mm washers. The bars contribution here is more significant than in the series of tests described above. The maximum bar contribution is reached for a displacement equal to about one half of the bar diameter in the models with joints inclined at 45 degrees, and one diameter for joints inclined at 60 degrees. The failure occurs rapidly, shortly after mobilization of the bar maximum contribution.

The maximum contribution of the bar in the CE series of tests, realized on the limestone models reinforced by bars which were fully bonded, is approximately equal to the bar tension strength.

Though the results of the tests were relatively unscattered, some deviation in the results was observed. In fact, it is difficult to be sure that all the bars were mobilized at the same time.

4.6. Summary and conclusions

The tests realized in the present study take into account two types of mechanical behaviour. The plaster models reinforced by the bars fixed at their extremities revealed a behaviour similar to that which is observed in stratified rock masses reinforced by pointwise fixed anchors. The limestone models reinforced by fully bonded bars represent more accurately the case of masses reinforced by fully grouted rockbolts.

The effect of the loading conditions is expressed by the augmentation of the deformability modulus due to the application of the confining pressure. The tangent modulus of the plaster models is much higher in the triaxial tests than in the simple compression tests. This can be explained as the effect of a closer contact of joint surfaces in triaxial conditions. It was also observed that a greater number of joints caused a decrease of the deformability modulus. On the other hand, no dependence between the number of joints and model strength was noted.

In the case of end-fixed bars, the influence of joint orientation was noticed as strength and deformability variations. Augmentation of the angle between the bar and joint caused a diminution of the shear strength of the models due to a lower contribution of the bars. The displacement necessary to mobilize total contribution of the bars was greater, when the value of the angle between the bar and joint was higher.

	Test	n_b -	β o	σ_3 [kPa]	F_3 [kN]	ΔF_1 [kN]	T_b^{max} [kN]	U_j^{Tbm} [mm]	U_j^{max} [mm]
	PL45.01			**0**	0	**165**	**2.35**	**23.1**	-
	PL45.02	8	45	**204**	18	**352**	**2.27**	**11.9**	-
PL SERIE	**PL45.03**			**406**	37	**552**	**2.43**	**10.4**	-
Plaster σ_c = 7.0 MPa	**PL45.04**			**0**	0	**172**	**2.45**	**23.1**	-
ϕ_j = 40 degrees	**PL45.05**	8	45	**238**	21	**368**	**2.06**	**7.0**	-
N_{max} = 3.0 kN	**PL45.06**			**439**	40	**587**	**2.49**	**7.7**	-
	PL60.07			**0**	0	**64**	**3.58**	**22.3**	-
	PL60.08	8	60	**220**	34	**127**	**2.93**	**21.6**	-
	PL60.09			**404**	63	**199**	**3.45**	**16.4**	-
PF SERIE	**PF45.10**	4	45	**0**	0	**220**	**6.26**	**2.32**	**2.74**
Plaster σ_c = 7.0 MPa	**PF45.11**	6	45	**0**	0	**272**	**5.16**	**2.06**	**2.71**
ϕ_j = 40 degrees	**PF60.12**	6	60	**0**	0	***65***	***4.84***	***2.38***	***2.45***
N_{max} = 3.5 kN	**PF60.13**	8	60	**0**	0	**97**	**5.39**	**3.38**	**3.72**
	CE45.14	6	45	**0**	0	**79**	**4.98**	**0.94**	**2.23**
	CE45.15	6	45	**0**	0	**79**	**4.96**	**1.61**	**2.60**
CE SERIE	**CE45.16**	8	45	**198**	18	**125**	**4.42**	**1.36**	**2.76**
Limestone	**CE45.17**	8	45	**395**	36	**159**	**4.59**	**1.44**	**2.55**
σ_c =150 MPa	**CE60.18**	6	60	**0**	0	**44**	**4.61**	**1.24**	**2.07**
ϕ_j = 25 degrees	**CE60.19**	8	60	**0**	0	**59**	**4.65**	**1.13**	**2.17**
N_{max} = 4.9 kN	**CE60.20**	8	60	**397**	62	**113**	**4.74**	**2.10**	**2.63**
	CE60.21	10	60	**402**	63	**130**	**4.87**	**2.21**	**3.12**

Table 4.2 : *Recapitulating of the tests results*

The role played by the strength of the surrounding medium can not be directly established, as the fixing conditions of the bars were different for the tests of two types of specimen materials. It seems, however, that if the material is weak (i.e., plaster), the displacements necessary for mobilization of the total strength of the bars are greater.

The strength of the models increases proportionally to the cross-sectional area of the reinforcing steel bars. Displacements at the failure are independent of the number of bars. In other words, the number of bars is not a parameter influencing the deformability of reinforced joint.

It should be finally stated that weak material reinforced by pointwise fixed bars constitutes a flexible system, whereas hard material reinforced by fully bonded bars forms a rigid system.

Chapter 5

Analytical Formulation of the Behaviour of Reinforced Joint

Analysis of the mechanical behaviour of the reinforced joint begins with the description of the action mode of the reinforcing bar. The relation between the force mobilized at the point where the bar intersects the joint plane and the corresponding displacement should be established. The deformational process of the bar should be taken into account, and the equilibrium of the system must be satisfied.

The analytical approach developed in this chapter needs the a priori knowledge of the direction of the displacement, U_o. This is defined by β, the angle between the displacement direction and the bar axis. According to the sign convention presented in Figure 5.1, the axial force in the bar is positive (tension) for the range of β values between $-\pi/2$ and $+\pi/2$. If the angle lies between $\pi/2$ and $3\pi/2$, the axial force in the bar is negative (compression). Though the axial force can be negative in certain cases, the actual study is limited to the most common situation, where the bar is inclined in the displacement direction and tensioned.

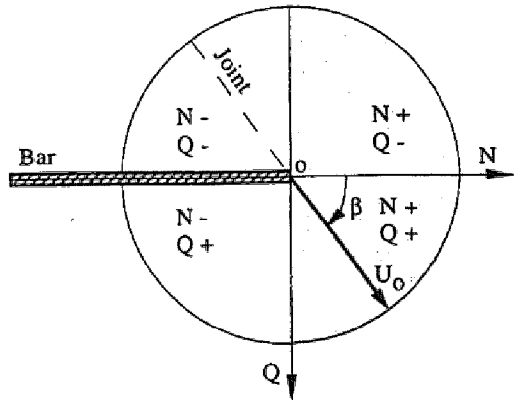

Figure 5.1 : *Convention of signs*

5.1. Loadings and deformations of a bar subjected to a displacement at its extremity

If the extremity of the fixed bar is subjected to a displacement of known direction, the bar is deformed and the reaction of the surrounding material is mobilized at the same time (Figure.5.2). The bar is thus, axially and transversely loaded by a set of forces composed of axial force, N, transversal force, Q, and bending moment, M. At the point of force application (point O), the bar curvature is equal to zero and the mobilized force is composed of normal and transversal forces. It can be observed in the general case that the directions of the resultant force and the displacement are not coaxial.

As the loading increases, the surrounding medium (i.e., rock or grout) supplies a reaction, p(x),acting on a bolt length which progressively increases until the bolt yields.

The failure of the bar can thus, be produced by the combination of normal and transversal forces at the point O or by the combination of the axial force and the bending moment at the point A, where the moment is maximal and the transversal force is equal to zero.

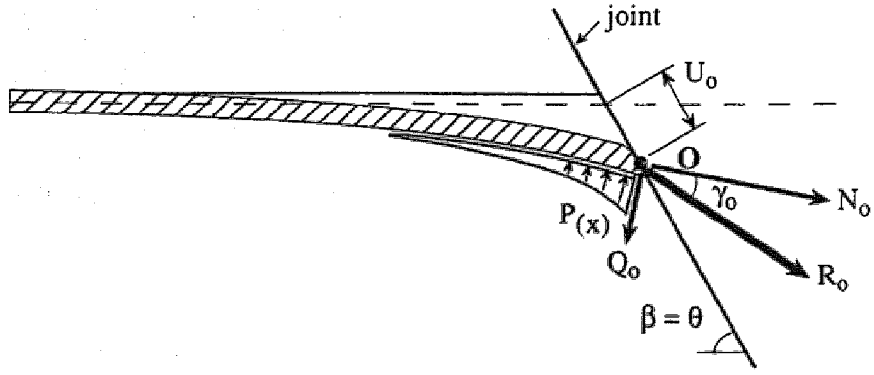

Figure 5.2 : *Loading and deformation of the bar*

It was observed in experiments performed by numerous authors **(Di Prisco, 1989)** that the relation between the resultant force mobilized in the bar and the associated joint displacement presents non-linearity. This is partially due to yielding of the bar and the rock (constitutive non-

linearity) and partially due to the development of large displacements (geometrical non-linearity). The combination of these two non-linearity sources leads to the study of the bar equilibrium in two phases. In the first, the bar is in elastic state, whereas in the second it is partially or completely yielded.

When the bar is in elastic state, the distribution of the normal stresses in the section of the maximum bending moment is linear (Figure 5.3a). The displacements are sufficiently small, and thus, the formulation in small displacements can be applied in this case.

As the bar reaches the yield limit in the section of the maximum bending moment, the distribution of normal stresses is further non-linearized and in the final state it becomes bi-rectangular (Figures 5.3b and 5.3c). The displacements significantly grow in comparison to the diameter of the bar and its stiffness progressively decreases.

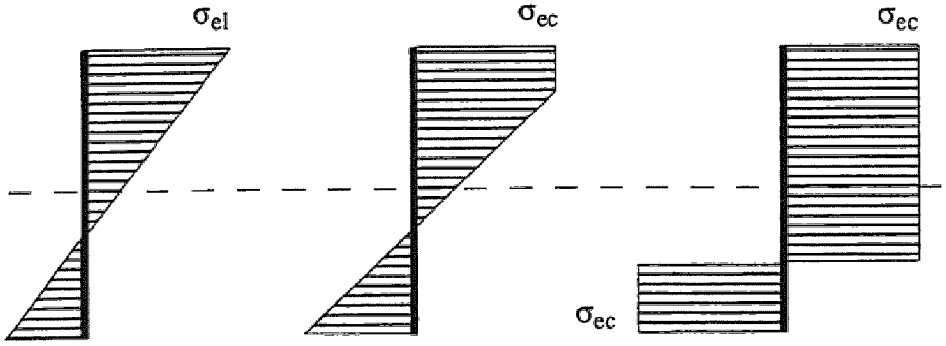

a- bar in elastic state *b- partially yielded bar* *c- completely yielded bar*

Figure 5.3 : *Normal stress distribution at the point of maximum moment*

5.2. General hypotheses and static system

The bar is considered as a beam of semi-infinite length, loaded at its end (at point where bar intersects joint plane) by shear force, Q_o, and axial force, N_o (Figure 5.4). The reaction of the surrounding medium (rock or grout) is

exerted along the bar, but the distribution of the reaction pressure is a priori unknown. It is assumed that the behaviour of the surrounding medium is perfectly rigid-plastic, and that the reaction pressure is constant until the point of maximum bending moment (point A). It is also supposed that the anchoring length of the bar is sufficient to avoid any failure by lack of pull out strength.

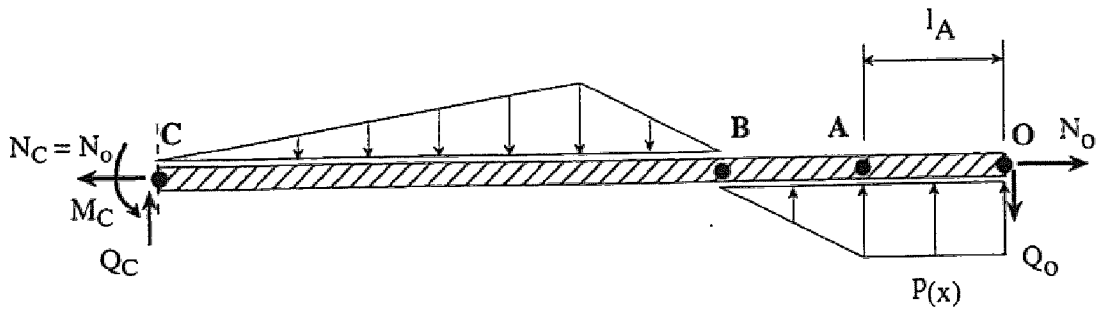

Figure 5.4 : *System of loading of the bar*

The loading length of the bar is a priori unknown. Yet, if the equilibrium of forces acting perpendicularly to the bar is studied, the distance l_A , from point O to point A, can be determined. Point A, is the point of zero shear force and maximum bending moment. It can be written :

$$\sum_y = 0 \Rightarrow Q_o = p_u l_A \qquad (5.1)$$

and :

$$l_A = \frac{Q_o}{p_u} \qquad (5.2)$$

where p_u is the maximum pressure of the rock reaction per unit length.

The bending moment, M_A, acting at point A, can be expressed as a function of the shear force, Q_o, by applying the principle of moments equilibrium :

$$\sum_{M} = 0 \Rightarrow M_A = Q_o\, l_A - p_u \frac{{l_A}^2}{2} \qquad (5.3)$$

M_A is calculated from the above formula as :

$$M_A = \frac{{Q_o}^2}{2\, p_u} \qquad (5.4)$$

It is also assumed that :

- bar material exhibits elastic - perfectly plastic behaviour
- rock reaction is normal to the bar, thus, friction at the bar-rock interface is neglected and the axial force along the deformed length of the bar is constant,
- cross-sections remain planar after deformation (Bernoulli's hypothesis)
- the shear strains of the bar are neglected.

5.3. Elastic limit and failure criteria of the bar

5.3.1. Elastic limit of the bar

If only axial force acts on the bar, then the distribution of normal stresses in any cross-section is uniform. In the case of composed bending loads, normal stress σ acting on external and internal fibers of the bar can be expressed as follows :

$$\sigma_{max} = \frac{M}{W_b} \pm \frac{N}{A_b} \qquad (5.5)$$

where, M : bending moment,
N : axial force,
A_b : area of bar cross-section,
W_b : section modulus,
D_b : diameter of bar,

and : $A_b = \pi D_b^2 / 4$
$W_b = \pi D_b^3 / 32$

If M is replaced by the formula (5.4), the relation between axial force, N_{oe}, and shear force, Q_{oe}, can be established when the external fiber reaches elastic limit at point A :

$$N_{oe} = A_b \left(\sigma_{el} - \frac{Q_{oe}^2}{2\ p_u\ W_b} \right) \qquad (5.6)$$

where σ_{el} signifies stress at the elastic limit of the bar material.

Replacing A_b and W_b in the above formula by functions expressing their dependencies on the diameter of the bar one obtains the following formula :

$$N_{oe} = \frac{\pi\ D_b^2\ \sigma_{el}}{4} - \frac{4\ Q_{oe}^2}{p_u\ D_b} \qquad (5.7a)$$

or :

$$Q_{oe} = \frac{1}{2} \sqrt{p_u\ D_b \left(\frac{\pi\ D_b^2\ \sigma_{el}}{4} - N_{oe} \right)} \qquad (5.7b)$$

5.3.2. Failure criteria for the bar

As the bending moment, the normal and the shear forces cannot reach the elastic limit in the same point, two cases can be studied :

- The failure of the bar at point O, resulting from the combined action of the axial force, N_{of}, and the shear force, Q_{of} ($M_o = 0$), is defined by the following interaction formula **(Neal, 1977)** :

$$\left(\frac{N_{of}}{N_p}\right)^2 + \left(\frac{Q_{of}}{Q_p}\right)^2 = 1 \qquad \textbf{(5.8a)}$$

and hence :

$$N_{of} = N_p \sqrt{1 - \left(\frac{Q_{of}}{Q_p}\right)^2} \qquad \textbf{(5.8b)}$$

or:

$$Q_{of} = Q_p \sqrt{1 - \left(\frac{N_{of}}{N_p}\right)^2} \qquad \textbf{(5.8c)}$$

In the above formulae, N_p and Q_p represent the values of the axial and the shear forces at the failure limit when they act separately.

- The failure of the bar at point O, occurring by the combination of the axial force and the bending moment ($Q_A = 0$), is determined by the following interaction formula :

$$\frac{M_A}{M_p} + \left(\frac{N_A}{N_p}\right)^2 = 1 \qquad \textbf{(5.9a)}$$

where M_p is the value of plastic bending moment when other loadings are absent.

If $N_A = N_o$ is assumed and M_A is replaced by the formula (5.4), then the following expression is obtained :

$$\frac{Q_{of}^2}{2\ p_u\ M_p} + \left(\frac{N_{of}}{N_p}\right)^2 = 1 \qquad \textbf{(5.9b)}$$

and :

$$N_{of} = N_p \sqrt{1 - \frac{Q_{of}^2}{2\ p_u\ M_p}} \qquad \textbf{(5.10a)}$$

and also :

$$Q_{of} = \sqrt{2\ p_u\ M_p \left[1 - \left(\frac{N_{of}}{N_p}\right)^2\right]} \qquad \textbf{(5.10b)}$$

If it is assumed that the bar material obeys Tresca's criterion, then the yield stress in tension is two times that of simple shear. For a circular cross-section, the forces at the failure can be expressed as follows :

$$M_p = 1.69\ W_b\ \sigma_{ec} = 1.69\ \frac{\pi\ D_b^3}{32}\ \sigma_{ec} \qquad \textbf{(5.11)}$$

$$N_p = A_b\ \sigma_{ec} = \frac{\pi\ D_b^2}{4}\ \sigma_{ec} \qquad \textbf{(5.12)}$$

$$Q_p = \frac{1}{2}\ A_b\ \sigma_{ec} = \frac{\pi\ D_b^2}{8}\ \sigma_{ec} \qquad \textbf{(5.13)}$$

where σ_{ec} indicates the stress at the yield point of bar material

Introducing the expressions for plastic forces to the equations 5.8a, 5.8b, 5.10a and 5.10b, one obtains two failure criteria for the bar :

- For failure of the bar at point O :

$$N_{of} = \frac{\pi D_b^2}{4} \sigma_{ec} \sqrt{1 - 64 \left(\frac{Q_{of}}{\pi D_b^2 \sigma_{ec}} \right)^2} \qquad \textbf{(5.14a)}$$

and :

$$Q_{of} = \frac{\pi D_b^2}{8} \sigma_{ec} \sqrt{1 - 16 \left(\frac{N_{of}}{\pi D_b^2 \sigma_{ec}} \right)^2} \qquad \textbf{(5.14b)}$$

- For failure of the bar at point A :

$$N_{of} = \frac{\pi D_b^2}{4} \sigma_{ec} \sqrt{1 - 16 \frac{Q_{of}^2}{p_u \, 1.69 \, \pi D_b^3 \sigma_{ec}}} \qquad \textbf{(5.15a)}$$

and :

$$Q_{of} = \sqrt{p_u \, 1.69 \frac{\pi D_b^3}{16} \sigma_{ec} \left[1 - 16 \left(\frac{N_{of}}{\pi D_b^2 \sigma_{ec}} \right)^2 \right]} \qquad \textbf{(5.15b)}$$

Equations 5.7b, 5.14b and 5.15b are represented in the coordinate system N_o - Q_o in Figure 5.5. The elastic limit (eq. 5.7b) is a parabola with the center situated in the N_o axis, whereas the failure criteria for the bar (eqs.

5.14b and 5.15b) are two ellipses, whose minor axes coincide with the shear force axis.

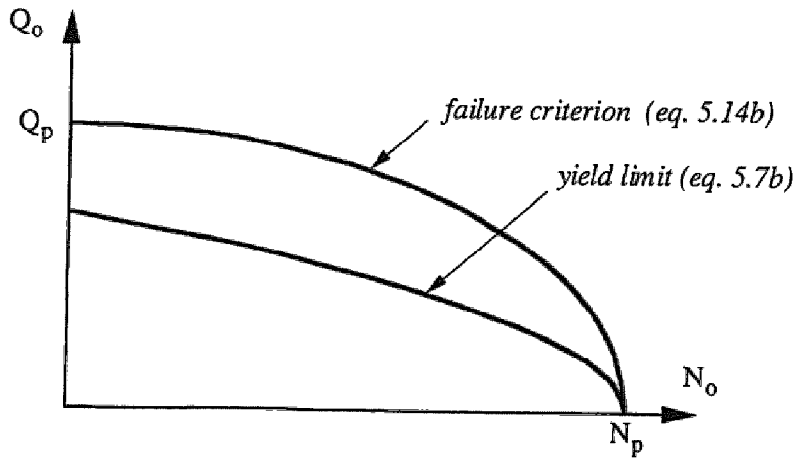

Figure 5.5 : *Elastic limit and failure criteria of the bar*

Comparing the lengths of the minor axes ($N_{of} = 0$) of the ellipses it is possible, for a given bar, to determine in a theoretical manner the failure mode depending on the rock reaction pressure.

If $p_u < 0.46\ D_b\ \sigma_{ec}$: failure occurs at point A (plastic hinge)

If $p_u = 0.46\ D_y\ \sigma_{ec}$: failure occurs simultaneously at points A and O

If $p_u > 0.46\ D_b\ \sigma_{ec}$: failure occurs at point O

The determination of the reaction pressure as a function of simple compressive strength of the rock will be considered later, in section 5.9. In practice, plastic hinges almost ever appear before the bar breaks at point O.

5.4. Behaviour of the bar in the elastic state

5.4.1. Equilibrium of beam section transversely and axially loaded

If a section of beam (as presented in Figure 5.6) is simultaneously loaded by transversal forces (distributed or punctual force) and by an axial force, the elastic line equation can be written in the following form :

$$EI \frac{d^4v}{dx^4} + N \frac{d^2v}{dx^2} - p_{(x)} = 0 \qquad (5.16)$$

where $v_{(x)}$ is a function describing the deformed transversal line of the bar.

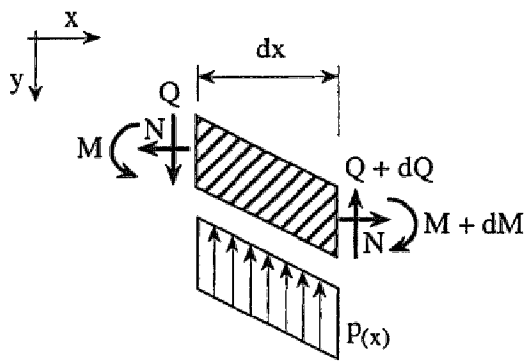

Figure 5.6 : *Equilibrium of a beam section*

If the axial force is not constant, but results from the deformation of the bar, then the above differential equation has the form :

$$EI \frac{d^4v}{dx^4} + EA_b \frac{d^2v}{dx^2}\left(\frac{dv}{dx}\right)^2 - p_{(x)} = 0 \qquad (5.17)$$

where, E = elastic modulus of the bar,
I = moment of inertia of the bar = $\pi D_b^4 / 64$

Such a differential equation has no simple solution. Therefore, it is proposed, based on the energetic principle, to apply a variational formulation to obtain an approximate solution.

5.4.2. Variational formulation of the bar equilibrium

Based on the principle of the virtual work, it is necessary to express the internal strain energy, as well as the external work of the loading. It is therefore required to choose, taking into account the boundary conditions, a function describing the deformed form of the bar. The total complementary energy of the system is thus calculated and the unknown parameters of the function are determined by energy minimization. This is the Rayleigh-Ritz method which constitutes the base of the Finite Element method. The principles of the method are presented by **Washizu (1975)**.

The quality of the solution depends on the ability of the selected function to describe the deformation of the bar. In the present case, the solution of the differential equation for a semi-infinite beam **(Hetenyi, 1946)** is chosen. This function properly describes transversal displacements observed by **Di Prisco (1989)**. It has the form :

$$v_{(x)} = v_o \, e^{-x/l_o} \cos\left(\frac{x}{l_o}\right) \qquad \textbf{(5.18a)}$$

and hence,

$$v'_{(x)} = -\frac{v_o}{l_o} \, e^{-x/l_o} \left[\cos\left(\frac{x}{l_o}\right) + \sin\left(\frac{x}{l_o}\right)\right] \qquad \textbf{(5.18b)}$$

$$v''_{(x)} = \frac{2\,v_o}{l_o^2} \, e^{-x/l_o} \sin\left(\frac{x}{l_o}\right) \qquad \textbf{(5.18c)}$$

It is supposed that the axial displacements vary linearly along the bar. As was previously postulated, the axial force is constant along the deformed part of the bar :

$$u_{(x)} = -u_o \left(1 - \frac{2\,x}{3\,\pi\,l_o} \right) \qquad \textbf{(5.19a)}$$

and hence,

$$u'_{(x)} = \frac{2\,u_o}{3\,\pi\,l_o} \qquad \textbf{(5.19b)}$$

$$u''_{(x)} = 0 \qquad \textbf{(5.19c)}$$

The $v_{(x)}$ function, as well as its first and second order derivatives normalized by their respective parameters, are shown in Figure 5.7.

The characteristic length, l_o, of the bar can then be expressed as a function of the maximum bending moment location :

$$l_o = \frac{4}{\pi}\, l_A \qquad \textbf{(5.20)}$$

It should be noticed that the axial and transversal displacements are equal to zero at a distance equal to $3\pi l_o / 2 = 6\, l_A$.

Calculation of the energy balance (described in details in appendix I) gives the following expressions for the internal stain energy, U, and for the external work, W :

$$U = \frac{E\,A_b\,u_o^2}{3\,\pi\,l} + \frac{E\,I\,v_o^2}{4\,l^3}$$

$$W = N_o u_o + Q_o v_o - p\, v_o\, l \left(\frac{1}{2} + \frac{\sqrt{2}\, e^{-\pi/4} - 2e^{-\pi/2}}{\pi} \right)$$

It should be pointed out that the linearized expression of the curvature was used for the elastic stage. It corresponds to a formulation in small strains, expressing the proportionality between the bending moment and the curvature of the bar. It is generally admitted that such a simplification is justified, if rotations are smaller than 0.1 radian (~ 6 degrees).

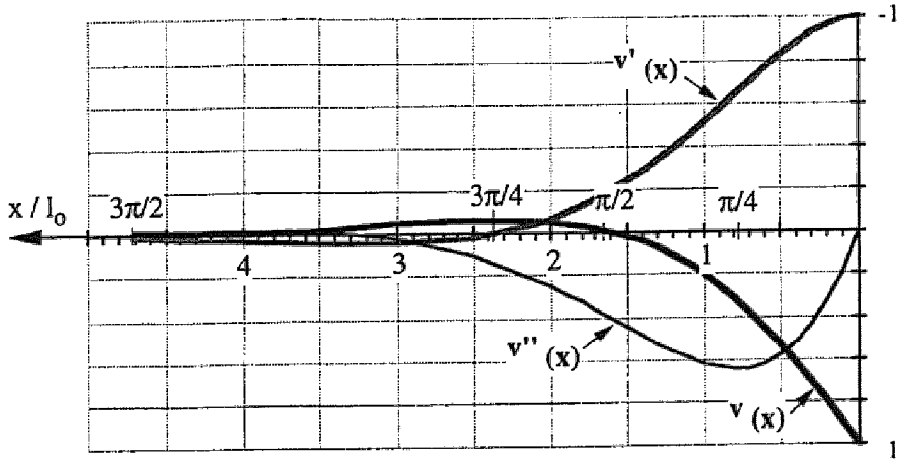

Figure 5.7 : *Displacement function and its derivatives*

5.4.3. Relationships between axial and transversal force

Expressions for axial and transversal displacements can be obtained by minimization of total complementary energy. In appendix, I details of the method and execution of calculations are given. Figure 5.8 presents the deformations of the bar and the forces acting in it.

Axial displacement, u_o, is expressed by the equation :

$$u_o = \frac{6\, N_o\, Q_o}{E\, A_b\, p_u} = \frac{24\, N_o\, Q_o}{E\, p_u\, \pi\, D_b^2} \qquad (5.21)$$

and transversal displacement, v_o, as :

$$v_o = \frac{128\, Q_o^4\, b}{E\, I\, \pi^3\, p_u^3} = \frac{8192\, Q_o^4\, b}{E\, \pi^4\, p_u^3\, D_b^4} \qquad (5.22)$$

where b (= 0.27) is a constant term defined in appendix I.

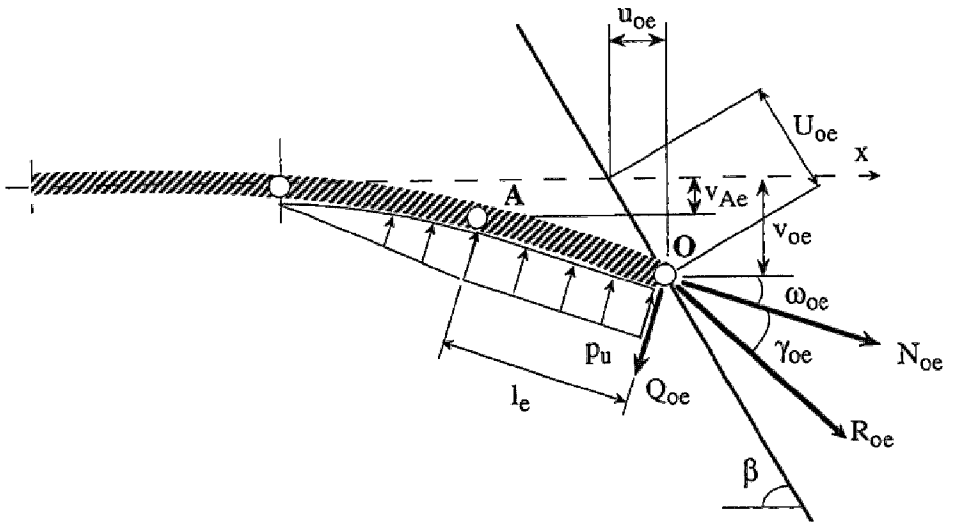

Figure 5.8 : *Loadings and deformation of the bar at the elastic limit*

Knowing, β, the angle between the bar axis and the direction of displacement, the following kinematic condition can be written :

$$tg\beta = \frac{v_o}{u_o} \qquad (5.23)$$

and further :

$$tg\beta = \frac{1024\, Q_o^3\, b}{3\, N_o\, p_u^2\, \pi^3\, D_b^2} \qquad (5.24)$$

The relation between the axial and the transversal force is obtained from the above equation, for the bar in elastic conditions :

$$N_o = \frac{1024\ Q_o^3\ b}{3\ p_u^2\ \pi^3\ tg\beta\ D_b^2} \qquad (5.25)$$

or :

$$Q_o = \sqrt[3]{\frac{3\ N_o\ p_u^2\ \pi^3\ tg\beta\ D_b^2}{1024\ b}} \qquad (5.26)$$

The determination of the elastic limit of N_{oe} and Q_{oe} is performed by calculation of the intersection point between equation 5.26 and 5.7b, which defines the elastic limit. The following third order equation is obtained :

$$Q_{oe}^3 + Q_{oe}^2\left(\frac{3\ p_u\ \pi^3\ D_b\ tg\beta}{256\ b}\right) - \left(\frac{3\ p_u^2\ \pi^4\ D_b^4\ tg\beta\ \sigma_{el}}{4096\ b}\right) = 0 \qquad (5.27)$$

Analytic solution of the above equation is done by calculation of the discriminant Δ.

$$\Delta = A^3 + B^2 \qquad (5.28)$$

where :

$$A = -\frac{\left(\left(\frac{3\ p_u\ \pi^3\ D_b\ tg\beta}{256\ b}\right)\right)^2}{9} \qquad (5.29)$$

$$B = \frac{27\left(\frac{3\ p_u{}^2\ \pi^4\ D_b{}^4\ tg\beta\ \sigma_{el}}{4096\ b}\right) - 2\left(\frac{3\ p_u\ \pi^3\ D_b\ tg\beta}{256\ b}\right)^3}{54} \qquad \textbf{(5.30)}$$

If the discriminant is greater than zero, then :

$$Q_{oe} = \sqrt[3]{B + \sqrt{\Delta}} + \sqrt[3]{B - \sqrt{\Delta}} - \frac{p_u\ \pi^3\ D_b\ tg\beta}{256\ b} \qquad \textbf{(5.31)}$$

In the case of the discriminant lower than zero :

$$Q_{oe} = 2\left[\sqrt{-A}\ \cos\left(\frac{1}{3}\ \arccos\left(\frac{B}{\sqrt{-A^3}}\right)\right)\right] - \frac{p_u\ \pi^3\ D_b\ tg\beta}{256\ b} \qquad \textbf{(5.32)}$$

The development of the shear and axial forces in the elastic domain, as well as the resultant force in the bar, are presented in Figure 5.9.

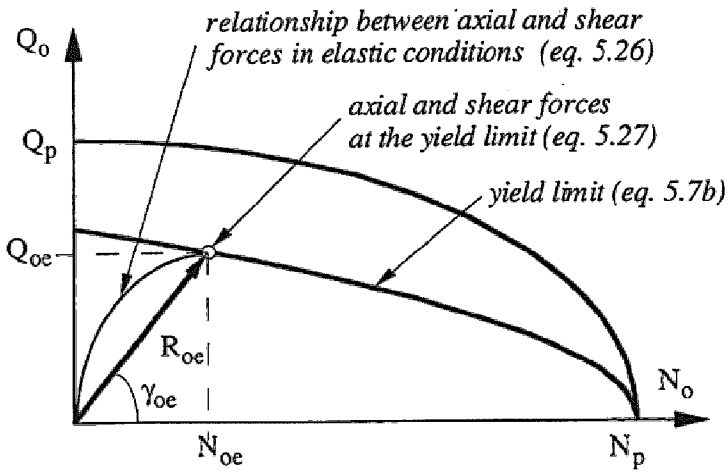

Figure 5.9 : *Evolution of the shear and axial forces in elastic domain*

5.4.4. Calculation of rotation and displacement of the bar extremity

Replacing v_o by the value of its first order derivative (eq.5.18b) and successively assuming $x = 0$ and $x = \pi l_o /4$, one obtains rotation of the bar at point O and at point A, respectively :

$$\omega_{oe} = -\frac{32\ Q_{oe}^{3}\ b}{E\ I\ \pi^2\ p_u^{2}} = -\frac{2048\ Q_{oe}^{3}\ b}{E\ p_u^{2}\ \pi^3\ D_b^{4}} \qquad (5.33)$$

$$\omega_{Ae} = -\frac{32\ Q_{oe}^{3}\ b}{E\ I\ \pi^2\ p_u^{2}} \left(e^{-\pi/4}\ \sqrt{2}\right) = 0.645\ \omega_{oe} \qquad (5.34)$$

In the same manner, when v_o is replaced in the displacement expression (eq.5.18a) in which $x = 0$ and $x = \pi l_o/4$ are successively introduced, the transversal displacement of the bar at point O and at point A are respectively obtained :

$$v_{oe} = \frac{128\ Q_{oe}^{4}\ b}{E\ I\ \pi^3\ p_u^{3}} = \frac{8192\ Q_{oe}^{4}\ b}{E\ p_u^{3}\ \pi^4\ D_b^{4}} \qquad (5.35)$$

$$v_{Ae} = \frac{128\ Q_{oe}^{4}\ b}{E\ I\ \pi^3\ p_u^{3}} \left(e^{-\pi/4}\ \frac{\sqrt{2}}{2}\right) = 0.322\ v_{oe} \qquad (5.36)$$

The resulting displacement in the joint direction is thus expressed by :

$$U_o = \frac{v_o}{\sin\beta} \qquad (5.37)$$

As the bar attains the elastic limit, the following equation can be written :

$$U_{oe} = \frac{8192\ Q_{oe}^{4}\ b}{E\ \pi^{4}\ D_b^{4}\ p_u^{3}\ \sin\beta} \qquad (5.38)$$

5.5. Behaviour of the bar in the plastic state

5.5.1. Complementary hypotheses

After the elastic limit is reached at the point of maximum bending moment (point A), the bar yields and plastic hinge is progressively developed.

It can be assumed that:

- The position of the plastic hinge is fixed with respect to the direction of x (see **Di Prisco 1989**),
- The deformed shape of the bar between points O and A is rectilinear,
- The axial strain, ε_x, is constant along the section O-A.

Figure 5.10 presents the deformation process of the bar as well as the forces, which load it.

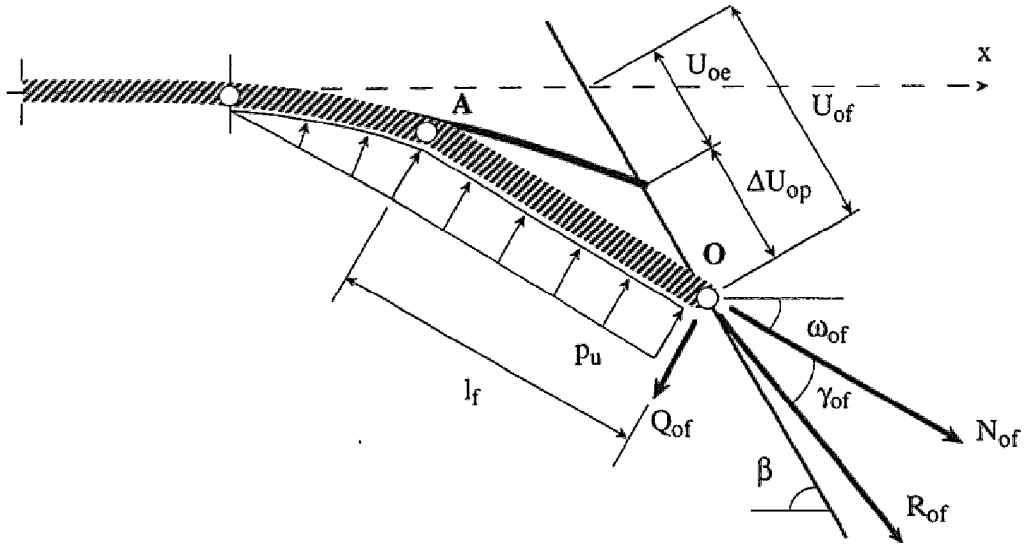

Figure 5.10 : *Loadings and deformation of the bar in plastic domain*

5.5.2. Relationships between normal and shear force

After the elastic limit is reached, it can be admitted that the bending moment at point A does not further increase, thus, the shear force, Q_o, remains constant up to the failure :

$$Q_{of} = Q_{oe} \tag{5.39}$$

The axial force, N_{of}, at the failure is obtained by calculation of the intersection of the straight line $Q_o = Q_{of}$ with the involved failure criterion.

If the failure occurs at point A, then the corresponding axial force is expressed by the combination of the axial force and the bending moment :

$$N_{of} = \frac{\pi D_b^2}{4} \sigma_{ec} \sqrt{1 - 16 \frac{Q_{oe}^2}{p_u \, 1.69 \, \pi \, D_b^3 \, \sigma_{ec}}} \tag{5.40}$$

To the contrary, if the failure occurs at point O, the axial force at the failure can be expressed by the combination of the axial and shear forces :

$$N_{of} = \frac{\pi D_b^2}{4} \sigma_{ec} \sqrt{1 - 64 \left(\frac{Q_{oe}}{\pi D_b^2 \sigma_{ec}} \right)^2} \tag{5.41}$$

The development of the shear and axial forces in the plastic domain, as well as the resultant force in the bar, are presented in Figure 5.11.

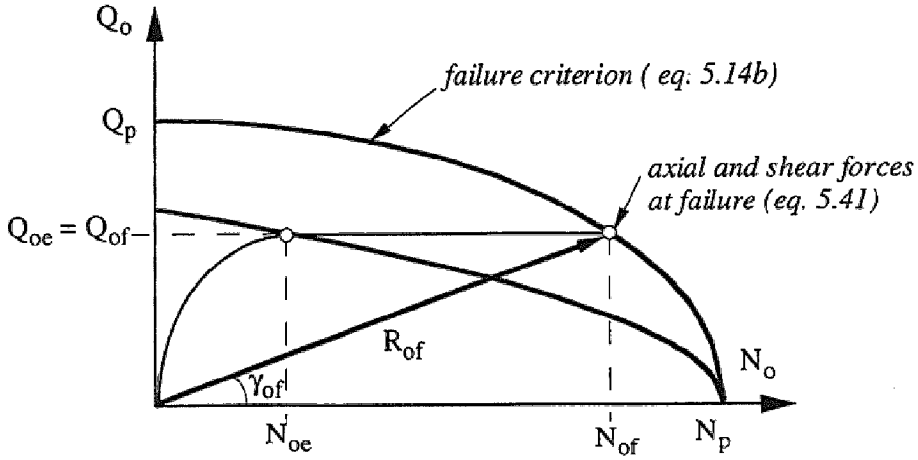

Figure 5.11 : *Evolution of the axial force in plastic domain*

Calculation of rotation and displacement of the bar extremity

ıcements significantly increase in the plastic domain. The following la expresses the bar's axial deformations, taking into account the large cement formulation :

$$\varepsilon_x = u'_{(x)} + \frac{1}{2} v'^2_{(x)}$$

isplacements calculation at the bar extremity is performed, considering ıe bar deformation reaches failure strain along the A-O section. Close ximation of the above differential equation is obtained by simple ətrical considerations, and applying the law of sine :

$$\frac{\Delta U_{op}}{\sin \Delta\omega_{op}} = \frac{l_f}{\sin\left(\pi - \beta + \omega_{oe}\right)} = \frac{l_e}{\sin\left(\beta - \Delta\omega_{op}\right)} \qquad \textbf{(5.42)}$$

', ΔU_{op} : increment of plastic displacement,
$\Delta\omega_{op}$: increment of plastic rotation,
l_e : elastic length of bar,
l_f : plastic length of bar.

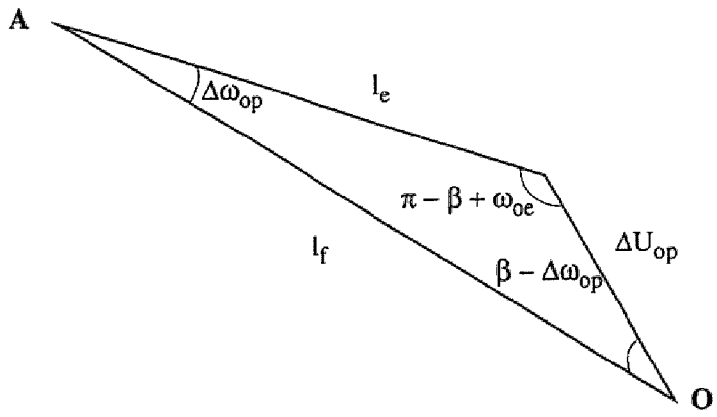

Figure 5.12 : *Simplified geometric representation*

Neglecting the term of elastic rotation ω_{oe} and considering that $\sin(\pi - \beta) = \sin\beta$ one obtains :

$$l_f \sin\left(\beta - \Delta\omega_{op}\right) = l_e \sin\beta \qquad (5.43)$$

and further :

$$l_f \left(\sin\beta \cos\Delta\omega_{op} - \cos\beta \sin\Delta\omega_{op}\right) = l_e \sin\beta \qquad (5.44)$$

Assuming $\sin\Delta\omega_{op} = \sqrt{1 - \cos^2\Delta\omega_{op}}$, the following second order equation is obtained :

$$\cos^2\Delta\omega_{op} - 2\frac{l_e}{l_f}\sin^2\beta\cos\Delta\omega_{op} + \left[\left(\frac{l_e}{l_f}\right)^2 \sin^2\beta - \cos^2\beta\right] = 0 \qquad (5.45)$$

The positive root of the above equation gives the increment of rotation angle $\Delta\omega_{op}$ at point O :

$$\Delta\omega_{op} = \arccos\left[\frac{l_e}{l_f}\sin^2\beta \pm \sqrt{\cos^2\beta\left(1 - \left(\frac{l_e}{l_f}\right)^2\sin^2\beta\right)}\right] \quad (5.46)$$

with $l_f = l_e\,(1 + \varepsilon_f)$ (5.47)

where ε_f is the failure strain of the bar material. The plastic displacement increment is given as follows :

$$\Delta U_{op} = \frac{Q_{oe}\ \sin\Delta\omega_{op}}{p_u\ \sin\left(\beta - \Delta\omega_{op}\right)} \quad (5.48)$$

The total deformation at failure is equal to the sum of the elastic and the plastic deformations. The rotation, ω_{of}, and the displacement, U_{of}, of the bar extremity at failure are expressed by the following formulae :

$$\omega_{of} = \omega_{oe} + \Delta\omega_{op} \quad (5.49)$$

$$U_{of} = U_{oe} + \Delta U_{op} \quad (5.50)$$

5.5.4. Reduction of the bar rigidity

The description of the displacements development between the elastic limit and failure of the bar is rather complex, as strains are, in fact, not uniform

in the maximum moment section (see Figure 5.3). The external fiber of the bar is yielded, whereas the middle part of the bar cross-section is still in the elastic conditions. On the other hand, the axial deformation varies along the section O–A. Additionally, the effect of the reduction of the bar diameter is neglected.

Calculation of the bar plastic lengthening as a function of the increment of the axial force is realized taking the mean axial rigidity of the bar :

$$\Delta N_o = K^* \Delta l_p \qquad (5.51)$$

where, ΔN_o : increment of the axial force in the bar,
Δl_p : plastic lengthening of the bar,
K^* : mean axial rigidity of the bar.

In the plastic domain (between the elastic limit and failure), the axial rigidity of the bar decreases due to the lowering of the material modulus. Axial rigidity, K_e, of the bar at the elastic limit ($N_o = N_{oe}$) is expressed as follows:

$$K_e = \frac{E\ A_b}{6\ l_e} \qquad (5.52a)$$

where, A_b : cross-sectional area of the bar,
E : elastic modulus of the bar,
l_e : elastic length of the bar.

Secant axial rigidity, K_f, of the yielded bar section (O-A) at failure is calculated as :

$$K_f = \frac{E_f\ A_b}{l_e} \qquad (5.52b)$$

E_f is the secant deformability modulus of the material at failure. Neglecting the elastic axial deformation, one obtains E_f from the following formula :

$$E_f = \frac{N_{of} - N_{oe}}{A_b \ \varepsilon_f} \qquad (5.53)$$

According to **Neal (1977)**, the diminution of the rigidity between the elastic limit and the failure of the bar can be described by a power function. Dividing the plastic domain into n intervals, secant rigidity can be calculated for each interval from the formula:

$$K_i^* = \frac{K_{i-1}^*}{(K_e \ / \ K_f)^{(1/n)}} \qquad (5.54)$$

where, K^*_i : axial rigidity at the considered step,
K^*_{i-1} : axial rigidity at the preceding step,
n : number of intervals between elastic limit and failure.

Figure 5.13a shows the evolution of the axial force as a function of the plastic lengthening of the bar for 11 calculation intervals, whereas Figure 5.13b presents the corresponding variation of the axial rigidity as a function of the axial force mobilized in the bar.

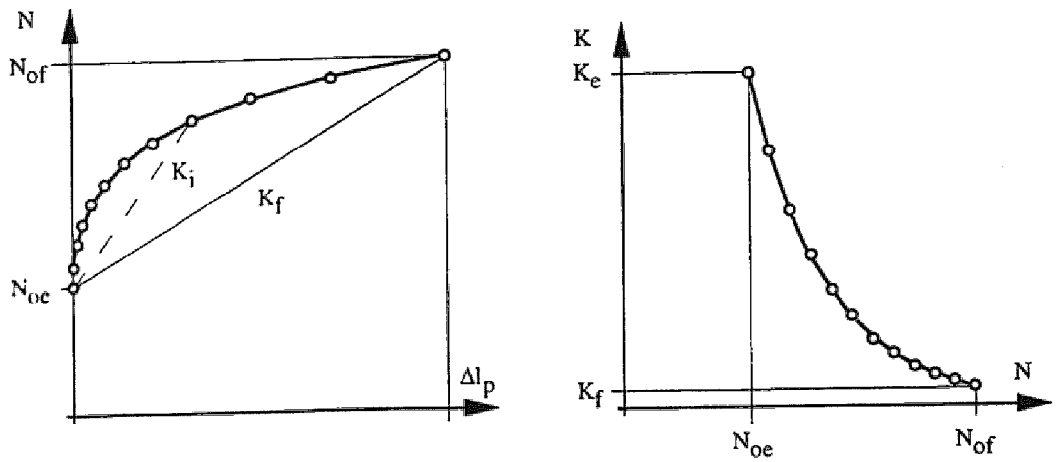

a- evolution of the axial force in function of plastic lengthening

b- decreasing of the axial rigidity in function of the axial force

Figure 5.13 : *Variation of the axial force and the axial rigidity in the plastic domain*

5.6. Bar contribution to the joint shear strength and the associated displacement

Figure 5.14 shows the decomposition of the different forces acting in the extremity of the bar and associated geometrical quantities.

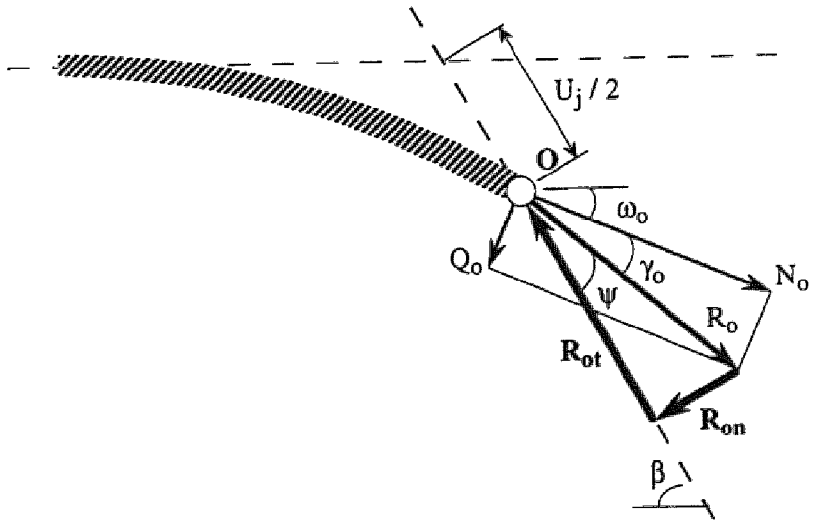

Figure 5.14 : *Projection of forces on the joint plane*

If shear and axial forces acting in the bar during the loading process are known, the resultant force, R_o, mobilized in the bar can be simply calculated using the following formula :

$$R_o = \sqrt{Q_o^2 + N_o^2} \qquad (5.55)$$

As can be seen in Figure 5.14, the direction of the forced displacement, U_j, is not coaxial with the direction of the resultant force, R_o. The angle ψ between these two directions is equal to :

$$\psi = \beta - \omega_o - \gamma_o$$

where γ_o is the angle between the direction of R_o and the axis of the bar after deformation. This angle is expressed as :

$$\gamma_o = \text{arctg}\left(\frac{Q_o}{N_o}\right) \tag{5.56}$$

In the case of smooth joints, the shear strength is generally determined by the Mohr-Coulomb failure criterion. The contribution of the bar can be found by the decomposition of the resultant force into the force R_{ot} parallel to the joint and the force R_{on} normal to the joint (Figure 5.14) :

$$R_{ot} = R_o \cos\left(\beta - \omega_o - \gamma_o\right) \tag{5.57}$$

$$R_{on} = R_o \sin\left(\beta - \omega_o - \gamma_o\right) \tag{5.58}$$

The total contribution, T_b, of the bar to the increase of shear strength of the joint is expressed by the formula :

$$\boxed{T_b = R_{ot} + R_{on} \text{ tg } \phi_j} \tag{5.59}$$

where ϕ_j is the joint friction angle.

The joint displacement corresponding to the maximum bar contribution is equal to two times the displacement of the point O :

$$\boxed{U_j = 2\ U_o} \tag{5.60}$$

5.7. Strength and deformability of the reinforced joint

5.7.1. Reinforcement cohesion and confining effects

The bar contribution to the shear strength of the joint is decomposed in term of cohesion and in term of confinement which are respectively connected to the parallel and the perpendicular component to the joint of the force mobilized in the bar. These two components can be simply calculated by the following formulae :

$$\Delta c_b = \frac{R_{ot}}{A_j} \qquad (5.61)$$

$$\Delta \sigma_b = \frac{R_{on}}{A_j} \qquad (5.62)$$

where, Δc_b : cohesion of reinforcement,
$\Delta \sigma_{nb}$: effect of confinement,
A_j : joint surface area.

5.7.2. Tangential and normal stiffness of the reinforced joint

Tangential stiffness of the reinforced joint is defined by the secant modulus at failure :

$$k_t = \frac{R_{ot}}{A_j \; U_{jf}} \tag{5.63}$$

Indirect normal stiffness, which expresses an increase of the normal stress acting on the joint during the tangential displacement is given as :

$$k_{nt} = \frac{R_{on}}{A_j \; U_{jf}} \tag{5.64}$$

5.8. Determination of the limit pressure of the rock reaction

The force mobilized in the bar and the associated displacement depend on the reaction provided on the bar by the surrounding material (rock or grout). Most of the methods allowing for analytical calculation of the bearing pressure are based on the theory of the expansion of a cylindrical hole. It can be stated that during the progressive displacement of the bar, the initially circular section becomes an oval. At the contact of the bar, the surrounding material is subjected to a multiaxial state of stress (Figure 5.15).

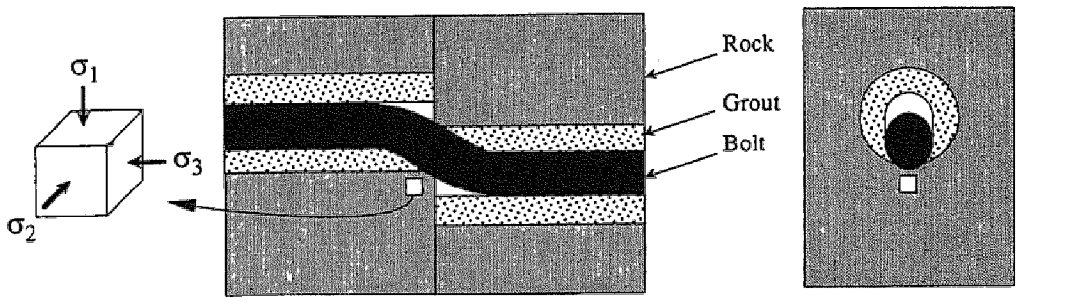

Figure 5.15 : *Deformation of the bar and state of stress in the grout*

The laboratory tests show that the elastic modulus of concrete varies insignificantly with confining stress, whereas strength is strongly influenced. Numerous authors presented results of tests realized on cubic specimens in triaxial compression. These results allow the establishment of the following law :

$$\frac{\sigma_1}{\sigma_c} = 1 + K \frac{\sigma_3}{\sigma_c} \qquad (5.65)$$

where, σ_c - unconfined compressive strength of material,
σ_1 - major principal stress,
σ_3 - minor principal stress.

Launay et al. (1970) determined the factor K. As shown in Figure 5.16, the maximum K value, equal to 6.5, is reached in triaxial compression, as the lateral stress attains the value of the surrounding material simple compressive strength. In a biaxial state of stress (i.e. $\sigma_3 = 0$), the maximum value of K is equal to 1.9.

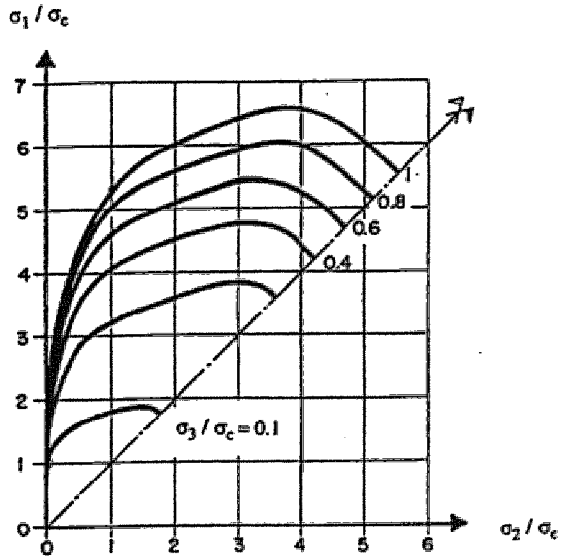

Figure 5.16 : *Triaxial compressive strength of concrete, after Launay et al. (1970)*

It can be considered, in the presented case, that due to the creation of a gap during the displacement along the joint, deconfinement is developed in a direction longitudinal to the bar (see Figure 5.15). As a consequence, σ_3 becomes nearly equal to zero and thus, the biaxial state of stress is created (with K = 1.9).

On the other hand, the material is subjected to a localized compression and the width on which the reaction pressure acts can be determined. Taking into account that the reaction vanishes when the angle between its direction and the normal to the bar is greater than the angle of friction of the bar-mortar interface, the width of reaction can be determined (Figure 5.17) :

$$L = D_b \sin \phi_i \qquad (5.66)$$

where, ϕ_i - angle of friction along bar-mortar interface,
L - width of reaction.

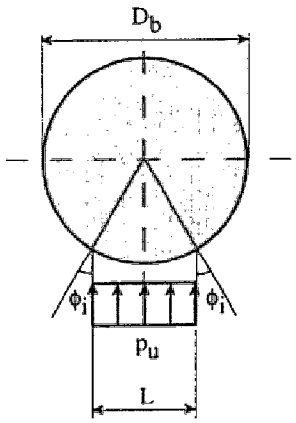

Figure 5.17 : *Width of application of the rock reaction*

The pressure of the rock reaction per unit length is expressed by :

$$p_u = K \sigma_c D_b \sin \phi_i = 1.9 \sigma_c D_b \sin \phi_i \qquad (5.67)$$

Considering a biaxial state of stress and the mean value of the friction angle of the bar-rock interface equal to 30 degrees, one can generally determine :

$$p_u \approx \sigma_c \, D_b \qquad (5.68)$$

It should be noted that if the grout is porous (as cement mortar), then the behaviour can be assumed plastic with brittle failure. It is thus, preferable to take the residual strength, instead of the peak strength.

5.9. Summary of the method

The presented method allows one to obtain the complete curve of the bar contribution to the shear strength of a rock joint as a function of the joint displacement.

In the elastic domain, the relation between the forces mobilized in the bar and the joint displacements is obtained by a variational formulation of the problem. The deformed shape of the bar is described by a hyperbolic cosine function, which accurately describes displacements experimentally measured. Forces mobilized in the bar at the elastic limit are obtained when the criterion of the plastic hinge initiation is fulfilled. The intersection of this criterion, which takes into account the interaction between the bending moment and the axial force, with the relationship describing the development of forces gives the solution in the form of a third order equation.

In the plastic domain, it is supposed that only the axial force mobilized in the bar increases. The axial force at failure is determined by the formula of interaction between the axial and shear forces, based on Tresca's criterion.

The displacements at failure are calculated by a large displacement formulation. It is supposed that the strain at failure is reached in the bar material, along the section delimited by the plastic hinge and the bar

INPUT DATA

Angle between bar and joint	β
Simple compressive strength of rock	σ_c
Bar diameter	D_b
Steel yield limit	σ_{ec}
Steel deformation at failure	ε_f
Joint friction angle	ϕ_j

CALCULATION OF ELASTIC LIMIT OF BAR

Shear force	Q_{oe}	eq.5.31 & 5.32
Axial force	N_{oe}	eq.5.25
Bar extremity rotation	ω_{oe}	eq.5.33
Bar extremity displacement	U_{oe}	eq.5.38

BAR FAILURE CALCULATION

Shear force at failure	Q_{of}	eq.5.39
Axial force at failure	N_{of}	eq.5.41
Plastic rotation of bar extremity	$\Delta\omega_{op}$	eq.5.46
Plastic displacement of bar extremity	ΔU_{op}	eq.5.48
Total rotation of bar extremity	ω_{of}	eq.5.49
Total displacement of bar extremity	U_{of}	eq.5.50

CALCULATION OF BAR CONTRIBUTION TO THE SHEAR STRENGTH OF JOINT AND ASSOCIATED DISPLACEMENT

Resultant force	R_{of}	eq.5.55
Component parallel to joint	R_{ot}	eq.5.57
Component perpendicular to joint	R_{on}	eq.5.58
Total contribution of bar	T_b	eq.5.59
Joint displacement	U_j	eq.5.60

extremity. In the plastic domain, the displacements are calculated by means of a secant axial stiffness, which progressively decreases as a function of the plastic lengthening of the bar.

Knowing the orientation and the intensity of the resultant force mobilized in the bar extremity and projecting it parallel and perpendicularly to the joint direction, it is possible to determine the shear strength of the reinforced joint, by dissociating the cohesion and the confining effects.

The principal stages necessary to calculate the maximum contribution of the bar to the joint shear strength and the associated displacement are summarized in the previous page. Additionally, numerical example is presented in appendix II.

Chapter 6

Parametric Study and Theory Evaluation

A parametric study is presented in this chapter, in order to appreciate the analytical procedure developed earlier. The influence of the principal mechanical and geometrical characteristics on the shear process of the reinforced joint will be studied.

The results obtained are subsequently compared with the most important analytical previsions published in the literature. The analytical model is also compared with the results of the tests presented in chapter 4 and with the results of tests realized in the past by different authors.

6.1. Selection and definition of the parameters

Parametric studies are realized beginning with the basic case which is defined by the following mechanical and geometrical characteristics :

- angle between bolt axis and joint: β = 60 degrees
- simple compressive strength of rock : σ_c = 50 MPa
- angle of joint friction : ϕ_j = 30 degrees

Parameters vary between the following limits :

β : 5 - 90 degrees
σ_c : 10 - 150 MPa
ϕ_j : 15 - 50 degrees

Mechanical characteristics of the reinforcing bolt are constant and equal to :

- bolt diameter:	D_b	=	12 mm
- elasticity and yield limit of steel:	σ_{ec}	=	600 MPa
- elasticity modulus of steel:	E	=	210000 MPa
- strain of steel at failure:	ε_f	=	20%

It is also assumed that the reaction pressure is equal to the product of the uniaxial compressive strength of the rock and the bolt diameter. Failure of the bolt occurs at the point in which it crosses the joint.

In order to simplify any comparisons, the results are presented in the form of normalized parameters. The forces are related to the axial force at the failure by tension, N_p, whilst the displacement along the joint is related to the bolt diameter. Normalized parameters are defined below :

- Shear force in the bolt $$F_Q = \frac{Q_o}{N_p}$$
- Axial force in the bolt $$F_Q = \frac{Q_o}{N_p}$$
- Resultant force in the bolt at the contact with the joint $$F_{Ro} = \frac{R_o}{N_p}$$
- Component of force in the bolt parallel to the joint $$F_{Rt} = \frac{R_t}{N_p}$$
- Component of force in the bolt normal to the joint $$F_{Rt} = \frac{R_t}{N_p}$$
- Contribution of the bolt to the joint shear strength $$F_T = \frac{T_b}{N_p}$$
- Displacement along the joint plane $$F_U = \frac{U_j}{D_b}$$

The deformability of the reinforced joint is characterized by the secant moduli at failure. Tangential stiffness is the ratio of the normalized tangential component of force mobilized in the bolt to the normalized displacement :

$$F_{Kt} = \frac{R_t \; D_b}{N_p \; U_j}$$

The term relating the augmentation of the axial force acting on the joint and the tangential displacement is called the indirect normal stiffness. It is defined as the ratio of the normalized axial component of the force mobilized in the bolt to the normalized displacement :

$$F_{Knt} = \frac{R_n \; D_b}{N_p \; U_j}$$

The scheme of forces acting in the bolt and along the joint is shown in Figure 6.1.

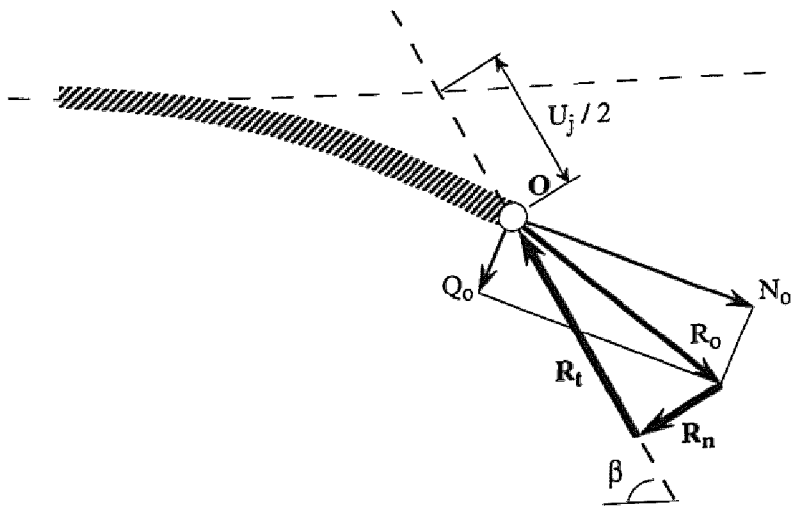

Figure 6.1 : *Decomposition with respect to the joint of forces in the bolt*

6.2. Curves of force versus joint displacement

6.2.1. Total contribution of the bolt

Rough results of the reinforced joint shear tests furnish total shear force as a function of displacement along the joint. The bolt contribution is obtained by subtracting the actual strength of the joint. The evolution of the bolt

contribution, F_T, as a function of the joint displacement, F_U, is calculated beginning with the basic case defined in the preceding section. Variations of the angle between the bolt and the joint as well as in the uniaxial compressive strength were encountered in the program. As shown in Figures 6.2 and 6.3, the contribution of the bolt progressively increases until its failure occurs.

The influence of the angle between the bolt axis and the joint is presented in Figure 6.2. For a single bolt installed perpendicularly to the joint plane (i.e., $\beta = 90^o$), the bolt contribution rapidly increases in the first portion of the curve. The progression then slows and the failure occurs after a significant displacement. The transition in the curve corresponds to the appearance of plastic hinges, which contribute a small fraction of the maximum contribution of the bolt.

For the case of a substantially inclined bolt (i.e., $\beta = 30^o$), the bolt contribution increases very quickly and reaches its maximum value after a very small displacement. The transition between the elastic and the plastic sections of the curve occurs progressively for a high contribution of the bolt. It can be stated that the displacement at failure increases and the stiffness of the reinforced joint decreases as the angle between the bolt and the joint increases.

The influence of the strength of the surrounding medium is shown in Figure 6.3. The bolt contribution curves as functions of the displacements have similar shapes. However, it is observed that in the case of rock having a low strength (σ_c = 10 MPa), the joint displacement at failure is greater in comparison to the case of very strong rock (σ_c = 100 MPa).

It can be finally said that the augmentation of the angle between the bolt and the joint causes increasing displacement at failure. On the other hand, the strength augmentation causes diminution of this same displacement. Thus, joints reinforced by bolts installed in weak rock at an angle equal to 90 degrees are flexible system. If the joint is reinforced by a strongly inclined bolt and rock is very hard, then the system is rigid, but not much more resistant.

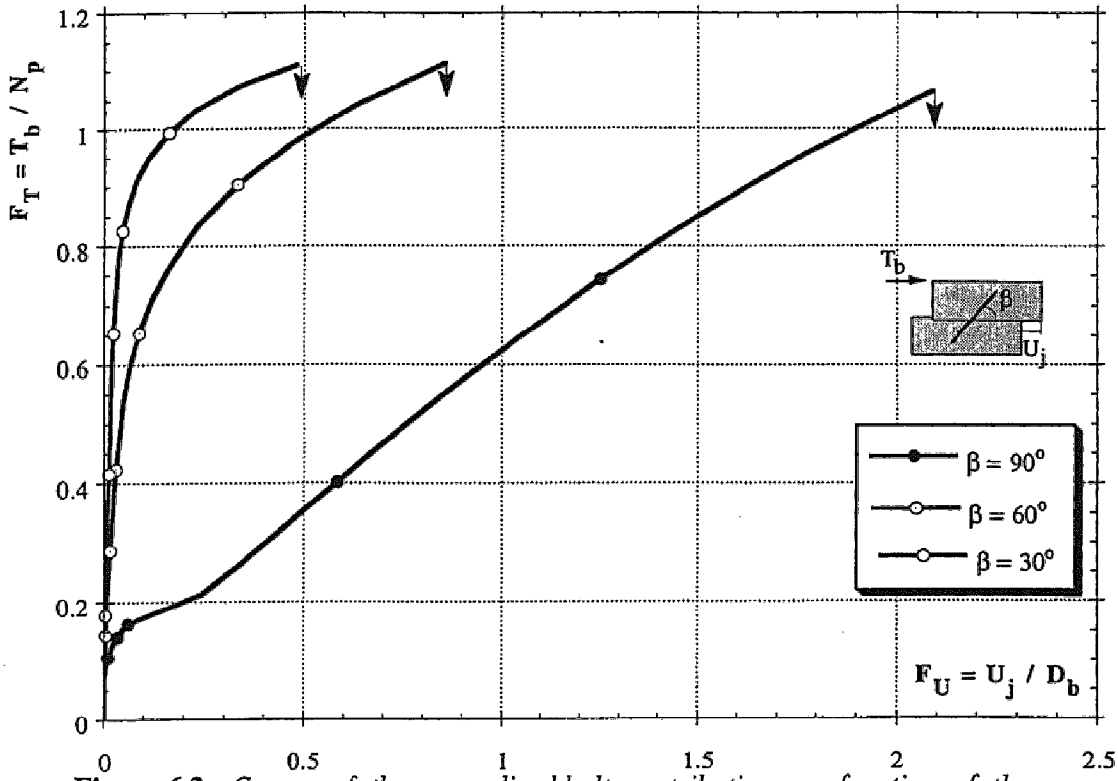

Figure 6.2 : *Curves of the normalized bolt contribution as a function of the normalized joint displacement, for σ_c = 50 MPa, ϕ_j = 30 degrees*

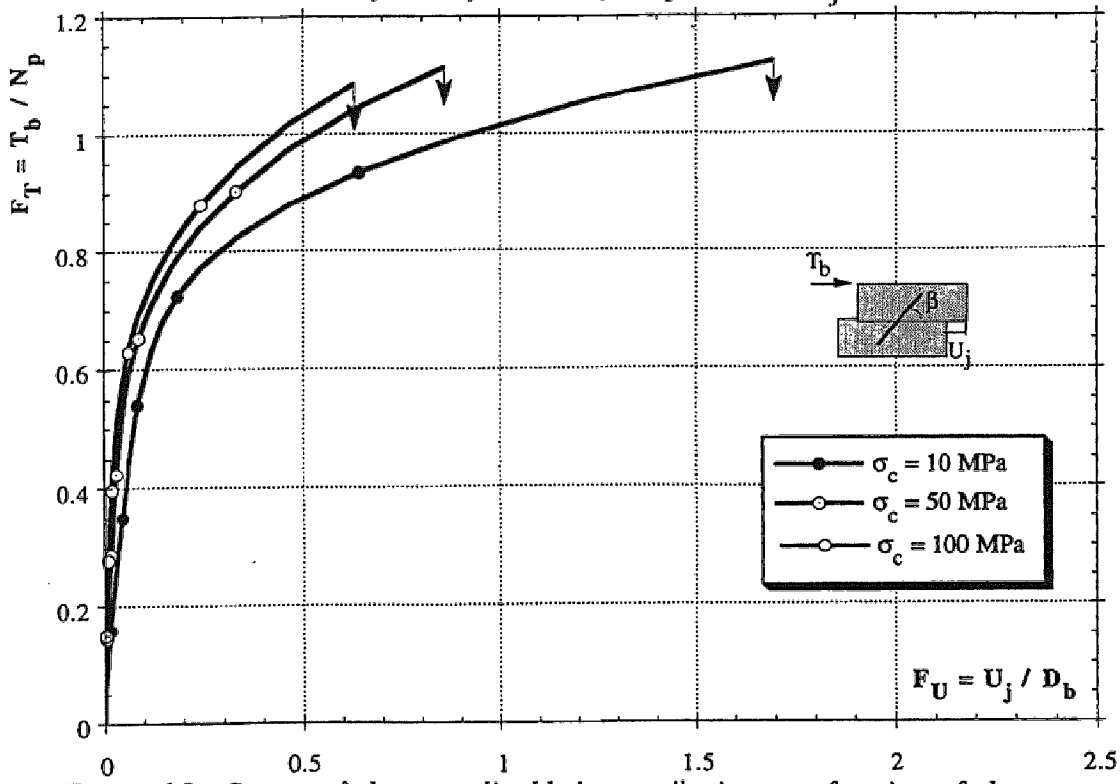

Figure 6.3 : *Curves of the normalized bolt contribution as a function of the normalized joint displacement, for β = 60 degrees, ϕ_j = 30 degrees*

6.2.2. Mobilization of forces in the bolt and on the joint

In order to better understand the way in which the bolt contribution is mobilized during the displacement process, it seems necessary to represent the evolution of the different forces composing the total contribution. The curves were drawn for a bolt installed perpendicularly to the joint plane (Figure 6.4) and for the case of an inclined bolt (Figure 6.5).

Independent of the bolt orientation, the shear force, Q_o, is very rapidly mobilized from the very beginning of the loading process. It attains a maximum value at the elastic limit of the bolt and remains constant up to the failure.

The rate of axial force mobilization depends on the bolt orientation. For the case of the bolt installed perpendicularly to the joint (i.e., $\beta = 90^o$), this force is not mobilized until the elastic limit. It then increases in the plastic domain until failure. If the bolt is more inclined (i.e., $\beta = 30^o$), the force is mobilized from the beginning of the loading and attains at the elastic limit, a relatively high value in comparison with its final value at failure. In the plastic domain, the force increases less rapidly. The maximum is reached at the failure point. In all cases, the values of the shear forces are distinctly lower than the axial forces. As a result, the forces mobilized in the bolt at failure have approximately the same value as the axial forces.

The component R_t parallel to the joint, representing the reinforcement cohesion, is mobilized immediately, and is independent of the bolt orientation. If the bolt is greatly inclined, then its evolution in the plastic domain is similar to that of the axial force. For a bolt placed perpendicularly to the joint, the curve of the reinforcement cohesion and that of the axial force diverge. The component perpendicular to the joint, representing the confining effect, follows, in the elastic domain, a course similar to that of the axial force. Comparable magnitudes of the confining and the cohesion effects are observed at failure, if the angle between the bolt axis and the joint is great. If the bolt is more inclined, the influence of the reinforcement cohesion becomes distinctly dominant.

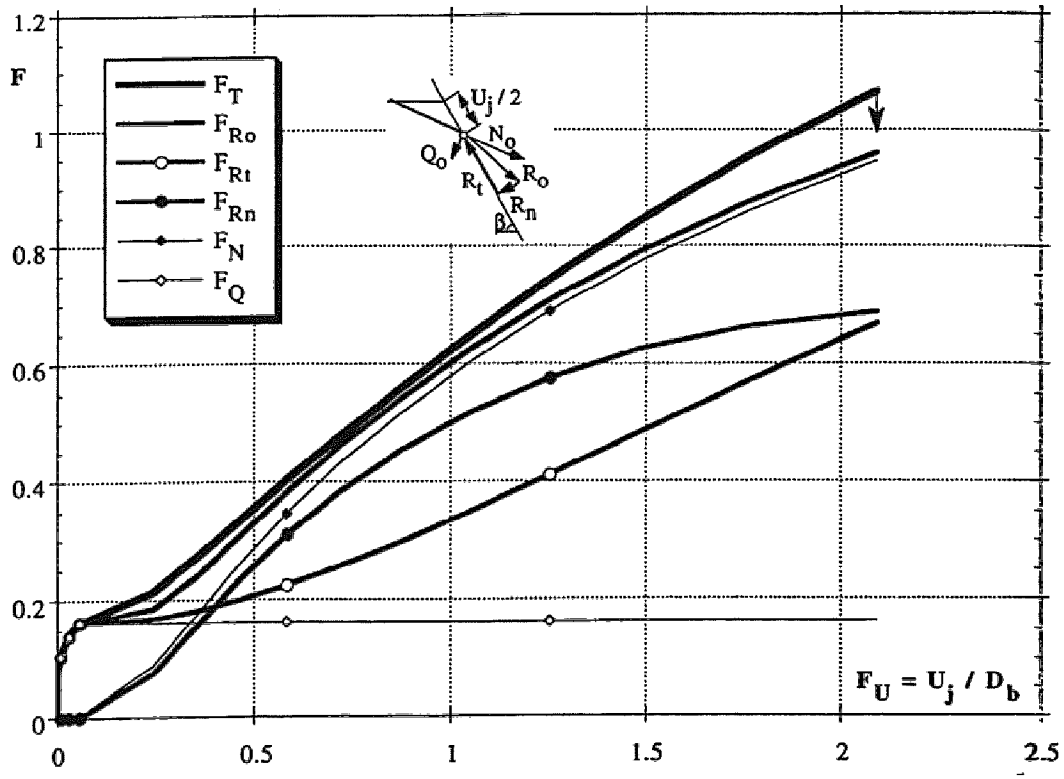

Figure 6.4 : *Forces versus joint displacements, represented by normalized parameters for* $\beta = 90$ *degrees,* $\sigma_c = 50$ *MPa,* $\phi_j = 30$ *degrees*

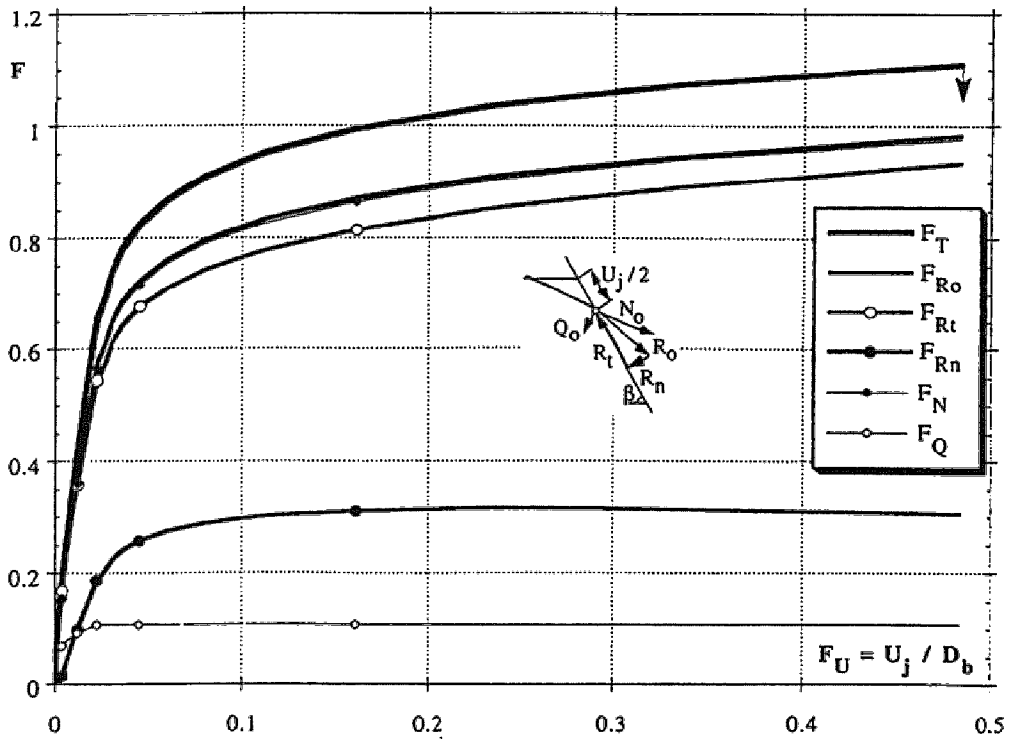

Figure 6.5 : *Forces versus joint displacements, represented by normalized parameters for* $\beta = 30$ *degrees,* $\sigma_c = 50$ *MPa,* $\phi_j = 30$ *degrees*

It can be finally said that a bolt installed perpendicularly to the joint constitutes a flexible system, which will be rapidly yielded. It is characterized by the relatively low bolt contribution at the elastic limit in comparison to its maximum value. The system is very stiff if the bolt is significantly inclined. In this case, the difference between the bolt contribution at the elastic limit and at the failure is reduced.

6.2.3. Evolution of normal and shear force

It is important to examine the development of the axial and shear forces during the loading process, one with respect to other. Different angles between the bolt and the joint, as well as different rock strengths were investigated. The elastic limit is represented by the parabola with the center situated on the axial force axis. The bolt failure across the joint is defined by the ellipse with its minor axis coinciding with the axis of the shear force.

It is observed in Figure 6.6 that if the angle between the bolt axis and the joint augments, then the shear force mobilized at the elastic limit increases, whereas, the axial force decreases. In the case of the bolt which is perpendicular to the joint, the axial force at the elastic limit is equal to zero. However, if the angle is great, the essential part of the force mobilization is developed in the plastic domain. This explains the low stiffness revealed by such a system. On the other hand, the resultant force mobilized in the bolt at failure diminishes as the angle between the bolt and joint increases.

The higher the uniaxial compressive strength of the rock, the greater the elastic domain defined by the parabola will be. As a result, when the rock strength increases, the shear force increases and the axial force decreases (Figure 6.7).

In summary, both the diminution of the angle between the joint and the bolt and the diminution of the rock strength cause the augmentation of the resultant force in the bolt.

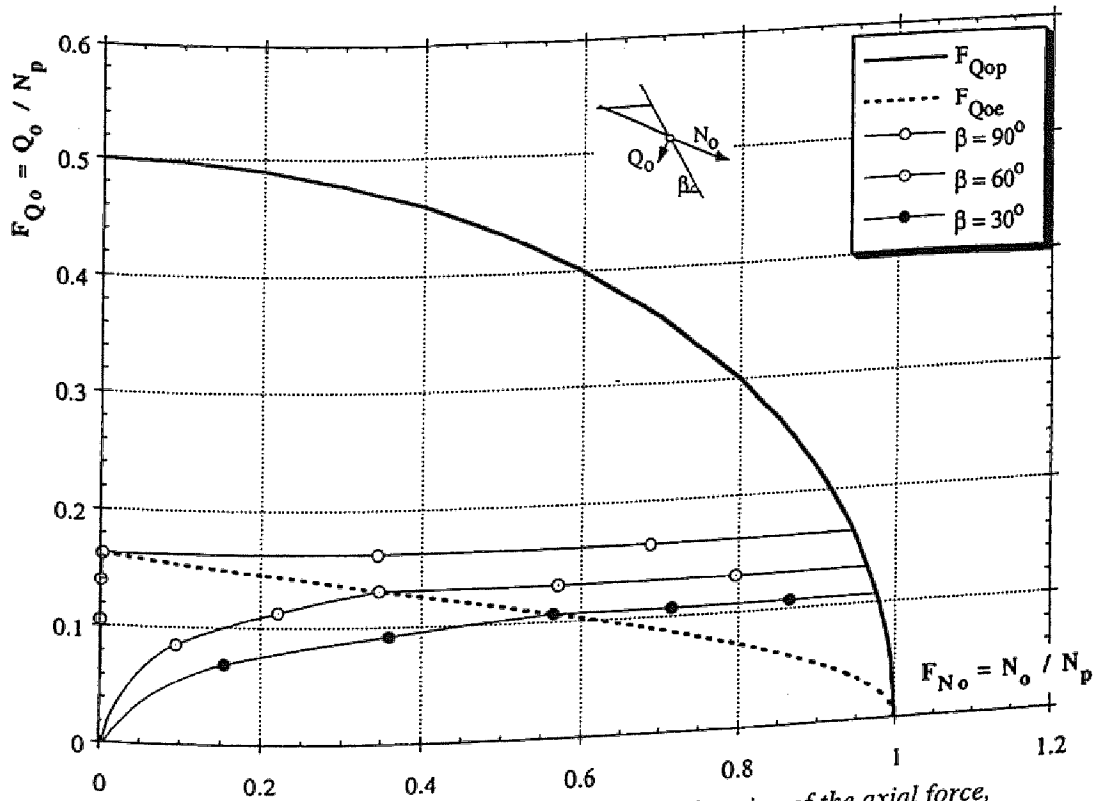

Figure 6.6 : *Evolution of the shear force as a function of the axial force, for different β values , σ_C = 50 MPa*

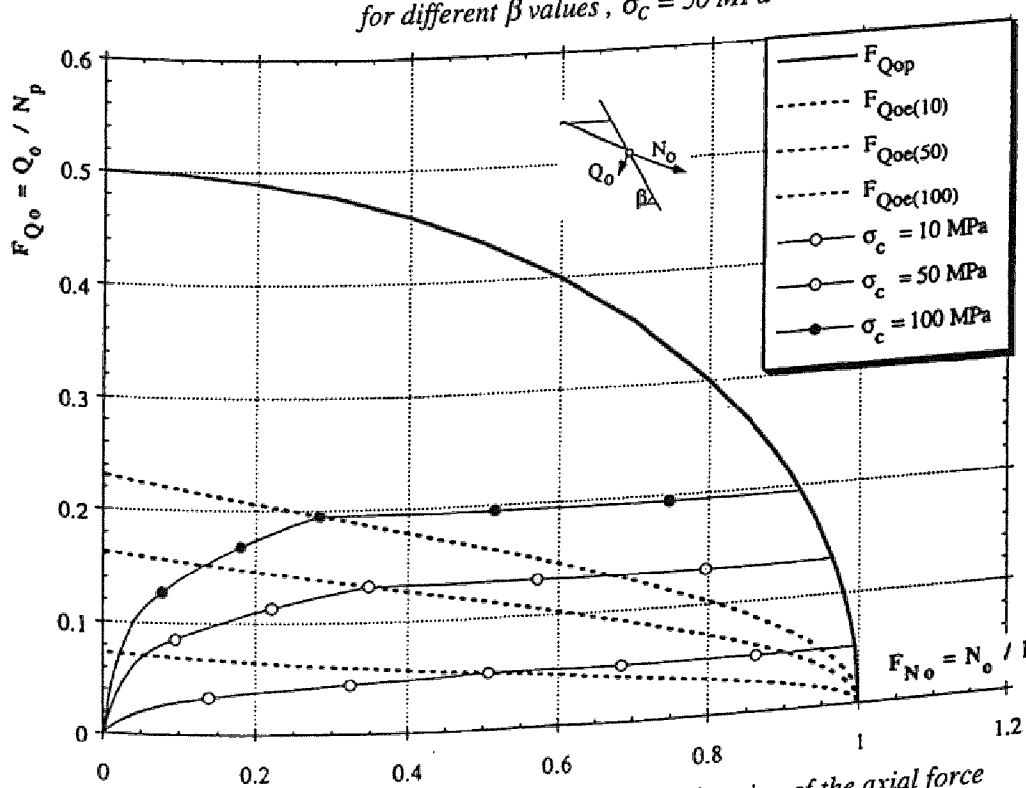

Figure 6.7 : *Evolution of the shear force as a function of the axial force for different σ_C values , β = 60 degrees*

6.3. Maximum contribution of the bolt to the joint shear strength and associated displacement

The manner in which the total contribution of the bolt and the forces composing it are mobilized as a function of the joint displacement was described in earlier sections. Below, the influence of different geometrical and mechanical characteristics on the maximum bolt contribution to the joint shear strength, as well as on the associated displacement, will be analyzed in detail. The role of the joint friction angle, which has not been analyzed until now, is also brought forward.

6.3.1. Influence of the angle between the bolt and the joint

The variation of the bolt contribution as a function of the angle between the bolt and the joint for different friction angles is presented in Figure 6.8. Though the bolt contribution is more significant if the friction angle is higher, the variation of the curves as a function of this angle is observed. For higher friction angles ($\phi_j = 45^o$), the maximum contribution occurs for a greater angle between the bolt and joint because the confining effect is greater in this case, as was proven in the previous sections. To the contrary, as the friction angle is lowered ($\phi_j = 15^o$), the significance of the confining is reduced and the maximum bolt contribution occurs for a smaller value of the angle between the bolt and joint. This value corresponds to the case in which the reinforcement cohesion dominates. In the extreme situation of a bolt steeply inclined to the joint direction, the contribution becomes independent of the friction angle and is approximately equal to the plastic axial force in the bolt (i.e., $F_T = 1$).

The maximum joint displacement at failure, which is independent of the joint friction angle, is represented in Figure 6.9 as a function of the bolt inclination and for different rock strengths. The maximum displacement is observed when the bolt crosses the joint plane perpendicularly ($\beta = 90^o$). As this angle diminishes, the displacement rapidly decreases and tends to a minimum.

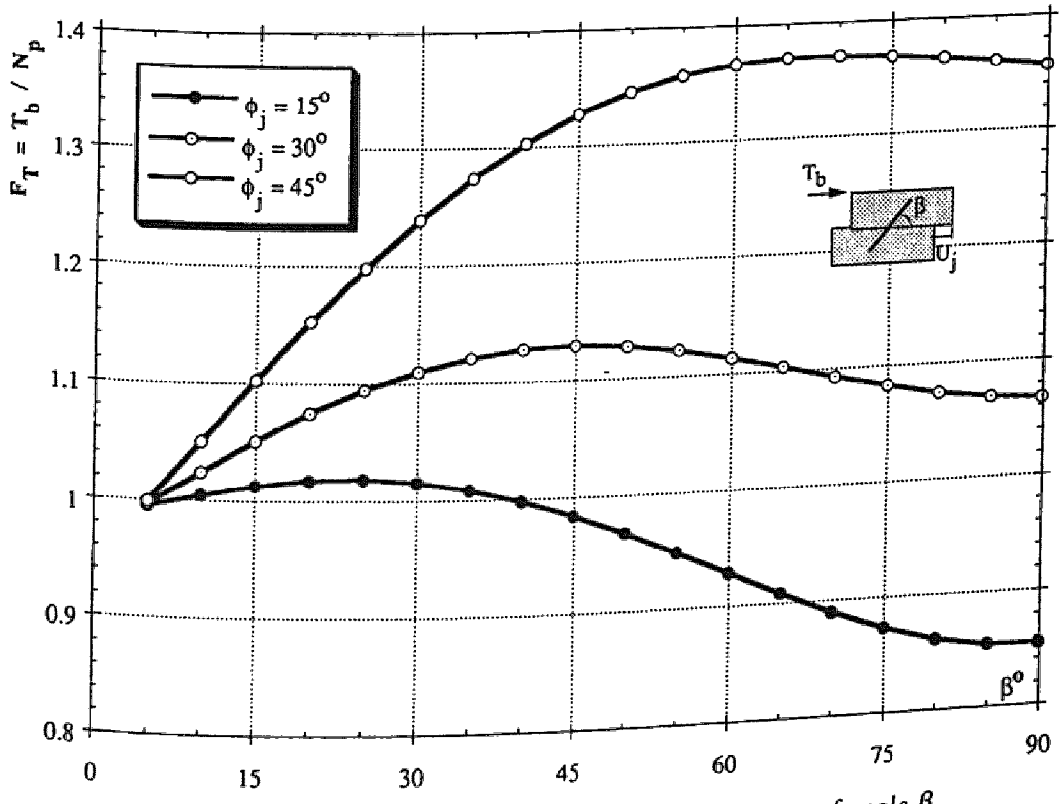

Figure 6.8 : *Total contribution of the bolt as a function of angle β, for different ϕ_j values , σ_c = 50 MPa*

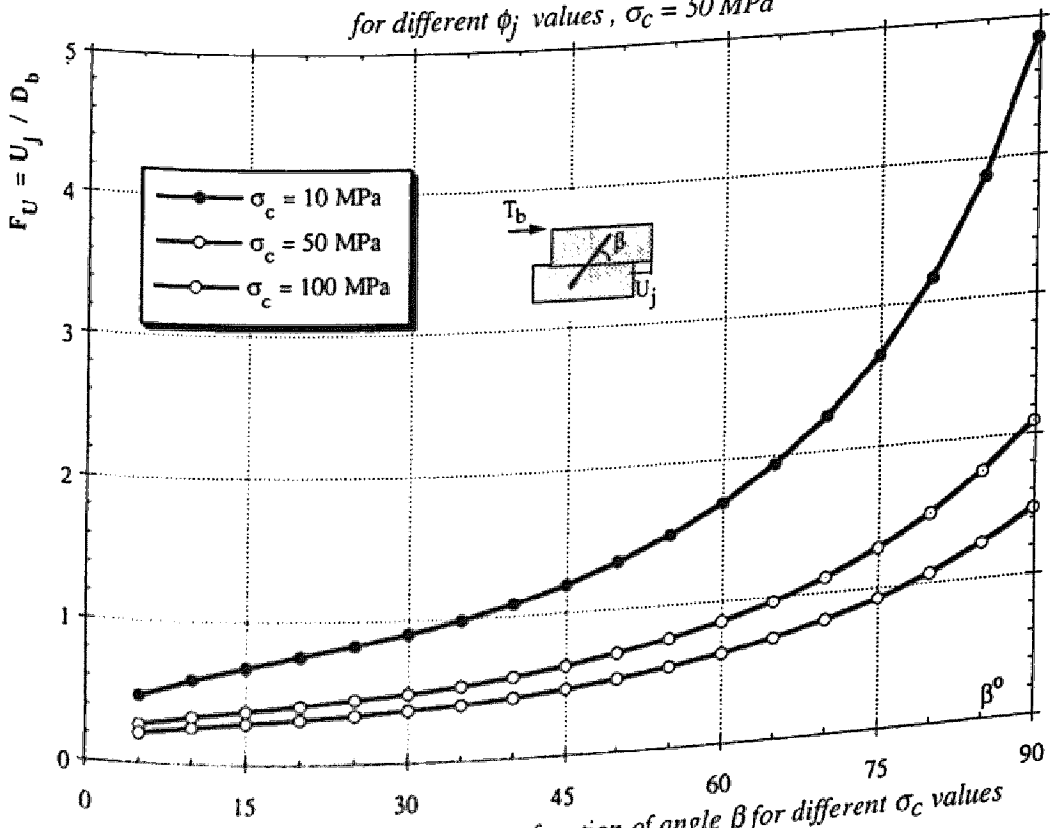

Figure 6.9 : *Joint displacement as a function of angle β for different σ_c values*

6.3.2. Influence of the rock strength

The influence of the rock uniaxial strength variation on the bolt contribution and on the associated displacement is shown for different values of the angle between the bolt axis and joint in Figures 6.10 and 6.11.

As can be seen in Figure 6.10, the rock strength σ_c has little influence on the shear strength of the reinforced joint. Yet, it should be noticed that the bolt contribution is slightly higher if the rock strength is low.

In fact, in weak rock, the bolt can mobilised a greater axial force because of its ability to be deformed. To the contrary, the rock strength has a significant influence on the displacement at failure, whatever the bolt orientation may be (Figure 6.11). The displacements are larger for a weak rock and decrease very rapidly with the augmentation of the rock strength.

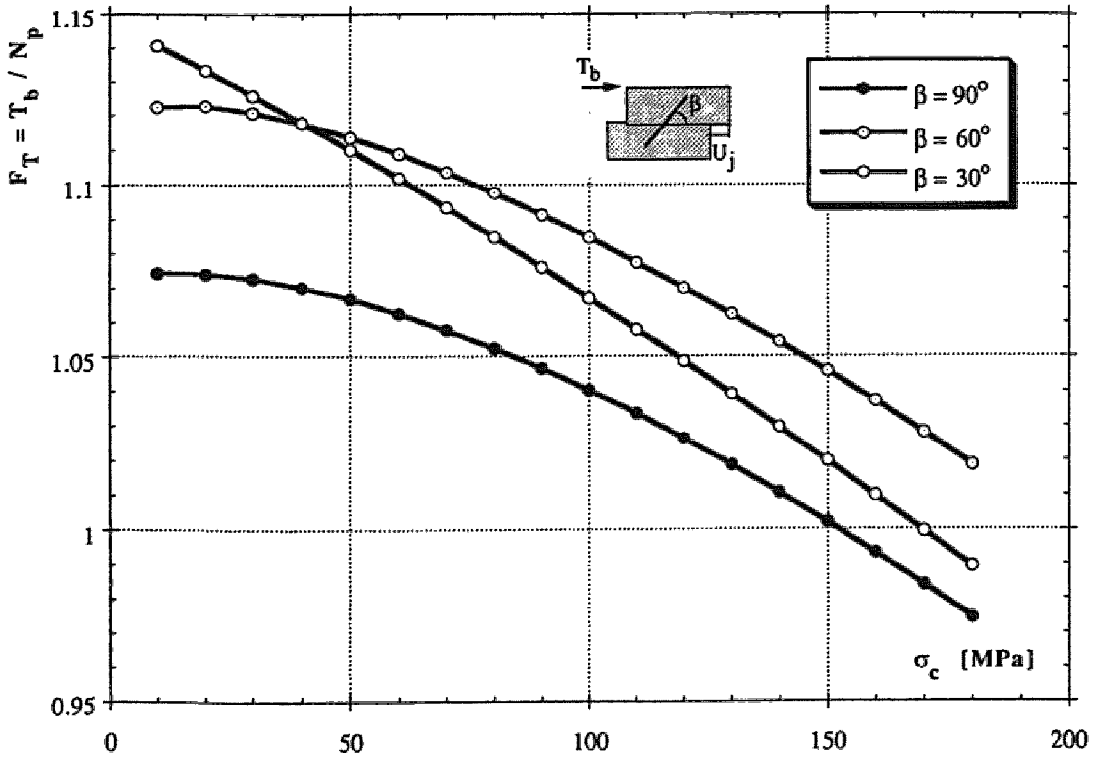

Figure 6.10 : *Total contribution of the bolt as a function of the rock strength for different β values , ϕ_j = 30 degrees*

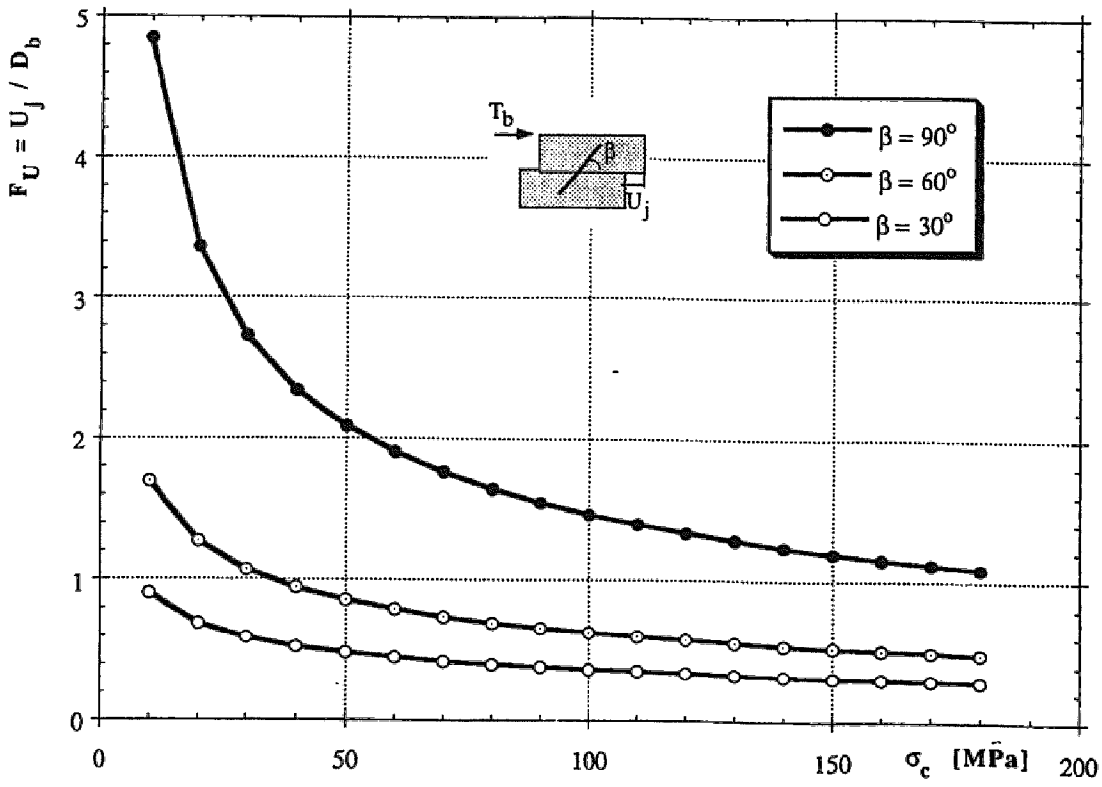

Figure 6.11 : *Joint displacement as a function of rock strength for different values of angle*

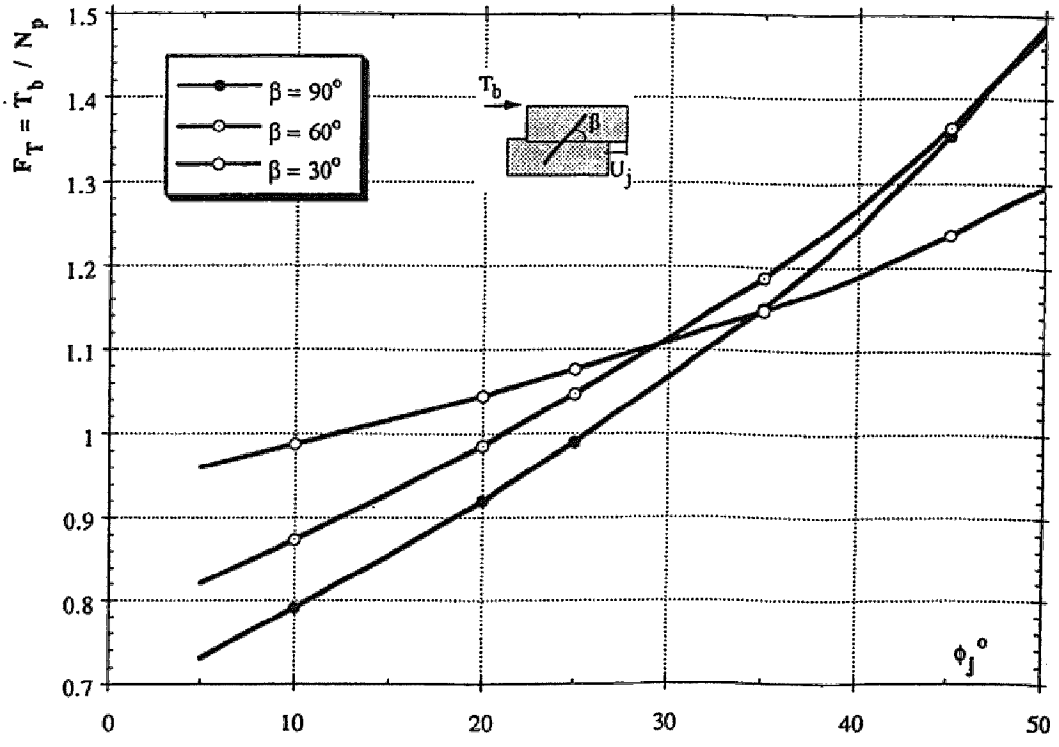

Figure 6.12 : *Total contribution of the bolt as a function of the joint friction angle for different values of angle β*

6.3.3. Influence of the joint friction angle

In Figure 6.12, the influence of the variation of the joint friction angle on the bolt contribution is shown for different bolt orientations.

The bolt contribution to the joint shear strength increases with the augmentation of the friction angle, whatever of the bolt orientation is. It is also observed that the greater the angle between the bolt and the joint, the more rapid the augmentation of the bolt contribution will be. As was already explained in previous sections, this is due to the important role of the confining in the case of a great angle between the bolt and the joint.

6.3.4. Evolution of the reinforcement cohesion and the confining on the joint

The bolt contribution to the joint shear strength results from the normal stress developed by the normal component of the force in the bolt and from the reinforcement cohesion related to the parallel component of the same force. The variation of the reinforcement cohesion and the confining effects as a function of the angle between the bolt and joint is presented in Figure 6.13. It is observed that the confining effect is more significant when this angle is great, whatever the rock strength may be. To the contrary, the cohesion decreases when the angle between the bolt and the joint increases. For a steeply inclined bolt ($\beta < 15^o$), the confining term is nearly equal to zero whereas the cohesion term attains its maximum. If the bolt is perpendicular to the joint ($\beta = 90^o$), the reinforcement cohesion has a minimum value, whilst the confining reaches its maximum. For this case, the magnitudes of the cohesion and the confining, composing the total bolt contribution, are comparable.

The influence of rock strength on the development of reinforcement cohesion and confining is presented for different values of the bolt orientation in Figure 6.14. It is observed that the cohesion term is not very sensitive to strength variation, whereas the confining very distinctly decreases with the augmentation of rock strength, whatever the bolt orientation is.

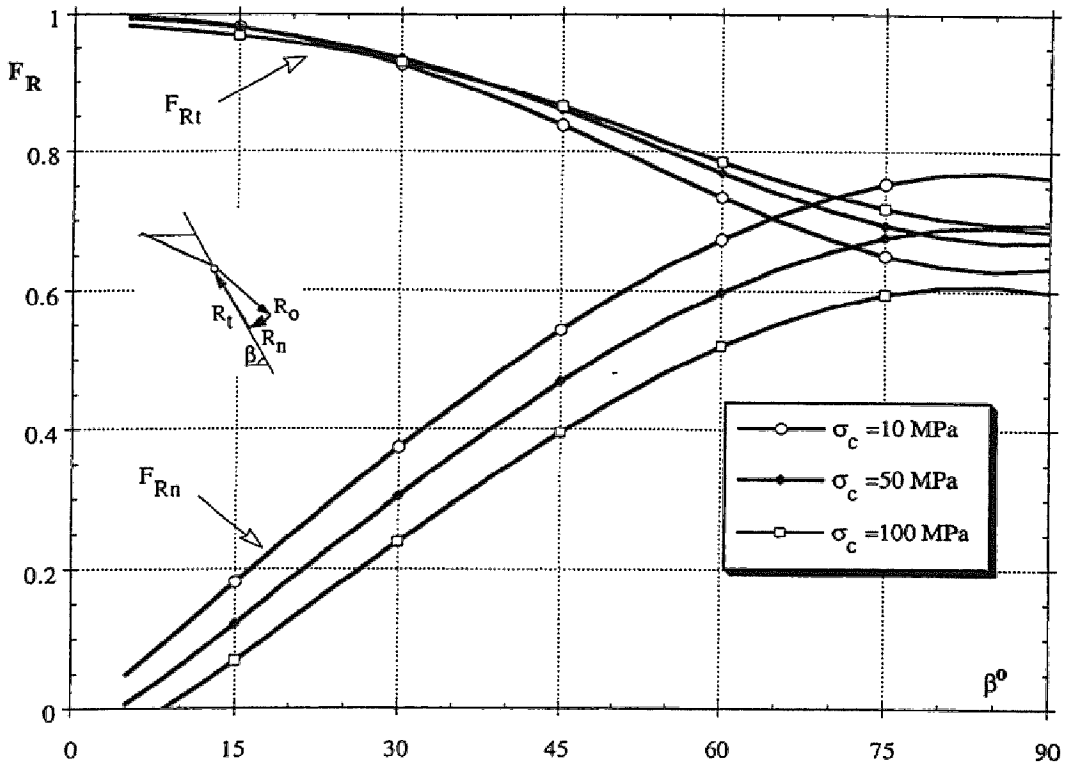

Figure 6.13 : *Evolution of reinforcement cohesion, R_t, and confining, R_n, as a function of angle β for different rock strength values, ϕ_j = 30 degrees*

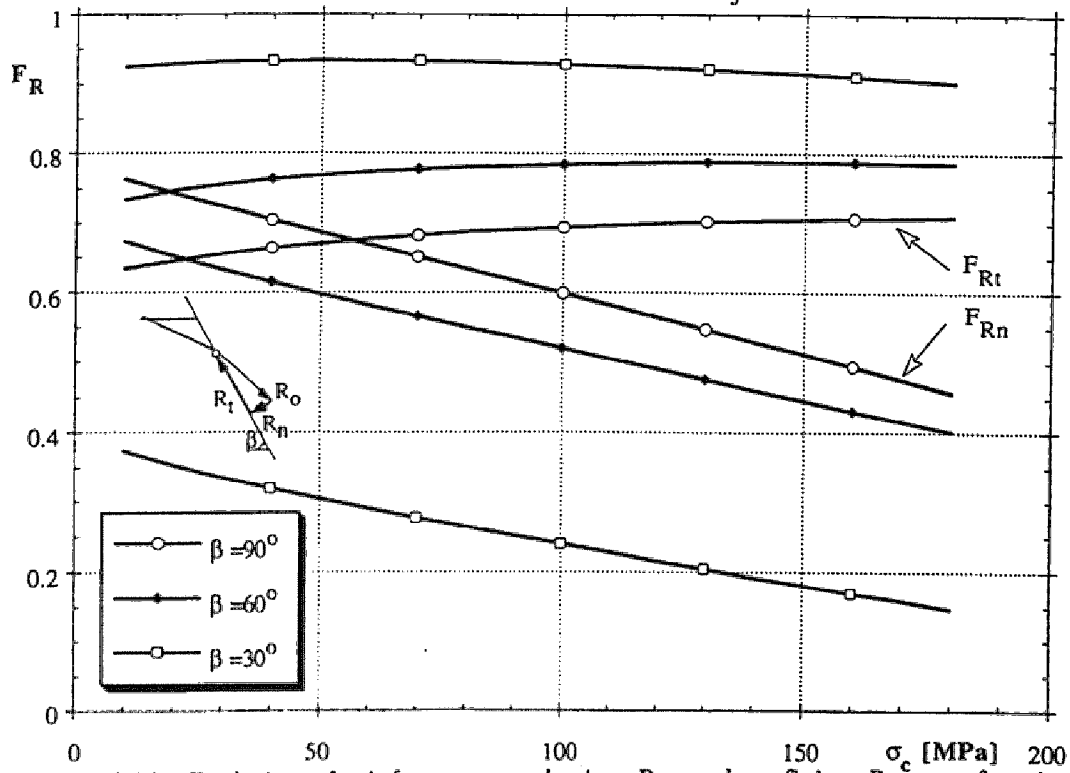

Figure 6.14 : *Evolution of reinforcement cohesion, R_t, and confining, R_n, as a function of rock strength for different angles β, ϕ_j = 30 degrees*

6.3.5. Normal and tangential stiffness of the joint

Functions of the forces parallel and normal to the joint versus displacement are not linear. Thus, for estimation of the reinforced joint deformability, the secant moduli can be determined. They are defined as the ratios of the forces mobilized at failure to the corresponding displacements. Evolution of the stiffness moduli as a function of the angle between the bolt and the joint is shown for the different rock strength values in Figure 6.15. Whatever the rock strength is, the tangential stiffness of the reinforced joint decreases proportionally to the augmentation of the angle between the bolt and the joint. The indirect normal stiffness increases and then diminishes after attaining its maximum. Evolution of the stiffness moduli as a function of the uniaxial compressive strength of the rock is presented for different values of the bolt orientation in Figure 6.16. The smaller the angle between the bolt and joint, the more rapid the augmentation of the tangential stiffness of the reinforced joint will be. The indirect normal stiffness is much less sensitive to the variation of rock strength.

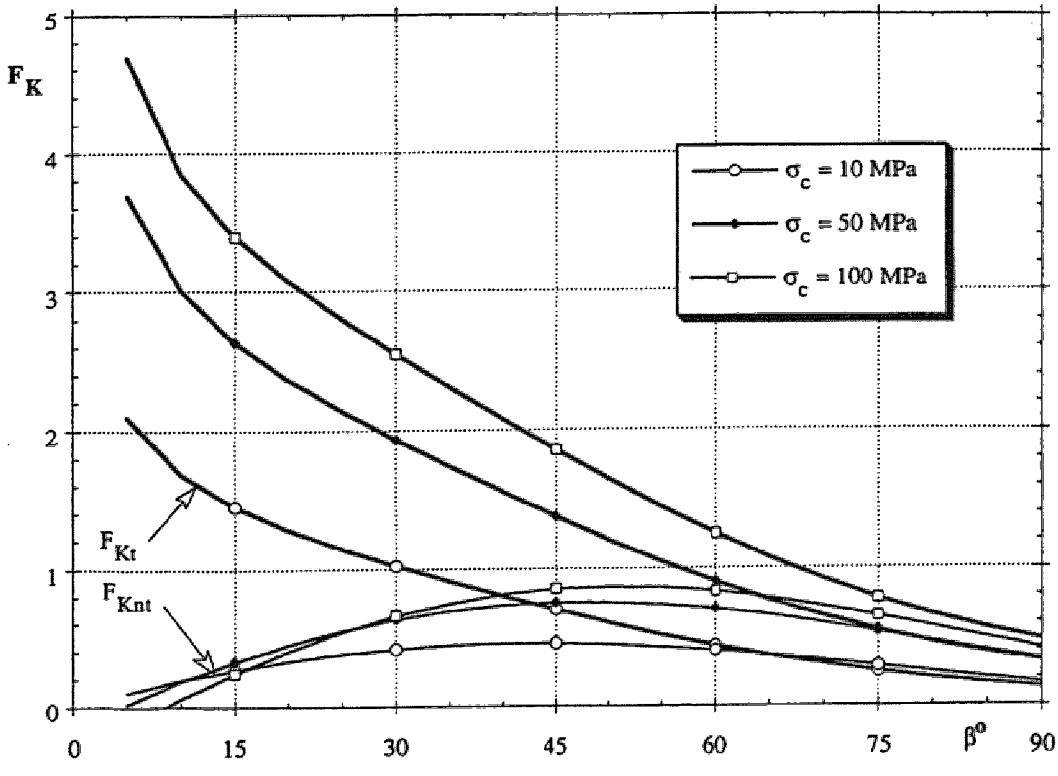

Figure 6.15 : *Evolution of rigidity modulus as a function of angle β for different values of rock strength*

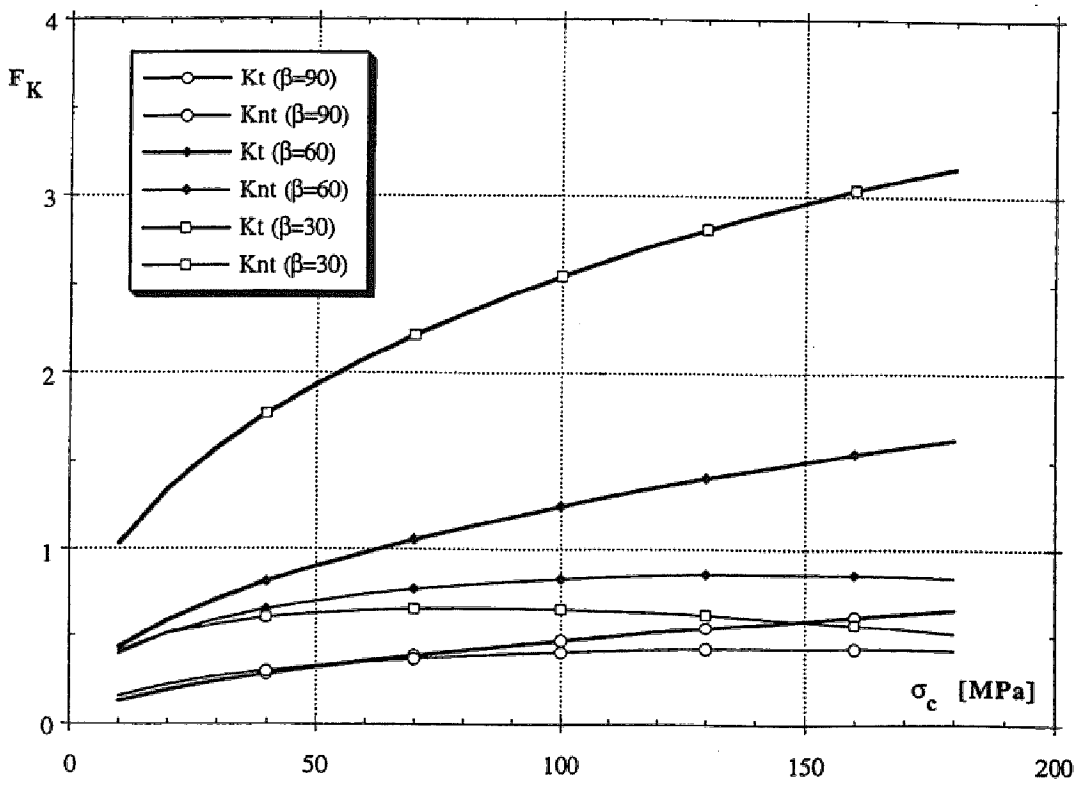

Figure 6.16 : *Evolution of rigidity modulus as a function of rock strength for different angles β*

6.4. Comparisons with the analytical formulations published in the literature

Several authors, whose studies were presented in chapter 3, elaborated formulae allowing one to calculate the bolt contribution to the shear strength of the joint. The most simple formula (**Bjurström, 1974**) consists of the decomposition with respect to the joint plane of the axial force mobilized in the bolt :

$$T_b = N_p \left(\cos\beta + \sin\beta \tan\phi_j\right)$$

where, N_p = axial force at yield limit of bolt,
β = angle between bolt and joint,
ϕ_j = joint friction angle.

Spang (1988) established the formulae, based on a great number of test results. Due to their semi-empirical character, the formulae are valid for rock compressive strengths of 10 to 70 MPa and for angles between the bolt and the joint of 60 to 90 degrees. They have the following forms :

$$T_b = N_p \left[1.55 + 0.011\ \sigma_c^{1.07}\ \sin^2(\alpha + i)\right] \sigma_c^{-0.14} \left(0.85 + 0.45\ \tan\phi_j\right)$$

$$U_j = D_b \left(15.2 - 55.2\ \sigma_c^{-0.14} + 56.2\ \sigma_c^{-0.28}\right) \left[1 - \frac{\tan\alpha}{\cos\alpha^{0.5}} \left(\frac{70}{\sigma_c}\right)^{0.125}\right]$$

where, σ_c = uniaxial compression strength of rock, in MPa,
α = angle between bolt and normal to joint,
D_b = bolt diameter

The above formulae, applied to the previously studied basic case, are compared with the predictions of the present theory. It can be observed in Figure 6.17a that the presented analytical formulation agrees with the expression of Spang for large angles between the bolt and the joint ($\beta > 60^o$), whereas the formula of Bjurström underestimates the bolt contribution. To the contrary, the results of the presented study and those from Bjurström's formula are comparable for the strongly inclined bolt ($\beta < 60^o$). The rock strength is taken into account in Figure 6.17b. It is observed that in the domain of low strength, Spang's formula gives a more rapid decrease of the bolt contribution values in comparison to those computed by the present theory.

Concerning the previsions of the joint displacement, both the presented theory and Spang's formula indicate a decrease due to the diminution of the angle between the bolt and the joint (Figure 6.18a) and the augmentation of the rock strength (Figure 6.18b).

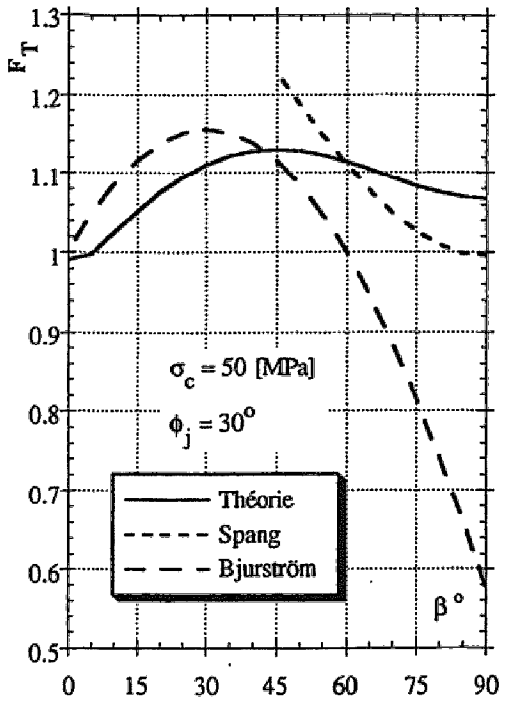

a- versus the angle between bolt and joint

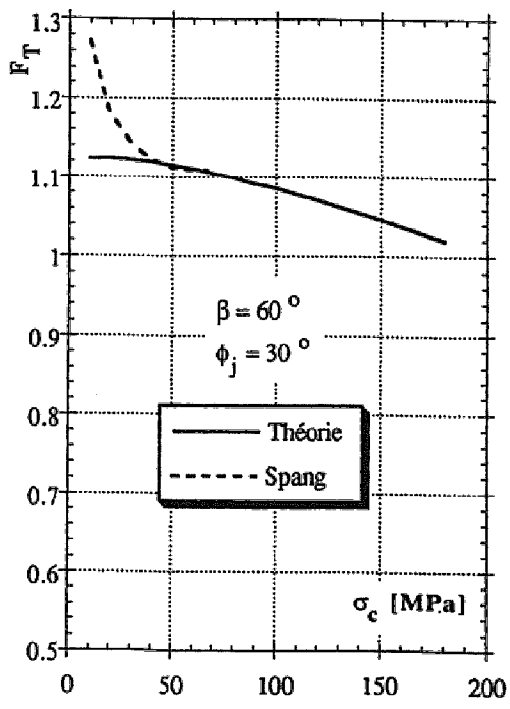

b- versus the rock strength

Figure 6.17 : *Normalized bolt contributions calculated analytically*

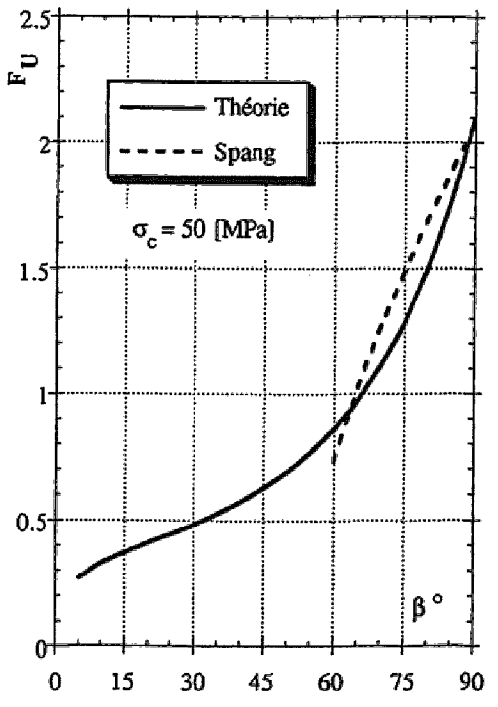

a- versus the angle between bolt and joint

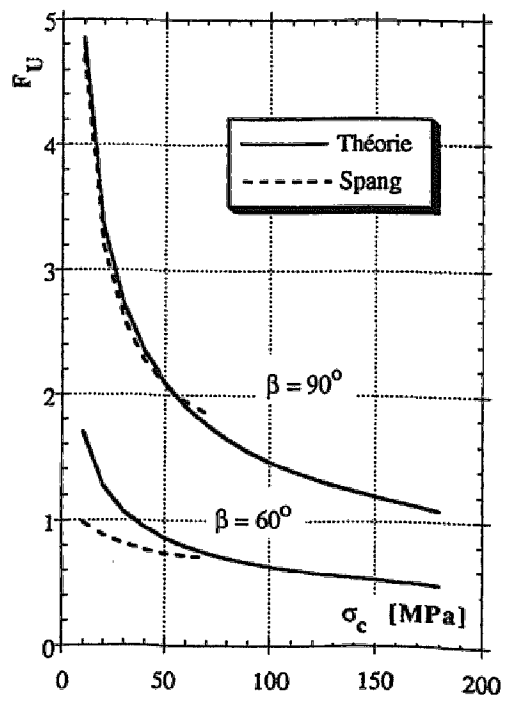

b- versus the rock strength

Figure 6.18. *Normalized joint displacements, calculated analytically*

In Figure 6.19, performances of the analytical formulation are compared with the results from the numerical model proposed by **Swoboda & Mareñce (1992)**, (see section 3.5.2). Good accordance is observed, especially for the case of a bolt perpendicular to the joint. A maximum deviation is equal to 10% for angle of 45 degrees.

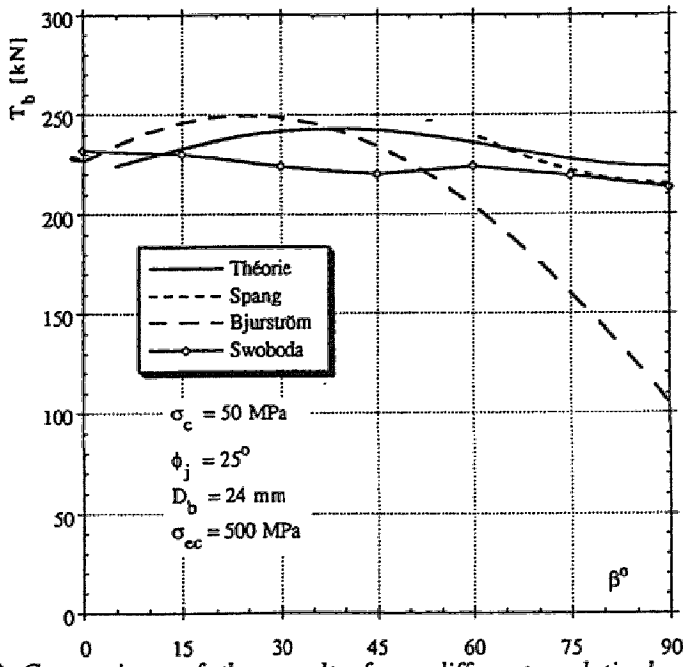

Figure 6.19. *Comparison of the results from different analytical methods with the results of Swoboda & Mareñce (1992) finite element calculations*

6.5. Comparisons with the experimental results

6.5.1. Tests realized in the TRIROC press

Analytical previsions are compared with the results of the tests described in chapter 4. Only the tests realized on models reinforced by fully bonded bolts are under consideration. The results are summarized in Table 6.1.

For models with the joints inclined at 45 degrees, the difference between the calculated and the measured values of the maximum bolt contribution is lower than 5%. To the contrary, the displacement calculated by the theory is 29% lower than that of the test. In the case of models with joint inclined at 60 degrees, the computed bolt contribution is higher by about 2% with

respect to the measured value and the calculated displacement at the failure is a little lower than the measured one.

Test	βo	T_b [kN]	T_{bm} [kN]	S_{xt} [kN]	T_b^{th} [kN]	e_t %	U_j [mm]	U_{jm} [mm]	S_{xu} [mm]	U_j^{th} [mm]	e_u %
CE 45.14	45	4.98	4.74	0.28	4.93	+4	2.23	2.54	0.22	1.80	-29
CE 45.15		4.96					2.60				
CE 45.16		4.42					2.76				
CE45.17		4.59					2.55				
CE 60.19	60	4.61	4.72	0.12	4.80	+2	2.07	2.50	0.48	2.46	-2
CE 60.20		4.65					2.17				
CE 60.21		4.74					2.63				
CE60.22		4.87					3.12				

Table 6.1 : *Comparison of the experimental results to analytical previsions*

T_{bm} : average value of the bolt contribution,
S_{xt} : standard deviation of the bolt contribution,
T_b^{th} : bolt contribution calculated by the presented theory,
e_t : difference between average and calculated bolt contribution,
U_{jm} : average value of the joint displacement,
S_{xu} : standard deviation of the joint displacement,
U_j^{th} : the joint displacement calculated by the theory,
eu : difference between average and calculated joint displacement.

The above results, presented in a graphic form in Figures 6.20a and 6.20b, prove that the proposed analytic solution accurately corresponds to the experimental results. One also observes that the Bjurström's formulation is valid for low and for moderate angles, whereas Spang's equation can be applied to cases of great angles.

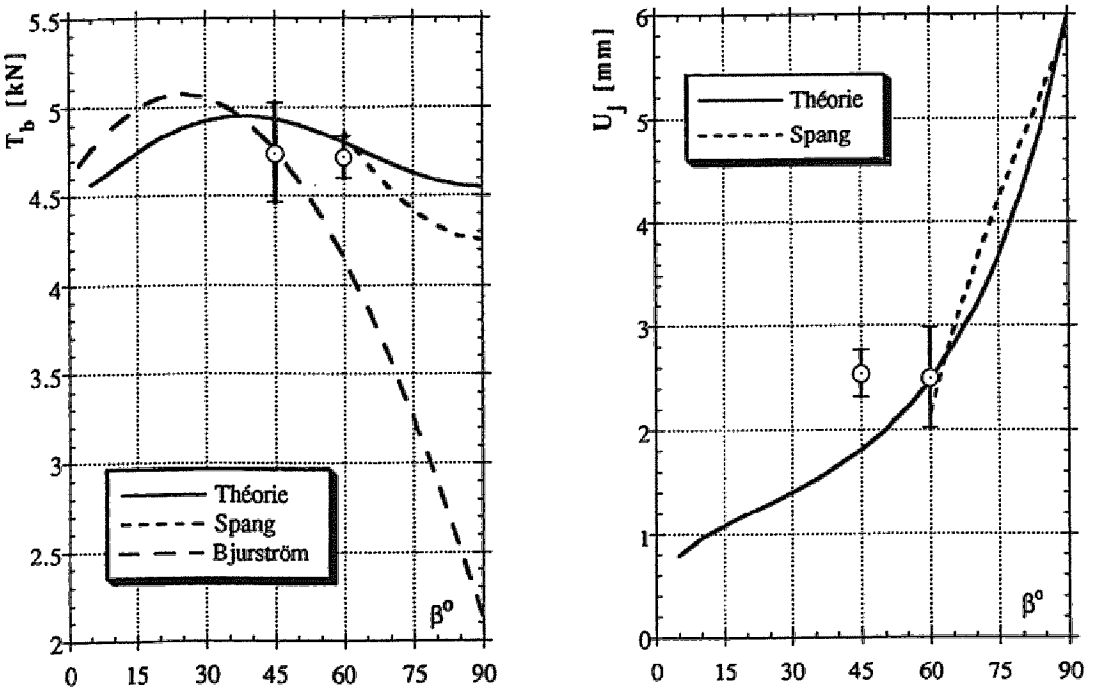

a- bolt contribution versus bolt orientation *b- joint displacement versus bolt orientation*

Figure 6.20 : *Comparison of the results from experiments in TRIROC press with those from different analytical methods*

In Figure 6.21, the curves are presented showing complete development of the bolt contribution versus joint displacement in the tests realized on the specimens with a single joint inclined at 45 degrees. The curves of the same kind, in Figure 6.22, present the results of the tests for joints oriented at 60 degrees to the horizontal.

The general trends of experimental and theoretical curves show a good accordance, although it can be observed that the curves obtained from the calculations insufficiently express the plastic portion in which the bolt contribution remains constant. To the contrary, the slopes of the curves at the initial loading stage are relatively similar.

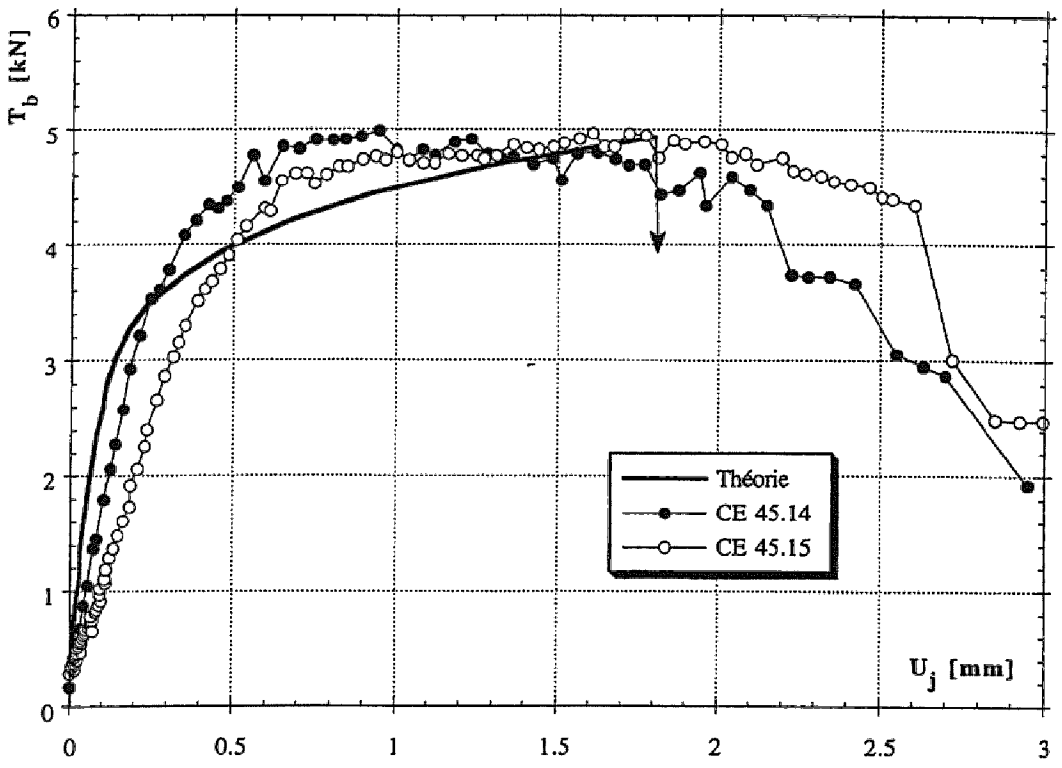

Figure 6.21 : *Comparison of bolt contribution for the models with joints inclined at 45 degrees*

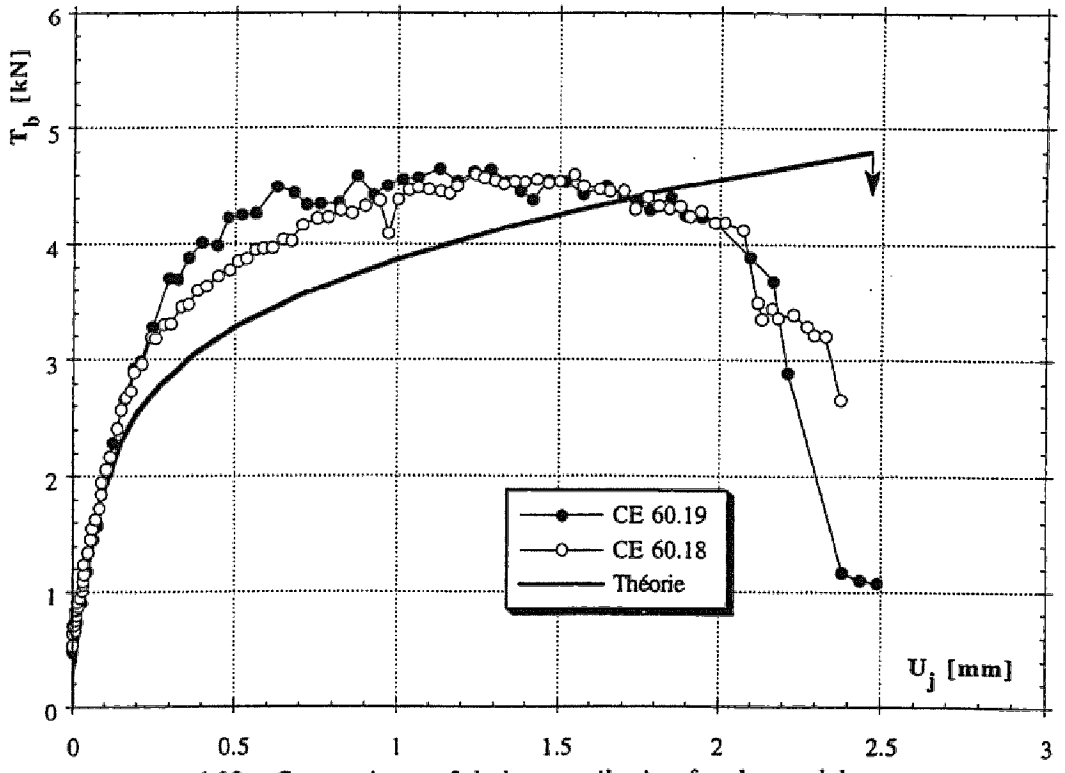

Figure 6.22 : *Comparison of bolt contribution for the models with joints inclined at 60 degrees*

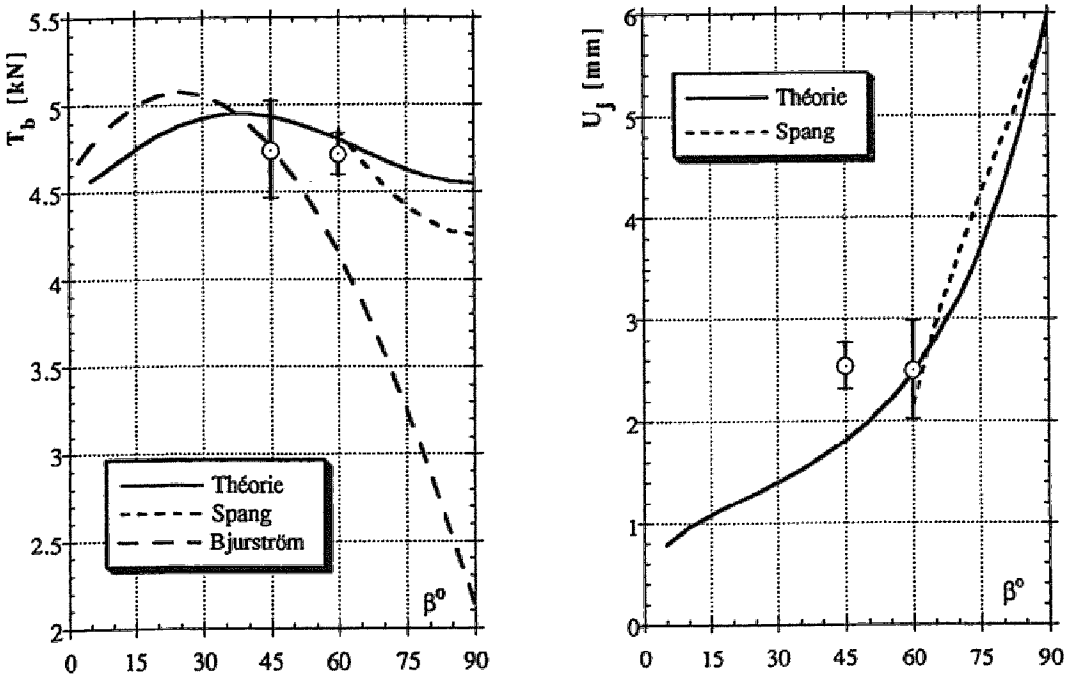

a- bolt contribution versus bolt orientation *b- joint displacement versus bolt orientation*

Figure 6.20 : *Comparison of the results from experiments in TRIROC press with those from different analytical methods*

In Figure 6.21, the curves are presented showing complete development of the bolt contribution versus joint displacement in the tests realized on the specimens with a single joint inclined at 45 degrees. The curves of the same kind, in Figure 6.22, present the results of the tests for joints oriented at 60 degrees to the horizontal.

The general trends of experimental and theoretical curves show a good accordance, although it can be observed that the curves obtained from the calculations insufficiently express the plastic portion in which the bolt contribution remains constant. To the contrary, the slopes of the curves at the initial loading stage are relatively similar.

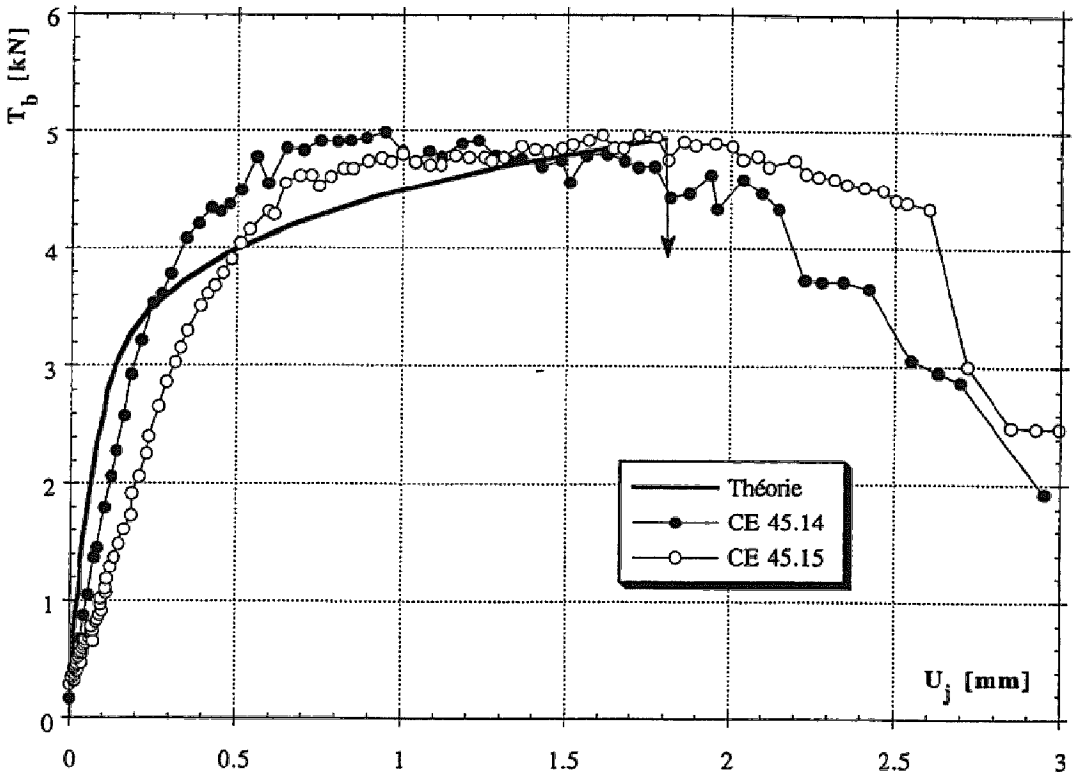

Figure 6.21 : *Comparison of bolt contribution for the models with joints inclined at 45 degrees*

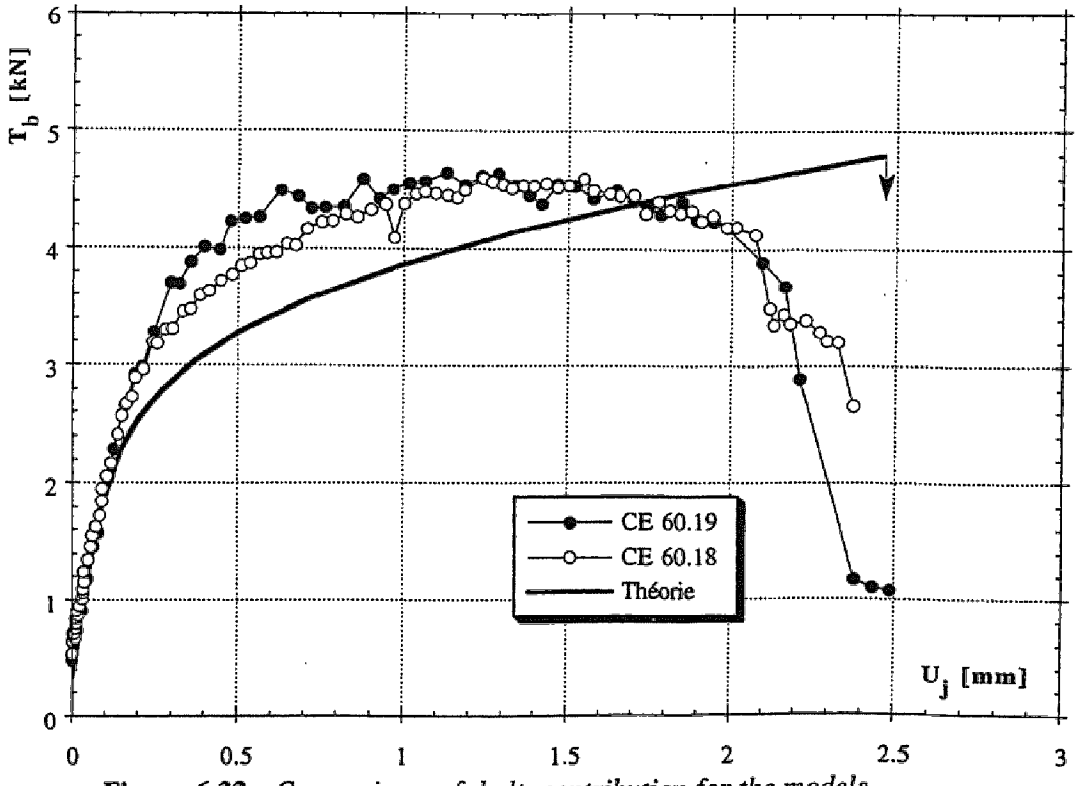

Figure 6.22 : *Comparison of bolt contribution for the models with joints inclined at 60 degrees*

6.5.2. Tests realized by Spang

The tests reported by **Spang (1988)** were carried out on granite, sandstone and concrete specimens, by direct shear tests. The specimens were reinforced by a single steel bolt of 8 mm diameter. The bolts were installed in holes whose diameters were equal to twice the bolt diameter. The bonding mortar was composed of a bentonite-cement mixture. Mechanical characteristics were as follows :

- Uniaxial compressive strength	Granite:	σ_c = 105 MPa
	Concrete :	σ_c = 40 MPa
	Sandstone:	σ_c = 10 MPa
	Mortar:	σ_{cg} = 36 MPa
- Bolt characteristics	Diameter:	D_b = 8 mm
	Elasticity limit:	σ_{el} = 630 MPa
	Yield limit:	σ_{ec} = 670 MPa
	Strain at failure:	ε_f = 13.5%

The joint friction angle was varied between 30 and 34 degrees, and the orientation of the bolts with respect to the joint varied between 60 and 90 degrees. Figures 6.23 to 6.26 show experimentally measured and analytically computed bolt contribution as a function of the joint displacement.

In the tests performed on the concrete specimens, favorable accordance between experimental and analytical results was observed. For the bolt perpendicular to the joint (Figure 6.23), displacement at the failure was two times greater than the bolt diameter, whereas the same displacement was reduced to about half of the diameter for an inclination of 60 degrees (Figure 6.24).

Accurate forecasting of the maximum bolt contribution is noted in the tests of sandstone (Figure 6.25). To the contrary, the displacement at the failure is underestimated, because of greater mortar strength with respect to that of the surrounding rock. For granite tests (Figure 6.26), the situation is inversed and the calculated displacement is markedly lower than that of the measurements.

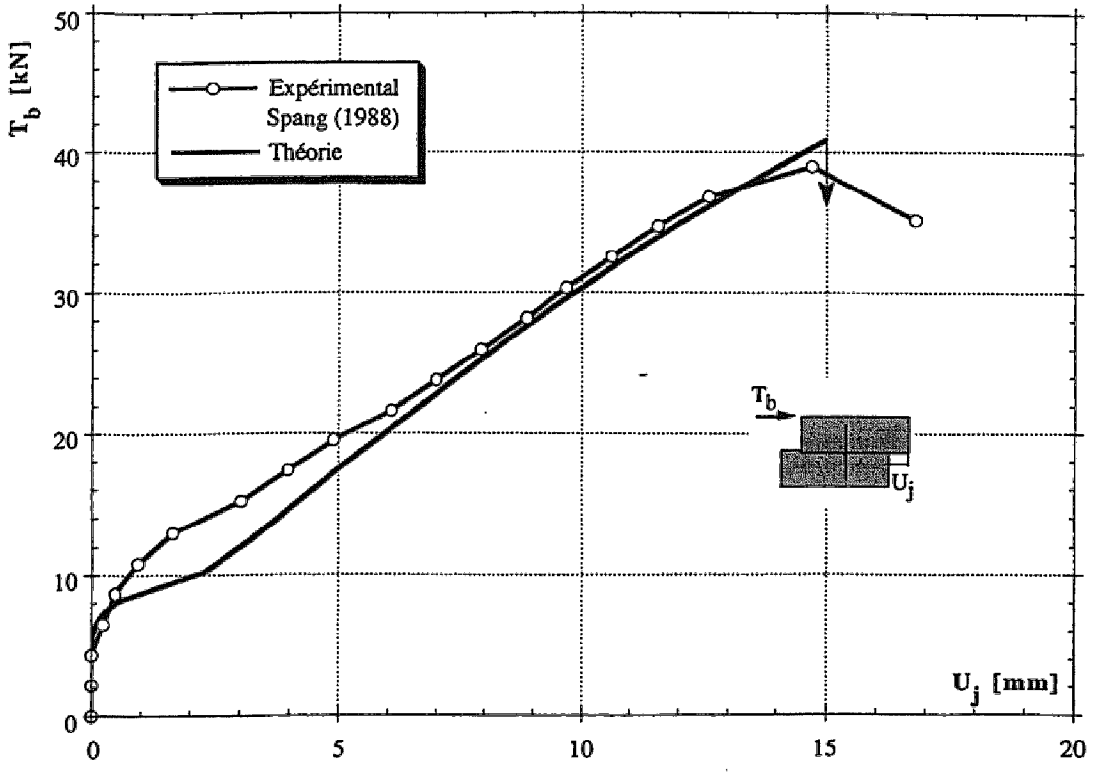

Figure 6.23 : *Bolt contribution versus joint displacement for concrete specimen reinforced by a single bolt of 8 mm diameter, perpendicular to the joint (β = 90 degrees)*

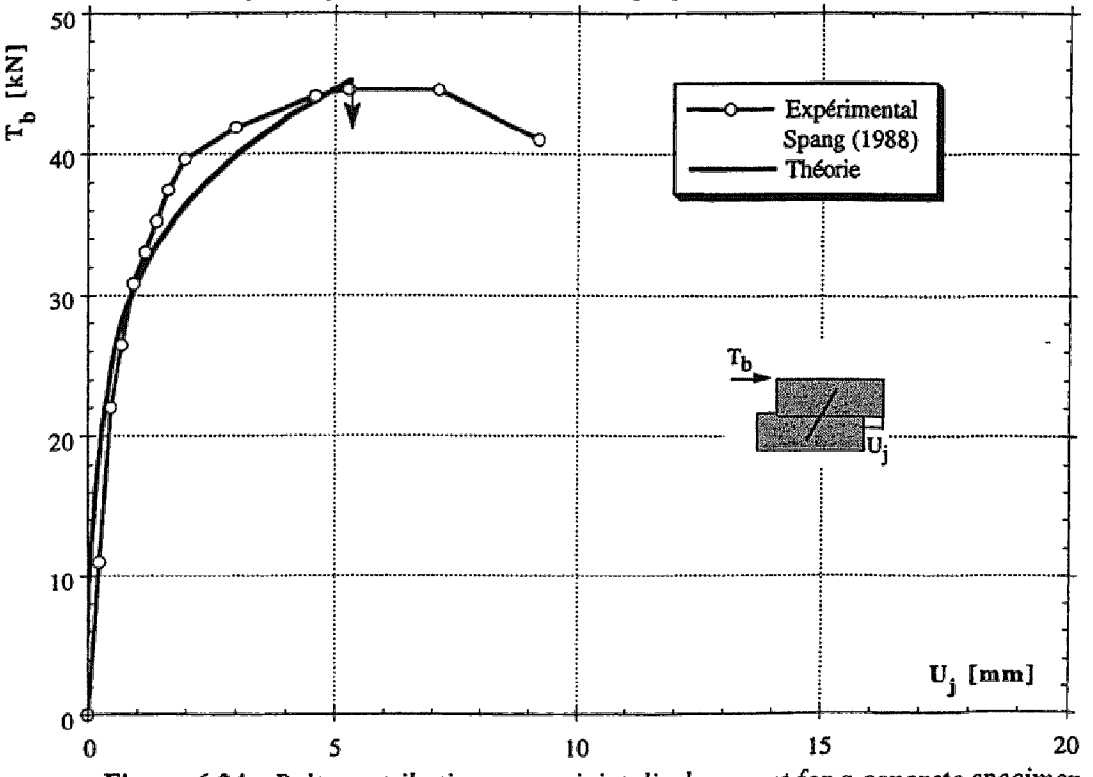

Figure 6.24 : *Bolt contribution versus joint displacement for a concrete specimen reinforced by a single bolt of 8 mm diameter, inclined at 60 degrees*

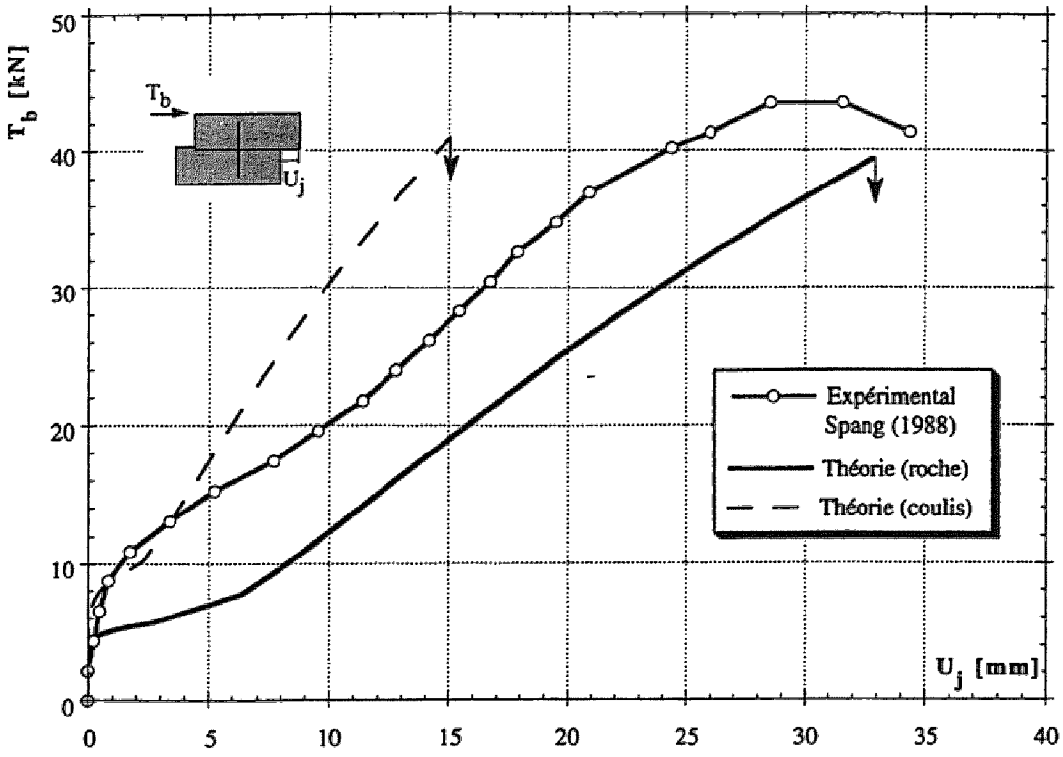

Figure 6.25 : *Bolt contribution versus joint displacement for a sandstone specimen reinforced by a single bolt of 8 mm diameter perpendicular to the joint*

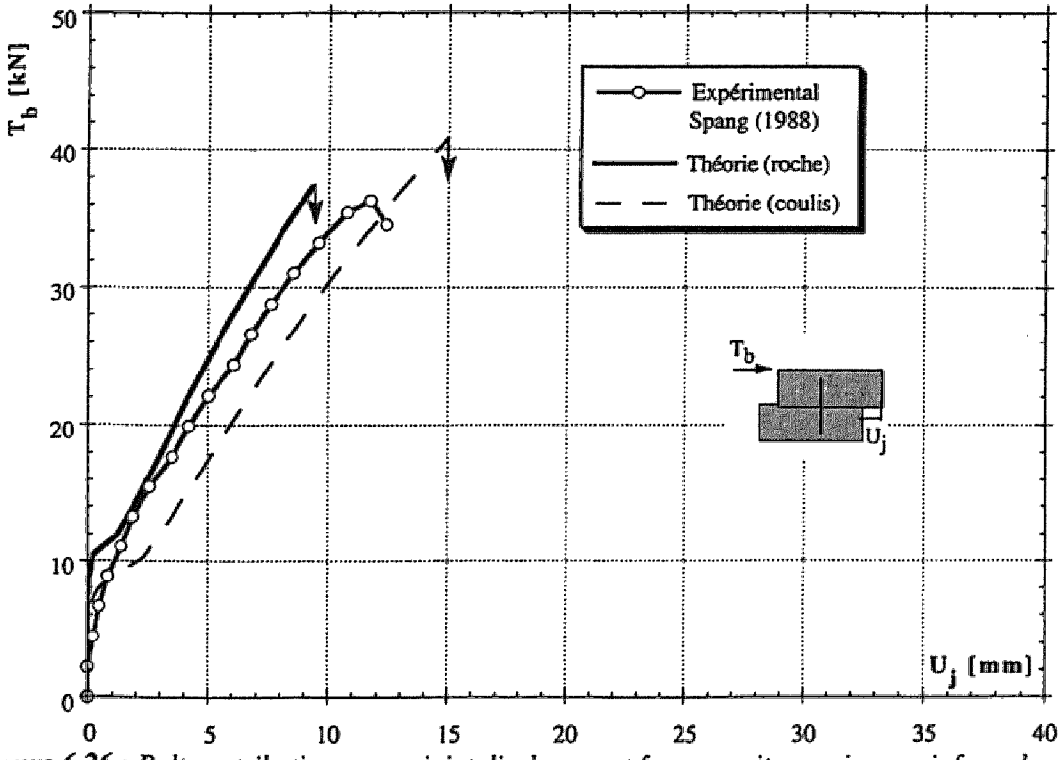

Figure 6.26 : *Bolt contribution versus joint displacement for a granite specimen reinforced by a single bolt of 8 mm diameter perpendicular to the joint*

The curves from the calculations, taking into account the mortar strength, are represented in the figure by dotted lines. One can also observe that the experimental curves are encircled by those of the calculations.

It can be finally stated that the favorable prevision of the bolt contribution and the joint displacement is obtained if the difference between the rock and the mortar strength is small.

6.5.3. Other tests published in the literature

The performance of the present analytical model is confronted with the test results reported by **Haas (1976-1981), Dight (1983), Egger & Fernandes (1983)** and **Ferrero (1993)**. The parameters of the tests and the principal results are summarized in Table 6.2.

The comparisons of the bolt contribution to the shear strength and the associated displacements of the joint are illustrated in Figures 6.27 and 6.28, respectively.

As previously mentioned, it is also observed here that in the case of a steeply inclined bolt (i.e., when the angle between the bolt and joint is small), the present theory and the Bjurström's decomposition furnish appropriate prediction of the total bolt contribution (see Figure 6.27). If the angle between the bolt and the joint is great, then Bjurström's curve is far from the experimental results, whereas both Spang's curves and those of the present theory are in agreement with them.

The joint displacements obtained from Spang's formula and the present theory are in accordance with the experimental results (see Figure 6.28).

Excepting one test of the Egger & Fernandes series, the maximum deviation is equal to 10% for the bolt contribution, and equal to 34% for the joint displacements.

Authors	Characteristics	β°	T_{bm} [kN]	S_{xt} [kN]	T_b^{th} [kN]	e_t %	U_{jm} [mm]	S_{xu} [mm]	U_j^{th} [mm]	e_u %
Haas (1981)	Limestone σ_c = 62 MPa ϕ_j = 42° D_b = 22 mm σ_{ec} = 483 MPa ε_f = 20 %	90	**210**	22.5	**231**	*+ 10*	**39.0**	11.9	**36.7**	*- 6*
		45	**231**	22.7	**229**	*- 1*	**22.7**	5.3	**11.4**	*- 50*
Egger & Fernandes (1983)	Concrete σ_c = 50 MPa ϕ_j = 33° D_b = 6 mm σ_{ec} = 500 MPa ε_f = 20 %	90	**10.9**	2.0	**15.7**	*+ 44*	**8.5**	1.5	**11.4**	*+ 34*
		60	**16.0**	0.7	**16.3**	*+ 2*	**3.9**	3.5	**4.7**	*+ 21*
		45	**16.9**	-	**16.3**	*- 4*	**3.6**	3.0	**3.4**	*- 6*
		30	**15.3**	1.8	**15.9**	*+ 4*	-	-	**2.7**	-
Dight (1983)	Plaster σ_c = 25 MPa ϕ_j = 37° D_b = 4.8 mm σ_{ec} = 210 MPa ε_f = 20 %	90	**4.6**	0.6	**4.4**	*- 4*	**8.7**	1.6	**8.2**	*- 6*
Ferrero (1993)	Granite σ_c = 41 MPa ϕ_j = 37° D_b = 12 mm σ_{ec} = 720 MPa ε_f = 25 %	90	**105**	7.1	**98.4**	*- 6*	**28.5**	0.1	**34.6**	*+ 21*

Table 6.2 : *Comparison of the experimental results to analytical previsions*

T_{bm} : average value of the bolt contribution,
S_{xt} : standard deviation of the bolt contribution,
T_b^{th} : bolt contribution calculated by the presented theory,
e_t : difference between average and calculated bolt contribution,
U_{jm} : average value of the joint displacement,
S_{xu} : standard deviation of the joint displacement,
U_j^{th} : the joint displacement calculated by the theory,
eu : difference between average and calculated joint displacement.

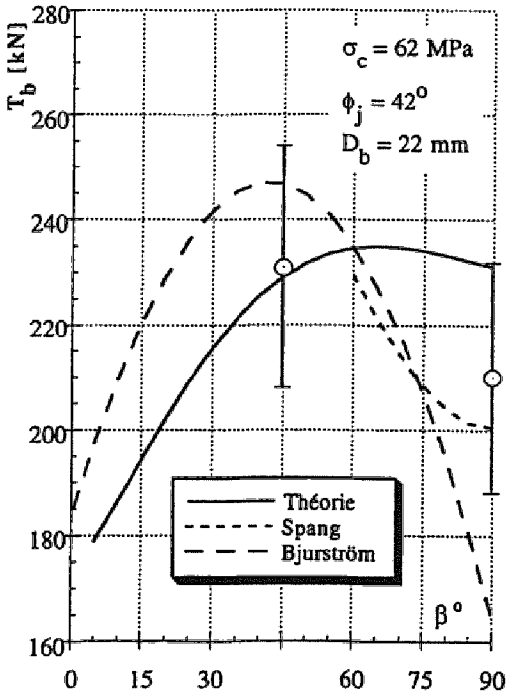

a- test results after Haas (1981)

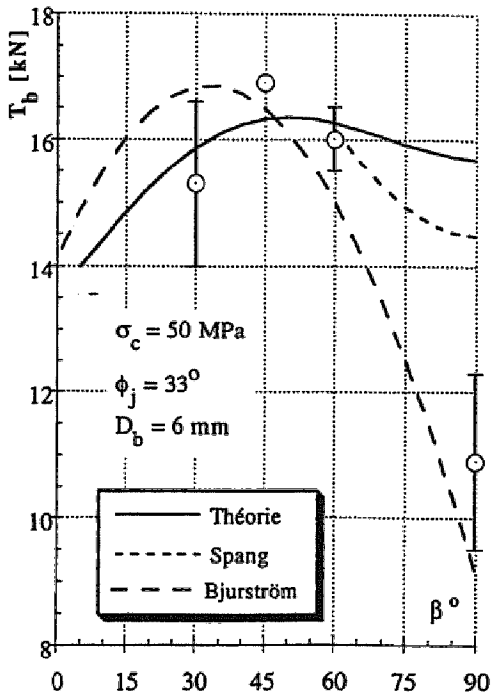

b- test results after Egger & Fernandes (1983)

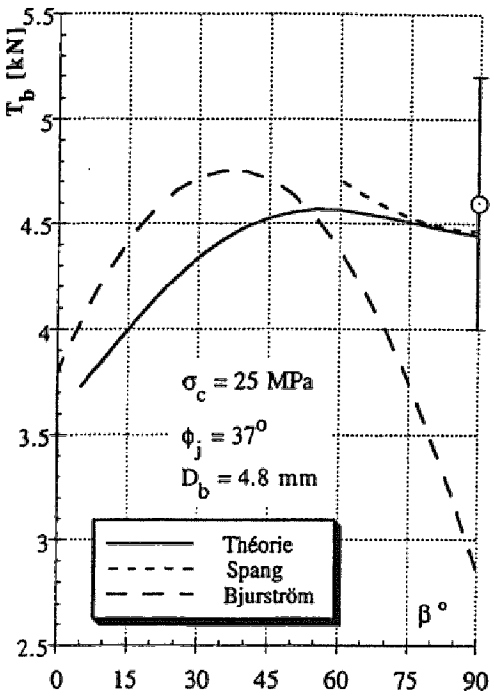

c- test results after Dight (1983)

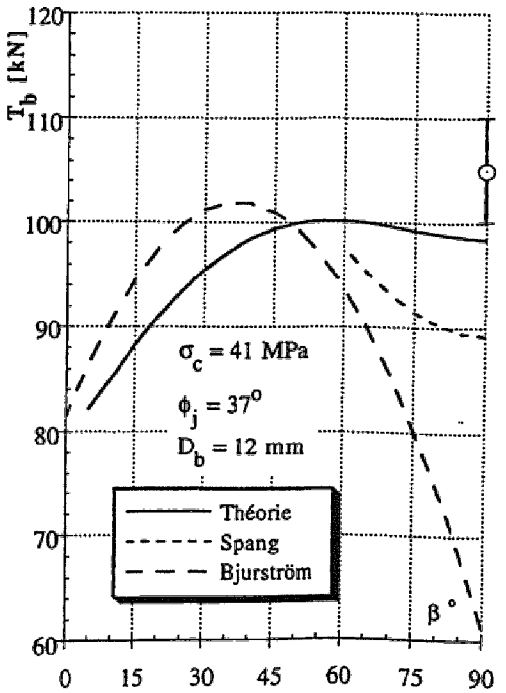

d- test results after Ferrero (1993)

Figure 6.27. *Comparison of calculated contributions of the bolts with these from the experiments performed by different authors*

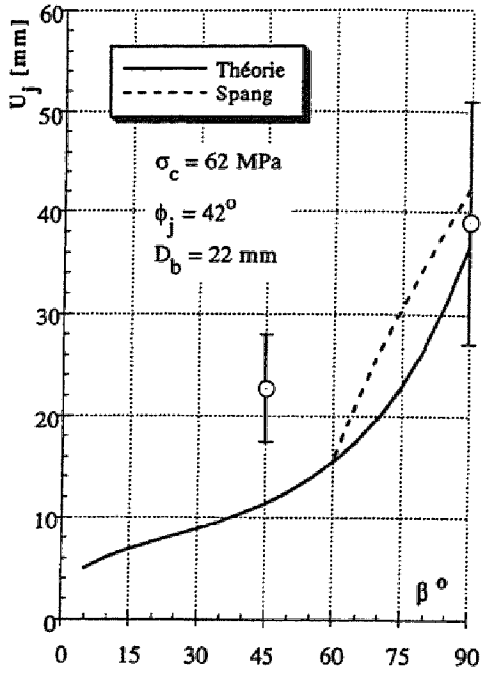

a- test results after Haas (1981)

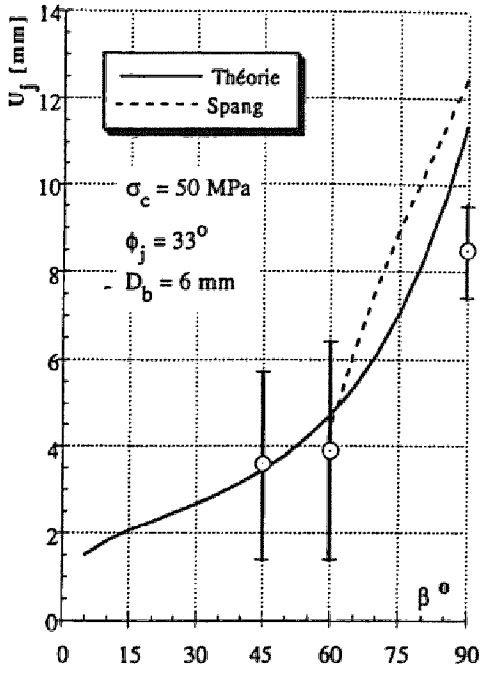

b- test results after Egger & Fernandes (1983)

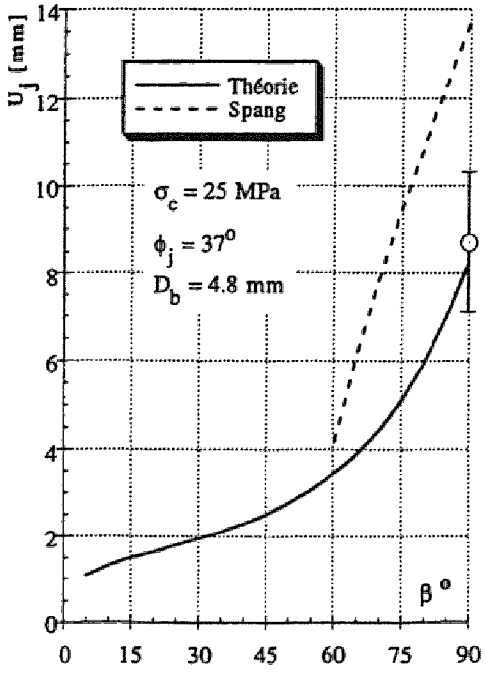

c- test results after Dight (1983)

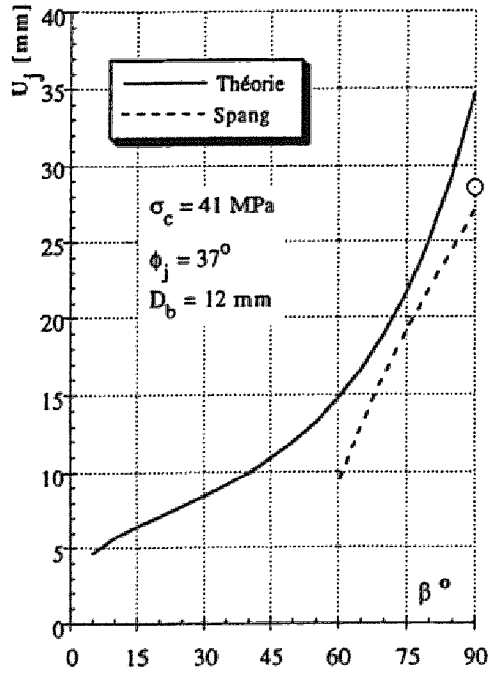

d- test results after Ferrero (1993)

Figure 6.28. *Comparison of calculated joint displacements with experimental values obtained by different authors*

6.6. Conclusions

The systematic study of the parameters influencing the behaviour of a reinforced joint, realized by the analytical formulation and confirmed by the principal test results, allows one to formulate the following conclusions.

The rock strength slightly influences the shear strength of the reinforced joint. To the contrary, if the strength diminishes, then the displacements required to mobilize the maximum strength considerably increase. If the grout annulus is thick, then the strength of the grouting agent is more important than that of the rock.

The inclination of the bolt to the joint surface very considerably influences the mechanical behaviour of the reinforced joint. If the angle is great (perpendicular bolt), the confining effect and the reinforcement cohesion have a comparable significance. To the contrary, if the angle is small (very inclined bolt), the role of the confining is negligible in comparison to that of the reinforcement cohesion. Therefore, the optimum position of the bolt varies as a function of the joint friction angle. On the other hand, the displacement required for the mobilization of the total contribution of the bolt increases with the angle between the bolt and the joint.

It summary, a perpendicular bolt installed in weak rock composes a flexible system, whereas a steeply inclined bolt in hard rock forms a rigid system. The strength of these systems depends on the joint friction angle.

In comparison to the previous analytical solutions, the presented theory can be applied to a wide range of values for the bolt orientation angles and for differentiated rock strength conditions. It also makes it possible to calculate analytically the complete curve of the bolt contribution as a function of the joint displacements.

Chapter 7

Applications to the Dimensioning of Rock Engineering Structures

In this chapter, the analytical formulation developed in chapter 5 and discussed in chapter 6 will be applied to the dimensioning of rock engineering structures.

7.1. Stability of excavated slope

Let us consider an excavated slope with a vertical wall of 15 meters height (Figure 7.1). The layers are 1.5 meter thick and the dip angle of the layers is 60 degrees. The reinforcement is realized by fully grouted steel bolts.

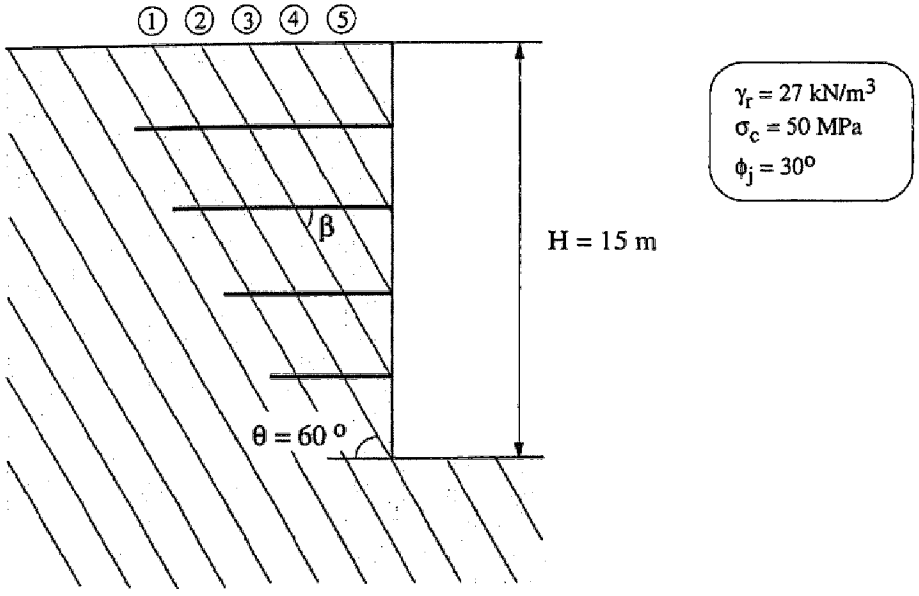

Figure 7.1 : *Geometry of the studied slope*

The geometrical and mechanical characteristics assumed in the calculations are as follows :

Rock:	- unit volumetric weight	$\gamma_r = 27$ kN/m3
	- uniaxial compressive strength	$\sigma_c = 50$ MPa
	- joint friction angle	$\phi_j = 30o$
Bolts:	- yield limit	$\sigma_{ec} = 600$ MPa
	- elasticity modulus	E = 210000 MPa
	- deformation at the failure	$\varepsilon_f = 20\%$

7.1.1. Equilibrium of unstable rock volume

The equilibrium of the unstable volume of rock is studied by force decomposition (Figure 7.2).

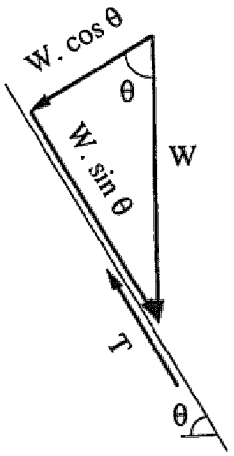

Figure 7.2 : *Decomposition of forces acting on the unstable volume of rock*

Considering the equilibrium equation with respect to the slide plane, one obtains the formula for the safety factor :

$$F = \frac{W \cos\theta \ tg\phi_j + T}{W \sin\theta}$$

where T is the additional resistance provided by the reinforcing bolts and W is the weight of the unstable volume of rock.

For reasons of the ratio between volumetric and surface forces, the discontinuity number 1 is considered as the critical failure plane. As the cohesion is equal to zero, the forces are proportional to the square of the slope height and the weight of unstable volume is calculated as follows :

$$W = \frac{\gamma_r \ H^2}{2 \ tg\theta} = \frac{27 \ 15^2}{2 \ tg60} = 1754 \ kN/m$$

As the safety factor at the limit equilibrium state is equal to 1.0, the supplementary resistance, which must be provided by the reinforcement to ensure the slope stability, can be obtained using the following formula :

$$T = W \left(\sin\theta - \cos\theta \ tg\phi_j\right) = 1754 \ (\sin 60 - \cos 60 \ tg30) = \mathbf{1012 \ kN/m}$$

Following the same procedure, one can calculate the force T, which is required to ensure the stability for each of the discontinuities :

- joint 2:	H = 12 m	W = 1122 kN	T = 648 kN/m
- joint 3:	H = 9 m	W = 631 kN	T = 365 kN/m
- joint 4:	H = 6 m	W = 281 kN	T = 162 kN/m
- joint 5:	H = 3 m	W = 70 kN	T = 41 kN/m

7.1.2. Reinforcement dimensioning for the critical discontinuity

In the calculations based on the relation between the force mobilized in the bolt and the joint displacements, it is necessary to assume a priori the bolt diameter. The reaction pressure exerted by the surrounding medium is

calculated with the assumption that the grout mixture strength is equal to the rock strength :

$$p_u = \sigma_c \, D_b$$

Detailed calculation of the forces mobilized in the bolt and associated displacements along the joint is presented in Appendix II. For a bolt of 20 mm diameter, installed horizontally ($\beta = 60^o$), the contribution, T_b, and the associated joint displacements, U_j, are equal :

- at the elastic limit of the bolt

$$\mathbf{T_{be} = 80\ kN} \qquad \mathbf{U_{je} = 0.6\ mm}$$

- at the failure of the bolt

$$\mathbf{T_{bf} = 210\ kN} \qquad \mathbf{U_{jf} = 17.1\ mm}$$

As the bolt contribution (T_b) to the shear strength of the joint is known, the bolting scheme can be determined. The number of bolts, n_b, installed in one profile as well as their spacing, e, are calculated for the equilibrium state of the unstable volume and for the adopted bolting scheme. If a square pattern of bolts is assumed then :

$$n_b = \sqrt{\frac{T\ H}{T_b}}$$ where n_b is the theoretic number of bolts

$$e = \frac{n_b\ T_b}{T} = \frac{H}{n_b}$$ with n_b rounded to the superior integer

For the present case, one obtains :

- at the failure of the bolts

$$n_b = \sqrt{\frac{1012\ 15}{210}} = \mathbf{8.5} \Rightarrow \mathbf{9\ bolts\ in\ a\ profile}$$

$$e = \frac{n_b\ T_b}{T} = \frac{9\ 210}{1012} = \mathbf{1.87\ m}$$

- at the elastic limit of the bolts

$$n_b = \sqrt{\frac{1012\ 15}{80}} = 13.8 \Rightarrow \mathbf{14\ bolts\ in\ a\ profile}$$

$$e = \frac{n_b\ T_b}{T} = \frac{14\ 80}{1012} = \mathbf{1.10\ m}$$

For e = 1.1 m and n_b = 14, the safety factor of the bolts is equal to :

$$F_b = \frac{T_{bf}}{T_{be}} = \frac{210}{80} = \mathbf{2.64}$$

The safety factor for the slope stability, F_b, is :

$$F = \frac{W \cos\theta\ tg\phi_j + T}{W \sin\theta} = \frac{1754\ 0.5\ 0.577 + \left(14\ 210/1.1\right)}{1754\ 0.866} = \mathbf{2.09}$$

This reinforcement arrangement is one of the possible solutions. In Table 7.1, results of calculations performed in the same manner for different diameters and orientations of the bolt are presented.

		bolts failure				bolts elastic limit				
D_b	β	T_{bf}	U_{jf}	n_b	e	T_{be}	U_{je}	n_b	e	F_b
[mm]	o	[kN]	[mm]	-	[m]	[kN]	[mm]	-	[m]	-
16	90	129	33.5	11	1.40	20	1.0	28	0.54	**6.6**
	60	134	13.7	11	1.46	51	0.5	18	0.91	**2.6**
	45	136	10.0	11	1.48	66	0.4	16	1.04	**2.3**
20	90	201	41.9	9	1.79	31	1.2	23	0.69	**6.6**
	60	**210**	**17.1**	**9**	**1.87**	**80**	**0.6**	**14**	**1.10**	**2.6**
	45	213	12.5	9	1.89	103	0.5	13	1.32	**2.3**
24	90	290	50.3	8	2.29	44	1.4	19	0.83	**6.6**
	60	302	20.6	8	2.39	115	0.7	12	1.36	**2.6**
	45	306	15.0	7	2.42	148	0.6	11	1.61	**2.3**

Table 7.1 : *Solutions for different bolt diameters and different bolt orientations*

Examination of this table proves logical relations, i.e., if the bolt diameter increases, the number of bolts decreases, whereas their spacing augments. The joint displacement considerably increases with the diameter of the bolts. For a given bolt diameter, the bolt contribution varies insignificantly when the angle between the bolt and the joint diminishes. The joint displacement, however, is considerably reduced at the same time. If it is assumed that the bolts only have to work to their elastic limit, then the number of installed bolts should be significantly increased. The joint displacement is limited and the bolting safety factor augments as a function of the orientation of the bolts.

The curves presented in Figure 7.3 show the augmentation of the safety factor of the bolts and the diminution of the joint displacement when the spacing between the bolts decreases. The last point consists of verifying that the bonded length of the bolts is sufficient to prevent pulling-out of the holes.

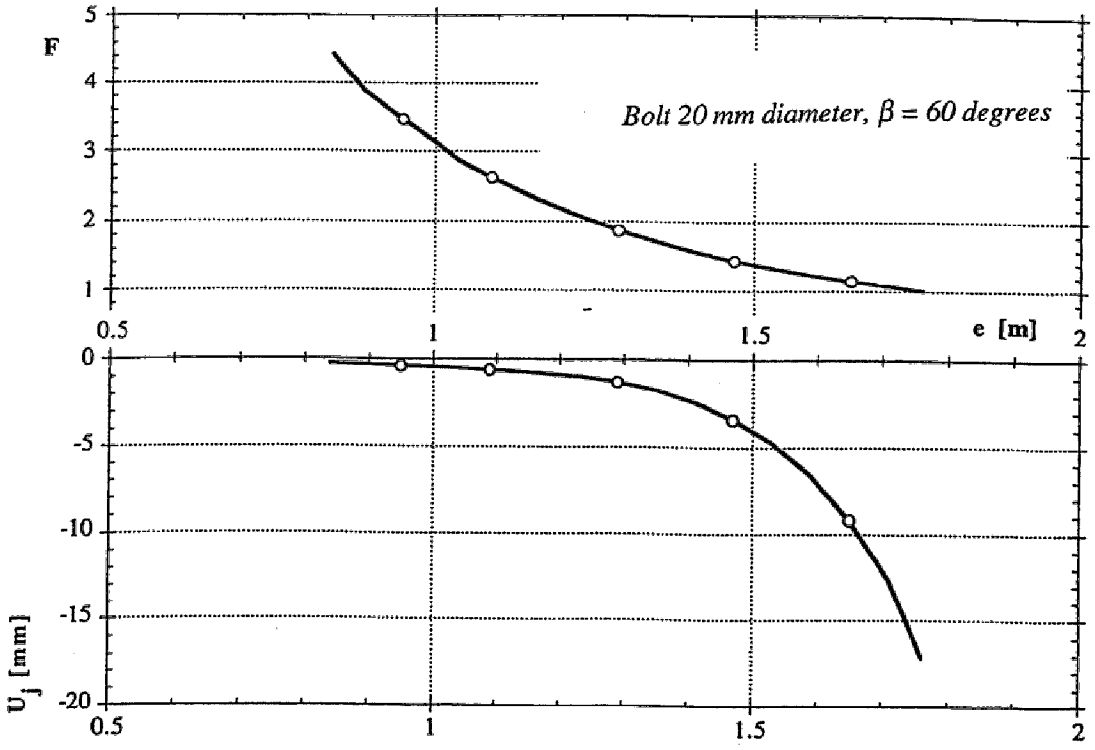

Figure 7.3 : *Evolution of the safety factor and the joint displacement as a function of the theoretical spacing between bolts*

7.1.3. Total displacement of the mass

The total displacement between the top of the slope and the stable part of the mass is obtained by adding the displacements occurring along each individual discontinuity. In doing this, it is necessary to calculate the force which loads each bolt of each discontinuity. The following values are obtained for the case of the bolts working at the failure :

- joint 2:	T = 648 kN/m	$n_b = 7$	$T_b = 173$ kN
- joint 3:	T = 365 kN/m	$n_b = 5$	$T_b = 136$ kN
- joint 4:	T = 162 kN/m	$n_b = 3$	$T_b = 101$ kN
- joint 5:	T = 41 kN/m	$n_b = 1$	$T_b = 76$ kN

As the force which loads each individual bolt is known, the displacement of each joint can be determined by utilizing the curve of the bolt contribution.

The bolt contribution versus the joint displacement, for a horizontal bolt (β = 60°) of 20 mm diameter is shown in Figure 7.4. The vertical component of the sum of the displacements along the joints is the total settlement, s, i.e., the vertical distance between the top of the slope and the stable part of the mass :

$$s = \sum_{n=1}^{n_j} \left(U_j \sin\theta \right) = (17.1 + 7.1 + 2.5 + 1.0 + 0.6) \sin 60 = \mathbf{24.5\ mm}$$

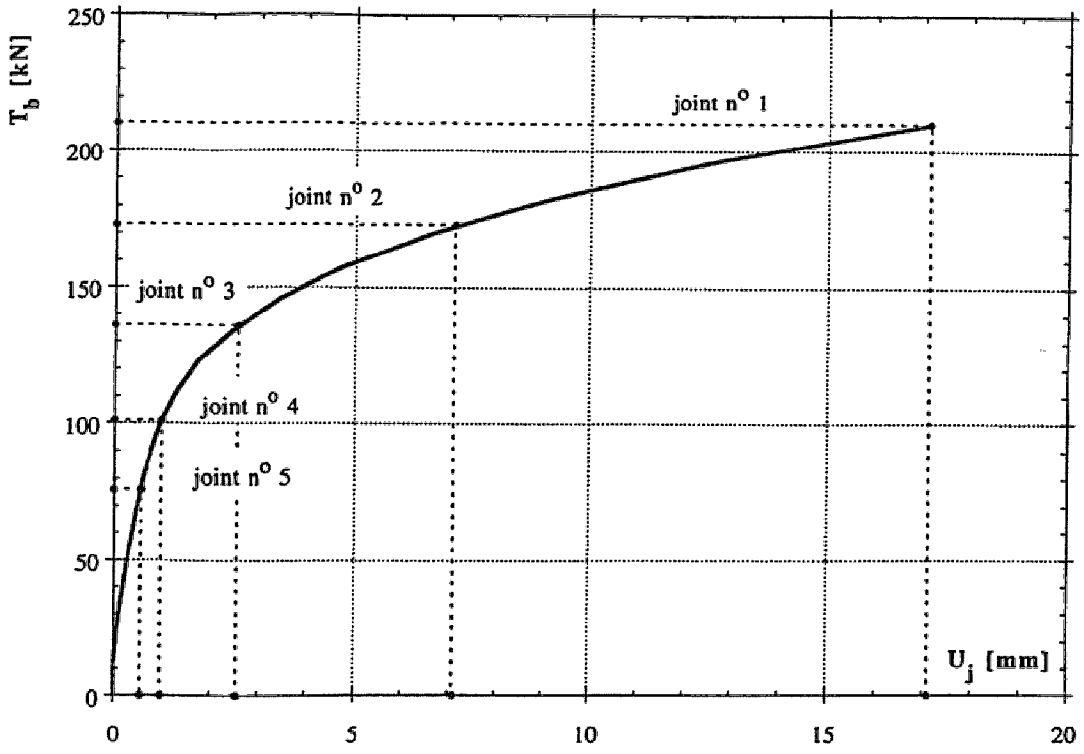

Figure 7.4. *Contribution of the bolt of 20 mm diameter, installed at β = 60 degrees, as a function of joint displacement*

7.2. Stability of shallow tunnel

Let us consider a tunnel of 10 meters diameter at a depth of 20 meters (Figure 7.5). The excavation is realized in weak formations and bolting is required to ensure the roof stability. It is assumed that the volume of the mass which can collapse is delimited by two vertical planes.

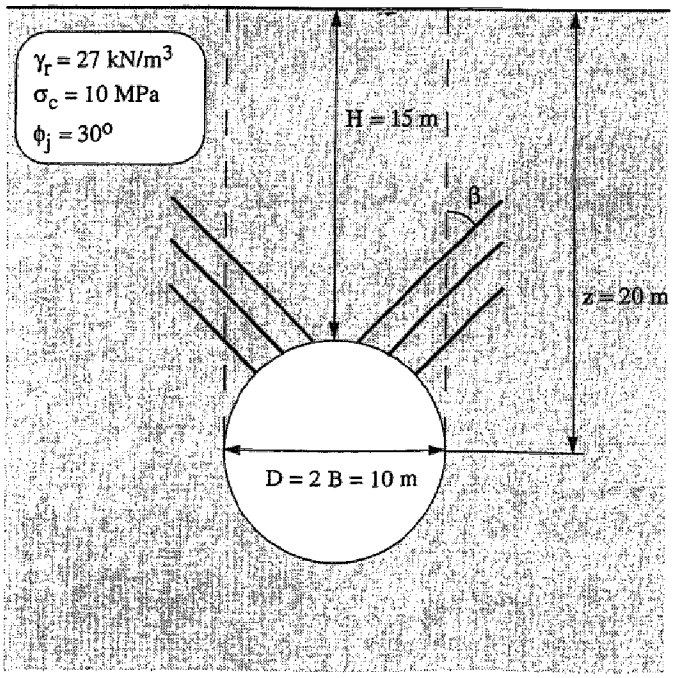

Figure 7.5 : *Geometry of the studied tunnel*

7.2.1. Overburden pressure which has to be supported by the reinforcement

The pressure acting on the roof can be calculated based on Terzaghi's theory. In the case of cohesionless material, this leads to the following formula :

$$p_v = \frac{\gamma\ B}{k_o\ tg\phi}\left(1 - e^{-k_o tg\phi \frac{H}{B}}\right) = \frac{27\ 5}{0.5\ 0.577}\left(1 - e^{-0.5\ 0.577\ \frac{15}{5}}\right) = \mathbf{271\ kPa}$$

Thus, the total force is equal to :

$$T = p_v \; D = 271 \; 10 = \mathbf{2710 \; kN/m}$$

7.2.2. Reinforcement dimensioning

The calculation of the bolt contribution is identical to that which was presented in the preceding section. After the bolt diameter and the orientation are chosen, the bolt's contribution and the associated displacement can be calculated. Table 7.2 summarizes possible solutions for different diameters of the bolts, placed at 60 and 45 degrees to the vertical. The letter "e" signifies the longitudinal spacing between the bolts.

			Failure of the bolts				**Elastic limit of the bolts**				
ϕ_j	D_b	β	T_{bf}	U_{jf}	n_b	e	T_{be}	U_{je}	n_b	e	F_b
o	[mm]	o	[kN]	[mm]	-	[m]	[kN]	[mm]	-	[m]	-
30	**20**	45	217	23.97	13	1.04	132	1.27	21	1.02	1.64
		60	211	33.87	13	1.01	102	1.68	27	1.02	2.08
	30	45	487	35.96	6	1.08	296	1.90	10	1.09	1.64
		60	476	50.81	6	1.05	229	2.51	12	1.02	2.08

Table 7.2 : *Solutions for different bolt diameters and different bolt orientations*

Examination of the table proves that the decrease of β causes, as before, considerable limitation of the displacement, whilst the contribution significantly increases simultaneously.

7.2.3. Settlement as a function of forces carried by the bolts

Let us suppose that the vertical load acting at the roof level is uniformly distributed. Then, the evolution of the pressure, calculated by subtraction of the pressure provided by the bolts from the initial pressure, can be determined as a function of the vertical displacement of the roof.

Evolution of the vertical pressure for 30 mm bolts, inclined at 45 degrees is shown in Figure 7.6. For a bolting system working at the elastic limit, 10 bolts with longitudinal spacings of 1.1 meter are required. If bolts work until the failure, 6 have the same longitudinal spacing. In this hypothesis, bolting must be associated with a concrete support, having a stiffness determined based on the admissible displacements and the required security of the bolts. The support stiffness represented in Figure 7.6 corresponds to the case where the elastic limit of the bolts cannot be exceeded.

Figure 7.7 illustrates the evolution of the vertical pressure acting on the roof for the case of bolts inclined at 60 degrees to the vertical. It should be noted that the displacements are significantly greater in this configuration.

7.2.4. Note on the length of the bolts

As was already mentioned, it is advantageous from the mechanical point of view to incline the bolts with respect to the joint plane. However, doing this, it is necessary to increase the length of the bolts to ensure their bonding outside of the unstable zone. In general cases, the minimum length of the bonding length is equal to at least 20 diameters of the bolt. As a result, the optimization of the bolting system requires one to study the ratio between the number of bolts installed in a profile and their respective lengths.

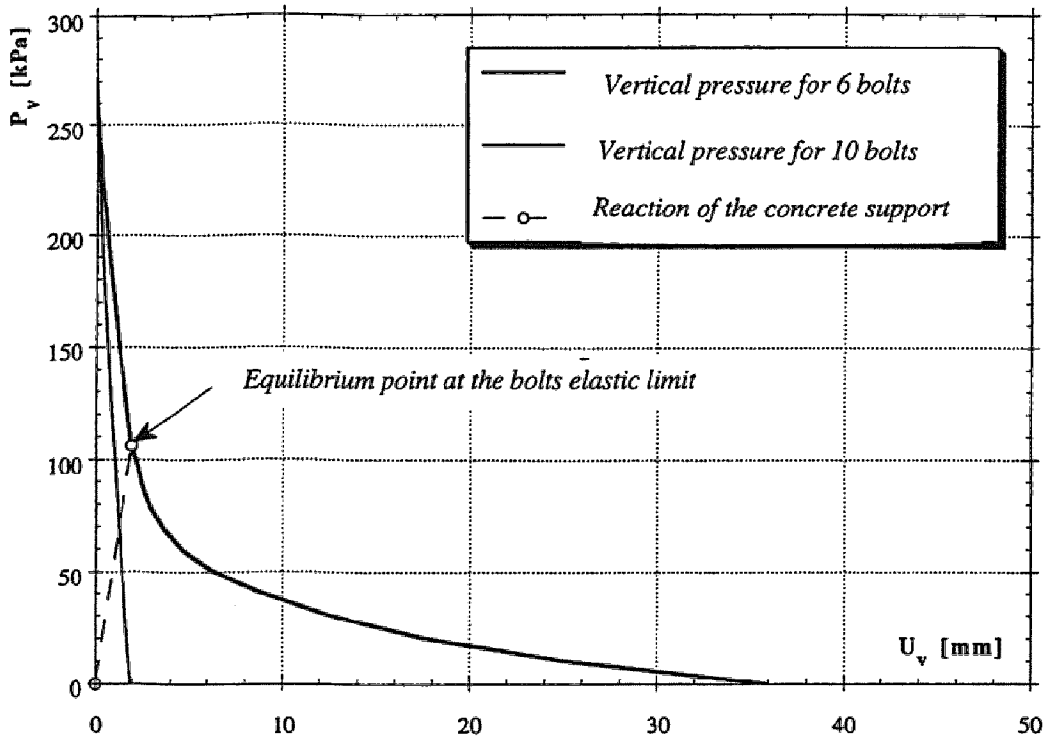

Figure 7.6 : *Pressure exerted on the roof as a function of the vertical displacement for bolts of 30 mm diameter, installed at 45 degrees to the vertical*

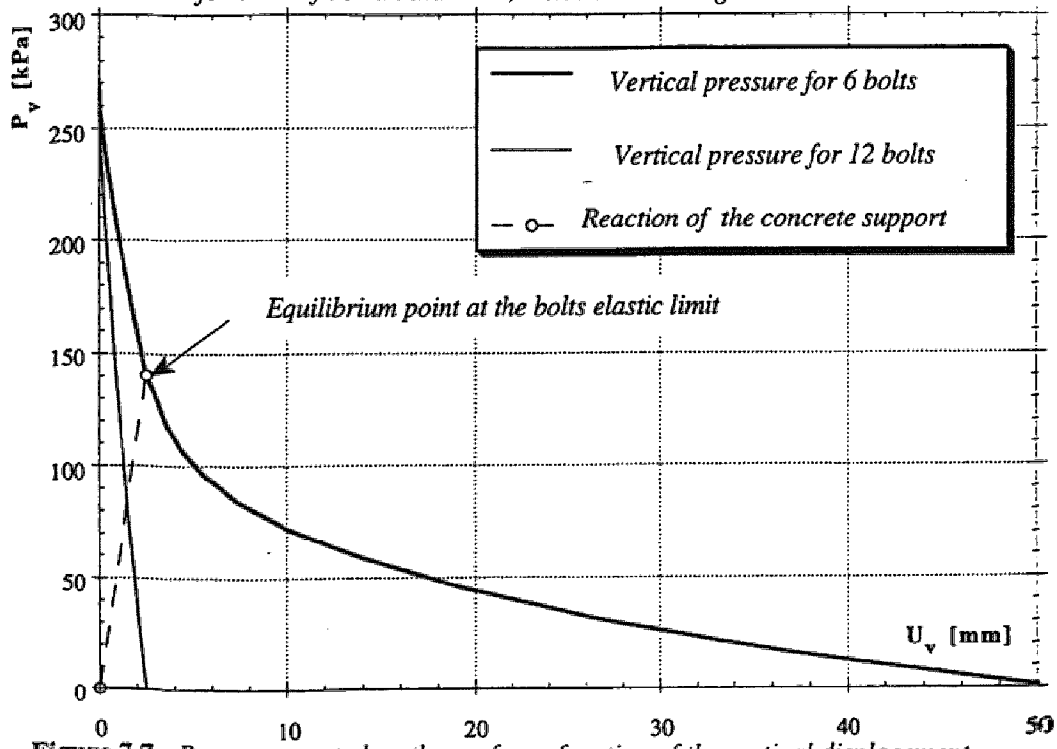

Figure 7.7 : *Pressure exerted on the roof as a function of the vertical displacement for bolts of 30 mm diameter, installed at 60 degrees to the vertical*

7.3. Practical suggestions

Some practical conclusions, resulting from the theoretical analysis of the mechanical behaviour of the fully grouted bolt, are drawn below. Beside the design criteria, economic or technical reasons may lead the constructor to others solutions.

7.3.1. Selection of the bolt type

The selection of the bolt type essentially depends on the function which the bolting has to achieve. For example, if it is necessary to ensure temporary support in any section of a tunnel before its final section is excavated, tubular or resin grouted bolts are very frequently utilized, allowing one to protect the excavating machines. Resin grouted bolts are also installed if the occurrence of electric currents, which accelerate the corrosion of the metallic elements, is possible.

Generally, it is most favorable to utilize full cross-section steel bolts, having high strength. This enables one to increase the bolt contribution. If it is required to limit the joint displacements, the use of steel exhibiting small failure strain would be preferred.

7.3.2. Selection of the bolt diameter

For a given configuration, the contribution of the bolt increases linearly with its cross-section area, whilst the joint displacement increases linearly with the bolt diameter. If it is required that the rock mass displacements be limited, the most preferable scheme will be densely spaced bolting with bolts of small diameter. In practical applications, the diameter of the bolts range between 20 and 30 mm.

For a stratified rock mass, it must be verified (Figure 7.8) that the deformed length of the bolt (up a magnitude about six times the elastic length, based on the present theory) is not greater than one half of the layer thickness divided by the sine of the joint orientation angle. If such a case is observed, the reinforcement effectiveness is reduced.

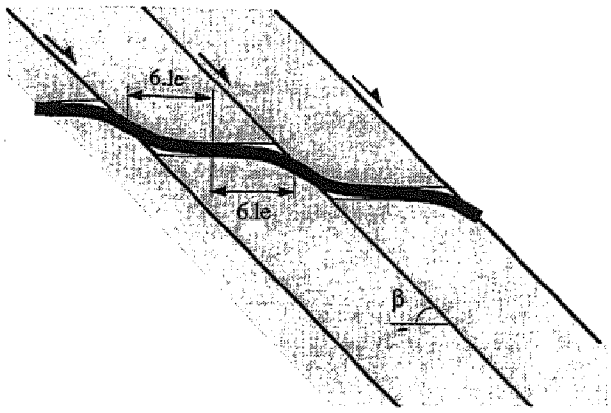

Figure 7.8 : *Deformational mechanism of the bolt installed in stratified rock mass*

7.3.3. Selection of the bolt orientation

The bolt contribution to the shear strength of the joint varies as a function of the bolt orientation, depending on the joint friction angle (see section 6.4.1). This relation shows that the lower the angle of friction, the more the bolts have to be inclined to the joint. On the other hand, if limitation of the rock mass displacements is required, it is recommended to incline the bolts with respect to the joint. Generally, the selected angle between the bolt and the joint should be lie in the range of 45 to 60 degrees.

7.3.4. Selection of the grout type

The quality of bonding between the bolt and the rock is of the greatest importance. In addition to bonding the bolt, the grout transmits the forces developed in the bolt to the rock. Thus, if high strength grout is used, the displacements necessary for the mobilization of the total bolt contribution will be limited.

Some authors recommend the utilization of grout with low shrinkage and high compressive strength, which exhibits dilatant behaviour. The epoxy resins, however, are very efficient. Their resistance is very high and their fluidity allows for the reduction of the borehole diameter.

Chapter 8

Conclusions

Numerous research programs realized in the past have highlighted the role played by an anchored bolt in rock joint reinforcement. Beside the characteristic properties of the reinforcing element, the bolt contribution and the resulting joint displacement essentially depend on the bolt inclination, the rock strength, and the joint friction angle. Although these conclusions could be established in a qualitative manner, the calculation of the rock structures in terms of strength and deformability were still rudimentary. Most of the proposed expressions for the calculations of bolt contribution and its associated displacements have an empirical character. In addition, they are based on simple hypotheses regarding bolt deformation and decomposition of forces.

8.1. Synthesis of the study

The experimental part of the study, realized on large scale models with a triaxial press having high capacities, allowed confirmation of the role played by the anchored bolt, and permitted the extension of the conclusions on specimens having several discontinuities. It was established that the number of joints does not affect the strength of the reinforced specimens. However, an increasing number of discontinuities causes deformability augmentation. The nature of the fixing condition of the bolt is a very important factor. For instance, a weak material reinforced by pointwise fixed bolts constitutes a flexible system, whereas any strong material reinforced by fully grouted bolts constitutes a rigid system. The system's strength varies as a function of the bolts inclination and the joint friction angle.

The analytical part, which allows for prevision of the bolt contribution and its associated joint displacement, is based on the accurate description of the bolt deformation process. The interdependence between axial and shear forces in the bolt is taken into account in both the elastic and the plastic domains. The consideration of large displacements in the plastic domain allows one to determine the bolt contribution and the associated joint displacement at failure.

The evaluation of the performances of this formulation proved its capacity to explain the observed phenomenon. The reinforcement cohesion and the confining effect are quantified. Comparison with the experimental results shows the reliability of this formulation. On the other hand, the formulation agrees with previous solutions, but covers a wide range of initial conditions.

Henceforth, the analytical formulation is at one's disposal, allowing one to obtain the complete curve of the bolt contribution as a function of the joint displacement. If the failure mechanism of a rock mass is clearly identified, this formulation is easily applicable for the calculation of the rock structures, such as slopes or underground excavations, whatever the orientation of the bolts and the rock strength may be.

8.2. Axes of future research

It would be sensible from an experimental point of view to perform more measurements of the displacements of the bolt during loading. It would facilitate the determination of the force distribution in the bolt. On the other hand, a certain lack of precision always exists in the determination of the reaction pressure exerted by the surrounding medium. It would be desirable to explain it by appropriately designed measurements. It should also be mentioned that the quantity of data collected on full scale constructions is rather small.

The analytical solution presented in this study deals with the case where the displacements occur by sliding along the joint for a bolt plunging in the joint direction. Although it covers most real situations, it would be advisable to extend the solution to the cases where the displacements cause the joint

opening and where the angle between the bolt and the joint is negative. The complete generalization of the formulation requires its adaptation for the cases of dilatant joints, where the failure occurs by shearing across the asperities.

The mechanical parameters calculated by the analytical development could be more generally included in numerical codes, to facilitate the analysis of complex rock structures.

Appendix I

Solution of the Bar Equilibrium by Rayleigh-Ritz Method

The method consists of the selection of a function which describes the deformation line of the bar and satisfies the boundary conditions. The total complementary energy of the system is calculated, and the unknown parameters, u_o and v_o, corresponding to the sought displacements, are obtained by minimization (more exact information can be found in **Washizu, 1975**). The bar geometry and the loading forces are shown in Figure I.1.

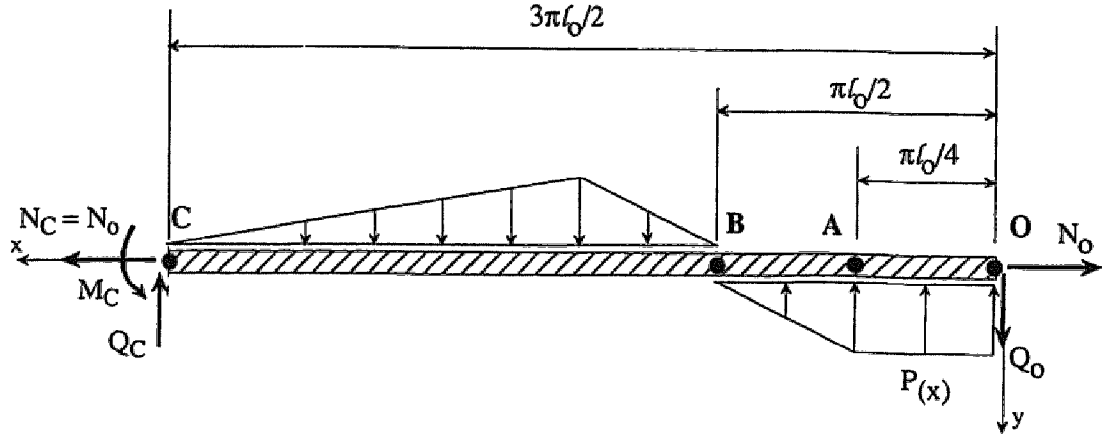

Figure II.1 : *Geometry of the bar and system of loading*

For simplification, as well as clarity, the characteristic length, $\mathbf{l_o}$, of the bar is denoted ℓ and the maximum pressure exerted by the rock, $\mathbf{p_u}$, is **p**.

- ***Displacement functions***

The chosen function describing transversal displacements is the solution of the differential equation of the beam elastic line having semi-infinite length, established without taking into account the normal force.

$$v_{(x)} = v_o\, e^{-x/\ell} \cos\left(\frac{x}{\ell}\right)$$

$$v'_{(x)} = -\frac{v_o}{\ell}\, e^{-x/\ell} \left[\cos\left(\frac{x}{\ell}\right) + \sin\left(\frac{x}{\ell}\right)\right]$$

$$v''_{(x)} = \frac{2\, v_o}{\ell^2}\, e^{-x/\ell} \sin\left(\frac{x}{\ell}\right)$$

It is supposed, that the axial displacements of the bar vary linearly along the bar's deformation line.

$$u_{(x)} = -u_o\left(1 - \frac{2\, x}{3\, \pi\, \ell}\right)$$

$$u'_{(x)} = \frac{2\, u_o}{3\, \pi\, \ell}$$

$$u''_{(x)} = 0$$

- ***Boundary conditions***

at x=0:

$$v_{(x)} = v_o$$

$$v'_{(x)} = -\frac{v_o}{\ell}$$

$$v''_{(x)} = 0$$

$$u_{(x)} = -u_o$$

at $x = 3\pi l / 2$:

$$v_{(x)} = 0$$

$$v'_{(x)} = \frac{v_o}{\ell} e^{-3\pi/2} \approx 0$$

$$v''_{(x)} = -\frac{2v_o}{\ell^2} e^{-3\pi/2} \approx 0$$

$$u_{(x)} = 0$$

- ***Deformation energy, U***

The deformation energy U is expressed as follows:

$$U = \frac{1}{2} \int_0^{3\pi\ell/2} \left[E A_b u'^2_{(x)} + E I v''^2_{(x)} \right] dx$$

or:

$$U = \frac{1}{2} \int_0^{3\pi\ell/2} E A_b \frac{4 u_o^2}{9\pi^2\ell^2} dx + \frac{1}{2} \int_0^{3\pi\ell/2} E I \frac{4 v_o^2}{\ell^4} e^{-2x/\ell} \sin^2\left(\frac{x}{\ell}\right) dx$$

Integration gives:

$$U = \frac{E A_b u_o^2}{3\pi\ell} + \frac{E I v_o^2}{4\ell^3}$$

where: E - elasticity modulus of bar,
A_b - cross-section of bar,
I - moment of inertia of bar.

- ***Work of external forces, W***

The calculation proves, that it is sufficient to integrate the work of the rock reaction pressure over the length from 0 to $\pi l/2$. On the other hand, the

forces acting at the left end of the bar (point C) do not produce any work, as the displacements and the rotation at this point are equal to zero.

$$W = N_o u_o + Q_o v_o - \int_0^{\pi\ell/2} p_{(x)}\ v_{(x)}\ dx$$

The reaction pressure is constant from 0 to $\pi l/4$, whereas it varies linearly from $\pi l/4$ to $\pi l/2$, following the function:

$$p_{(x)} = p\left(2 - \frac{4x}{\pi\ell}\right)$$

or:

$$W = N_o u_o + Q_o v_o - p\ v_o \int_0^{\pi\ell/4} e^{-x/\ell}\ \cos\left(\frac{x}{\ell}\right) dx$$
$$- p\ v_o \int_{\pi\ell/4}^{\pi\ell/2} \left(2 - \frac{4x}{\pi\ell}\right) e^{-x/\ell}\ \cos\left(\frac{x}{\ell}\right) dx$$

and after integration:

$$W = N_o u_o + Q_o v_o - p\ v_o\ \ell \left(\frac{1}{2} + \frac{\sqrt{2}\, e^{-\pi/4} - 2e^{-\pi/2}}{\pi}\right)$$

- ***Complementary total energy***

The complementary total energy Π of the system is expressed as the difference between the energy of deformation, U, and the work, W, of external forces.

$$\Pi = U - W$$

or:

$$\Pi = \frac{E\ A\ u_o^2}{3\ \pi\ \ell} + \frac{E\ I\ v_o^2}{4\ \ell^3} - N_o u_o - Q_o v_o + p\ v_o\ \ell \left(\frac{1}{2} + \frac{\sqrt{2}\, e^{-\pi/4} - 2e^{-\pi/2}}{\pi} \right)$$

- ***Calculation of displacements at O***

Minimization of the energy function gives:

$$\frac{\partial \Pi}{\partial v_o} = \frac{E\ I\ v_o}{2\ \ell^3} - Q_o + p\ell \left(\frac{1}{2} + \frac{\sqrt{2}\, e^{-\pi/4} - 2e^{-\pi/2}}{\pi} \right) = 0$$

$$v_o = \frac{2\ \ell^3}{E\ I} \left[Q_o - p\ell \left(\frac{1}{2} + \frac{\sqrt{2}\, e^{-\pi/4} - 2e^{-\pi/2}}{\pi} \right) \right]$$

Substituting $\ell = 4\ Q_o / \pi p$ one obtains:

$$v_o = \frac{128\ Q_o^4}{E\ I\ \pi^3\ p^3} \left[1 - \frac{4}{\pi} \left(\frac{1}{2} + \frac{\sqrt{2}\, e^{-\pi/4} - 2e^{-\pi/2}}{\pi} \right) \right]$$

or:

$$v_o = b\ \frac{128\ Q_o^4}{E\ I\ \pi^3\ p^3}$$

where b=0.27

For displacement u_o :

$$\frac{\partial \Pi}{\partial u_o} = \frac{2\ E\ A\ u_o}{3\ \pi\ \ell} - N_o = 0$$

$$u_o = \frac{3\ \pi\ \ell\ N_o}{2\ E\ A}$$

Substitution $\ell = 4\ Q_o / \pi p$ gives:

$$u_o = \frac{6\ N_o\ Q_o}{E\ A\ p}$$

Appendix II

Calculation Example of Bar Contribution and Joint Displacement

- ***Input data***

Geometry :	- angle between bar and joint	$\beta = 60^o$
Rock:	- uniaxial compressive strength	$\sigma_c = 50$ MPa
	- joint friction angle	$\phi_j = 30^o$
Bars:	- bar diameter	$D_b = 20$ mm
	- yield limit	$\sigma_{ec} = 600$ MPa
	- elasticity modulus	$E = 210000$ MPa
	- deformation at the rupture	$\varepsilon_f = 20$ %

Reaction pressure exerted by rock is equal to :

$$p_u = \sigma_c \; D_b = 50 \; 20 = 1'000 \text{ N/mm}$$

- ***Calculation of the bar contribution and the joint displacement at the elastic limit***

Figure II.1 reminds decomposition of forces and displacements in the bar in the elastic domain. Calculation begins with the determination of the forces mobilized in the bar at its elastic limit.

The shear force, Q_{oe}, is expressed by the equation 5.27 :

$$Q_{oe}^3 + Q_{oe}^2\left(\frac{3\ p_u\ \pi^3\ D_b\ tg\beta}{256\ b}\right) - \left(\frac{3\ p_u^2\ \pi^4\ D_b^4\ tg\beta\ \sigma_{ec}}{4096\ b}\right) = 0$$

and taking the considered parameters one obtains :

$$Q_{oe}^3 + Q_{oe}^2\left(\frac{3\ 1000\ \pi^3\ 20\ tg60}{256\ 0.27}\right) - \left(\frac{3\ 1000^2\ \pi^4\ 20^4\ tg60\ 600}{4096\ 0.27}\right) = 0$$

$$Q_{oe}^3 + 46618\ Q_{oe}^2 - 4.3937\ 10^{13} = 0$$

Solution of this equation requires the calculation of the discriminant Δ, expressed by the equation 5.28 :

$$\Delta = A^3 + B^2$$

where :

$$A = -\frac{46618^2}{9} = -2.4148\ 10^8$$

$$B = \frac{27\ 4.393710^{13} - 2\ 46618^3}{54} = 1.8216\ 10^{13}$$

Hence :

$$\Delta = -\left(2.4128\ 10^8\right)^3 + \left(1.8216\ 10^{13}\right)^2 = 3.1774\ 10^{26}$$

The value of the shear force at the steel elastic limit is obtained from expression 5.31 :

$$Q_{oe} = \sqrt[3]{1.8216\ 10^{13} + \sqrt{3.1774\ 10^{26}}} + \sqrt[3]{1.8216\ 10^{13} - \sqrt{3.1774\ 10^{26}}} - \cancel{46618}\ 15\,539 = \mathbf{24'803\ N}$$

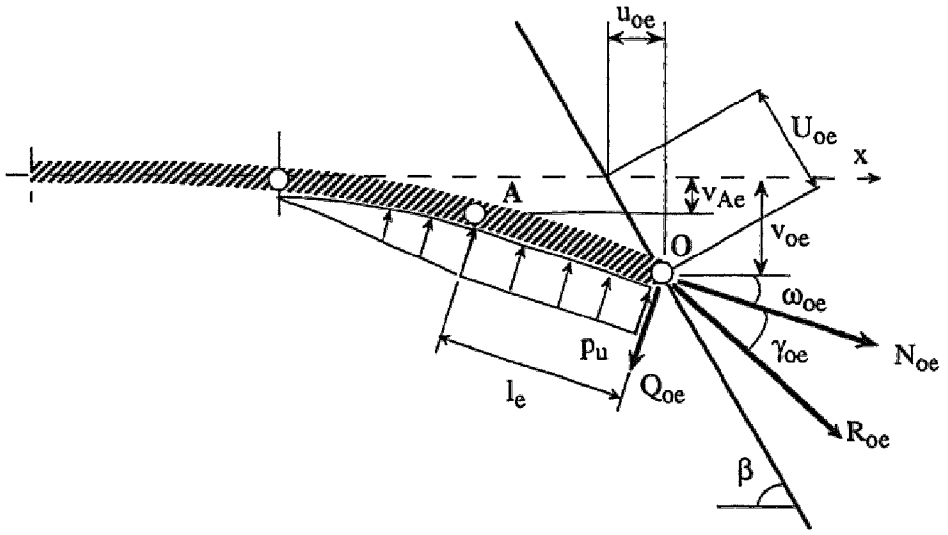

Figure II.1 : *Decomposition of forces and displacements of the bar in elastic domain*

The normal force is calculated from 5.25 :

$$N_{oe} = \frac{1024\ Q_{oe}^{3}\ 0.27}{3\ p_u^{2}\ \pi^{3}\ tg\beta\ D_b^{2}} = \frac{1024\ 24803^{3}\ 0.27}{3\ 1000^{2}\ \pi^{3}\ tg60\ 20^{2}} = \mathbf{65'460\ N}$$

The resultant force mobilized in the bar is simply calculated using the formula 5.55 :

$$\mathbf{R_{oe}} = \sqrt{Q_{oe}^2 + N_{oe}^2} = \sqrt{24'803^2 + 65'460^2} = \mathbf{70'001\ N}$$

The bar rotation at the elastic limit is obtained from 5.33 :

$$\omega_{oe} = \frac{2048\ Q_{oe}^3\ b}{E\ p_u^2\ \pi^3\ D_b^4} = \frac{2028\ 24803^3\ 0.27}{210000\ 1000^2\ \pi^3\ 20^4} = 0.008\ \text{rad} = \mathbf{0.5^o}$$

Angle between the force direction and deformed axis of the bar is given by the equation 5.56 :

$$\gamma_{oe} = \text{arctg}\left(\frac{Q_{oe}}{N_{oe}}\right) = \text{arctg}\left(\frac{24'803}{65'460}\right) = \mathbf{20.8^o}$$

Knowing the intensity and the orientation of the force mobilized in the bar, the components normal and tangential to the joint direction can be calculated (eqs. 5.57 and 5.58) :

$$\mathbf{R_{ot}} = R_{oe} \cos(\beta - \omega_{oe} - \gamma_{oe}) = 70'001 \cos(60 - 14.3 - 7.8) = \mathbf{54'594\ N}$$

$$\mathbf{R_{on}} = R_{oe} \sin(\beta - \omega_{oe} - \gamma_{oe}) = 70'001 \sin(60 - 14.3 - 7.8) = \mathbf{43'814\ N}$$

Thus, total contribution, T_b, of the bar to the shear strength of the joint is expressed by the equation 5.59 :

$$R_{ot} + R_{on} \text{ tg } \phi_j = 54'594 + 43'814 \text{ tg}30 = \mathbf{79'890\ N}$$

:

$$\boxed{T_b = 80\ \text{kN} \quad \text{per bar}}$$

-

ɪplacement of the bar extremity in the joint direction is calculated ıe equation 5.38 :

$$\frac{8192\ Q_{oe}^4\ b}{E\ \pi^4\ D_b^4\ p_u^3\ \sin\beta} = \frac{8192\ 24803^4\ 0.27}{210000\ \pi^4\ 20^4\ 1000^3\ \sin 60} = \mathbf{0.30\ mm}$$

nt displacement is two times as big as the displacement of the bar ty :

$$U_{je} = 2\ U_{oe} = \mathbf{0.6\ mm}$$

ılation of the bar contribution and the joint displacement e rupture

ear force constantly decreases beginning from the elastic limit. ɔosition of the forces and the displacements in the plastic domain are in Figure II.2. The normal force at the rupture is obtained from the n 5.41 :

$$N_{of} = \frac{\pi\ D_b^2}{4}\ \sigma_{ec}\ \sqrt{1 - 64\left(\frac{Q_{oe}}{\pi\ D_b^2\ \sigma_{ec}}\right)^2}$$

$$\mathbf{R_{oe}} = \sqrt{Q_{oe}^2 + N_{oe}^2} = \sqrt{24'803^2 + 65'460^2} = \mathbf{70'001\ N}$$

The bar rotation at the elastic limit is obtained from 5.33 :

$$\omega_{oe} = \frac{2048\ Q_{oe}^3\ b}{E\ p_u^2\ \pi^3\ D_b^4} = \frac{2028\ 24803^3\ 0.27}{210000\ 1000^2\ \pi^3\ 20^4} = 0.008\ \text{rad} = \mathbf{0.5^o}$$

Angle between the force direction and deformed axis of the bar is given by the equation 5.56 :

$$\gamma_{oe} = \text{arctg}\left(\frac{Q_{oe}}{N_{oe}}\right) = \text{arctg}\left(\frac{24'803}{65'460}\right) = \mathbf{20.8^o}$$

Knowing the intensity and the orientation of the force mobilized in the bar, the components normal and tangential to the joint direction can be calculated (eqs. 5.57 and 5.58) :

$$\mathbf{R_{ot}} = R_{oe} \cos(\beta - \omega_{oe} - \gamma_{oe}) = 70'001 \cos(60 - 14.3 - 7.8) = \mathbf{54'594\ N}$$

$$\mathbf{R_{on}} = R_{oe} \sin(\beta - \omega_{oe} - \gamma_{oe}) = 70'001 \sin(60 - 14.3 - 7.8) = \mathbf{43'814\ N}$$

Thus, total contribution, T_b, of the bar to the shear strength of the joint is expressed by the equation 5.59 :

$$T_b = R_{ot} + R_{on} \text{ tg } \phi_j = 54'594 + 43'814 \text{ tg}30 = \mathbf{79'890\ N}$$

so, it is :

$$\boxed{T_b = \mathbf{80\ kN} \quad \text{per bar}}$$

The displacement of the bar extremity in the joint direction is calculated using the equation 5.38 :

$$U_{oe} = \frac{8192\ Q_{oe}^4\ b}{E\ \pi^4\ D_b^4\ p_u^3\ \sin\beta} = \frac{8192\ 24803^4\ 0.27}{210000\ \pi^4\ 20^4\ 1000^3\ \sin 60} = \mathbf{0.30\ mm}$$

The joint displacement is two times as big as the displacement of the bar extremity :

$$U_{je} = 2\ U_{oe} = \mathbf{0.6\ mm}$$

- ***Calculation of the bar contribution and the joint displacement at the rupture***

The shear force constantly decreases beginning from the elastic limit. Decomposition of the forces and the displacements in the plastic domain are shown in Figure II.2. The normal force at the rupture is obtained from the equation 5.41 :

$$N_{of} = \frac{\pi\ D_b^2}{4}\ \sigma_{ec}\ \sqrt{1 - 64\left(\frac{Q_{oe}}{\pi\ D_b^2\ \sigma_{ec}}\right)^2}$$

or :

$$\mathbf{N_{of}} = \frac{\pi\ 20^2}{4}\ 600\ \sqrt{1 - 64\left(\frac{24803}{\pi\ 20^2\ 600}\right)^2} = \mathbf{181'851\ N}$$

The resultant force in the bar is equal to :

$$\mathbf{R_{of}} = \sqrt{{Q_{of}}^2 + {N_{of}}^2} = \sqrt{24803^2 + 181851^2} = \mathbf{183'535\ N}$$

Increment of the plastic rotation is calculated using the equation 5.46 :

$$\Delta\omega_{op} = \arccos\left[\frac{l_e}{l_f}\sin^2\beta \pm \sqrt{\cos^2\beta\left(1 - \left(\frac{l_e}{l_f}\right)^2\sin^2\beta\right)}\right]$$

or :

$$\Delta\omega_{op} = \arccos\left[\frac{1}{1.2}\sin^2 60 \pm \sqrt{\cos^2 60\left(1 - \left(\frac{1}{1.2}\right)^2\sin^2 60\right)}\right] = \mathbf{13.8^o}$$

Total rotation of the bar with respect to the joint is the sum of elastic and plastic rotations (eq.5.49) :

$$\omega_{of} = \omega_{oe} + \Delta\omega_{op} = 0.5 + 13.8 = \mathbf{14.3^o}$$

Angle between direction of the resultant force and the deformed axis of the bar is equal to :

$$\gamma_{of} = \text{arctg}\left(\frac{Q_{of}}{N_{of}}\right) = \text{arctg}\left(\frac{24803}{181851}\right) = \mathbf{7.8^{o}}$$

The normal and tangential components to the joint and the resultant force mobilized at the bar extremity are calculated as follows :

$$\mathbf{R_{ot}} = R_{of} \cos(\beta - \omega_{of} - \gamma_{of}) = 183'535 \cos(60 - 14.3 - 7.8) = \mathbf{144'889\ N}$$

$$\mathbf{R_{on}} = R_{of} \sin(\beta - \omega_{of} - \gamma_{of}) = 183'535 \sin(60 - 14.3 - 7.8) = \mathbf{112'660\ N}$$

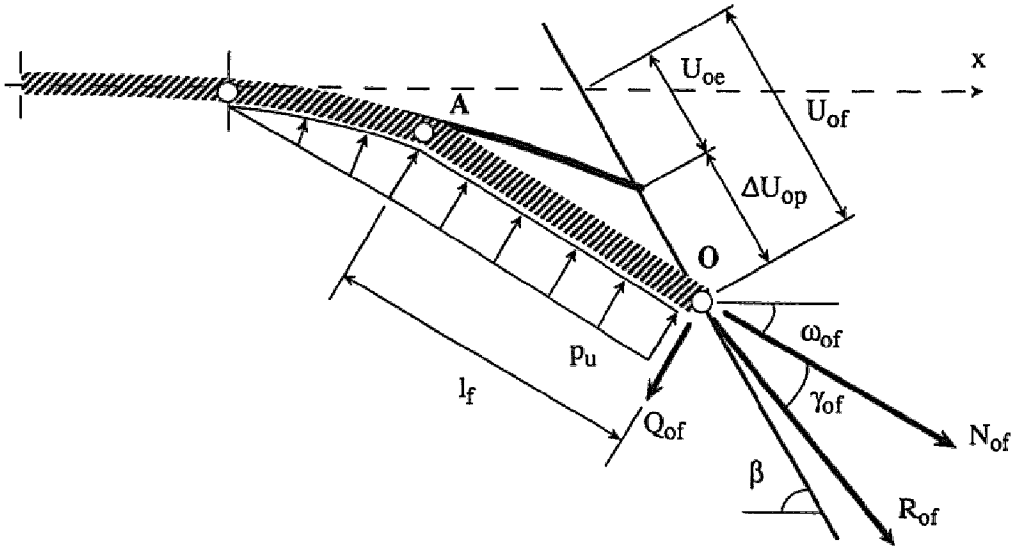

Figure II.2 : *Decomposition of forces and displacements of the bar in plastic domain*

The bar contribution to the shear strength of the joint is equal to :

$$T_b = R_{ot} + R_{on} \text{ tg } \phi_j = 144'889 + 112'660 \text{ tg}30 = \mathbf{209'893\ N}$$

and hence :

$$\boxed{T_b = \mathbf{210\ kN} \quad \text{per bar}}$$

The increment of the plastic displacement can be obtained from the equation 5.48 :

$$\Delta U_{op} = \frac{Q_{oe} \sin \Delta\omega_{op}}{p_u \sin\left(\beta - \Delta\omega_{op}\right)} = \frac{24803 \sin 13.8}{1000 \sin (60 - 13.8)} = \mathbf{8.20\ mm}$$

Total displacement of the joint is equal to :

$$U_j = 2\ U_{of} = 2\left(U_{oe} + \Delta U_{op}\right) = 2\ (0.30 + 8.20) = \mathbf{17.1\ mm}$$

Bibliography

Amadei B., Goodman R.E. 1981
A 3-D constitutive relation for fractured rock masses
Proc. Int. Symp. on the Mechanical Behaviour of Structured Media, Ottawa, Canada, pp 249 - 268

Aydan Ö. 1989
The stabilisation of rock engineering structures by rockbolts
Ph.D Thesis, Nagoya University, Japan

Aydan Ö., Kawamoto T. 1992
The stability of slopes and underground openings against flexural toppling and their stabilisation
Rock Mech. Rock Engng., Vol 25, no 3, pp 143-165

Aydan Ö., Kyoya T., Ichikawa Y., Kawamoto T. 1987
Anchorage performance and reinforcement effect of fully grouted rockbolts on rock excavations
Proc. 6th ISRM Cong., Montréal, Canada, pp 757-760

Azuar J.J. 1977
Stabilisation de massifs rocheux fissurés par barres d'acier scellées.
Rapport de recherche No 73, Laboratoire Central des Ponts et Chaussées, Paris, France

Azuar J.J., Debreuille, Habib P, Londe P, Panet M, Rochet L 1979
Le renforcement des massifs rocheux par armatures passives
Proc. 4th ISRM Cong., Montreux, Suisse

Azuar J.J., Panet M. 1980
Le comportement au cisaillement des aciers passifs dans les massifs rocheux
Industrie Minérale, Mine 4-78, Document S.I.M., B5, Boulonnage Tome 2, pp 93-98

Ballivy G., Benmokrane B., Aitcin P.C. 1986
Rôle du scellement pour les ancrages actifs scellés au rocher.
Revue Canadienne de Géotechnique, Vol 23, No 4, pp 481-489

Ballivy G., Benmokrane B., Lahoud A. 1987
Méthode intégrale de dimensionnement d'ancrages cimentés dans le rocher.
Proc. 6th ISRM Cong., Montréal, Canada, pp 761-768

Bergman S.G.A., Bjurström S. 1983
Swedish experience of rock bolting - A keynote lecture
Proc. Int. Symp on Rock bolting, Abisko, Sweden, pp 243-255

Bjurström S. 1974
Shear strength of hard rock jointed reinforced by grouted untensioned bolts
Proc. 3rd ISRM Cong., Denver, USA, pp 1194-1199

Blondeau F., Christiansen M., Guilloux A., Schlosser F. 1984
Talren : Méthode de calcul des ouvrages en terre renforcée
Proc. Int. Symp. in Situ Soil and Rock Reinforcement, Paris, France, pp 219-224

Chappell B.A. 1989
Rock bolts and shear stiffness in jointed rock masses
J. of the Soil Mech.and Found. Div., ASCE, Vol 115, No 2, pp 179-197

Coates D.F., Yu Y.S. 1970
Three dimensional stress distributions around a cylindrical hole and anchor
Proc. 2nd ISRM Cong., Belgrad, Yugoslavia, pp 175-182

Colombet G., Glories M. 1983
Confortement des talus rocheux de la carrière chenal de Montezic
Proc. 5th ISRM Cong., Melbourne, Australia, pp C25-C29

Descoeudres F. 1986
Ancrages actifs ou passifs, en terrain meuble et en rocher
Publication Société Suisse de Mécanique des Sols et des Roches, No 112, pp 5-11.

Di Prisco M. 1989
Sul comportamento a taglio delle barre d'armatura nel calcestruzzo. L'azione di spinotto : Risultati sperimentali e modellazione matematica
Doctoral Thesis, Politecnico di Milano, Italia

Dight P.M. 1983a
A case study of the behaviour of a rock slope reinforced with fully grouted rock bolts
Proc. Int. Symp on Rock bolting, Abisko, Sweden, pp 523-538

Dight P.M. 1983b
Improvements to the stability of rock walls in open pit mines
Ph.D Thesis, Monash University, Australia

Dight P.M. 1985
The Theoretical behaviour of full contact bolts subject to shear and tension
Proc. Int. Symp. on the Role of Rocks Mechanics, Zacatecas, pp 215-222

Dulacska H. 1972
Dowel action of reinforcement crossing cracks in concrete
American Concrete Institute J. Proc., Vol 69, No 12, pp 754 - 757

Dunham R.K. 1976
Anchorage tests on strain gauged resin bonded bolts
Tunnels & Tunnelling, pp 73-76

Egger P. 1973
Einfluss des Post-Failure-Verhaltens von Fels auf den Tunnelausbau unter besonderer Berücksichtigung des Ankerausbau
Veröff. Inst. Böden und Felsmech., no 57, Univ. Karlsruhe, Germany

Egger P. 1978
Dimensionnement des ancrages en souterrain
Publication Société Suisse de Mécanique des Sols et des Roches, No 98, pp 1-6

Egger P., Fernandes H. 1983
Nouvelle presse triaxiale - Etude de modèles discontinus boulonnés
Proc. 5th ISRM Cong., Melbourne, Australia, pp A171-A175

Egger P., Pellet F. 1990
Behaviour of reinforced jointed models under multiaxial loadings
Proc. Int. Symp. on Rock Joints, Loen, Norway, pp 191-194

Egger P., Pellet F. 1991
Strength and deformation properties of reinforced jointed media under true triaxial conditions
Proc. 7th ISRM Cong., Aachen, Germany, pp 215-220

Egger P., Pellet F. 1992
Numerical and experimental investigations of the behaviour of reinforced jointed media
Proc. Int. Conf. on Fractured and Jointed Rock Masses, Lake Tahoe, USA

Egger P., Spang K. 1987
Stability investigations for ground improvement by rock bolts at a large dam
Proc. 6th ISRM Cong., Montréal, Canada, pp 349-354

Egger P., Zabuski L. 1991
Behaviour of rough bolted joints in direct shear tests
Proc. 7th ISRM Cong., Aachen, Germany, pp 1285-1288

Einstein H.H., Hirschfeld R.C. 1973
Model studies on mechanics of jointed rock
J. of the Soil Mech.and Found. Div., ASCE, Vol 99, No SM3, pp 229-248

Farmer I.W. 1975
Stress distribution along a resin grouted rock anchor
Int. J. Rock Mech. Min. Sci. & Geomech Abstr., Vol 12, pp 347-351

Ferrero A.M. 1993
Resistenza al taglio di discontinuita' rinforzate
Doctoral Thesis, Politecnico di Torino, Italia

Freeman T.J. 1978
The behaviour of fully-bonded rock bolts in the Kielder experimental tunnel
Tunnels & Tunnelling, pp 37-40

Fuller P.G., Cox R.H.T. 1978
Rock reinforcement design based on control of joint displacement
Proc. 3rd Australian Tunneling Conf., Sidney, Australia, pp 28-35

Gaziev E.G., Lapin L.V. 1983
Passive anchor reaction to shearing stress on a rock joint
Proc. Int. Symp. on Rock Bolting, Abisko, Sweden, pp 101-108

Gerrard C.M. 1982
Joint compliances as a basis for rock mass properties and the design of supports
Int. J. Rock Mech. Min. Sci. & Geomech Abstr., Vol 19, pp 285-305

Gerrard C.M. 1983
Rock bolting in theory - A keynote lecture
Proc. Int. Symp. on Rock Bolting, Abisko, Sweden, pp 3-32

Gerrard C.M., Pande G.N. 1983
Predicted response of two cases of reinforcement jointed rock
Proc. Int. Symp. Rock bolting, Abisko, Sweden, pp 47-53

Gerrard C.M., Pande G.N. 1985
Numerical modelling of reinforced rock masses - I. Theory
Computers and Geotechnics, Vol 1, PP 293-318

Ghaboussi J., Wilson E.L., Isenberg J. 1973
Finite element for rock joints and interfaces
J. of the Soil Mech.and Found., Div.ASCE, pp 833-848

Gudehus G. 1982
Clouage des sols : règles de dimensionnement et leur vérification expérimentale
Revue Française de Géotechnique, no 19, pp 29-37

Haas C.J. 1976
Shear resistance of rock bolts
Transactions AIME, Vol. 260, pp 32-41

Haas C.J. 1981
Analysis of rock bolting to prevent shear movement in fracturated ground
Mining Engineering, Vol 33, no 6, pp 698-704

Hart R.D. 1991
An introduction to distinct element modelling for rock engineering
Proc. 7th ISRM Cong., Aachen, Germany, pp 1881-1891

Hetényi 1946
Beam on elastic foundation - Theory with applications in the fields of civil and mechanical engineering
Ann Arbor - The University of Michigan Press

Heuze F.E. 1979
Dilatant effect of rock joints
Proc. 4th ISRM Cong., Montreux, Switzerland, pp 169-173

Heuze F.E., Goodmann R.E. 1973
Finite Element and physical model studies of tunnel reinforcement in rock
Proc. 15th U.S. Symp. on Rock Mech., pp 37-67

Hibino S., Motijama M. 1981
Effects of rock bolting in jointy rock
Proc. Int. Symp. on Weak Rock, Tokyo, Japan, pp 1057-1062

Hofbeck J.A., Ibrahim I.O., Mattock A.H. 1969
Shear transfer in reinforced concrete
American Concrete Institute Journal, pp 119-128

Holmberg M. 1991
The mechanical behaviour of untensionned grouted rock bolts
Ph. D. Thesis, Royal Institute of Technology, Stockholm, Sweden

Holmberg M., Stille H. 1992
The mechanical behaviour of a single grouted bolt
Proc. Int. Symp. on Rock Support in Mining and Underground Construction, Sudbury, Canada, pp 473-481

Indraratna B. 1990
Development and applications of a synthetic material to simulate soft sedimentary rocks
Géotechnique, Vol 40, No , pp 189-200

Indraratna B., Kaiser P.K. 1990
Analytical model for the design of grouted rock bolts
Int. J. for Numerical and Analytical Methods & Geomech. Abstr, Vol 14, No 4, pp 227-251

Jewell R.A., Pedley M.J. 1992
Analysis for soil reinforcement with bending stiffness
J. of Geotechnical Engineering, ASCE, Vol 118, no 10, pp 1505-1528

Keddi W. 1992
Numerische Untersuchungen zum Tragverhalten vermörtelter Felsdübel in klüftigem Fels
Doctoral Thesis, Institutes für Grundbau, Bödenmechanik, Felsmechanik und Verhehrswasserbau der RWTH Aachen, Germany

Larsson H., Olofsson T. 1983
Bolt action in jointed rock
Proc. Int. Symp. on Rock Bolting, Abisko, Sweden, pp 33-46

Larsson H., Olofsson T., Stephansson O. 1985
Reinforcement of jointed rock mass - a non linear continuum approach
Proc. Int. Symp. on Fundamentals of Rocks Joints, Björkliden, Sweden, pp 567-577

Launay P., Gachon H., Poitevin P. 1970
Déformation et résistance ultime du béton sous étreinte triaxiale
Annales de l'Institut Technique du Bâtiment et des Travaux Publics, No 269, pp 22-48

Littlejohn G.S., Bruce D.A. 1975
Rock anchors - State of the art, Part 1 : Design
Ground Engineering, pp 25-32

Londe P., Bonazzi D. 1974
La roche armée
Proc. 3rd ISRM Cong., Denver, USA, pp 1208-1211

Lorig L.J. 1985
A simple numerical representation of fully bonded passive rock reinforcement for hard rocks
Computers and Geotechnics, Vol 1, pp 79-87

Ludvig B. 1983
Shear tests on rock bolts
Proc. Int. Symp. on Rock Bolting, Abisko, Sweden, pp 113-123

Moore D.P., Imbrie A.S. 1982
Rock slope reinforcement with passive anchors
Proc. 23rd U.S. Symp. on Rock Mech., Berkeley, USA

Neal B.G. 1977
The plastic methods of structural analysis
Third Edition, Chapmann and Hall, London

Pande G.N., Beer G., Williams J.R. 1990
Numerical methods in rock mechanics
John Wiley and Sons, England

Pande G.N., Gerrard C.M. 1983
The behaviour of reinforced jointed rock masses under various simple loading states
Proc. 5th ISRM Cong., Melbourne, Australia, pp F217-F223

Panet M. 1987
Renforcement des fondations et des talus à l'aide d'ancrages actifs et passifs
Proc. 6th ISRM Cong., Montréal, Canada, pp 1569-1578

Patton F.D. 1966
Multiple modes of shear failure in rock
Proc. 1st ISRM Cong., Lisboa, Portugal, pp 509-513

Pells P.J.N. 1974
The behaviour of fully bonded rockbolt
Proc. 3rd ISRM Cong, Denver, USA, pp 1212-1217

Piguet J.P., Revalor R. 1988
Rappels fondamentaux sur le boulonnage et lignes d'évolution actuelle
Séminaires Boulonnage et Renforcement des Terrains, Institut National Polytechnique de Lorraine, Nancy, France, pp 3-40

Reik G., Zacas M. 1978
Strength and deformation characteristics of jointed media in true triaxial compression
Int. J. Rock Mech. Min. Sci. & Geomech. Abstr., Vol 15, pp 295-303

Rosegren K.J., Friday R.G., Parker R.J. 1987
Preplaced cable bolts for slope reinforcement in open cut mines
Proc. 6th ISRM Cong., Montréal, Canada, pp 491-495

Schubert P. 1984

Das Tragvermögen des Mörtelversetzten Ankers unter Aufgezwungener Kluftverschiebung

Doctoral Thesis, Montanuniversität, Loeben, Austria

Sharma K.G., Pande G.N. 1988

Stability of rock masses reinforced by passive, fully grouted rock bolts

Int. J. Rock Mech. Min. Sci. & Geomech Abstr., Vol 25, No 5, pp 273-285

Spang K. 1988

Beitrag zur rechnerischen Berücksichtigung vollvermörtelter Anker bei der Sicherung von Felsbauwerken in geschichtetem oder geklüftetem

Thèse de doctorat No 740, Ecole Polytechnique Fédérale de Lausanne, Switzerland

Spang K., Egger P. 1990

Action of fully-grouted bolts in jointed rock and factors of influence

Rock Mech. and Rock Eng., Vol 23, pp 201-229

ST. John C.M., Van Dillen D.E. 1983

Rockbolts : A new representation and its application in tunnel design

Proc. 24th U.S. Symp. on Rock Mechanics, pp 13-25

Stillborg B. 1986

Professional users handbook for rock bolting

Trans Tech Publication, Series on Rock and Soil Mechanics, Vol 15

Stille H. 1992

Keynote lecture : Rock support in theory and practice

Proc. Int. Symp. on Rock Support in Mining and Underground Construction, Sudbury, Canada, pp 421-438

Stille H., Holmberg M., Nord G. 1989

Support of weak rock with grouted bolts and shotcrete

Int. J. Rock Mech. Min. Sci. & Geomech. Abstr., Vol 26, No 1, pp 99-113

Stimpson B. 1987
An analytical method for determining shear stiffness of an inclined grouted bolt installed across an open discontinuity
Int. J. of Mining and Geological Eng, Vol 5, pp 299-305

Swoboda G., Mareñce M. 1991
FEM modelling of rockbolts
Proc. Comp. Meth. and Adv. in Geomech.,Cairns, Australia, pp 1515 - 1520

Swoboda G., Mareñce M. 1992
Numerical modelling of rock bolts in intersection with fault system
Proc. Numerical models in Geomechanics, NUMOG IV, Swansea, U.K., pp 729-738

Ward W.H., Tedd P., Berry N.S.M. 1983
The Kielder experiment tunnel : final results
Géotechnique, Vol 33, no 3, pp 275-291

Washizu K. 1975
Variational methods in elasticity and plasticity
Second Edition, Pergamon Press

Wullschläger D., Natau O. 1983
Studies of the composite system of rock mass and non prestressed grouted rock bolt
Proc. Int. Symp. Rock bolting, Abisko, Sweden, pp 75-85

Wullschläger D., Natau O. 1987
The bolted rockmass as an anisotropic continuum - Material behaviour and design suggestion for rock cavities
Proc. 6th ISRM Cong., Montréal, Canada, Vol 1, pp 1321 - 1324

Yamachi H., Hirai M., Nakata M., Sakurai S. 1989
Mechanical behaviour of jointed rock masses supported with rock bolts
Proc. Int. Symp. on Rock at Great Depth, Pau, France, pp 497 - 504

Yoshinaka R., Sakaguchi S., Shimizu T., Arai H., Kato E. 1986
Reinforcing effect of rockbolt in rock joint model
Proc. Int. Symp. on Engineering in Complex Rock Formations, Beijing, China, pp 922-928

Yoshinaka R., Sakaguchi S., Shimizu T., Arai H., Kato E. 1987
Experimental study on the rock bolt reinforcement in discontinuous rocks
Proc. 6th ISRM Cong., Montréal, Canada, Vol 1, pp 1329-1332

Principal Notations

Mechanical properties

σ_c uniaxial compressive strength of intact rock
ϕ_r friction angle of intact rock
c_r cohesion of intact rock
E_r elasticity modulus of intact rock
ν_r Poisson's coefficient of intact rock

p_u maximum pressure applied by the rock or the grout on the bolt

ϕ_j joint friction angle
c_j joint cohesion
i dilatation angle of joint

σ_{el} stress at elastic limit of bolt material
σ_{ec} stress at yield limit of bolt material
E elasticity modulus of bolt material
ε_f strain at failure of bolt material

Δc_b cohesion of reinforcement (due to bolt contribution)
$\Delta\sigma_{nb}$ effect of confinement (due to bolt contribution)
k_n normal stiffness of reinforced joint
k_t tangential (shear) stiffness of reinforced joint
k_{nt} indirect normal stiffness of reinforced joint

Geometrical characteristics

r_h borehole radius
r_b bolt radius
D_b bolt diameter
A_b bolt cross-section
W_b moment of resistance of bolt
I moment of inertia of bolt

l_o characteristic length by theory of elastically supported beam
l_A distance between bolt extremity (point O) and point (A) of maximum bending moment
l_e elastic length of bolt (distance between O and A at the elastic limit)
l_f plastic length of bolt (distance O-A at the failure)
Δl_{pl} plastic elongation of bolt

A_j joint area
s spacing between joints
e thickness of layers

Angles and displacements

θ dip angle of discontinuity (angle between joint and horizontal)
β angle between bolt axis and joint
α angle between bolt axis and normal to joint

ω rotation angle of bolt
ω_o rotation angle of bolt extremity (point O)
ω_{oe} rotation angle of bolt extremity at elastic limit
ω_{of} rotation angle of bolt extremity at failure
$\Delta\omega_{op}$ plastic rotation of bolt extremity

γ_o angle (at point O) between resultant force and deformed axis of bolt
γ_{oe} angle between resultant force and deformed axis of bolt at elastic limit
γ_{of} angle between resultant force and deformed axis of bolt at failure

Ψ angle between direction of the resultant force in the bolt and the joint

u axial displacement of bolt
u_o axial displacement of bolt extremity (point O)
u_{oe} axial displacement of bolt at elastic limit (point O)
u_{of} axial displacement of bolt at failure (point O)

v transversal displacement of bolt
v_o transversal displacement of bolt extremity (point O)
v_{oe} transversal displacement of bolt at elastic limit (point O)
v_{of} transversal displacement of bolt at failure (point O)

U_o displacements of bolt extremity (point O) in joint direction
U_{oe} displacements of point O in joint direction at elastic limit of bolt
U_{of} displacements of point O in joint direction at failure of bolt
ΔU_{op} increment of plastic displacement
U_j total displacement of joint

Forces and moments

N normal force in bolt
N_p normal force in bolt at yield limit
N_o normal force at bolt extremity
N_{oe} normal force at bolt extremity at elastic limit
N_{of} normal force at bolt extremity at failure

Q shear force in bolt
Q_p shear force in bolt at yield limit
Q_o shear force at bolt extremity
Q_{oe} shear force at bolt extremity at elastic limit
Q_{of} shear force at bolt extremity at failure

M bending moment in bolt
M_p full plastic bending moment in bolt
M_A bending moment at point A
R_o resultant force in bolt on joint level
R_{oe} resultant force in bolt at elastic limit on joint level
R_{of} resultant force in bolt at failure on joint level

R_{on} resultant force component in bolt, normal to joint
R_{ot} resultant force component in bolt, tangential to joint
T total contribution of bolt to shear strength of joint
T_{be} contribution of bolt at elastic limit
T_{bf} contribution of bolt at failure

σ_1 major principal stress
σ_2 intermediate principal stress
σ_3 minor principal stress

Numbers

n_j number of joints
n_b number of bolts

Normalized parameters

F_T ratio of total contribution to normal plastic force in bolt
F_R ratio of resultant force to normal plastic force in bolt
F_{Rn} ratio of force component normal to joint to normal plastic force in bolt
F_{Rt} ratio of force component parallel to joint to normal plastic force in bolt
F_N ratio of normal force mobilized in bolt to normal plastic force in bolt
F_Q ratio of transversal force mobilized in bolt to normal plastic force in bolt
F_U ratio of joint displacement to diameter of bolt